University of Cyprus

DEPARTMENT OF BIOLOGICAL SCIENCES

MOLECULAR AND CELLULAR INVESTIGATION OF GLOMERULAR FILTRATION BARRIER COMPONENTS IN THIN BASEMENT MEMBRANE NEPHROPATHY

DOCTOR OF PHILOSOPHY DISSERTATION

CHARALAMBOS D. STEFANOU

2015

University of Cyprus

DEPARTMENT OF BIOLOGICAL SCIENCES

MOLECULAR AND CELLULAR INVESTIGATION OF GLOMERULAR FILTRATION BARRIER COMPONENTS IN THIN BASEMENT MEMBRANE NEPHROPATHY

CHARALAMBOS D. STEFANOU

A Dissertation Submitted to the University of Cyprus in Partial Fulfillment of the Requirements for the Degree of Doctor of Philosophy

April 2015

VALIDATION PAGE

Doctoral Candidate: Charalambos D. Stefanou

Doctoral Thesis Title: Molecular and cellular investigation of glomerular filtration barrier components in thin basement membrane nephropathy

The present Doctoral Dissertation was submitted in partial fulfillment of the requirements for the Degree of Doctor of Philosophy at the ***Department of Biological Sciences*** *and was approved on the ……. [date of approval] by the members of the* ***Examination Committee***.

Examination Committee:

Research Supervisor:_____

(Name, position and signature)

Committee Member:_____

(Name, position and signature)

Committee Member: _____

(Name, position and signature)

Committee Member: _____

(Name, position and signature)

Committee Member: _____

(Name, position and signature)

DECLARATION OF DOCTORAL CANDIDATE

The present doctoral dissertation was submitted in partial fulfilment of the requirements for the degree of Doctor of Philosophy of the University of Cyprus. It is a product of original work of my own, unless otherwise mentioned through references, notes, or any other statements.

……..[Full Name of Doctoral Candidate]

……..[Signature]

Περίληψη

Η Νεφροπάθεια της Λεπτής Βασικής Μεμβράνης (ΝΛΒΜ) και το σύνδρομο Alport αποτελούν κληρονομικές σπειραματοπάθειες, οι οποίες κατά κύριο λόγο οφείλονται σε μεταλλάξεις στα γονίδια COL4A3/A4/A5 τα οποία κωδικοποιούν για τις α3, α4 και α5 αλυσίδες αντίστοιχα του κολλαγόνου τύπου IV. Οι ασθενείς με σύνδρομο Alport παρουσιάζουν τυπικά μικροσκοπική ή/και μακροσκοπική αιματουρία από την παιδική ηλικία. Με την πάροδο του χρόνου, η εξελισσόμενη νεφρική βλάβη οδηγεί σε πρωτεϊνουρία, έκπτωση της νεφρικής λειτουργίας και αναπόφευκτα σε τελικό στάδιο νεφρικής ανεπάρκειας στη $2^{η}$-$3^{η}$ δεκαετία της ζωής. Η ΝΛΒΜ χαρακτηρίζεται τυπικά από μεμονωμένη μικροσκοπική αιματουρία σπειραματικής προέλευσης, απουσία κλινικά σημαντικής πρωτεϊνουρίας, φυσιολογική αρτηριακή πίεση και νεφρική λειτουργία. Ωστόσο, σημαντικός αριθμός δημοσιεύσεων αναφέρουν ότι ασθενείς με ΝΛΒΜ παρουσιάζουν σημαντική φαινοτυπική ετερογένεια, με κλινική εικόνα που ποικίλει ευρέως από μεμονωμένη μικροσκοπική αιματουρία μέχρι και τελικό στάδιο νεφρικής ανεπάρκειας σε ηλικίες πέραν των 40 ετών. Εντούτοις, τα ακριβή αίτια της ευρείας αυτής φαινοτυπικής ετερογένειας, καθώς επίσης και οι μοριακοί μηχανισμοί οι οποίοι ενεργοποιούνται σε έδαφος μεταλλάξεων στα γονίδια COL4A3/A4/A5 εξακολουθούν να παραμένουν άγνωστοι.

Στην προσπάθεια εύρεση του μοριακού μηχανισμού ο οποίος οδηγεί στο σύνδρομο Alport ή στη ΝΛΒΜ, υποθέσαμε πως μεταλλάξεις στα γονίδια COL4A3/A4/A5, προκαλούν τη μη φυσιολογική ενεργοποίηση ενδοκυττάριων μονοπατιών, οδηγώντας στο συγκεκριμένο φαινότυπο. Για τη μελέτη αυτή έγινε υπερέκφραση της φυσιολογικής και της μεταλλαγμένης αλυσίδας του κολλαγόνου COL4A3 (μετάλλαξη *COL4A3*-p.G1334E) σε ανθρώπινα αδιαφοροποίητα ποδοκύτταρα προκειμένου να ελεγχθούν οι επιπτώσεις τους στα διάφορα ενδοκυττάρια μονοπάτια. Δεδομένα τα οποία προέκυψαν από σειρά πειραμάτων εισηγούνται πως η υπερέκφραση του κολλαγόνου COL4A3 οδηγεί σε ανώμαλη εντόπιση της συγκεκριμένης αλυσίδας στο ενδοπλασματικό δίκτυο, ενεργοποιώντας το μονοπάτι των μη σωστά αναδιπλωμένων πρωτεϊνών (unfolded protein response-UPR). Παρόμοια αποτελέσματα παρατηρήθηκαν σε μοντέλο knockin ποντικού, το οποίο φέρει τη μετάλλαξη *Col4a3*-p.G1332E καθώς επίσης και σε βιοψίες ασθενών με ΝΛΒΜ οι οποίοι ήταν φορείς της μετάλλαξης *COL4A3*-p.G1334E.

Επιπλέον, παρατηρώντας την ύπαρξη φαινοτυπικής ετερογένειας σε ασθενείς με ΝΛΒΜ, υποθέσαμε πως κάποια γονίδια μπορεί δυνητικά να δρουν ως τροποιητικά γονίδια. Πραγματοποιήθηκε *in silico* ανάλυση και αλληλούχηση γονιδίων τα οποία εκφράζονται

στο σχισμοειδές διάφραγμα των ποδοκυττάρων για εντοπισμό επιβλαβών μη συνώνυμων πολυμορφισμών. Μετά από γονοτύπηση έξι υψηλού ρίσκου πολυμορφισμών σε 103 ασθενείς με ΝΛΒΜ, οι οποίοι είχαν κατηγοριοποιηθεί βάσει κλινικών κριτηρίων σε σοβαρά και ήπια επηρεασμένους ασθενείς, επισημάνθηκε ο συσχετισμός του πολυμορφισμού *NEPH3*-p.V353M με το σοβαρό φαινότυπο της ΝΛΒΜ (p=0.036). Ακολούθησε έλεγχος για το συγκεκριμένο πολυμορφισμό μεγαλύτερης συλλογής ασθενών με αιματουρία (*HEMATURIA*) η οποία αποτελείται από 524 ασθενείς, επίσης κατηγοριοποιημένους ως σοβαρά ή ήπια πάσχοντες. Και πάλι εντοπίστηκε η σχέση του πολυμορφισμού *NEPH3*-p.V353M με τη σοβαρότητα της πορείας της νόσου ($p=3.0x10^{-3}$). Επιπλέον, ακολούθησε η γονοτύπηση 6,531 ατόμων από τη συλλογή Framingham Heart Study (FHS), η οποία αποκάλυψε τη συσχέτιση του ομόζυγου γονοτύπου 353M/M με τη μικροαλβουμινουρία ($p=1.0x10^{-3}$). Δύο ανεξάρτητες πληθυσμιακές συλλογές, KORAF4 και SAPHIR, επιβεβαίωσαν το αποτέλεσμα αυτό ενώ μέτα-ανάλυση και των τριών συλλογών (11,258 άτομα) παρουσίασε αυξημένη στατιστική σημαντικότητα ($p=1.3x10^{-5}$). Επιπρόσθετες λειτουργικές μελέτες παρουσίασαν την επίδραση του *NEPH3*-p.V353M στον ομοδιμερισμό και ετεροδιμερισμό της φιλτρίνης με τη νεφρίνη. Επίσης, χρήση πρωτεομικής ανάλυσης σε συνδυσμό με πειράματα ανοσοκατακρήμνισης και ανοσοφθορισμού, επέτρεψαν την ταυτοποίηση της Myh9 ως νέου μορίου αλληλεπίδρασης με τη φιλτρίνη. Η παρουσία του πολυμορφισμού *NEPH3*-p.V353M είχε ως αποτέλεσμα τη σημαντικότερη αλληλεπίδραση της φιλτρίνης με τη Myh9. Επίσης, υπερέκφραση της *NEPH3*-p.V353M στην παρουσία tunicamycin οδήγησε σε ένα διαφορετικό τρόπο ενεργοποίησης του μονοπατιού UPR.

Επιπρόσθετα, αλληλούχηση του γονιδίου της ποδοσίνης οδήγησε στον εντοπισμό των πολυμορφισμών *NPHS2*-p.E237Q και *NPHS2*-p.R229Q σε επτά σοβαρά επηρεασμένους ασθενείς με ΝΛΒΜ. Οι ασθενείς αυτοί ανήκουν σε δυο διαφορετικές οικογένειες με χαρακτηριστικό γνώρισμα τη συγκληρονόμηση της μετάλλαξης *COL4A3*-p.G1334E. Πειράματα ανοσοφθορισμού ανέδειξαν μεταβολή στον εντοπισμό της φυσιολογικής ποδοσίνης ή νεφρίνης στην παρουσία των δύο πολυμορφισμών, εμφανίζοντας περιπυρηνική χρώση. Επιπλέον, πειράματα ανοσοκατακρήμνισης παρουσίασαν ισχυρότερη σύνδεση των δύο μεταλλαγμένων μορφών της ποδοσίνης με τη φυσιολογική ποδοσίνη ή νεφρίνη.

Τα αποτελέσματα αυτά δείχνουν ότι το στρες στο ενδοπλασματικό δίκτυο, το οποίο προκαλείται από το μη φυσιολογικό εντοπισμό των αλυσίδων του κολλαγόνου IV στα ανθρώπινα ποδοκύτταρα, συμβάλλει στην παθογένεση της ΝΛΒΜ και του συνδρόμου

Alport μέσω της ενεργοποίηση του UPR. Ένα αρκετά υποσχόμενο εύρημα για την εφαρμογή καινοτόμων θεραπευτικών παρεμβάσεων για τις διάφορες κολλαγονοπάθειες. Τα αποτελέσματα τα οποία προέκυψαν από τις γενετικές και λειτουργικές μελέτες σε ότι αφορά στον πολυμορφισμό *NEPH3*-p.V353M ενισχύουν το σημαντικό ρόλο του σπάνιου αυτού πολυμορφισμού, ο οποίος φαίνεται να επιδρά αρνητικά στην εξέλιξη της αιματουρίας. Συμπληρωματικές γενετικές μελέτες παρουσίασαν ότι ο συγκεκριμένος πολυμορφισμός σε ομοζυγωτία αποτελεί προδιαθεσικό παράγοντα για την ανάπτυξη μικροαλβουμινουρίας σε άτομα του γενικού πληθυσμού. Τέλος, γενετικές και λειτουργικές μελέτες υποστηρίζουν την άποψη ότι συγκεκριμένοι πολυμορφισμοί οι οποίοι εντοπίζονται στην ποδοσίνη μπορούν να δράσουν ως τροποιητικά γονίδια, όταν συγκληρονομηθούν με μεταλλάξεις στα γονίδια *COL4A3/A4*, προδιαθέτοντας ίσως για FSGS και σοβαρότερο φαινότυπο.

Abstract

Thin-basement-membrane nephropathy (TBMN) and Alport syndrome (AS) are hereditary collagen IV glomerulopathies caused by mutations in the COL4A3/A4/A5 genes. Clinical presentation of AS includes hematuria, progressive nephritis with proteinuria and declining renal function leading to end-stage renal disease. TBMN represents the carrier state of AS and is typically characterized by persistent microscopic hematuria of glomerular origin, minimal proteinuria, normal arterial blood pressure and normal renal function. However, scarce reports suggest that, occasionally, TBMN can be progressive, leading to impairment of renal function of variable degree causing even end-stage renal disease (ESRD). Nonetheless, the cause of this phenotypic variability observed in TBMN patients and the exact molecular mechanisms by which these mutations exert their deleterious effects on the glomerulus remain elusive.

Therefore, it was hypothesized that defective trafficking of the COL4A3 chain causes a strong intracellular effect on the cell responsible for COL4A3 expression, the podocyte. To this end, normal and mutant COL4A3 chains (*COL4A3*-p.G1334E mutation) were overexpressed in human undifferentiated podocytes in order to verify their effects in various intracellular pathways employing a microarray approach. COL4A3 overexpression caused chain retention in the endoplasmic reticulum (ER) leading to the activation of unfolded protein response (UPR)–related markers of ER stress. Remarkably, the overexpression of normal or mutant COL4A3 chains differentially activated the UPR pathway. Similar results were observed in a novel knockin mouse carrying the *Col4a3*-p.G1332E mutation, which produced a phenotype consistent with AS and in biopsy specimens from patients with TBMN carrying a heterozygous *COL4A3*-p.G1334E mutation.

Additionally, it was hypothesized that genetic modifiers could explain the observed variability of symptoms in TBMN patients. To this end, *in silico* analysis and re-sequencing in genes expressed in the slit diaphragm was performed, in an effort to detect potentially deleterious non-synonymous SNPs. Genotyping for six high-scored variants in 103 TBMN adult patients with founder mutations, who were classified as mildly or severely affected, pointed to an association with variant *NEPH3*-p.V353M (filtrin) ($p=0.036$). This result prompted testing in a larger pooled cohort (*HEMATURIA*) of 524 patients, which also included IgA nephropathy patients, categorized as “Severe” or “Mild”. This indicated an association of the *NEPH3*-p.V353M variant with disease severity under the dominant model ($p=3.0x10^{-3}$). Subsequently, genotyping 6,531 subjects of the

Framingham Heart Study (FHS) revealed an association of the homozygous 353M/M genotype with microalbuminuria ($p=1.0x10^{-3}$). Two further general population cohorts, KORAF4 and SAPHIR confirmed the association, and a meta-analysis of all three cohorts (11,258 individuals) was highly significant ($p=1.3x10^{-5}$). Moreover, functional studies exhibited a slight distortion in homodimerization or heterodimerization of Neph3 with nephrin caused by the *NEPH3*-p.V353M. Interestingly, a combination of a proteomics approach followed by immunoprecipitation and immunofluorescence experiments, identified Myh9 as a new interacting partner of filtrin. The filtrin *NEPH3*-p.V353M substitution resulted in a significantly stronger interaction with Myh9 protein. Additionally, overexpression of *NEPH3*-p.V353M in the presence of tunicamycin, exhibited a differential activation of the UPR pathway.

Furthermore, resequencing of *NPHS2* led to the detection of *NPHS2*-p.E237Q and *NPHS2*-p.R229Q in seven severely affected TBMN patients, belonging in two families, which segregated mutation *COL4A3*-p.G1334E (combined concordance probability 0,003). Immunofluorescence experiments suggested altered localization of *wt* podocin or nephrin when co-expressed with each of the two these variants, demonstrating perinuclear staining. Additionally, immunoprecipitation experiments showed stronger binding of mutant podocin to *wt* podocin or nephrin.

These results suggest that ER stress arising from defective localization of collagen IV chains in human podocytes contributes to the pathogenesis of TBMN and AS through activation of the UPR, a finding that may pave the way for novel therapeutic interventions for a variety of collagenopathies. Moreover, genetics and functional studies support a “rare variant-strong effect” role for *NEPH3*-p.V353M, by exerting a negative modifier effect on primary hematuria. Additionally, genetics studies support a role in predisposing homozygous subjects of the general population to micro-albuminuria. Finally, genetics and functional studies support the hypothesis that certain hypomorphic podocin variants may act as adverse modifiers when co-inherited with *COL4A3/A4* mutations, thus predisposing to FSGS and severe kidney function decline. Overall, the current study, using an interdisciplinary approach, shed light to the pathophysiology of TBMN, a serious health issue in Cyprus and around the world.

"If I have seen further it is by standing on the shoulders of giants"

Isaac Newton

Acknowledgements

The current work was performed at the Molecular Medicine Research Centre of the University of Cyprus during 2009-2015.

First and foremost, I would like to express my sincere gratitude to Professor Constantinos Deltas for allowing me to conduct this research under his auspices and especially for the confidence placed on me. His valuable time is highly appreciated as well as his enduring support and inspirational guidance that, taken together, make him a great mentor.

Words cannot express my gratitude to my academic "mother", Dr Myrtani Pieri for spreading happiness on those scientifically dark days. Without her enthusiasm and encouragement, I could never finish my doctoral work at the UCY. For me, she is not just a supervisor, but also a lifetime friend and advisor.

My deep appreciation also goes to Dr Konstantinos Voskarides for his patience and valuable insights he has provided me with, throughout my PhD time. I have been extremely lucky to work with such a committed individual.

Heartfelt thanks goes to my lab-buddies Isavella and Georgia for their invaluable advice and feedback as well as for their never-ending support. In addition, I would like to thank past and present members of the Delta lab; Penny and Kyriacos for their brief but invaluable supervision. Big thanks go to Gregory for sharing his exceptional scientific calibre and for being such a great coach. Thanks to Panagiota for being my sweet Toulla and keeping me company and entertained all those late nights spent at the lab. Thanks to Andrea for helping me with the writing hell and the proofread as well as for being the best cell co-worker ever. Thanks to Louiza for giving life to the lab. Thanks to Despina for sharing her knowledge and for answering questions in general. I am grateful for their help and for the good times shared together inside and outside the lab. I would also like to thank Apostolis, Kamil and Revekka for their support and contribution during the preparation of our manuscript. Moreover, I have to express my sincere gratitude to all the other members of the Delta group Maria Louca, Amir, Constantina, Anastasia, Vasileia, Nada, Demetris and Eliza. Many thanks to the members of the Santama lab (Antoni, Andri, Yianni, Elena, Anna and Despina) for being the ultimate lab-neighbours, providing a great work environment and for their help and chats.

I cannot express my gratitude enough for our collaborators starting with the doctors of the Nephrology Departments at the public and private hospitals in Cyprus, especially Dr Alkis Pierides, for their continuous support. I would also like to extend my sincerest thanks and appreciation to our patients and their families. Appreciation is also expressed to Dr Ioanna

Zouvani and Dr Natasa Anastasiadou for providing us all the needed help for the immunohistochemistry experiments, Dr George Lapathiti and Mr Christo Karaisko for their invaluable assistance with the creation and maintenance of our mouse model and Dr Dimitrios Goumenos for supplying us with tissue samples from their collection. Additionally, I would like to express my gratitude to the Benzing Group, specifically Dr Martin Hohne, for assisting us with the accomplishment of the immunoprecipitation experiments and for kindly providing us with the nephrin construct. Special thanks is also extended to Dr Kostas Stylianou and Dr Dontscho Kerjaschki for performing all the EM experiments. Likewise, I would like to acknowledge Dr Stavros Malas, Dr Elena Panayiotou and Mr Neoklis Makrides for their contributions and Dr Moin Saleem for kindly providing us with the human podocyte cell line. I am also grateful for the priceless support of the Skourides and Santama group to the immunofluorescence analyses.

Furthermore, my thanks are due to the members of my oral defense committee Dr Anna Greka, Dr Niovi Santama, Dr Paris Skourides and Dr Ioannis Georgiou for their time and insightful questions.

Very special thanks go to Nico and Kyriaco Yiannouka for their motivation, encouragement and support. You both have been great mentors for me. I also thank the members of the Yiannoukas Medical Laboratories especially Chrystalla, Maro, Louiza, Maria, Andriani and Michaella for their constant encouragement.

Words cannot express the thanks to my dear friends who have supported me over the last few years: Costas Symeonides, Nikolas Varnavas, Eliana Sergiou Varnava, Varnavas Varnava Junior, Eleni Panagiotou, Petros Zapitis, Louis Vakanas, Stalo Solea, Demetra Stavrou, Emily Sophocleous, Petroulla Tzortzi, Avgoustinos Petrakkides, Kyriaki Sofocleous Makridou and George Makrides. Having you guys in my life makes it as wonderful and fun as it is, and your support has been essential all these years.

Finally yet importantly, special thanks go to my family for all the sacrifices that they have made for me. For my parents who have always been there next to me supporting and helping me in all my endeavours. Your endless love and encouragement has enabled me to follow my dreams and be the person I am today. You are my greatest strength and I am blessed to be your son. I would also like to thank my beloved sister and brother for being my best friends. Thank you for supporting me to everything, and especially for encouraging me through this experience.

If I have not thanked you personally then you know who you are and consider yourself thanked. Special thanks go as well to all of you who have spent some time reading my thesis.

I dedicate my thesis to my family and my friends.
For their endless love, support and encouragement

Harris D. Stefanou

List of contents

List of figures

List of tables

List of abbreviations

AB8/13	human podocytes
ADAS	autosomal dominant Alport syndrome
ARAS	autosomal recessive Alport syndrome
AS	Alport syndrome
ATF6	activating transcription factor-6
BSA	bovine serum albumin
CASK	calcium/calmodulin-dependent serine protein kinase
CD2AP	CD-2 associated protein
CFHR5	complement factor related protein 5
CHOP	C/EBP homologous protein
D-MEM	Dulbecco's Modified Eagle's Medium
DMSO	dimethyl sulfoxide
ECM	extracellular matrix
EDEM	ER degradation enhancer mannosidase a-like
EDTA	ethylenediaminetetraacetic acid
eIF2a	eukaryotic initiation factor 2a
ELC	essential light chains
EM	electron microscopy
EMBL	European Molecular Biology Laboratory
ER	endoplasmic reticulum
ERAD	endoplasmic reticulum associated degradation
ESKD	end stage kidney disease
ESL	endothelial cell surface layer
ESRD	end stage renal disease
EST	expressed sequence tag
FBS	fetal bovine serum
FH	familial hematuria
FSGS	Focal Segmental Glomerulosclerosis
GADD34	growth arrest and DNA damage-inducible protein 34
GBM	glomerular basement membrane

GFB	glomerular filtration barrier
GPCR	G-protein coupled receptors
HBSS	Hank's balanced salt solution
HEK	human embryonic kidney cells
HRP	horseradish peroxidase
HT	hypertensive nephropathy
Ig	immunoglobulin
IQGAP1	IQ motif-containing GTPase-activating protein 1
IRE1	inositol-requiring protein-1
LC-MSMS	liquid chromatography-mass spectrometry
MAGI-2/S-SCAM	membrane-associated guanylate kinase inverted 2/synaptic scaffolding molecule
MAP	mitogen activated protein
MCD	minimal change disease
MGN	membranous glomerulonephropathy
NF-κB	nuclear factor kappa-B
NGS	next generation sequencing
NM	non-muscle myosins
OCT	optimal cut temperature
PAGE	polyacrylamide gel electrophoresis
PAN	puromycin aminonucleoside nephrosis
PBS	phosphate buffered saline
PERK	protein kinase RNA (PKR)-like ER kinase
PFA	paraformaldehyde
PVDF	polyvinilidene fluoride
RGD	integrin-recognition site
RLC	regulatory light chains
RTKs	receptor tyrosine kinases
SD	slit diaphragm
SDS	sodium dodecyl sulfate
SH2	Src homology 2
SNAP	*S*-nitroso-*N*-acetyl-dl-penicillamine
SP1	specific protein 1

SRNS	steroid resistant nephrotic syndrome
SSNS	steroid sensitive nephrotic syndrome
TBMN	thin basement membrane nephropathy
TM	tunicamycin
TRAF2	tumor necrosis factor receptor (TNRF) associated factor-2
TRPC6	transient receptor potential cation channel 6
UPR	Unfolded Protein Response
v/v	volume/volume
VEGF-A	vascular endothelial growth factor A
XBP1	X-box-binding-protein-1
XLAS	X-linked Alport syndrome

Chapter 1: Introduction

1.1 Urinary system structure and function

The urinary system is a group of organs participating in the production and excretion of urine. It consists of the kidneys, the ureters, the urinary bladder and the urethra. More specifically, the kidneys' function is to filter the blood and produce the urine, while ureters along with the bladder and the urethra form the urinary tract, which transfers, stores and excretes urine to the environment. Additionally, kidneys contribute to the regulation of electrolyte balance, acid-base homeostasis and control of arterial pressure (Rosdahl and Kowalski, 2008).

1.2 Kidney structure and function

Kidneys are bean shaped organs located on each site of the spinal cord in the upper abdominal area. Kidneys consist of nephrons, the structural and functional unit of the kidney, as well as the collecting ducts and the microvasculature. Each kidney contains approximately one million nephrons, which are the functional and structural units of this organ *(Figure 1A)*.
The human kidneys are responsible for conserving the homeostasis of the extracellular fluid through specialized retention or excretion of water, electrolytes and other metabolites. This procedure takes place via three different processes, including filtration of circulating blood at the glomerulus, selective reabsorption from tubular fluid to the blood and selective secretion from peritubular capillary blood to the tubular fluid (Feehally et al., 2007).
In addition, the kidneys take part in the production or activation of hormones essential for the regulation of the arterial blood pressure, the process of erythropoiesis and the maintenance and integrity of the skeletal system (Walser and Thrope, 2004).

1.2.1 Nephrons

A kidney nephron develops from the mesenchymal metanephric blastemal by induction through the ureteric bud (Pavenstadt et al., 2003). It consists of two parts: the renal corpuscle *(Figure 1B)*, where the blood plasma is filtered, and the renal tubule, which is attached to the collecting duct.
The renal tubule is the portion of the nephron where the filtrate passes. It is divided in structurally and functionally defined fragments, consisting of the proximal convoluted tubule, the Loop of Henle (descending and ascending limb) and the distal convoluted tubule. The distal convoluted tubules are connected through the collecting tubules to the cortical collecting ducts.

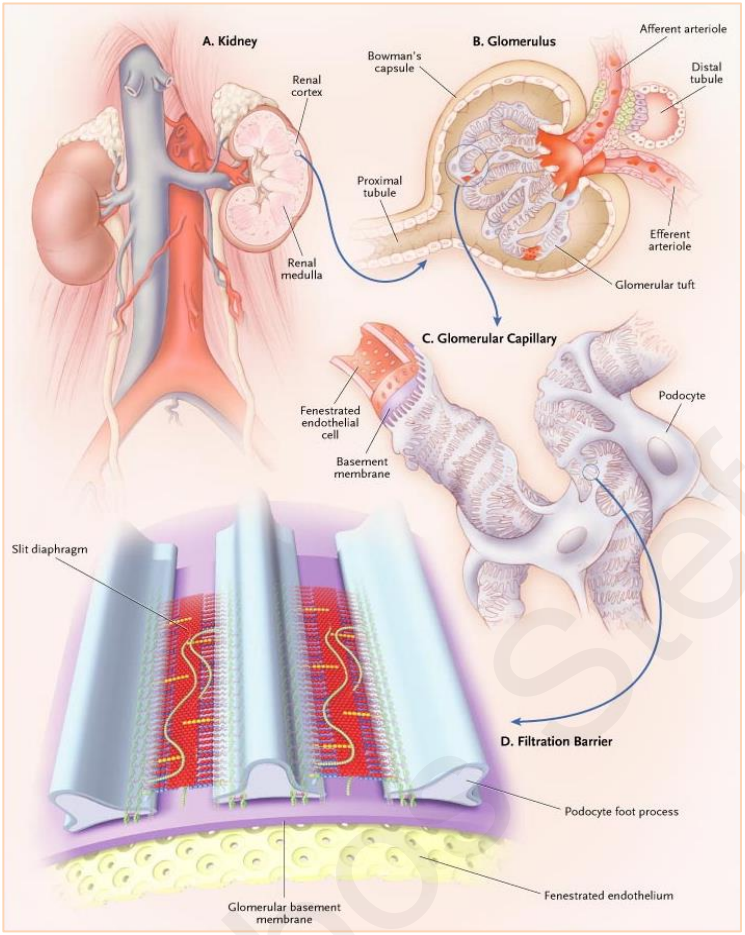

Figure 1: Kidney, glomerulus and glomerular filtration barrier

Typically, a human kidney contains nearly one million glomeruli in the renal cortex, as is indicated in panel (A). Afferent arterioles enter the Bowman's capsule branch into several capillaries and form the glomerular tuft, as shown in panel (B). The product of plasma filtration, a process performed by the capillary walls, is guided to the proximal tubule, whereas the unfiltered blood returns back to the circulation via the efferent arteriole. The filtration barrier of the capillary wall is demonstrated in panel (C), consisting of the innermost fenestrated endothelium, the glomerular basement membrane and the epithelial cells with their interdigitating foot processes. Panel (D) shows a cross-section of the glomerular filtration barrier, illustrating the fenestrated endothelial layer and the glomerular basement membrane with the overlying podocyte foot processes (Tryggvason et al., 2006).

1.2.2 The glomerular filtration barrier

The renal glomerulus is a knot of specialized capillaries attached to the mesangium, all of them surrounded by a pouch-like formation named Bowman's capsule. These specialized capillaries are able to filter enormous amounts of blood while retaining the blood cells and at least 99.9% of the albumin and other proteins. They are comprised by the fenestrated endothelium, the glomerular basement membrane which has a unique composition and the visceral epithelial cells (podocytes), which play a crucial role in regulating the glomerular filtration *(Figure 2)* (Welsh and Saleem, 2012).

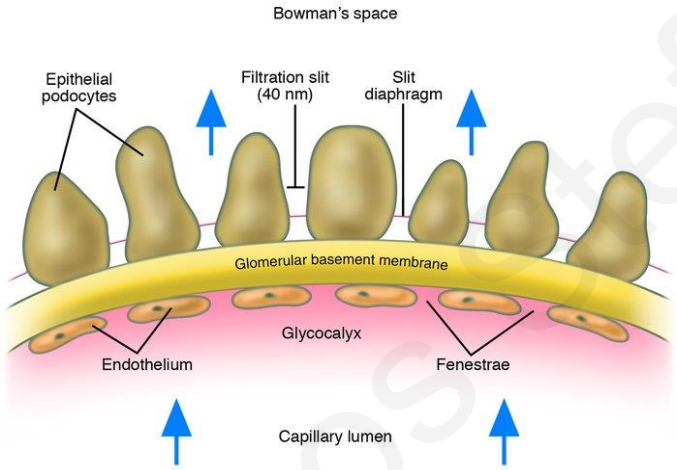

Figure 2: The glomerular filtration barrier.

The glomerular filtration barrier consists of the fenestrated endothelium, the glomerular basement membrane and the epithelial foot processes. The foot processes form filtration slits spanned by slit diaphragms. Also shown are the subepithelial space and the endothelial glycocalyx (Deen, 2004).

1.2.2.1 Fenestrated endothelium

Glomerular capillaries, are characterized by a unique type of porous endothelial cells, featuring a large fenestrated region expanding to the 20-50% of the entire capillary surface area (Haraldsson et al., 2008). For many years, glomerular endothelial cells were not considered part of the glomerular filtration barrier (GFB) due to the existence of these fenestrations. However, electron microscopy studies revealed the existence of sialoglycoproteins covering the renal capillary fenestrations (Rostgaard and Qvortrup, 1997), while other studies reported the detection of the endothelial cell surface layer (ESL), consisting of the glycocalyx and the endothelial cell coat. Both structures have been shown to

form a barrier, which prevents the loss of plasma protein in the urine (Haraldsson and Jeansson, 2009).

Moreover, several studies have described that Vascular Endothelial Growth Factor-A (VEGF-A), produced and secreted by the podocytes, is an important factor for the formation and maintenance of the fenestrated endothelium (Eremina et al., 2008). Furthermore, there is evidence that endothelial cells are important for the synthesis and preservation of the glomerular basement membrane (GBM), and more specifically by participating in the production of major compounds such as laminin isoform LM-111 and early collagen trimer α1α1α2 (IV) (Abrahamson, 2012, St John and Abrahamson, 2001).

1.2.2.2 Glomerular Basement Membrane

The kidney GBM is an unusually thick, specialized, sheet-like, acellular type of matrix contributing to the barrier function (*Figure 3).* According to multiple reports, the mean thickness in male adults is 370±50 nm and in female adults 320±50 nm. In children the GBM thickness is 150 nm at birth, 200 nm at age 1 year and approaches adult-like thickness at age 11 years (Steffes et al., 1983, Vogler et al., 1987).

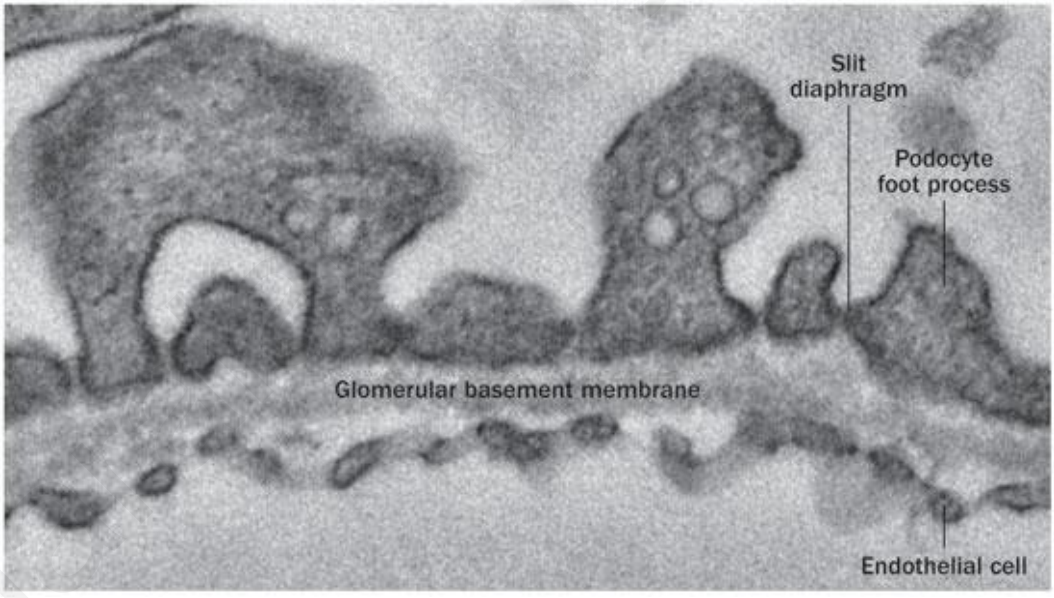

Figure 3: High-power electron microscopy image of murine podocyte foot processes attached to the glomerular basement membrane.

High-power electron microscopy image reveals the glomerular basement membrane, decorated with the fenestrated glomerular endothelial cells and the podocytes on the opposite sites (Brinkkoetter et al., 2013).

The GBM is divided into three layers; the dense lamina densa, the lamina rara interna, which lies between the lamina densa and the endothelial cells, and the lamina rara externa, which lies between the lamina densa and the epithelial cells (Nelson, 2011). The basic function of the GBM is to provide structural and functional support to the endothelial, mesangial and epithelial cells. It contains a unique composition of collagen IV and laminins, which are secreted by the endothelial and epithelial cells (Tryggvason et al., 2006). In detail, the immature GBM is composed of collagen α1α1α2 (IV), which is replaced by collagen α3α4α5 (IV). This transition occurs concurrently with the conversion of laminin chains from LM-111 to LM-521 (Suh and Miner, 2013). Moreover, recent proteomic analysis of the glomerular extracellular matrix (ECM), revealed the abundance of collagen VI and TINAGL1 (Lennon et al., 2014).

For the last 20 years, several groups have focused on the study of the consistency of the GBM, since there is evidence for the importance of the GBM in the selectivity of the glomerular filtration. Additionally, recent genetic and functional studies demonstrated the association of mutations in genes encoding components of the GBM with the development of kidney diseases, including Thin Basement Membrane Nephropathy (TBMN) and Alport syndrome (AS) (Miner, 2012a).

1.2.2.2.1 Collagen IV

Collagen type IV forms a flexible "chicken-wire" network and along with laminins, proteoglycans and entactin/nidogen, create the backbone of the GBM. It is the most abundant protein found in basement membranes and was first described by Kefalides in 1966, who defined its structure in canine glomerulus (Kefalides and Winzler, 1966, Kefalides, 1966). Since then, a significant number of research groups established the importance of collagen type IV in the structure of the GBM and its association with the development of different kidney diseases, such as AS, TBMN and Goodpasture syndrome. Molecular findings have proved the existence of six different collagen IV genes, arranged in a pairwise head-to-head orientation, positioned on three different chromosomes; *COL4A1-COL4A2* on chromosome 13, *COL4A3-COL4A4* on chromosome 2 and *COL4A5-COL4A6* on chromosome X (Hudson et al., 1993, Khoshnoodi et al., 2008).

Each collagen IV gene encodes for a different α-chain, which consists of three structurally distinct domains: A 15-residue non-collagenous amino terminus domain rich in cysteine and lysine residues, a long collagenous domain of 1400-residues of Gly-Xaa-Yaa (were X and Y are frequently prolines and 4-hydroxyprolines) repeats which are interrupted at several sites

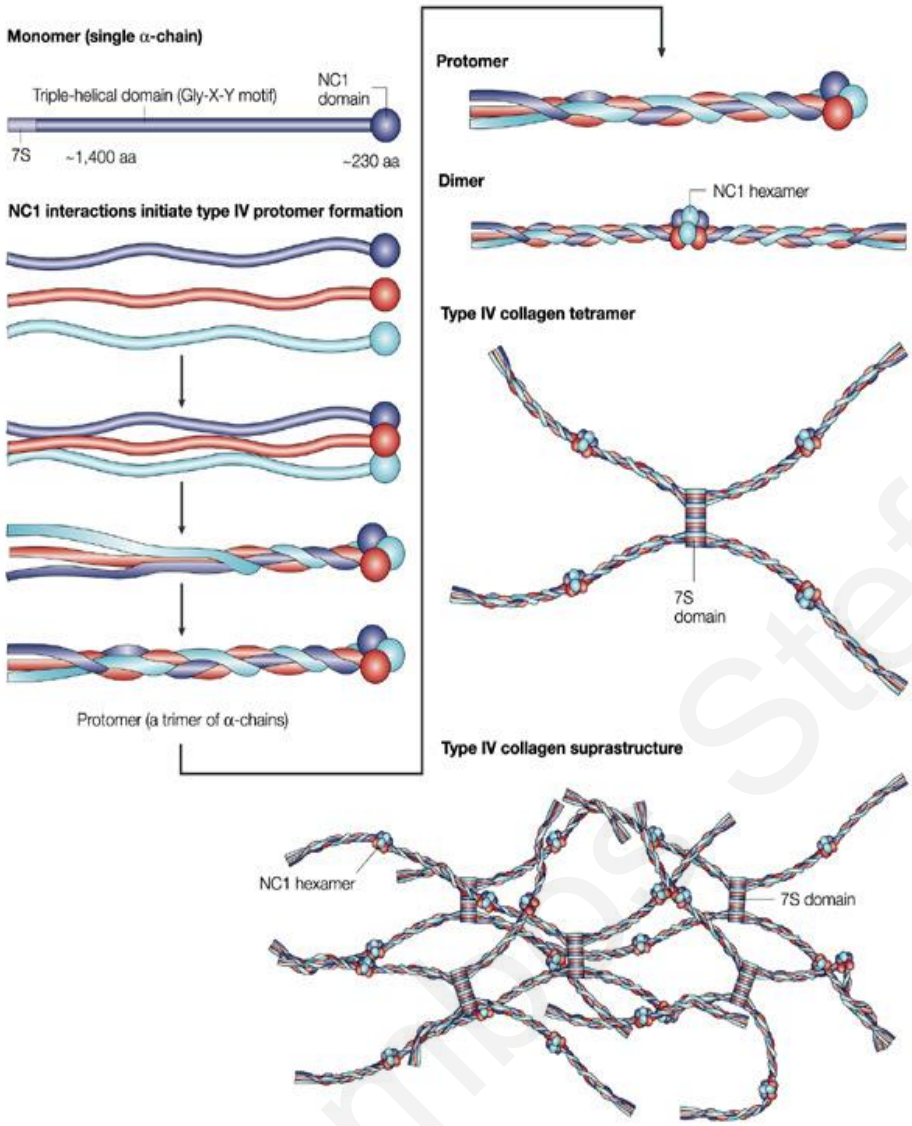

Figure 4: Type IV collagen network formation

Collagen IV helical heterotrimers (protomers) are synthesized and modified in the endoplasmic reticulum (ER). Protomers are secreted into the extracellular matrix where they self-associate via the interaction of their carboxy-terminal NC1 domain (covalent and noncovalent interactions), forming collagen dimers or via their glycosylated amino-terminal 7S domain (noncovalent interactions) promoting the establishment of tetramers (Cosgrove et al., 1996a). Both dimers and tetramers are considered to be the nucleus of the type IV collagen superstructure, providing an interacting scaffold for the ECM components (Kalluri, 2003).

by short non-collagenous sequences and a 230-residue long carboxy-terminal noncollagenous NC1 domain (Khoshnoodi et al., 2008).

Collagen IV α chains form heterotrimers (protomers) with each other, giving rise to three different types of protomers: α1α1α2, α3α4α5 and α5α5α6 (Hudson et al., 1993). The interruptions detected in the collagenous domain provide molecular flexibility for network formation and create sites for cell-binding or interchain crosslink (Khoshnoodi et al., 2008). Zhou and Reeders (Zhou and Reeders, 1996) reported the existence of variability in the number of interruptions between chains, with the lowest number found in the α1 chain and the highest in the α4 chain *(Table 1)*. The collagen IV helical protomers are synthesized and post-translationally modified. Once α-chains are synthesized and translocated to the endoplasmic reticulum (ER), the NC1 domain acts as the initial direction for the association of the triple-helical molecules. In the ER, co- or post-translational enzymatic modifications, take place, including signal peptide removal, proline and lysine hydroxylation, mannose-rich oligosaccharide addition and disulphide intrachain bonds formation.

Table 1: *Chromosomal localization, number of residues in different domains, number of interruptions in collagenous domain, and total number of cysteine residues for each chain is indicated. (Data adapted from Zhou and Reeders, 1996).*

	α1	**α2**	**α3**	**α4**	**α5**	**α6**
Gene localization on chromosome	13	13	2	2	X	X
Residues after translation	1,669	1,712	1,670	1,690	1,685	1,691
Residues in the mature chain	1,642	1,676	1,652	1,652	1,659	1,670
Residues in the collagenous domain	1,413	1,449	1,410	1,421	1,430	1,417
Residues in the NC1 domain	229	227	232	231	229	228
Interruptions in the collagenous domain	21	23	23	26	22	25
Cysteine residues (NC1 domain)	12	12	12	12	12	12
Cysteine residues (7S+collagenous domain)	8	9	12	20	8	9

Protomers are secreted into the extracellular matrix where they self-associate via the interaction of their carboxy-terminal NC1 domain (covalent and noncovalent interactions), forming collagen dimers or, via their glycosylated amino-terminal 7S domain (noncovalent interactions), promoting the establishment of tetramers (Cosgrove et al., 1996a). Both dimers and tetramers are considered to be the nucleus of the type IV collagen superstructure, as they provide an interacting scaffold for the ECM components *(Figure 4)* (Kalluri, 2003, Khoshnoodi et al., 2008, Suh and Miner, 2013).

During embryogenesis, the α1α1α2 heterotrimer is the main collagen component of the GBM, which is partially replaced by the α3α4α5 heterotrimer during development. This switch to the composition of collagen type IV heterotrimers is assumed to improve the stability of the GBM, since the α1α1α2 heterotrimer is highly susceptible to endoproteolysis (Kalluri et al., 1997). This is probably due to the fact that α3α4α5 heterotrimer contains more cysteine molecules, allowing collagen to be further cross-linked compared to the α1α1α2 heterotrimer (Tryggvason and Patrakka, 2006). Moreover, the GBM collagen α3α4α5 heterotrimer is solely produced by the epithelial podocytes, while heterotrimer α1α1α2 has been shown to be secreted by all three cell types found at the glomerulus, namely podocytes, endothelial cells and mesangial cells (Abrahamson et al., 2009).

Interestingly, the α3α4α5 (IV) network is expressed throughout the full thickness of the GBM in the distal tubule basement membrane and the specialized basement membranes of the eye and the cochlea (Cheong et al., 1994, Cosgrove et al., 1996b). On the contrary, the α1α1α2 (IV)-α5α5α6 (IV) network is expressed in the Bowman's capsule (but not in the GBM), in the collecting duct basement membrane and in epidermal and smooth muscle cell basement membrane (Peissel et al., 1995, Borza et al., 2001).

1.2.2.3 Podocytes

The glomerular podocyte is a remarkable, highly specialized cell type, displaying both epithelial and mesenchymal features (Welsh and Saleem, 2010). Podocytes have a restricted capability to multiply, even though recent findings are suggestive of podocyte regeneration resulting from progenitor cells within Bowman's capsule (Cheng and Harris, 2010).

A podocyte consists of a large cell body enclosing the organelles, including the nucleus, a well-developed Golgi system, the endoplasmic reticulum, the lysosomes and many mitochondria. Moreover, the cell gives rise to major, secondary and finely interdigitating foot processes extending toward the capillaries to which they attach through their interactions with the components of the underlying GBM (Patrakka and Tryggvason, 2009, Pavenstadt et al.,

2003). Additionally, a well-defined and described extracellular cell-cell protein complex, known as the slit diaphragm, connects the interdigitating foot processes forming a 40nm wide filtration slit (Pavenstadt et al., 2003, Welsh and Saleem, 2012).

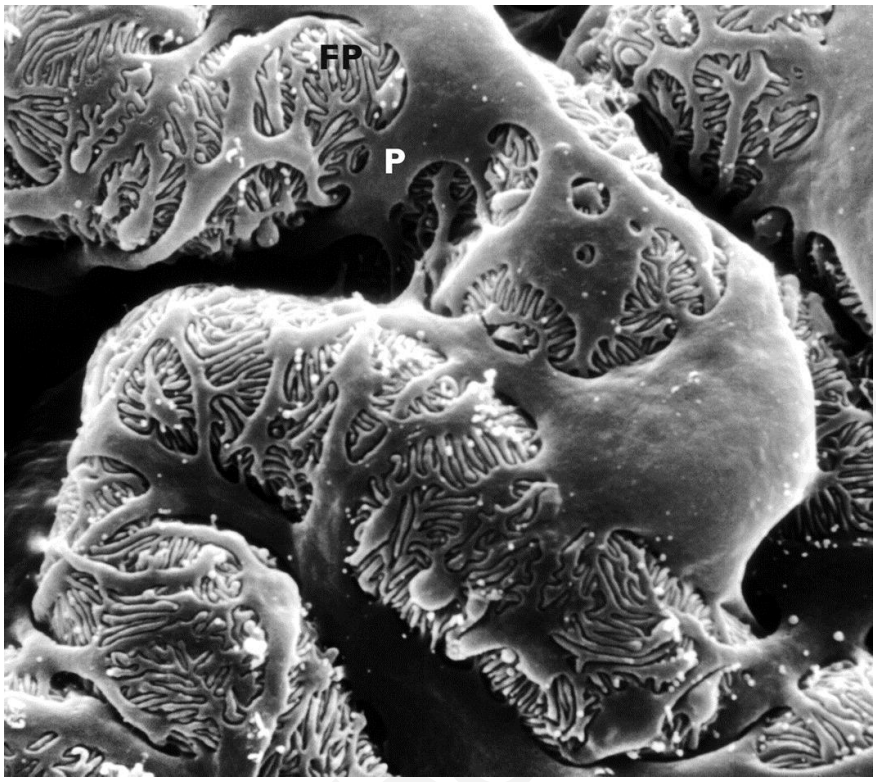

Figure 5: Scanning electron micrograph of normal rat glomerular capillaries.

The glomerular podocyte is a remarkable, highly specialized cell type, which displays both epithelial and mesenchymal features. They have a voluminous cell body, which bulges into the urinary space. Moreover, the cell gives rise to major, secondary and finely interdigitating foot processes extending toward the capillaries to which they attach through their interactions with the components of the underlying GBM. The figure above shows the urinary side of the capillary wall, which is covered by the highly branched podocytes (Pavenstadt et al., 2003).

These cells are polarized, as they have a luminal and an apical or basal cell membrane and the foot processes are bridged by the slit diaphragm. The luminal membrane and the slit diaphragm are covered with a thick coat, which is rich in sialoglycoproteins, including podocalyxin and podoendin, giving to the podocyte surface a highly negative charge. The basal membrane, which covers the soles of the foot processes, mediates the affixation to the GBM. More recently, Salmon and his colleagues proposed the existence of an additional

layer contributing to the structure of the GFB, named the subpodocyte space (SPS), which is positioned between the podocyte cell body and the GBM (*Figure 5)* (Salmon et al., 2009). Additionally, podocytes are characterized by a complex cytoskeleton, which controls the shape and processes of these cells. More specifically, the cell body as well as the primary and secondary foot processes contain microtubules and intermediate filaments (vimentin, and desmin) forming a dynamic cytoskeletal network, while foot processes contain long actin fibre bundles (Welsh and Saleem, 2012, Pavenstadt et al., 2003).

Modern molecular and genetic techniques have progressively extended our knowledge regarding the components and functions of the podocyte and its role in congenital nephrotic syndrome. Also, the establishment of human and rodent podocyte cell lines in addition to the recent identification in Drosophila melanogaster of podocyte-like cells, has enabled the study of podocyte biology *in vivo* and *in vitro* (Cheng and Harris, 2010).

1.2.2.3.1 Slit diaphragm

The slit diaphragm (SD) is a unique intercellular cell-cell protein complex, containing tight junction, adherens junction and neuronal adhesion molecules (Reeves et al., 1978). It is a remarkably highly conserved structure between species, participating either in the development or in the functional integrity of different tissues (Kramer-Zucker et al., 2005).

The glomerular SD is formed during metanephric development and is a well-organized, zipper-like substructure, spanning roughly 40nm between the interdigitating foot processes of neighbouring podocytes. It is proposed to be a major, if not the most important element, of the glomerular filtration barrier (*Figure 6)* (Johnstone and Holzman, 2006).

The first image of the slit diaphragm was taken in 1955 by Yamada (Yamada, 1955), while in the 1970s, Karnovsky and colleagues described for the first time the structure of this multiprotein complex (Rodewald and Karnovsky, 1974). Since then, a considerable number of studies have identified numerous genes whose mutations are causative for nephrotic syndrome, while their products are located either in the podocyte or directly within the SD. This effort contributed to the understanding of the molecular structure of the SD and to the identification of new proteins localized at the SD (Grahammer et al., 2013), including nephrin, nephrin-like proteins Neph1-3, podocin, Fat1, VE-cadherin, P-cadherin, CD2-associated protein (CD2AP) and transient receptor potential cation channel 6 (TRPC6) (Benzing, 2004, Grahammer et al., 2013, Holthofer, 2007).

Accumulating evidence demonstrates the expression of a number of signalling receptors (receptor tyrosin kinases-RTKs, G-protein coupled receptors-GPCRs and nuclear receptors),

emphasizing the importance of the signalling properties of the SD, which are critical for both podocyte function and glomerular filter viability and integrity (Benzing, 2004). Specifically, different extracellular signalling events activate this multiprotein complex of the plasma membrane, triggering the activation of transmembrane receptors, which control several pathways involved in the regulation of podocyte biology (Reiser et al., 2014, Patrakka and Tryggvason, 2007, Aaltonen and Holthofer, 2007).

A great example of slit diaphragm signalling is the phosphorylation of tyrosine residues of the intracellular domain of nephrin, which leads to the recruitment and activation of various signalling adaptors and thus controlling important functions such as endocytosis, actin remodelling and cell survival. Some of these proteins are the Nck adaptor proteins, which are associated with the regulation of actin dynamics (Jones et al., 2006, Verma et al., 2006) and CD2AP, which acts as linker between nephrin and actin-modifying proteins (Hutchings et al., 2003). CD2AP also recruits p85, which facilitates the nephrin-induced AKT activity leading to the inhibition of podocyte apoptosis (Huber et al., 2003a).

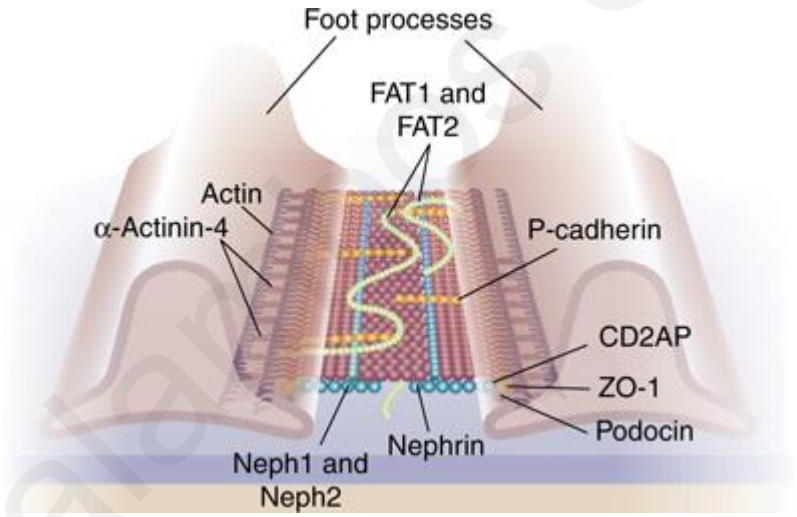

Figure 6: The glomerular slit diaphragm

The slit diaphragm (SD) is a unique intercellular cell-cell protein complex, containing tight junction, adherens junction and neuronal adhesion molecules. It is a remarkably highly conserved structure among different species, participating either in the development or in the functional integrity of different tissues (Pollak, 2009).

1.2.2.3.1.1 Nephrin

Nephrin was the first slit-diaphragm protein to be discovered (Kestila et al., 1998) and is a member of the immunoglobulin (Ig) superfamily of cell adhesion molecules. It was originally

found in Finnish patients diagnosed with congenital nephrosis (OMIM #256300) characterized by prenatal onset of massive proteinuria and nephrosis soon after birth (Hallman et al., 1967). Since then, researchers have demonstrated the importance of this molecule in glomerular filtration, even though additional information is needed to expand the knowledge on nephrin's exact properties (Li et al., 2013).

Nephrin is a transmembrane glycoprotein (~185-200 kDa) consisting of eight IgG-like domains shown to have nine N-glycosylation sites (Khoshnoodi et al., 2007), a single fibronectin type-3 motif and a short cytoplasmic domain with several phosphorylation sites that are modified by tyrosine kinases, including Fyn, Yes, Tec and PI3K (*Figure 7)* (Verma et al., 2003, Huber et al., 2003a, Drozdova et al., 2013).

Among human podocytopathies described, mutations in the *NPHS1* gene give rise to the earliest and most severe clinical phenotype observed, demonstrating the crucial role of this protein for intact filtration (Welsh and Saleem, 2010). Likewise, nephrin appears to be the first podocyte protein to be altered or down-regulated at the very first stages of most of proteinuric diseases compared to other podocyte proteins, such as podocin (Li et al., 2013). In addition, studies on rodents demonstrated that a lack of nephrin results in foot process effacement and absence of the slit diaphragm, while other studies have shown that missense mutations in the *NPHS1* gene lead to misfolding of the protein causing defective trafficking within the podocyte (Liu et al., 2001). More recently, it has been revealed that the misfolded nephrin mutants have an enhanced association with the endoplasmic reticulum (ER) chaperone calnexin, causing accumulation of the protein in the ER and thus leading to the induction of the unfolded protein response pathway (UPR) (Drozdova et al., 2013).

Nevertheless, in a recently published study, the authors surprisingly demonstrated that birds and reptiles do not possess any orthologue of *NPHS1* and *NEPH3* even though they form a properly functioning slit diaphragm. This finding clearly challenges our perception of the slit diaphragm, which has been considered as a nephrin-based structure for over a decade (Volker et al., 2012, Miner, 2012b).

Nephrin is the key regulator of podocyte intracellular signalling, controlling the activation of several pathways including the mitogen-activated protein (MAP) kinase and phosphoinositide 3-OH kinase-PKB pathway. Additionally, new findings demonstrate that upon phosphorylation, the intracellular domain of nephrin can act as a binding site for proteins containing Src homology 2 (SH2) domains, such us phosphatidylinositol-3-OH kinase and the Src kinase family member Fyn (Welsh and Saleem, 2010). Moreover, there is evidence

Table 2: *Known direct protein interactions of nephrin and postulated functional consequences of those interactions.*

Protein	Nephrin-binding site	Function
Podocin	C-terminal binding. Binding site identified as 1183-1208. Phosphorylated tyrosine 1193 increases binding	Regulation of nephrin trafficking. Stimulation of nephrin signalling.
CD2AP	Binding requires last 65 c-terminal amino acids of nephrin	Regulation of actin dynamics. Stimulation of nephrin signalling
Nck	Phosphorylated tyrosine 1176, 1193 and 1217	Regulation of actin dynamics
PI3 kinase	Phosphorylated tyrosine 1138	Regulation of actin dynamics. Inhibition of apoptosis
Phospholipase Cγ I	Phosphorylated tyrosine 1193	Regulation of actin dynamics. Ca^{2+} signaling
β-arrestin	C-terminal binding. Binding site identified as 1120-1125 (TGERDT). 1177-1208 has regulatory function for binding. Phosphorylated tyrosin 1193 inhibits binding	Induction of nephrin endocytosis. Inhibition of nephrin signaling
Atypical protein kinase C	C-terminal portion (1057-1241)	Regulation of podocyte cell polarity. Inhibition of NF-κB activity
IQGAP1	Intracellular domain	Effector protein of small GTPases RacI and Cdc42. Putative regulator of cell-cell adherens junctions
VAMP2	C-terminal portion (1057-1241)	Regulation of podocyte glucose homeostasis

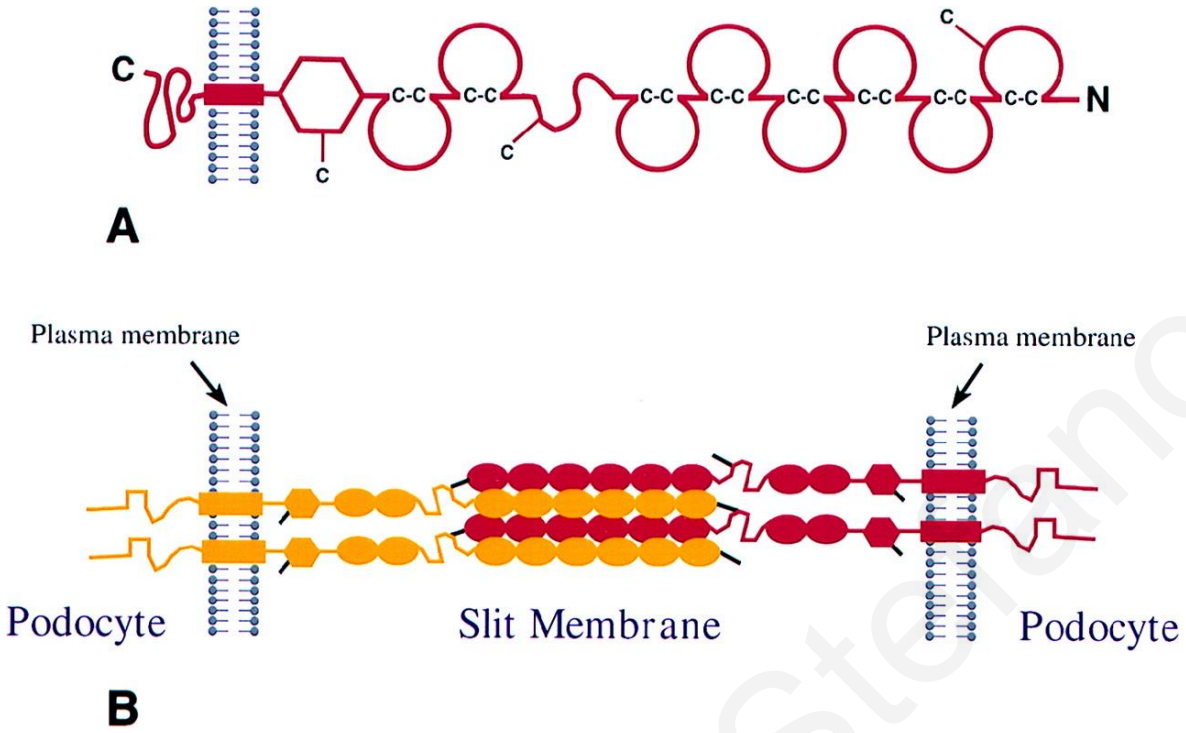

Figure 7: Hypothetical model of nephrin assembly to form the isoporous filter of the podocyte slit diaphragm

(A) Schematic overview of nephrin. The Ig repeats are presented by incomplete circles connected by disulfide bridges (C-C) (B) Possible mode of interdigitating association of four nephrin molecules in the slit between two-foot processes (Ruotsalainen et al., 1999).

that nephrin is localized in lipid rafts on the plasma membrane with the help of podocin (Huber et al., 2003b). In addition, Neph proteins support nephrin molecules in a *cis* configuration and both nephrin and Neph 1-3 seem to be involved in signalling events from the urinary space to the podocyte cytosol. Recently, mechanisms such as ubiquitination and phosphorylation have been shown to participate in regulating nephrin endocytosis and degradation (Godel et al., 2013).

Regarding the interactions of nephrin, cellular studies have shown that nephrin molecules interact in trans configuration with each other and, probably, overlap in the middle of the gap to form a dense midline, giving the slit diaphragm its zipper-like appearance (Grahammer et al., 2013, Heikkila et al., 2011). Moreover, pull-down assays have presented evidence that the cytoplasmic domain of nephrin interacts with scaffolding proteins such as membrane-associated guanylate kinase inverted 2/synaptic scaffolding molecule (MAGI-2/S-SCAM), IQ motif-containing GTPase-activating protein 1 (IQGAP1), calcium/calmodulin-dependent serine protein kinase (CASK), α-actinin, αII spectrin and βII spectrin (Lehtonen et al., 2005).

Additionally, co-immunoprecipitation assays in rat glomeruli have demonstrated that nephrin, under normal conditions, interacts with the tight-junction proteins JAM-A, occludin and cingulin, a fact that clearly indicates the uniqueness of the slit diaphragm (Fukasawa et al., 2009). Identified protein interactors of nephrin are described in *Table 2*.

1.2.2.3.1.2 Podocin

Podocin is a 42 kDa (383aa) hairpin-like membrane-attached protein of the stomatin family *(Figure 8)*. It is exclusively expressed in the glomerular podocytes, although a weak expression of podocin's RNA was detected in the adult testis Sertoli cells, fetal heart and fetal liver (Godel et al., 2013, Boute et al., 2000). It was first described by the Antignac group in 2000, who mapped the *NPHS2* gene in patients with steroid-resistant idiopathic nephrotic syndrome (SRNS). Since then, an important number of studies have contributed significantly to the understanding of the structure and function of this molecule and its involvement in different kidney diseases (Boute et al., 2000, Benzing, 2004).

In the renal glomerulus, podocin is exclusively localized at the cytoplasmic face of the slit diaphragm and it is predicted to form a hairpin structure with a short amino terminal tail, a transmembrane region and a longer carboxy terminal domain which regulates plasma membrane localization and internalization (Godel et al., 2013). Both domains reside in the cytoplasm and interact with a number of proteins localized at the slit diaphragm, including podocin itself, nephrin, CD2AP, Neph1-3 and TRPC6. Interestingly, the interaction of podocin with CD2AP and TRPC6 emphasizes the important role of this molecule, linking the slit diaphragm with the podocyte cytoskeleton (Huber et al., 2003b, Roselli et al., 2004b, Schwarz et al., 2001).

Moreover, podocin has been shown to be vital for the localization and function of nephrin, as the association of the carboxy terminal domain of podocin with specialized lipid raft microdomains of the plasma membrane is a prerequisite for the recruitment of nephrin into rafts (Huber et al., 2003b, Nishibori et al., 2004). Additionally, the Huber group demonstrated that podocin cholesterol-binding regulates the activity of the TRPC6 channel (Huber et al., 2006), while Roselli et al. showed that podocin is targeted at the plasma membrane via the classical exocytic pathway (Roselli et al., 2004b).

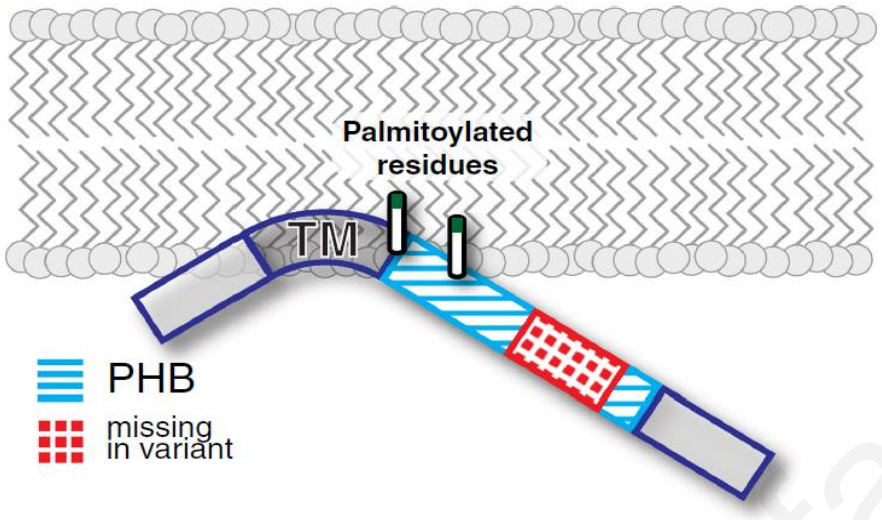

Figure 8: Schematic overview of the podocin short isoform.

Schematic drawing of podocin demonstrating the PHB domain missing in the short isoform (Volker et al., 2013).

More recently, Volker et al. identified an additional short isoform of podocin lacking part of the PHB domain, which is essential for the binding of podocin to nephrin and Neph proteins, as well as for the recruitment of cholesterol to the plasma membrane lipid bilayer and thus enabling lipid raft formation (Volker et al., 2013, Huber et al., 2003b). Furthermore, podocin knockout mice have been shown to die within the first weeks of life because of kidney failure, which proves the importance of this protein for the integrity and function of the glomerular filter (Roselli et al., 2004a).

Genetic studies have revealed a considerable number of mutations located in the *NPHS2* gene, causing childhood onset SRNS, focal segmental glomerulosclerosis (FSGS) (Godel et al., 2013, Bouchireb et al., 2014) and adult-onset SRNS (Tsukaguchi et al., 2002). In a recent review, Bouchireb et al. give an exhaustive summary of all *NPHS2* mutations published between October 1999 and September 2012. Interestingly, most of the 126 reported mutations are missense mutations, with *NPHS2*-p.R138Q being the most prevalent mutation in Northern Europe (Bouchireb et al., 2014).

Additionally, in genotype-phenotype correlation reports, children bearing two identified pathogenic mutations showed a lower mean age of onset. Likewise, Weber et al. demonstrated that patients carrying two pathogenic *NPHS2* mutations presented early-onset SRNS, while renal biopsies from compound heterozygotes exhibited altered podocin expression and localization, causing secondary changes in the distribution of nephrin,

CD2AP and α-actinin-4 (Zhang et al., 2004, Weber et al., 2004). Moreover, Ruf et al. found that patients bearing homozygous or compound heterozygous mutations in *NPHS2* exhibit primary steroid resistance with a reduced rate of FSGS recurrence after renal transplant, when compared with patients lacking *NPHS2* mutations (Ruf et al., 2004).

Interestingly, a significant number of additional studies have revealed the association of *NPHS2*-p.R229Q polymorphism with the progression of SRNS, TBMN or CFHR5 nephropathy (Weber et al., 2004, Voskarides et al., 2012, Tonna et al., 2008a), showing that the *NPHS2* gene can act as a modifier gene. According to these findings, *NPHS2*-p.R229Q is found to be insufficient to alone cause a disease, even though it has been suggested that p.R229Q can predispose to proteinuria in the general population (Pereira et al., 2004). However, this variant appears to enhance the progression of renal disease in homozygosity or compound heterozygosity. Recently, Tory et al. presented that the pathogenicity of *NPHS2*-p.R229Q depends on the trans-associated mutation, with disease associated 3' mutations exerting a dominant-negative effect on p.R229Q podocin, but behaving as recessive alleles when associated with wild-type podocin (Tory et al., 2014). Moreover, Ruf et al. and Weber et al. (Ruf et al., 2004, Weber et al., 2004) reported the detection of the *NPHS2*-p.E237Q polymorphism (0.3% in general population) in patients with steroid sensitive nephrotic syndrome (SSNS) or SRNS, which, as stated by the authors, could have a functional defect similar to *NPHS2*-p.R229Q. Interestingly, Weber et al. reported the detection of *NPHS2*-p.E237Q and p.R229Q in patients with sporadic SRNS and recurrence of proteinuria after transplantation. (Tsukaguchi et al., 2002, Tory et al., 2014, Voskarides et al., 2012, Tonna et al., 2008a, Ruf et al., 2004).

Furthermore, functional studies have shown that disease-causing mutations in the *NPHS2* gene could actually alter the function and localization of this protein. For instance, Ohashi et al. found that the *NPHS2*-p.R138Q mutation of podocin has an effect on the localization of this protein, leading to ER retention (Ohashi et al., 2003). Use of chemical chaperones including glycerol, trimerhylamine-N-oxide and DMSO corrected this phenotype by releasing the ER retained R138Q podocin. In a different study, Huber et al. confirmed these findings, by showing that the missense mutations *NPHS2*-p.R138Q and *NPHS2*-p.R138X had an effect on the intracellular trafficking of podocin causing again ER retention (p.R138Q) or reduced association with the lipid rafts (p.R138X) (Huber et al., 2003b). Likewise, Roselli et al. showed that podocin's mutants, which cause ER retention, were associated with earlier onset of SRNS phenotype compared to mutants that were correctly targeted to the plasma membrane (Roselli et al., 2004b). Moreover, Nishibori et al. showed that mutations located at

the proximal C-terminal part of podocin again failed to localize to the plasma membrane, causing additionally altered localization of wild-type nephrin (Nishibori et al., 2004).

Regarding the polymorphism *NPHS2*-p.R229Q, Tsukaguchi et al. using in vitro-translated podocin and purified nephrin, found decreased nephrin binding to the R229Q podocin, whereas Tory et al. showed altered membrane localization of R229Q when co-expressed with *NPHS2*-p.Ala284Val, p.Ala288Thr, p.Arg291Trp, p.Ala297Val or p.Glu310Lys (Tory et al., 2014).

1.2.2.3.1.3 Filtrin

Filtrin (Neph3, Kirrel2, NLG1) is a transmembrane-type I protein, member of the immunoglobulin superfamily and of the SD multiprotein complex. It consists of an extracellular region containing five Ig-like domains highly homologous to human nephrin, an α-helical transmembrane region (23 amino acids) and a cytoplasmic domain (178 amino acids) (*Figure 9)* (Ihalmo et al., 2003).

The human *NEPH3* gene maps on chromosome 19q12.13 adjacent to the *NPHS1* gene and has 15 exons. It possesses a promoter with an activating regulatory region lacking the classic TATA- and CAAT- boxes and contains a GC rich area and two Alu-repeat sequences. Additionally, *NEPH3* transcription was found to be regulated by nuclear factor kappa-B (NF-κB) and specificity protein 1 (Sp1) (Ristola et al., 2009).

Filtrin was, initially, described to have two alternative splicing forms: the α-form, lacking the first Ig-like domain, and a soluble form termed as the β-form (Ihalmo et al., 2003). Sequence comparisons, using pancreas cDNA clones, and Expressed Sequence Tag (EST) sequences have revealed two more alterative splicing mRNAs (Sun et al., 2003).

Various studies, in the past 10 years, have provided novel insights into the interactions, function and localization of filtrin in the kidney (Hartleben et al., 2008). Filtrin has been found to be highly homologous to *Drosophila* RST (irregular chiasm C–roughest) protein, mammalian KIRREL (kin of irregular chiasm C–roughest), Neph1, Neph2 and Nphs1 proteins (Ihalmo et al., 2007), while it is conserved from rodents to primates (Sun et al., 2003), with an exception in *Gallus gallus* (Liu et al., 2001, Volker et al.). Filtrin has been shown to be primarily expressed in the kidney glomerulus, the *β* cells of pancreas (Sun et al., 2003) and the lymph nodes and, similarly to nephrin and Neph1-2 to localize at the SD (Ihalmo et al., 2003).

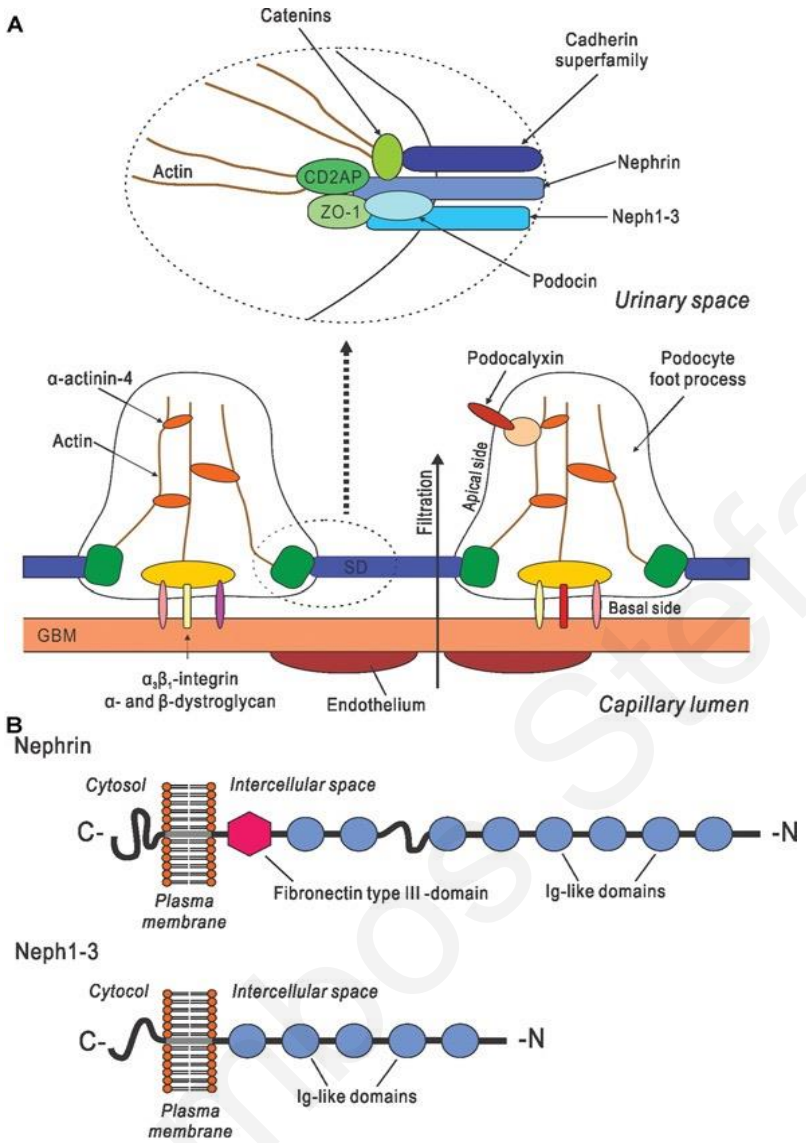

Figure 9: Nephrin and Neph-family proteins are central components of the glomerular filtration barrier

(A) Schematic representation of the glomerular filtration barrier and a simplified presentation of the molecular composition of the podocyte foot processes and the SD, indicating key proteins and protein families. (B) Domain structure of nephrin and Neph1–3. (Ristola and Lehtonen, 2014).

A number of studies have revealed several functional domains of filtrin, located both at the cytoplasmic as well as at the extracellular region. More specifically, filtrin has been found to possess a cell attachment sequence RGD (integrin-recognition site) (Ihalmo et al., 2003), a conserved Grb2 SH2-binding site and a C-terminal PDZK1-binding site (Sellin et al., 2003). A 2003 study has revealed the existence of a proline-rich region located in the intracellular part of the filtrin. Interestingly, proline-rich regions are reported to interact with SH3- and WW- domain containing proteins, such as CD2AP and MAGI-1 (Ihalmo et al., 2003). In

addition, a review paper of Takahashi describes an interaction between the proline-rich region of protein WAVE2 with the SH3-like domain of Myh9 (Takahashi, 2012).

Functional studies revealed that filtrin homo/heterodimerizes with nephrin and Neph1 inducing cell adhesion. The same study revealed an increase of filtrin in nephrin deficient mouse podocytes, indicating the important role of filtrin in the function and morphology of podocytes (Heikkila et al.).

In addition, Sun et al. using a diabetes type I mouse model, showed a decrease in the number of filtrin positive β-cells, while the disease was developing (Sun et al., 2003). Moreover, another group described filtrin and densin as autoantigens in patients with diabetes type 1, showing the existence of autoantibodies against these two proteins (Lehtonen et al., 2005, Rinta-Valkama et al., 2007).

In regards to the contribution of filtrin to nephropathies, Ihalmo et al. demonstrated decreased mRNA levels of *NEPH3* in human glomerular diseases, such as minimal change disease (MCD), hypertensive nephropathy (HT), membranous glomerulonephritis (MGN) and FSGS. Additionally, filtrin was shown to have an altered glomerular distribution in MCD biopsies, a finding suggesting its involvement in the mechanism of proteinuria development (Ihalmo et al., 2007).

Currently, there are no reports on *NEPH3* mutations in humans associated with disease. Nonetheless, recent findings of our group have suggested that *NEPH3* could be acting as a modifier gene by predisposing to a more severe phenotype of TBMN (Voskarides et al, submitted). More specifically, in a set of 96 patients with TBMN categorized as severe or mild according to the presence or not of proteinuria, our group detected a deleterious SNP, causing a substitution of the highly evolutionary conserved valine in position 353 by methionine (*NEPH3*-p.V353M). Genotyping in four additional hematuric cohorts confirmed the association of *NEPH3*-p.V353M with the severity of the phenotype. Additionally, co-immunoprecipitation experiments showed an increase in the interaction of *NEPH3*-p.V353M with *NPHS1*-wt and with *NEPH3*-wt or *NEPH3*-p.V353M itself (Voskarides et al, submitted).

All reports stated above show the important contribution of filtrin in the formation and function of the SD. Therefore, the association of the *NEPH3*-p.V353M variant with a more severe phenotype of nephropathy should be studied in greater detail.

1.2.2.3.1.4 Non-muscle myosin II

Myosins are actin-associated motor proteins mediating muscle contraction, cell division, axoplasmic organelle motions and material transport in cells in an ATP-dependent manner (Noris, 2012).

Myosin superfamily is divided into 24 classes with the most abundant being class II myosins, which, along with actin form the contractile apparatus of cardiac, skeletal and smooth muscle. In addition to muscle myosins, class II includes three ubiquitously expressed non-muscle myosins, NMII-A, NMII-B and NMII-C, whose heavy chains are encoded by the MYH9, MYH10 and MYH14 genes respectively (Vicente-Manzanares et al., 2009, Noris, 2012).

Cellular myosin NM-IIA, in addition to its important role in cytoskeleton reorganization, focal contacts formation and lamellipodia retraction, also appears to play an important role in protein trafficking by acting as a motor protein. Rey at al., using a proteomic approach, proved the interaction and co-localization of NMII-A with the C-terminus of the chemokine receptor CXCR4 in T-lympocytes (Rey et al., 2002). Likewise, Huang et al. revealed that NM-IIA could act as a physical link between nucleolin and cytoskeleton, thus modulating the translocation of nucleolin from nucleus to the cell surface (Huang et al., 2006). Additionally, NM-IIA has been proven to bind to WAVE2, a member of WASP/WAVE family of actin cytoskeletal regulatory proteins. The binding of NM-IIA to WAVE2 is suggested to occur through the interaction between the SH3-like domain of NM-IIA and the proline-rich region of WAVE2 (Takahashi, 2012).

Similar to muscle myosin II, non-muscle myosin II molecules consist of three pairs of peptides: two heavy chains of 230 kDa, two 20 kDa regulatory light chains (RLCs), that regulate NMII activity, and two 17 kDa essential light chains (ELCs) that stabilize the heavy chain architecture *(Figure 10)* (Vicente-Manzanares et al., 2009).

In the kidney, NMII-A is the most widely expressed non-muscle myosin, localized in podocytes as well as in mesangial, tubular, endothelial and parietal epithelial cells (Noris, 2012, Hays et al., 2014). Knockout of *MYH9* in mice has been shown to be lethal (Conti et al., 2004), while knockdown of NM-IIA in zebrafish glomerulus resulted in malformation of the glomerular capillary tuft, characterized by few and dilated capillaries in pronephros. Additionally, endothelial cells of zNM-IIA morphants failed to develop fenestrations, whereas GBM appeared to be non-uniformly thickened (Muller et al., 2011). Interestingly, knockdown of NM-IIA did not compromise the formation of foot processes or slit diaphragms, even though recent findings demonstrated that NMHC-IIA knockdown in

podocytes caused smaller body size and lack of stress fibers, which are typical of differentiation (Hays et al., 2014).

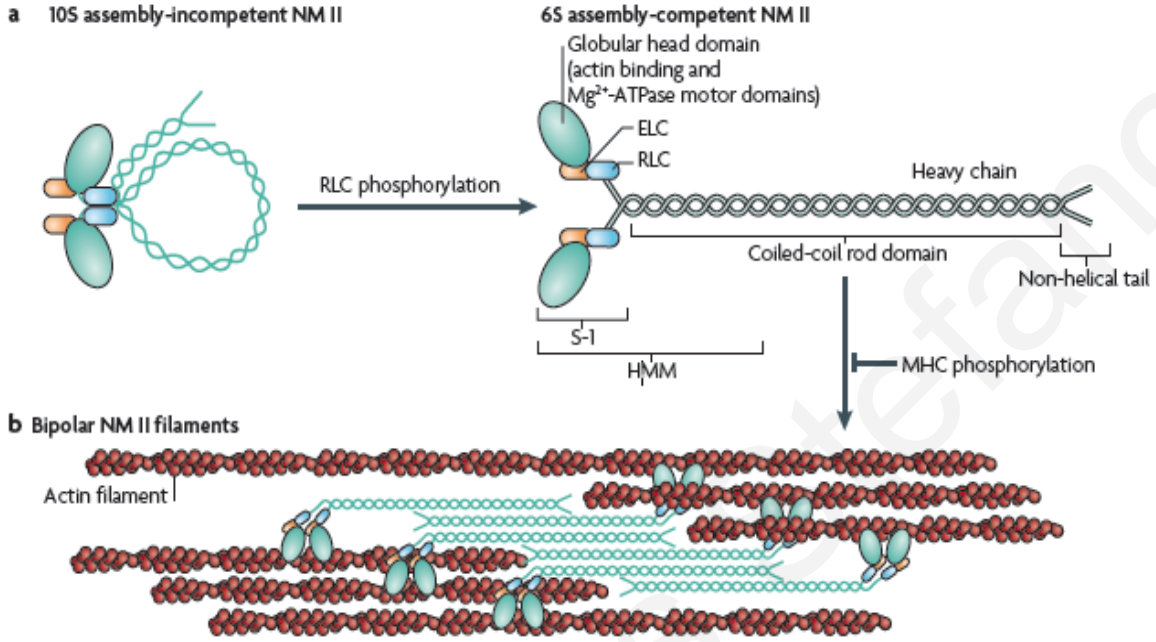

Figure 10: Domain structure of NM II

A. Schematic representation of the subunit and domain structure of non-muscle myosin II (NM II), forming a dimer through interactions among the α-helical coiled-coil rod domains. The actin-binding regions and enzymatic Mg2+-ATPase motor domains are located on the globular head domain. Both essential light chains (ELCs) and regulatory light chains (RLCs) bind to the heavy chains at the lever arms that link the head and rod domains. In the absence of RLC phosphorylation, NM II forms a compact molecule, 10S competent form (left), which is incapable to associate with other NM II dimers. Upon RLC phosphorylation, the structure unfolds and becomes an assembly-competent form (6S). The motor and neck domain is contained at the S-1 of NM II, while heavy meromyosin (HMM) is the fragment which includes the motor domain, neck and enough of the rod to cause dimerization. B. It represents the assembling of NM II molecules into bipolar filaments, which bind to actin through their head domains. ATPase activity of the head allows conformational changes that move actin filaments in an anti-parallel manner (Vicente-Manzanares et al., 2009).

A number of several mutations (missense, nonsense and deletions) in *MYH9* have been reported as the cause of a set of overlapping autosomal-dominant syndromes, so-called

MYH9-related diseases, including May-Hegglein anomaly, Fechtner syndrome, Sebastian syndrome, Epstein syndrome and isolated sensorineural deafness. All these syndromes are characterized with macrothrombocytopenia, associated with cataracts, sensorineural deafness, granulocyte inclusions and glomerular injury (Epstein and Fechtner syndromes) (Muller et al., 2011, Kopp, 2010). More recently, multiple *MYH9* SNPs were recessively associated with FSGS and hypertensive end-stage kidney disease (ESKD) among African Americans (Kopp et al., 2008, Kao et al., 2008), even though an independent study in the same population discovered an association with the *APOL1* gene, located contiguous to the *MYH9* gene (Genovese et al., 2010). Our group demonstrated the association of *MYH9* variant rs11089788 with complement factor H related protein 5 (*CFHR5*) nephropathy and familial hematuria (FH) (Voskarides et al., 2013).

Glomerular findings from renal biopsies obtained from patients with autosomal dominant *MYH9* disorders, included mesangial proliferation, segmental and global glomerulosclerosis, GBM thickening, lamellation and foot process effacement. Biopsies showing segmental glomerulosclerosis could be attributed to a nonspecific response to mesangial proliferation or, alternatively, to a manifestation of podocyte injury since podocyte foot process effacement was present in some cases (Sekine et al., 2010, Alhindawi and Al-Jbour, 2009, Epstein et al., 1972, Ghiggeri et al., 2003, Moxey-Mims et al., 1999, Naito et al., 1997, Peterson et al., 1985, Turi et al., 1992, Yap et al., 2009, Clare et al., 1979). Interestingly, GBM abnormalities are similar to Alport's syndrome findings, something which suggests that NM-IIA could be engaged in the cellular processes by which podocytes organize GBM assembly and remodeling (Kopp, 2010).

Despite all the evidence implicating NM-IIA in podocytopathies, the function of this protein in podocytes remains unknown.

1.3 Glomerular basement membrane diseases

1.3.1 Alport syndrome

Alport syndrome is a hereditary glomerulopathy, originally described in 1927 by Arthur C. Alport, caused by mutations affecting the collagen IV proteins localized in the GBM (Alport, 1927). AS is a rare disease, with a prevalence of 1/10000 for X-linked AS (XLAS) and 1/50000 for autosomal recessive AS (ARAS) (Hertz et al., 2012).

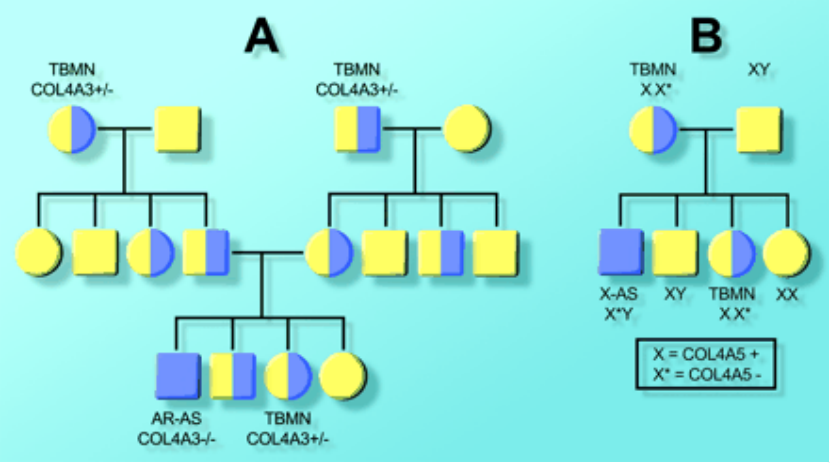

Figure 11: Illustration of possible modes of inheritance for autosomal and X-linked forms of TBMN and Alport syndrome

(A) Illustration of TBMN and autosomal recessive AS inheritance in two families with a mutation in COL4A3. Half-shaded symbols represent TBMN patients and fully shaded represent AS patients. (B) X-linked inheritance of AS and TBMN. Half-shaded symbols represent heterozygosity and TBMN in females while fully shaded symbols represent AS in males (Tryggvason and Patrakka, 2006).

To some extent, the phenotype severity of Alport syndrome depends on the nature and the location of the mutation. Clinical presentation includes hematuria, progressive nephritis with proteinuria and declining renal function, which inevitably, leads to end-stage renal disease (Demosthenous et al., 2012, Ciccarese et al., 2001, Fallerini et al., 2014, Jais et al., 2000, Heidet et al., 2001, Jais et al., 2003). Additionally, patients diagnosed with Alport syndrome, frequently develop sensorineural hearing loss and/or ocular abnormalities (anterior lenticonus, macular or peripheral flecks) (Jais et al., 2000, Jais et al., 2003). In a number of affected families, a contiguous gene syndrome that includes the deletion of *COL4A5* and part of *COL4A6*, there is leiomyomatosis of the esophagus and tracheobronchial tree (Antignac et al., 1992, Zhou et al., 1993).

Three different modes of AS inheritance are currently known, including the X-linked Alport syndrome (XLAS), caused by mutations in the *COL4A5* gene (~80-85% of patients), and the autosomal recessive syndrome (ARAS, ~10-15% of patients), resulting from compound heterozygous or homozygous mutations in the *COL4A3* or *COL4A4* genes. Additionally, several research groups have identified Alport syndrome cases on the background of heterozygous mutations in the *COL4A3* or *COL4A4* genes, providing evidence for the existence of a more rare form of autosomal dominant AS (ADAS, ~1% of patients) (*Figure*

11) (Lin et al., 2014b, Crockett et al., 2010, Kruegel et al., 2013, Kashtan, 2005a, van der Loop et al., 2000, Marcocci et al., 2009, Ciccarese et al., 2001).

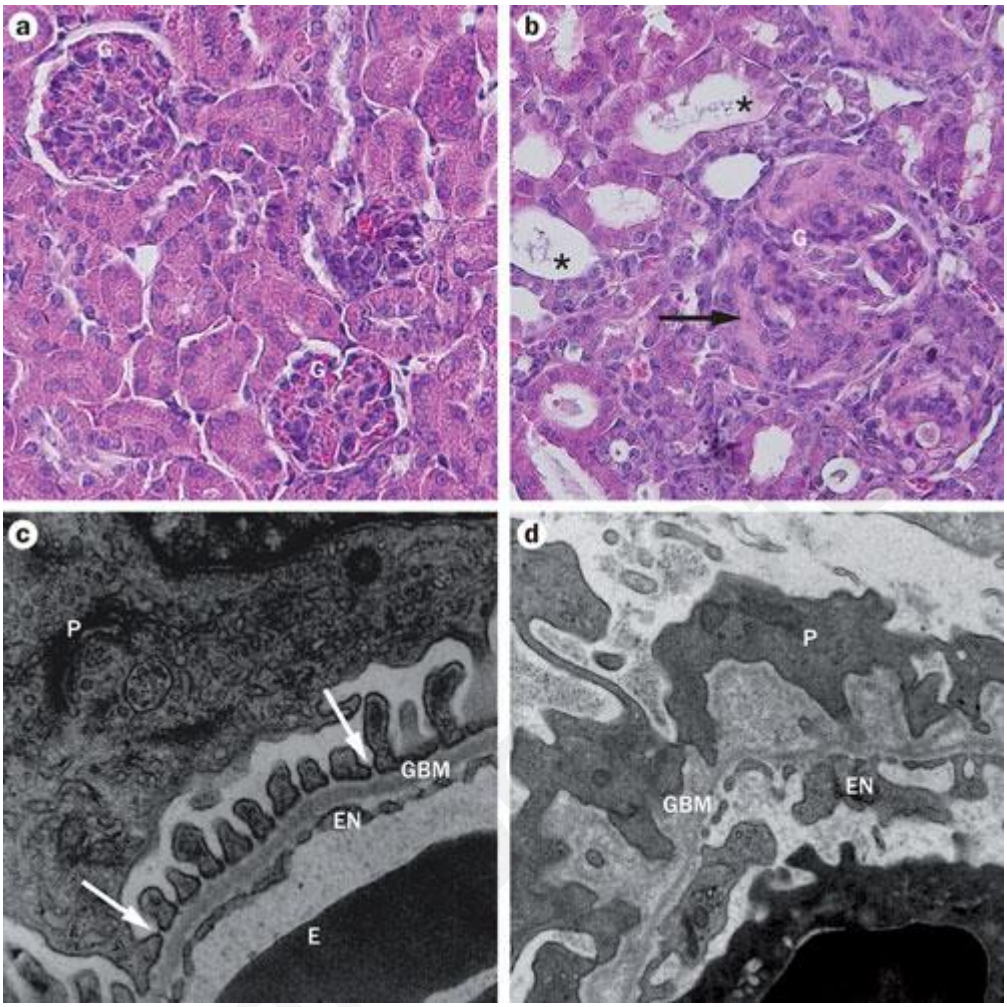

Figure 12: Ultrastructural nature of the GBM in Alport syndrome

(A) Light microscopy images of kidneys from 9-week-old normal mice. (B) Light microscopy images of kidneys from 9-week-old COL4A3$^{-/-}$ mice. Black arrows indicate focal segmental glomerulosclerosis and asterisks enlarged and partially destroyed tubuli. (C) Electron microscopy images of glomeruli from 9-week-old normal mice demonstrating normal GBM, slit diaphragms and fenestrated endothelium. White arrows demonstrate a normal GBM, podocytes with foot processes and slit diaphragms. (D) Electron microscopy of glomeruli from 9-week-old COL4A3$^{-/-}$ mice showing typical wave-like thickening and splitting of the GBM and podocyte effacement (Kruegel et al., 2013).

More recent findings are presenting evidence of digenic inheritance in AS, caused by two pathogenic mutations in two different genes. In the author's words, "segregation analysis revealed three possible digenic segregation models; (i) autosomal inheritance with mutations on different chromosomes, (ii) autosomal inheritance with mutations on the same chromosome, resembling dominant inheritance and (iii) unlinked autosomal and X-linked inheritance, with a peculiar segregation" (Mencarelli et al., 2015).

The XLAS represents the leading model of inheritance of AS caused by different types of mutations. Today 771 *COL4A5* (Crockett et al., 2010) AS mutations have been identified worldwide and an association has been attempted between the type and side of the underlying mutation and the resulting phenotype (Jais et al., 2003, Jais et al., 2000, Gross et al., 2002, Bekheirnia et al., 2010, Tsiakkis et al., 2012). The course of the disease is gender dependent, with hemizygous male patients progressing to ESRD more frequently and much earlier than women. Women carriers of the XLAS present with variable penetrance, depending on the exact type of the mutation and the imprinted inactivation of the X chromosome (Demosthenous et al., 2012, Jais et al., 2000). Moreover, male patients hemizygous for mutations in *COL4A5* have similar clinical findings with men and women who are homozygous or compound heterozygous for mutations in *COL4A3* or *COL4A4 (Kruegel et al., 2013).* Patients with heterozygous mutations in *COL4A3* or *COL4A4* present TBMN and exhibit significant phenotypic heterogeneity, with their clinical presentation varying widely between isolated microscopic hematuria and later onset ESRD (Voskarides et al., 2007, Temme et al., 2012).

The most important structural abnormality of the kidney in AS patients is the variable thickening, thinning, splitting and lamellation of the GBM ("basket-weaving" appearance), as it appears in electron microscopy studies. Adjunctive finding is the foot process effacement. The GBM abnormalities found on EM are considered pathognomonic of Alport syndrome. In contrast, light microscopy findings are not disease specific.

In XLAS, most mutations in the α5 gene prevent normal triple-helix formation and secretion, leading in male patients to the absence of the respective collagen IV chains from the GBM and Bowman's capsule. On the contrary, in cases of ARAS, in male and female patients as well, an absence of staining for α3, α4 and α5 chains in the GBM is noted but the α5 staining is still normal in the Bowman's capsule *(Figure 12)* (Deltas et al., 2013b, Nakanishi et al., 1994, Heidet et al., 2000).

In an attempt to understand the molecular mechanisms of Alport syndrome, different groups, using gene-targeting technologies, proceeded in the creation of collagen IV knockout mouse

models, with phenotypes resembling those of AS in humans (*Table 3*). Cosgrove et al. were the first to develop a *COL4α3* knockout mouse model by constructing a gene targeting vector, which was disrupting the exon 5 (reverse orientation) of murine *COL4α3* by inserting the *Neo* cassette. This model exhibited microhematuria and proteinuria and reached ESRD at ~14 weeks of age. In more detail, the current model developed hematuria at the earliest time points measured (2 weeks of age), while proteinuria occurred at the age of ~5 weeks. In addition, serum urea was shown to rise at ~10 weeks of age and continued to increase until death. Transmission electron microscopy analysis revealed the progression of the disease at the ultrastructural level, starting with focal multilamellation and thinning of the GBM, which, at the age of 12-15 weeks, became thick and heavily rarefied. Additionally, analysis of the basement membrane-associated proteins (fibronectin, entactin/nidogen, laminin, and HSPG) showed them to accumulate at the GBM, something that was suggested to play a role in the disease pathogenesis (Cosgrove et al., 1996a).

Table 3: *Mouse models of Alport syndrome*

Gene	**Mutation**	**Ref.**
ARAS		
COL4A3	exon 48	(Cosgrove et al., 1996a)
COL4A3	exon 48-50	(Miner and Sanes, 1996)
COL4A3-COL4A4	COL4A3 exon 1-2/COL4A4 exon 1-12	(Lu et al., 1999)
XLAS		
COL4A5	exon 1	(Rheault et al., 2004)

Later in the same year, Miner and Sanes announced the generation of a second *COL4α3* knockout mouse model, with the deletion of three exons located at the NC1 domain. The model created was characterized by decreased glomerular filtration (causing increase in serum creatinine and urea levels) and increased glomerular permeability (resulting in proteinuria; no hematuria was observed). Additionally, light microscopy revealed glomerulosclerosis and tubular atrophy, whereas electron microscopy displayed a characteristic basket-weave thickening and lamellation of the glomerular basal laminae. Interestingly, immunohistochemical analysis of the kidneys demonstrated absence of collagens α4 (IV) and α5 (IV) from the GBM and increase of collagens α1, 2 (IV),

fibronectin, perlecan and collagen VI. These findings resembled the phenotype of Alport syndrome, confirming the previous results of Cosgrove (Miner and Sanes, 1996).

In addition, insertional mutation of the collagen genes *COL4α3* and *COL4α4* resulted in another mouse model of Alport syndrome, lacking exons one through twelve of *COL4α4*, exons one and two on *COL4α3* and the intergenic promoter region. Routine histopathology and ultrastructural analysis of the kidney revealed morphological abnormalities of the GBM, causing hematuria and proteinuria at the age of two weeks. Additionally, administration of BrdU (5-bromo-2'-deoxyuridine) showed an increased number of proliferating cells, including parietal epithelial cells, endothelial, mesangial and infiltrating inflammatory cells (Lu et al., 1999).

Furthermore, Rheault et al. generated a knock-in mouse model, carrying the nonsense mutation G5X in *COL4α5*. This resulted in the creation of a model where the expression of α5 (IV) chain, was absent in the kidneys of male mutants while in female carriers was mosaic. This resembled the XLAS phenotype, as male mice died at 6 to 34 weeks of age, while female carriers died at 8 to 45 weeks of age. Their death was caused by ESRD. Histopathological findings comprised of capillary loop dilation, capsular adhesion and focal sclerosis. GBM was described with diffuse abnormalities, including lamellation and splitting, while there was evidence of podocytes injury and foot processes effacement, vesiculation and denudation (Rheault et al., 2004).

Table 4: *The efficacy of pharmacological drugs in COL4A3 -/- mice*

Drug	Survival (d)	Efficacy
Vasopeptidase inhibitor	172	(+++)
ACE inhibitor	150	(+++)
ARB	98	(++)
HMG-CoA reductase inhibitor	91	(++)
Drug	Survival (d)	Efficacy
CCR1 inhibitor	86	(+)
TNF-alpha antagonist	81	(+)
Renin inhibitor	78	(+)
Vitamin D analog	75	(+)
Untreated (129SvJ)	71	

Currently, there is no curative treatment for Alport syndrome. ACE inhibitors and AT_1-receptor antagonists are the recommended pharmaceutical agents for delaying the disease progression (Alport Syndrome Research Collaborative)(Gross et al., 2012). Additionally, studies in Alport mouse models have uncovered a number of novel therapies having a positive effect regarding the progression of renal injury (*Table 4*) (Katayama et al., 2014, Gross et al., 2014).

1.3.2 Thin basement membrane nephropathy

Thin basement membrane nephropathy (TBMN), also known as "benign familial hematuria", "thin basement membrane disease", "benign persistent hematuria" and "benign essential hematuria", is the most common cause of glomerular bleeding. It is typically characterized by persistent microscopic hematuria of glomerular origin (dysmorphic urinary red blood cells with irregular shape and size), minimal proteinuria, normal arterial blood pressure and normal renal function. Definite diagnosis of TBMN can be made only by renal biopsy and EM study of the renal tissue, where the diffuse thinning of the glomerular basement membrane, with a width of <200 to 250nm in children and <200nm to 264nm in adults (adjusted for age, gender and technical differences) is demonstrated *(Figure 13)* (Vogler et al., 1987).

TBMN represents the carrier state for autosomal recessive AS and is inherited in an autosomal dominant mode, primarily segregating with the *COL4A3/COL4A4* locus or X-linked segregating with *COL4A5 (Figure 11) (Savige et al., 2003, Buzza et al., 2003, Kashtan, 2005b).*

Genetic analysis of patients diagnosed with TBMN revealed the detection of heterozygous mutations distributed throughout these genes, while a number of mutations detected are identical with mutations found in patients with autosomal recessive or X-linked Alport Syndrome. Interestingly, Pierides et al. reports that X-linked *COL4A5* mutations exhibit a spectrum of phenotypes, ranging from classical AS to TBMN (Pierides et al., 2013, Kaneko et al., 2010, Slajpah et al., 2007). Nevertheless, a number of patients which does not segregate with the *COL4A3, COL4A4* or *COL4A5* genes, is assumed to carry mutations in other unknown genes (Zhang et al., 2007).

TBMN has been reported in all races, including Caucasians, Chinese, Indians and Africans. It is more common in females than in males, while hematuria from TBMN has been reported at all ages. The prevalence of TBMN is difficult to be assessed, however, using approximation from the known frequencies of glomerular hematuria in the population and from the prevalence of autosomal-recessive Alport syndrome and its known relationship with TBMN,

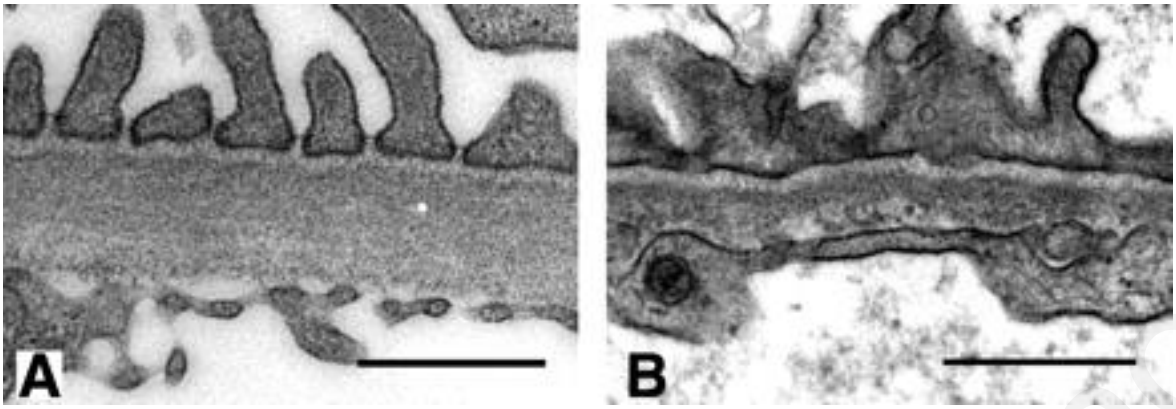

Figure 13: Ultrastructural nature of the GBM in thin basement membrane nephropathy

(A) Glomerular basement membrane of a normal adult male kidney normally located between the fenestrated endothelial cells and the podocytes. (B) The uniformly thinned GBM of a TBMN patient, with endothelial cells and podocytes maintaining normal morphologic features (Tryggvason and Patrakka, 2006).

it is widely accepted that the overall prevalence of TBMN in the population is more than 1% (but <10%). This makes TBMN the commonest inherited renal disease and one of the most prevalent conditions affecting the kidney, after infections, hypertension and stones (Wang and Savige, 2005).

Typically, the prognosis of TBMN is good, something that urges most clinicians to consider it as the mildest end of the spectrum of diseases due to type IV collagen defects of the basement membrane. However, older scarce reports had suggested that occasionally, TBMN could be progressive, leading to impairment of renal function of variable degree. Voskarides et al. (Voskarides et al., 2007) showed that *COL4A3/COL4A4* heterozygous mutation carriers could develop FSGS and progressive loss of renal function. Others have reported cases of heterozygous carriers of *COL4A3/COL4A4* mutations presenting with the pathognomonic EM features of Alport abnormalities of the GBM and progressive renal damage with or without the characteristic extrarenal manifestations, labelling these cases as autosomal dominant Alport syndrome (ADAS).

Interestingly, in 2007, Voskarides et al. (Voskarides et al., 2007) presented the largest series of patients with founder mutations in either the *COL4A3* or the *COL4A4*, where more than 50% of these TBMN patients developed clinically significant proteinuria and chronic renal failure (CRF) due to late-onset FSGS, manifesting after the age of 30 years. Equally

importantly, in a Greek-Cypriot cohort of 230 patients, about 30% of the patients reached ESKD by the age of 70 years (Pierides et al., 2009, Papazachariou et al., 2014, Deltas et al., 2013b, Deltas et al., 2012). These findings were more recently confirmed by two different independent studies, which searched for mutation in *COL4A3 or COL4A4* genes, using the latest technology of Next Generation Sequencing (NHS). The first study describes the discovery of rare variants in *COL4A3* or *COL4A4* in 7 out of 70 families (10%) with a diagnosis of FSGS. Interestingly, a compound heterozygote variant was detected in the index family, while the other six families had a single heterozygous variant. These data suggest that mutations in GBM collagen IV may result in FSGS development and that phenotypes induced by mutations in GBM collagen IV genes may phenocopy primary FSGS (Malone et al., 2014). Additionally, a new study of 40 Chinese families with familial FSGS and 50 cases with sporadic FSGS confirmed the association of FSGS with *COL4A3* mutations (12.5% of familial FSGS and 2% of sporadic FSGS) (Xie et al., 2014).

The cause of this adverse development is not known. Many support the idea that this could be attributed to the probable co-inheritance of IgA nephropathy or focal segmental glomerulosclerosis and to misdiagnosed IgA disease or X-linked Alport. More recently though, environmental and genetic factors have been invoked in explaining the progressive nature of TBMN in a subset of patients. As previously mentioned, *NPHS2*-p.R229Q variant was shown to be an indicator for TBMN patients at increased risk of proteinuria and renal impairment (Tonna et al., 2008a, Voskarides et al., 2012).

1.4 Unfolded protein response

The endoplasmic reticulum (ER) is a cellular organelle formed by a network of flattened, membrane-enclosed sacs of tubes, extending from the outer membrane of the nuclear envelope through the cytoplasm of cells. There are two types of ER, rough and smooth, serving as the site for the folding and assembly of nearly all-signaling proteins, as well as for the synthesis of steroids, cholesterol and other lipids (Alberts B, 2002).

One of the principal functions of the ER is to apply a quality control on the proteins it synthesizes, confirming that these components are assembled with high fidelity. Properly folded proteins are then transported to the Golgi complex moving onwards to plasma membrane. However, misfolded proteins, which are considered harmful to the cell, accumulate in the ER causing ER stress. In an effort to decrease the misfolded protein load in the ER, the cell has in place quality control mechanisms, including the unfolded protein

response (UPR) first described in 1988 (Kozutsumi et al., 1988) and ER associated degradation (ERAD) *(Figure 14)* (Meusser et al., 2005).

UPR promotes the ER protein folding capacity by increasing the production of molecular chaperones and attenuates general protein translation to decrease the misfolded protein load in the ER. If the UPR fails to resolve ER stress and restore cell homeostasis, cells will be eliminated by induction of tightly controlled apoptotic cell-death pathways (Walter and Ron, 2011, Schuck et al., 2009).

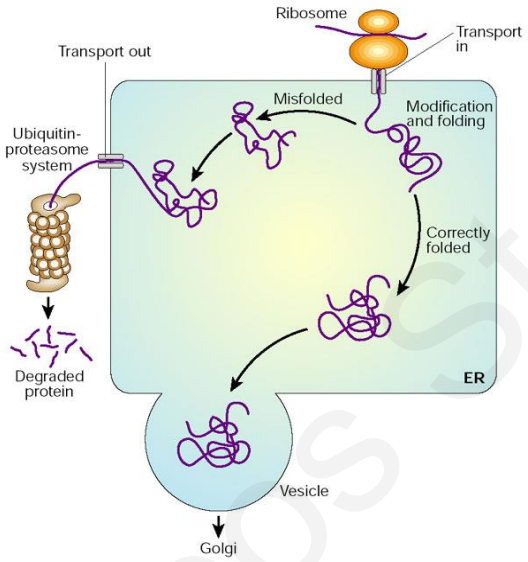

Figure 14: Protein folding

Newly synthesized proteins, fold into their three-dimensional structures with the help of a series of molecular chaperones and folding catalysts. Properly folded proteins are then transferred to the Golgi complex and from there are delivered to the extracellular environment. However, misfolded proteins are identified by a quality-control mechanism and sent along another pathway (the unfolded protein response), in which they are ubiquitinated and then degraded in the cytoplasm by proteasomes (Reynaud, 2010).

Three protein sensors initiate the UPR, including the inositol-requiring protein-1 (IRE1), the activating transcription factor-6 (ATF6) and the protein kinase RNA (PKR)-like ER kinase (PERK) *(Figure 15)*. In non-stressed cells, the three sensors are in an inactive state due to their association with ER chaperone BiP. Upon accumulation of misfolded proteins in the ER or depletion of the ER calcium stores, BiP dissociates from these three receptors, allowing their activation *(Ron and Walter, 2007)*.

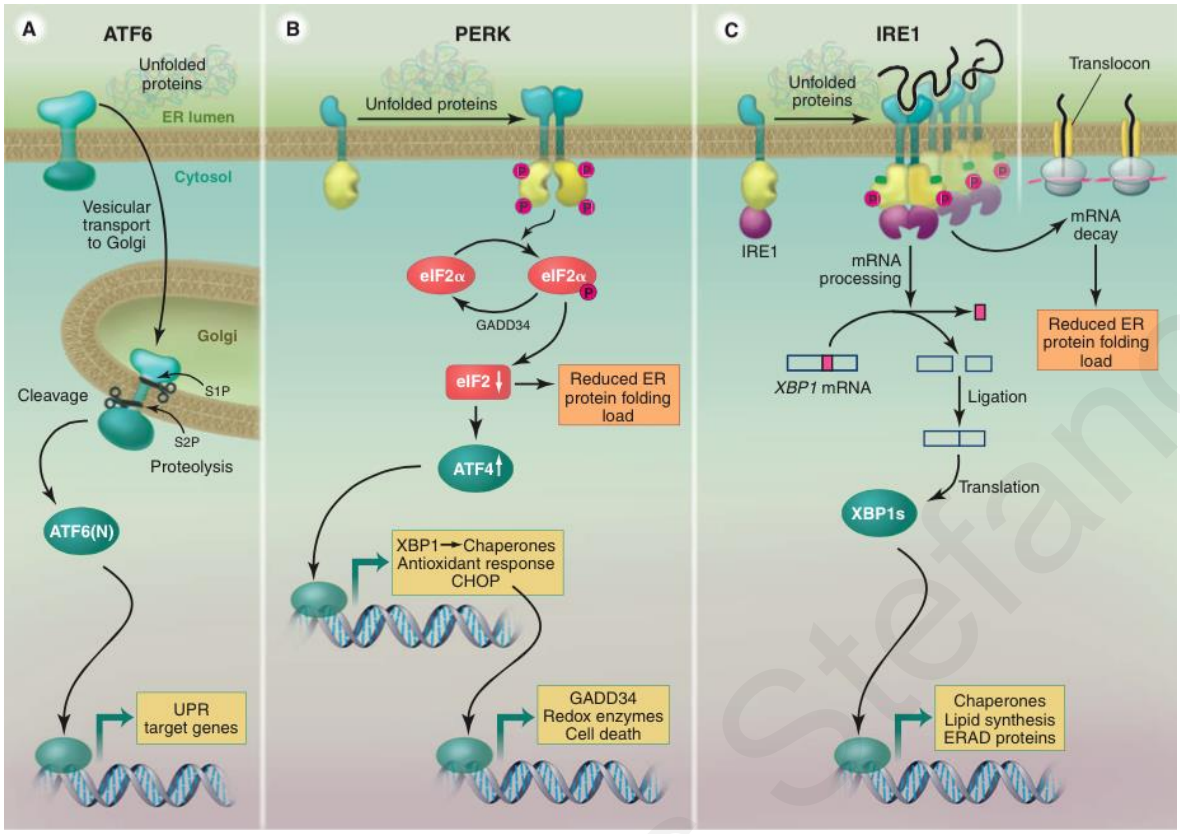

Figure 15: The three branches of the UPR

Three families of signal transducers (ATF6, PERK and IRE1) sense the protein-folding conditions in the ER lumen and transmit that information, resulting in production of bZIP transcription regulators that enter the nucleus to drive transcription of UPR target genes. Each pathway uses a different mechanism of signal transduction: ATF6 by regulated proteolysis, PERK by translational control, and IRE1 by nonconventional mRNA splicing. In addition to the transcriptional responses that largely serve to increase the protein-folding capacity in the ER, both PERK and IRE1 reduce the ER folding load by down-tuning translation and degrading ER-bound mRNAs, respectively (Walter and Ron, 2011)

During ER stress, ATF6 is released from BiP exposing a region containing two Golgi localization signals, GLS1 and GLS2. This event allows the translocation of ATF6 to the Golgi where it is recognized and cleaved by site-1 and site-2 proteases. The cleaved cytosolic fragment, which contains a DNA-binding domain, then migrates to the nucleus to activate transcription of ER chaperones and enzymes that promote protein folding, maturation, secretion and ERAD (Schindler and Schekman, 2009). Additionally, upon release of BiP, IRE1 is activated through autophosphorylation on Ser 724 residue (Hollien and Weissman, 2006). This event allows the activation of IRE1 endoribonuclease activity, causing the precise

endonucleolytic cleavage of X-box-binding-protein-1 (XBP1) mRNA. Following the excision of XBP1 intron, the 5' and 3' mRNA fragments are then ligated by the RTCB (the catalytic subunit of the tRNA ligase complex) and its co-factor archease (Jurkin et al., 2014, Reimold et al., 2001). Ligation of XBP1 mRNA causes a frame shift of the open reading frame enabling translation of spliced XBP1 (XBP1s). The protein product of XBP1s acts as a potent transcription factor, which functions in parallel with ATF6, triggering the transcription of the genes required to restore ER homeostasis such as chaperones or proteins involved in ERAD.

However, IRE1 other than the splicing of XBP1 it can also act by alternative means. In mammals the phosphorylated IRE1 can interact with TRAF2 (tumor necrosis factor receptor TNRF-associated factor-2) activating the JNK signaling while IRE1-TRAF2 complex has also been associated with caspase-12 activation and cell death. Moreover, in Drosophila cell cultures, activated IRE1 has been proven to promote the degradation of mRNAs localized on ER (Ron and Walter, 2007). The third aspect of the UPR involves PERK, which upon release of BiP, homodimerizes and subsequently trans-autophosphorylates. This allows activated PERK protein kinase domain, to phosphorylate the eukaryotic translation initiation factor-2α subunit (eIF2α), resulting in the inhibition of the guanine nucleotide exchange factor eIF2B. Lower levels of active eIF2B result in lower levels of translation initiation, decreasing the protein load on a damaged ER (Walter and Ron, 2011). Interestingly, although BiP is shown to serve as the major regulator of the UPR sensors, more recent studies suggest that IRE1 and probably PERK may bind misfolded proteins directly.

Current information concerning the role of ER stress and UPR in renal pathophysiology is still limited. However a number of studies revealed a link between ER stress, UPR and renal diseases (Cybulsky, 2010). For example, induction of ER stress in glomerular cells has been described in experimental models including the puromycin aminonucleoside nephrosis (PAN) rat model (Cybulsky et al., 2005), the knockin α-actinin-4 p.K256E mouse model (Cybulsky et al., 2009) and the transgenic rat overexpressing megsin (Inagi et al., 2005b). Additionally Inagi et al. reported the upregulation of the ER chaperones (BiP, p-eIF2a and p-PERK) in glomeruli of rats with anti-Thy1 nephritis (Inagi et al., 2005b, Inagi et al., 2008). Also, a cell culture model of proteinuria revealed that overexposure of tubular epithelial cells to albumin can actually lead to an increase in BiP and ORP150 expression, as well as apoptosis (Ohse et al., 2006). Likewise, in podocytes, a number of stressors including tunicamycin (TM), *S*-nitroso-*N*-acetyl-dl-penicillamine (SNAP), complement activation, ROS, palmitate, and thapsigargin have been associated with the induction of the ER stress response (Cybulsky et

al., 2002, Inagi et al., 2005a, Morse et al., 2010, Sieber et al., 2010). Nevertheless, hypoxia and high-glucose conditions did not induce the ER stress response in podocytes (Inagi et al., 2005a, Morse et al., 2010). Interestingly, expression of ER stress markers have been described in human kidney biopsies originating from patients diagnosed with FSGS and membranous nephropathy. Certain missense mutations in nephrin and podocin, as well as underglycosylation of nephrin, result in misfolding and retention in the ER, and eventually ERAD. Drozdova et al. recently proved the accumulation of nephrin mutants in the ER led to enhanced association with the ER chaperone calnexin and impaired glycosylation. This resulted in the activation of ATF6 pathway and in the increase of ER chaperone Grp64 (Drozdova et al., 2013). Similar results were reported by Fan et al. who demonstrated retention of *NPHS2*-p.R168H, resulting in significant up-regulation of ER stress markers Bip/grp78, p-PERK and caspase-12 (Fan et al., 2009).

Interestingly, understanding the various aspects of ER stress will provide an opportunity for developing novel therapeutic strategies for proteinuric diseases as was proven by Ohashi et al. (Ohashi et al., 2003) and Liu et al. (Liu et al., 2004) where both studies provided evidence for pharmacological correction of the mis-localized Nphs2 and Nphs1 defect respectively.

Chapter 2: Evidence for Activation of the Unfolded Protein Response in Collagen IV Nephropathies

2.1 Scientific hypothesis and specific aims

TBMN and AS are progressive collagen IV nephropathies, caused mainly by mutations in the *COL4A3/COL4A4/COL4A5* genes; the exact mechanism by which these mutations exert their deleterious effects remains elusive. In the course of this work, we generated data, which allowed us to hypothesize, that defective trafficking of the *COL4A3* causes a strong intracellular effect on the podocyte. Specific objectives were as follows:

1. *To test the effect on the overexpression of wild-type (wt) and mutant COL4A3 chains (mutation p.G1334E) on various intracellular pathways of the human podocyte.*

2. *To perform a transcriptomic profiling analysis in human podocytes transiently transfected with wt or mutant COL4A3-p.G1334E chain.*

3. *To investigate the expression of predicted markers in vivo, in renal biopsy specimens from patients with a confirmed COL4A3-p.G1334E mutation.*

4. *To generate a knockin mouse model, carrying the Col4a3-p.G1332E mutation (the equivalent of the COL4A3-p.G1334E mutation in patients with AS and TBMN), for a more detailed phenotypic evaluation in a murine model.*

To our knowledge, this is the first mouse model ever generated carrying a missense glycine COL4A3 mutation, which causes AS and TBMN in humans.

2.2 Materials and methods

2.2.1 Plasmid vectors

For the current experiments, a plasmid vector containing the full-length human *COL4A3* cDNA was purchased (Origene). The point mutation *COL4A3*-p.G1334E was inserted in the *wt* sequence of the *COL4A3 cDNA* using a standard site-directed mutagenesis approach (QuikChange Site-Directed Mutagenesis, Stratagene, La Jolla, CA). The desired mutation was designed to be in the middle of the mutagenic primers shown in the table below (*Table 5*). Restriction digestion and DNA sequencing was applied in order to confirm the correct incorporation of the mutation and in order to eliminate the possibility of any nonspecific changes occurring in the sequence. Both vectors were validated for expression of C-terminal fusion of the collagen α3 with the hemagglutinin (HA) tag.

From a great pool of glycine substitution mutations appearing in patients with TBMN, this study was focused on studying the *COL4A3*-p.G1334E mutation, due to its well-known pathogenicity as well as its high prevalence in Cypriot patients with TBMN (Deltas et al., 2012, Voskarides et al., 2007).

Table 5: *Sequences of mutagenic primers for inserting COL4A3-p.G1334E*

	Oligonucleotide name	Sequence	Length
1	COL4A3_G1334E_F	CCATTGGACCTCCAG**A**ACCAATTGG GCCAAAAGG	34
2	COL4A3_G1334E_R	CCTTTTGGCCCAATTGGT**T**CTGGAG GTCCAATGG	34

2.2.2 Cell culture

The AB8/13 undifferentiated podocyte cells (kindly provided by Dr. M. Saleem) were incubated at 33°C at 5% CO_2 and cultured in RPMI medium, supplemented with 10% FBS (Invitrogen, Carlsbad, CA), 1% of 100 U/ml penicillin/streptomycin (Invitrogen), and 1% insulin-transferrin-selenium (Invitrogen). Podocytes were differentiated by thermo-switching at the nonpermissive temperature of 37°C in 5% CO_2 for fourteen days as previously described (Saleem et al., 2002). At 70% confluence, cells were transiently transfected with vectors containing collagen cDNAs, *wt* or mutant, using Lipofectamine 2000 (Invitrogen) and according to manufacturer's instructions. After a 48h incubation, cellular lysates and cellular medium were collected for experiments. In order to improve collagen synthesis and secretion

from transfected podocytes, cells were treated with 50 mg/ml ascorbic acid, 12h prior to protein extraction (Sigma-Aldrich, St. Louis, MO) in serum-free medium.

Transfection efficiency and collagen expression were evaluated with immunofluorescence and qPCR respectively. In all experiments, the empty pCMV6-AC-HA plasmid was used as a control to determine transfection toxicity. Immunofluorescence experiments, using an anti-HA antibody demonstrated routinely a transfection efficiency of around 60%. Likewise, *COL4A3* mRNA expression post-transfection increased 30-fold, compared with nontransfected AB8/13 cells as determined by qPCR (data not shown).

Collagen construct expression was shown to be similar in all transfected cells according to qPCR results measuring collagen mRNA levels, using the primers listed in *Table 6*.

Table 6: *Sequences of primers for exogenous COL4A3 quantification*

	Oligonucleotide name	Sequence	Length
1	*COL4A3*_F	CCAGCTGGATCAGATGGAT	19
2	HA-FLAG-Rev	AGCGTAATCTGGAACATCGTATGGGTA	27

2.2.3 RNA preparation and microarray experimental design

High-throughput microarray profiling was performed for studying the cellular pathways affected by collagen overexpression in podocytes. Total RNA was extracted from podocytes transfected with the pcDNA6-HA-vector or with vectors expressing *COL4A3*-wt or the mutant *COL4A3*-p.G1334E chain. The quality of the isolated RNA was further evaluated, using the 2100 Bioanalyzer (Agilent Technologies, Santa Clara, CA) and the RNA 6000 LabChip kit (Agilent Technologies). High quality total RNA was selected, for obtaining biotin-labelled target cRNA using the GeneChip 39 IVT Express Kit (Affymetrix, Santa Clara, CA). Equal amounts of the labelled and fragmented RNA from V1 (vector only), *wt* (*COL4A3*-wt), and G (*COL4A3*-p.G1334E) were hybridized to the Affymetrix GeneChip Human Genome U133 Plus 2.0 Array, representing approximately 39,000 of the best-characterized human genes. Staining and washes were performed, following the hybridization step, using the GeneChip Fluicids Station 450 robot (Affymetrix) and the GeneChip Hybridization, Wash and Stain Kit (Affymetrix).

The resulting arrays were scanned at 5-mm resolution using the Affymetrix Gene-Chip Scanner 3000 7G. Quality control was performed using the Affymetrix expression Console. The raw microarray data were background corrected, quantile normalized and log2

transformed using the SAS JMP7 Genomics, version 4, package (SAS Institute, Cary, NC). Differential mRNA expression was analysed by one-way ANOVA. A p-value of 0.05 with false discovery rate 10% was considered as the cut off level of significance. These experiments were performed at the University of Mannheim in collaboration with Prof. N. Gretz.

2.2.4 Pathway analysis, gene ontology and clustering

Pathway analysis and gene ontology for the significantly deregulated genes was performed using the KEGG (http://www.genome.jp/kegg/ pathway.html) and the DAVID (http://david.abcc.ncifcrf.gov/) databases. A p value of 0.05 using the Fisher exact test with Bonferroni correction was set as a cut off. A two-way hierarchical clustering and K-means clustering with Euclidean distance was used as a metric, in an effort to group the most deregulated genes. Clustering was performed using Genesis software, version 1.7.6 (Graz University of Technology).

2.2.5 qPCR

In order to confirm the findings obtained from the microarray experiments, qPCR experiments were further employed. Firstly, total RNA was isolated from transiently transfected cells, using an RNA extraction kit (Macherey-Nagel, Düren, Germany). The integrity and concentration of the RNA was assessed through agarose gel electrophoresis and NanoDrop 2000C spectrophotometry (Thermo Scientific, Wilmington, DE) respectively. Total RNA was then reversely transcribed with the use of an oligo-dT (dT23VN) primer and the ProtoScript First-Strand cDNA Synthesis Kit (New England Biolabs, United Kingdom). All qPCR reactions were achieved using the LightCycler system (Roche Applied Science) and the LightCycler FastStart DNA Master SYBR Green I kit (Roche, Germany) in total reaction volume of 20 ul. Relative quantification analysis was performed through the LightCycler software, version 4.1. All primer sets for the gene expression analysis are shown in *Table 7 and 8*. All reactions were normalized against *GAPDH* and *L19* housekeeping genes.

Table 7: Primer sequences for UPR and housekeeping genes	
Human Genes	**Primer Sequence (5' to 3')**
BiP_F	TGTTCAACCAATTATCAGCAAACTC
BiP_R	TTCTGCTGTATCCTCTTCACCAGT
CHOP_F	AGAACCAGGAAACGGAAACAGA
CHOP_R	TCTCCTTCATGCGCTGCTTT
Calnexin_F	TCCGCCTCTCTCTTTACTGC
Calnexin_R	GCAACCACTTCCCTTCCAT
Calreticulin_F	GCAAATTCGTCCTCAGTTCTGG
Calreticulin_R	CCATGCATGTCCTTCTGGTC
Gadd34_F	ATGTATGGTGAGCGAGAGGC
Gadd34_R	GCAGTGTCCTTATCAGAAGGC
EDEM_F	CAAGTGTGGGTACGCCACG
EDEM_R	AAAGAAGCTCTCCATCCGGTC
Human genes	
sXBP-1_F	CTGAGTCCGCAGCAGGTGCAG
sXBP-1_R	CCAGAACATCTCCCCATGGAT
GAPDH_F	TTGGTATCGTGGAAGGACTCA
GAPDH_R	TTGGTATCGTGGAAGGACTCA
L19_F	GCGGAAGGGTACAGCCAAT
L19_F	GCAGCCGGCGCAAA
Mouse genes	**Primer Sequence (5' to 3')**
COL4A3_F	CCGAGCCAGTCCATTTATAGAAT
COL4A3_R	CAGCGAAGCCAGCCAGAA
BiP_F	TCATCGGACGCACTTGGAA
BiP_R	CAACCACCTTGAATGGCAAGA
CHOP_F	GTCCCTAGCTTGGCTGACAGA
CHOP_R	TGGAGAGCGAGGGCTTTG
sXbp1_F	CTGAGTCCGCAGCAGGTGCAG
sXbp1_R	CCAGAACATCTCCCCATGGAT
GAPDH_F	GCATGGCCTTCCGTGTTCCTA
GAPDH_R	CCTGCTTCACCACCTTCT

Table 8: Primer sequences for UPR and housekeeping genes	
Oligos for Xbp1 splicing assay	**Primer Sequence (5' to 3')**
hXbp1_F	GGAGTTAAGACAGCGCTTGG
hXbp1_R	ACTGGGTCCAAGTTGTCCAG
mXbp1_F	GAACCAGGAGTTAAGAACACG
mXbp1_R	AGGCAACAGTGTCAGAGTCC

2.2.6 Immunoblotting and densitometry

For confirming the findings obtained from the microarray experiments and qPCR reactions, western blot was performed in order to evaluate protein expression.

Forty-eight hours post transfection cellular lysates and medium were collected for further experiments. Cells were lysed in equal volumes of preheated 2xLaemmli sample buffer (SDS 25mM, Tris-HCl with pH of 6.8, 20%glycerol, 2%SDS, 2%b-mercaptoethanol, and bromophenol blue) and homogenized using a 27-28G needle (insulin syringe) or with sonication.

Equal amounts of samples were separated on a 7.5% SDS-polyacrylamide gel electrophoresis and then transferred overnight at 4^{o}C to polyvinylidene difluoride membranes (Millipore, Massachusetts, USA). Transblots were then incubated with a primary antibody (anti-HA; Santa Cruz Biotechnology), which targeted, to the fused HA-tag epitope engineered in the carboxyl terminus of the collagen chain. Moreover, in an effort to evaluate the activation of the UPR pathway, antibodies were used against BiP, PERK, calnexin (Cell Signaling Technology, Danvers, MA) CHOP and p-eIF2a (Santa Cruz Biotechnology). Transblots were further incubated by peroxidase labelled secondary antibodies, either goat anti-mouse or donkey anti-rabbit (Santa Cruz Biotechnology).

Proteins were detected using the Enhanced Chemi Luminescence Plus Blotting Detection system (Amersham Biosciences, Buckinghamshire, United Kingdom) and were visualized by autoradiography on photographic film (Kodak X-OMAT; Eastman Kodak, Rochester, NY). Band density was defined using the ImageJ Software (http://imagej.nih.gov/ij).

2.2.7 Semi quantitative analysis and XBP1 splicing

For the quantification of spliced and unspliced XBP1 mRNA, AB8/13 cells were transiently transfected with *COL4A3*-wt or *COL4A3*-p.G1334E constructs. Twenty-four hours post-

transfection, total RNA was isolated and reverse transcribed as described above. The resulting cDNA was further used for the semi quantitative analysis of XBP1 splicing.

2.2.8 *COL4A3* knockdown experiments

For knockdown experiments, 400.000 differentiated podocytes were sequentially transfected using *COL4A3* siRNA (Santa Cruz Biotechnology) and RNAiMax (Invitrogen) according to the manufacturer's instructions. Briefly, 7.5 ul of RNAiMax (Invitrogen) was mixed with 80 pmol of siRNA in 1 ml of Opti-MEM (Gibco). The mix was added to 4 ml of complete media (no antibiotics) and then transferred to the cells which were incubated overnight at 37°C and 5% CO_2. After 24 hours, the cells were transfected again using the same concentrations for siRNA and RNAiMax. Cells were harvested 72 hours after the first transfection.

2.2.9 Immunocytochemistry

Podocytes were seeded on coverslips and forty-eight hours post-transfection were fixed with 4% paraformaldehyde in PBS for 10 minutes. Following fixation, transfected cells were permeabilized using 0.5% Triton X-100 in PBS and quenched with 50 mM ammonium chloride in PBS for 10 minutes. Then, podocytes were blocked with 2% BSA, 2% FCS, 0.2% fish skin gelatin in PBS (blocking mix) for 30 minutes and incubated with primary antibody overnight at 4°C. Next, cells were incubated with the secondary antibodies in PBS, containing 5% blocking mix, for 1 hour at room temperature and then with Hoechst solution (DAKO, Denmark) at a 1:10000 dilution for 1 minute for nucleus staining. Finally, transfected cells were mounted with fluorescence mounting medium (DAKO).

2.2.10 Fluorescence microscopy

Immunofluorescent preparations were analysed on a Zeiss Axiovert 200M inverted fluorescence microscope equipped with Zeiss Axiovision 4.2 software and on a laser scanning confocal microscope Zeiss LSM 710 equipped with the ZEN 2010 software. Digital images were recorded and composed using Adobe Photoshop 5.0 and Illustrator 10 for Macintosh. Quantification and co-localization were determined using ImageJ software.

2.2.11 Immunohistochemistry

For human kidney staining experiments, kidney sections were cut and mounted on slides coated with suitable tissue adhesive. Sections were deparaffinised using xylene and

rehydrated through washes in graded alcohols. Endogenous peroxidase was neutralized using 0.5% v/v hydrogen peroxide/methanol for 10 minutes.

Slides were washed with water. Retrieval was carried out using 0.01 citrate retrieval solution (pH, 6.0). Sections were subsequently washed with TBS and blocked for 10 minutes using diluted normal serum (Novocastra Protein Block; Leica Microsystems). Moreover, sections were incubated with 1:200 primary antibody anti-BiP (Cell Signaling Technology), diluted in antibody diluent solution (DAKO) overnight at 4°C. Slides were then washed and incubated with DAKO REAL EnVision HRP Rabbit/Mouse (ENV). Subsequently, slides were incubated with a suitable peroxidase substrate, washed thoroughly in running tap water and counterstained with hematoxylin, before being dehydrated and mounted. Patient tissue was used after bioethics approval and informed consent. Immunohistochemistry experiments were performed at the Department of Histopathology of the Nicosia General Hospital, in collaboration with Dr N. Anastasiadou and Dr I. Zouvani.

2.2.12 Generation of *Col4a3*-p.G1332E Knock-In Mice

In order to generate a *Col4a3*-p.G1332E knock-in mouse model, a BAC encoded fragment (BAC bMQ-451l12) was obtained from Source Bioscience LifeSciences (Cambridge, UK), validated by PCR. This fragment was subloned into the pMV minimal vector (ColE1 origin of replication; apR resistance marker) via Red/ET Recombination. Targeting construct was generated by GeneBridges (Heidelberg, Germany).

A DNA-fragment carrying the *Col4a3*-p.G1332E mutation was then synthesized (Geneart/Life Technologies, Regensburg, Germany). This fragment was flanked by appropriate targeting and resistant cassette sequence regions, enabling neomycin/kanamycin resistance. At the same time, an engineered PCR construct was generated combining a DNA molecule and a neomycin/kanamycin resistance gene. Both products were fused with the pMV-Col4A3, derived from the verified BAC of the bMQ library, using a "triple recombination".

All constructs were verified through restriction digest analysis and sequencing, which was carried out at the University of California, DAVIS, Mouse Biology Program (MBP). Sequence analysis of agouti mice was accomplished through Big Dye-terminator technology and the ABI-3130*xL* Genetic Analyzer. Sequences were evaluated with the ABI PRISM 3100 Genetic Analyzer (Applied Biosystems) (*Figure 16)*.

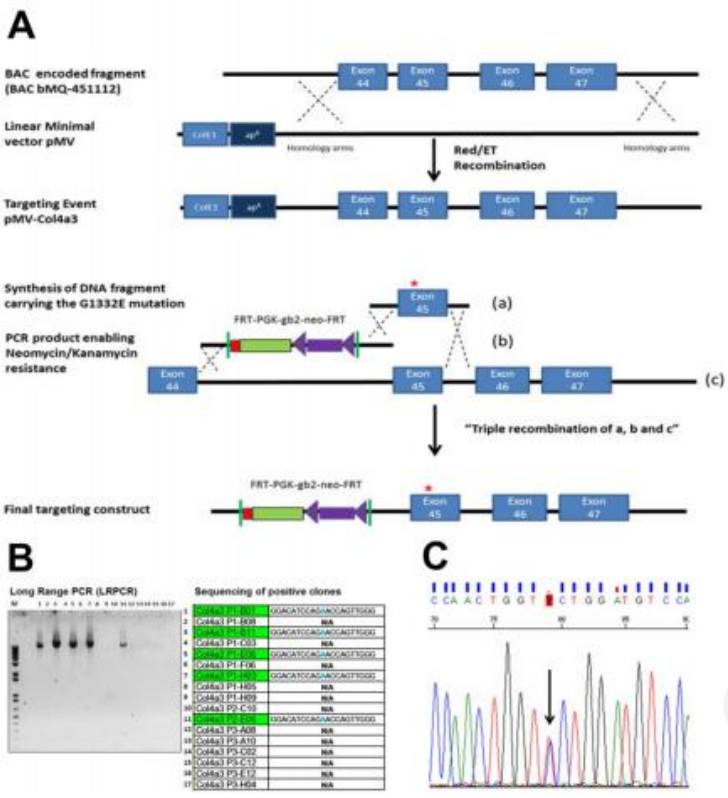

Figure 16: Generation of Col4a3-p.G1332E knock-in mice

(A) Map of targeting strategy, (B) Screening for correctly recombined alleles and (C) Sequence analysis of agouti heterozygous mice positive for the Col4a3-p.G1332E mutation.

Full phenotypic analysis of this line is currently in process. Animals are hosted in the Cyprus Institute of Neurology and Genetics animal house under specific pathogen-free conditions. All animal experiments were carried out in compliance with Cyprus law for protection of animals and were approved by the local authorities.

2.2.13 Electron microscopy of mouse kidney sections

For electron microscopy studies, left kidney sections were processed as usual and examined under a transmission electron microscope (JEM2100HR; JEOL, Inc., Tokyo, Japan) equipped with an ES500W Erlangshen CCD camera (Gatan GmbH,Munchen, Germany). GBM thickness was measured in open capillary loops using the Digital-Micrograph software (Gatan). These experiments were performed at the Heraklion University Hospital, in collaboration by Dr K. Stylianou.

2.2.14 Glomeruli isolation

Glomeruli were isolated as described in Takemoto et al. (2002). Briefly, mice were anesthetized by an intraperitoneal injection of Avertin (2,2,2-tribromoethyl and tertiary amyl alcohol; 17 ml/g mouse) and perfused with 8 x 10^7 Dynabeads (Invitrogen) diluted in PBS, through the heart. The kidneys from adult mice were removed, minced into 1-mm^3 and

digested in collagenase (1mg/ml collagenase A, 100U/ml deoxyribonuclease I) at 37^{o}C for thirty minutes. The digested tissue was gently pressed through a 100-μm cell strainer, which was then washed with 5ml of HBSS. The resulting cell suspension was centrifuged at 200 x g for 5 minutes. The supernatant was discarded and the cell pellet was suspended in Hank's balanced salt solution (HBSS). Finally, glomeruli containing Dynabeads were gathered by a magnetic particle concentrator and washed for at least three times with HBSS. During the procedure, kidney tissues were kept at 4^{o}C except for the collagenase digestion, which took place at 37^{o}C. Glomeruli total RNA was isolated using a commercially available kit (Macherey-Nagel) according to the manufacturer's instructions *(Figure 17)* (Takemoto et al., 2002).

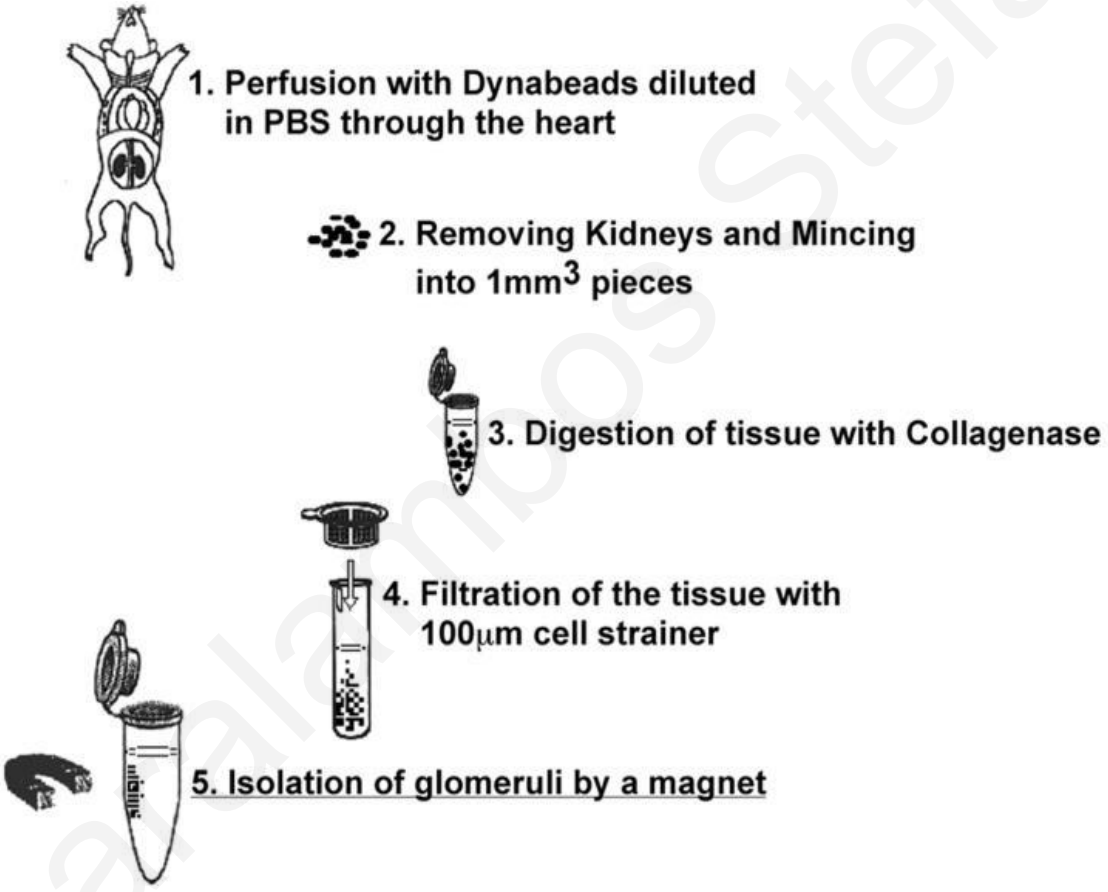

Figure 17: Flow chart depicting the basic steps for the isolation of mice glomeruli.

2.2.15 Statistical analysis

All data, with the exception of the microarrays, were statistically analysed using the GraphPad Prism software (GraphPad, LJ, USA). Mean SEM was compared among samples, whereas the Mann-Whitney U test was performed for pairwise comparisons. For comparisons

containing more than two groups, nonparametric analysis of relative contrasts was performed with Tukey post hoc analysis. No prior transformation of the data was implemented. For microarray analysis, we used the SAS JMP7 Genomics version 4 package (SAS Institute). Differential mRNA expression was analyzed by ANOVA. A P value of 0.05 with a false discovery rate 10% was established as the cut-off level of significance. For pathway analysis and gene ontology enrichment, a P value of 0.05 using the Fisher exact test with Bonferonni correction was set as the cut-off.

2.3 Results

2.3.1 Overexpression of *COL4A3*-wt and *COL4A3*-p.G1334E chains in AB8/13 podocyte cells

Human podocyte cells transiently transfected with constructs expressing *COL4A3*-wt or mutant *COL4A3*-p.G1334E, resulted in equal expression, as verified through quantitative real-time PCR (qPCR) analysis (data not shown). Interestingly, cells expressing the mutant form of *COL4A3* chain, exhibited significantly reduced secretion of the mutant protein in the cellular medium forty-eight hours post transfection (P<0.01) *(Figure 18, A and B).* In addition, the mutant *COL4A3*-p.G1334E was more abundant in the cellular lysate, compared to the *wt* chain, even though this was not statistically significant at the 48-hour time point *(Figure 18B).*

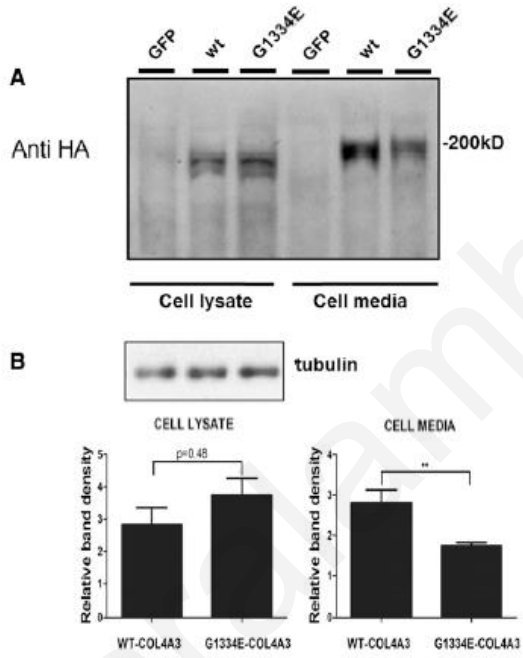

Figure 18: Mutant COL4A3 chain is secreted less efficiently when expressed in AB8/13 cells

*(A) and (B) AB8/13 cells were transiently transfected with vectors expressing COL4A3-wt or COL4A3-p.G1334E HA-tagged at C-terminus. Expression and secretion of single chains of collagen were measured through western blot analysis of the cell lysate and the cell medium respectively, 48 hours after transfection. No HA antigen was detected in AB8/13 cells transfected with a vector expressing the green fluorescent protein (GFP). (B) The levels of the secreted COL4A3-p.G1334E chain were significantly lower, reaching 70% of COL4A3-wt levels. Upper panel (A) demonstrates a representative western blot and lower panel (B) shows relative band density corresponding to HA tag immunoreactivity (i.e. COL4A3) that was normalized against tubulin. Data are represented as means ±SEM of n≥3 independent experiments; **P≤0.01.*

Moreover, in order to determine the cellular location of the expressed chains, immunocytochemistry experiments were performed employing the same cell line grown on coverslips. Results strongly suggested that overexpressed collagen chains were mainly retained into the cell's ER and colocalized with the ER marker calnexin *(Figure 19, A and B).* This colocalization was more apparent when the mutant *COL4A3*-p.G1334E chain was overexpressed. Further investigation through intensity correlation analysis plots, indicated that the colocalization of collagen and calnexin in the *wt* is more random, in contrast to the stronger association seen in the case of the mutant collagen chain *(Figure 19, C–H).*

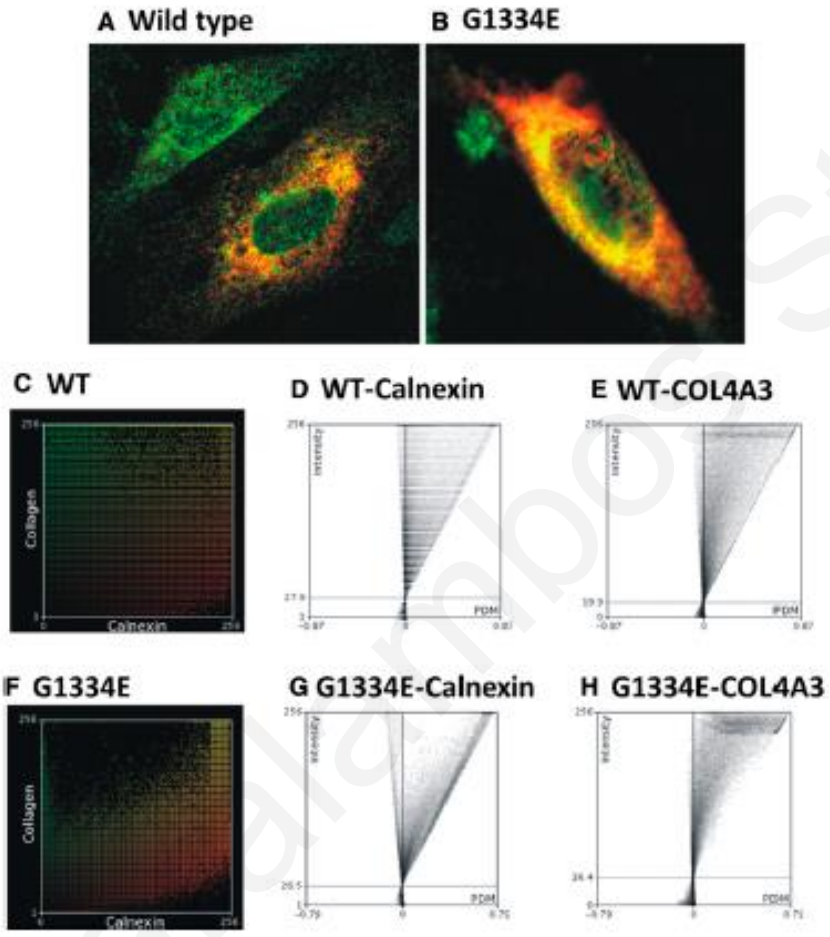

Figure 19: Mutant collagen IV chain demonstrates ER retention when expressed in AB8/13 cells

Human podocyte cells equally expressing wt (A) or G1334E mutant protein (B), exhibited ER retention of the mutant form, as indicated by the colocalization (yellow) of the ER marker calnexin (green) with the COL4A3 chain (red). Intensity correlation analysis of images C and F show the colour scatter plots of the red (collagen) and green (calnexin) channels. Intensity correlation analysis plots where for each pixel the product of differences from the mean value plotted with respect to its intensity. As indicated, the co-localization of collagen and calnexin in the wt is more random in contrast to the stronger association seen in the mutant. The intensity correlation analysis was performed using the ImageJ software (D, E, G and H).

2.3.2 Identification of significantly deregulated genes using microarrays

In order to identify the cellular pathways activated by collagen overexpression in the podocyte, microarray RNA profiling was performed. Experimental results identified 1835 differentially expressed genes between the empty vector, the *COL4A3*-wt and the *COL4A3*-p.G1334E expressing cells. Of these, 1512 genes were suggestively deregulated between the *wt* and vector and 1553 between the G1334E and vector. The top 40 significantly deregulated genes (20 top upregulated and 20 top down regulated) in the vector versus the *COL4A3*-wt are described in supplementary table 1 A and B. A similar relationship was observed when comparing the vector with the *COL4A3*-p.G1334E expressing cells *(supplementary table 1, C and D).* In addition, no genes were significantly deregulated, when the cells that overexpressed the *wt* were compared to the mutant chains.

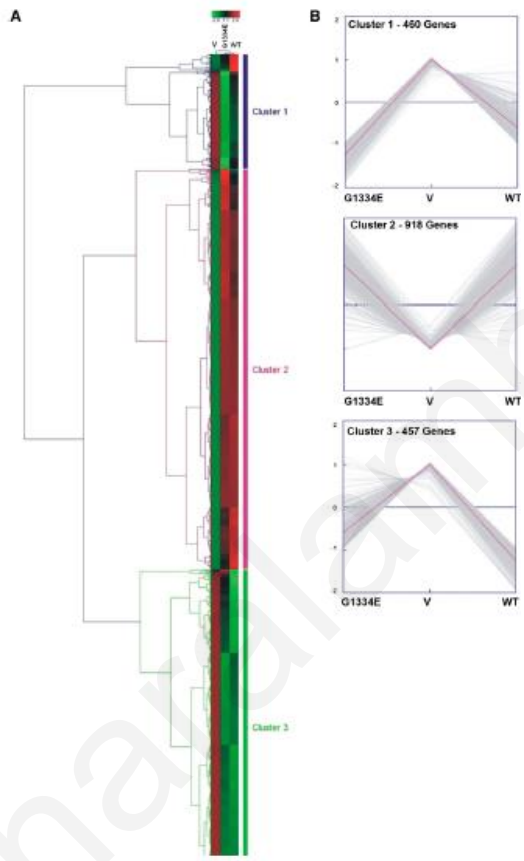

Figure 20: Unsupervised hierarchical cluster illustrating differentially expressed genes between vector only (V), wt and COL4A3-p.G1334E (G1334E)–expressing cells

(A) Unsupervised hierarchical clustering based on 1835 probe sets with the highest variation between podocyte cells transfected with three different vectors: an empty pcDNA6-HA vector (V) and vectors expressing the COL4A3-wt chain or the mutant COL4A3-p.G1334E chain (G1334E). Three main gene clusters were observed. Colour saturation is directly proportional to the measured expression ratio magnitude. Euclidian distance was used as the metric. Rows represent individual probe sets, whereas columns represent the three experimental conditions. Red and green bars indicate high and low expression respectively. (B) K-means clustering verified the existence of three main gene clusters: cluster 1 (460 genes), cluster 2 (918 genes), and cluster 3 (457 genes).

The deregulated genes were further clustered using unsupervised two-way hierarchical clustering with Euclidian distance and were divided into three main groups *(Figure 20A).*

Gene clustering using the K-means algorithm verified the existence of three main gene clusters *(Figure 20B)*.

2.3.3 Enrichment analysis on significantly deregulated pathways: Deregulation of the UPR pathway

Based on the microarray profiling, all genes found to be significantly deregulated were further subcategorized into two different groups; the upregulated or downregulated genes. These classifications were based on comparisons made between vector versus *COL4A3*-wt and vector versus *COL4A3*-p.G1334E.

According to these findings, 10 pathways were associated with the deregulated genes exhibiting p=0.05 when applying Benjamini correction *(supplementary table 2)*. The top three pathways with the highest score were the UPR pathway (P<0.00001), the p53 pathway (P=0.0023) and the glyoxylate and dicarboxylate metabolism pathway (P=0.0048). The UPR pathway was the pathway with the highest score, i.e. the highest number of deregulated genes, all the genes that were deregulated and thus could play a significant role (P=1.7E-9; Fisher exact test), were marked on the "protein processing in the endoplasmic reticulum" pathway, using the Kyoto Encyclopedia of Genes and Genomes (KEGG) database *(Figure 21A)*.

Moreover, the 118 genes involved in protein processing in the ER were further clustered, in order to verify the genes demonstrating altered expression *(Figure 21B)*. Thirty-one genes were upregulated and seven were downregulated, in the "protein processing in endoplasmic reticulum" pathway *(supplementary table 3)*. Genes encoding protein chaperones BiP, calnexin and calreticulin, as well as the downstream transcription factor X-box binding protein 1 (XBP1), the UPR target genes Gadd34 and EDEM and the proapoptotic marker C/EBP homologous protein (CHOP) were specifically selected for further evaluation.

2.3.4 Verification of UPR activation using qPCR and western blotting

Microarray results showing significantly increased expression of all UPR markers in cells expressing *wt* or *COL4A3*-G1334E versus the empty vector, were confirmed through qPCR *(Figure 22A, grey versus white and grey versus black bars)*.

Interestingly, qPCR results revealed significant differences in the expression of the BiP, CHOP, and XBP1 genes between cells expressing the *wt* versus cells transfected with the

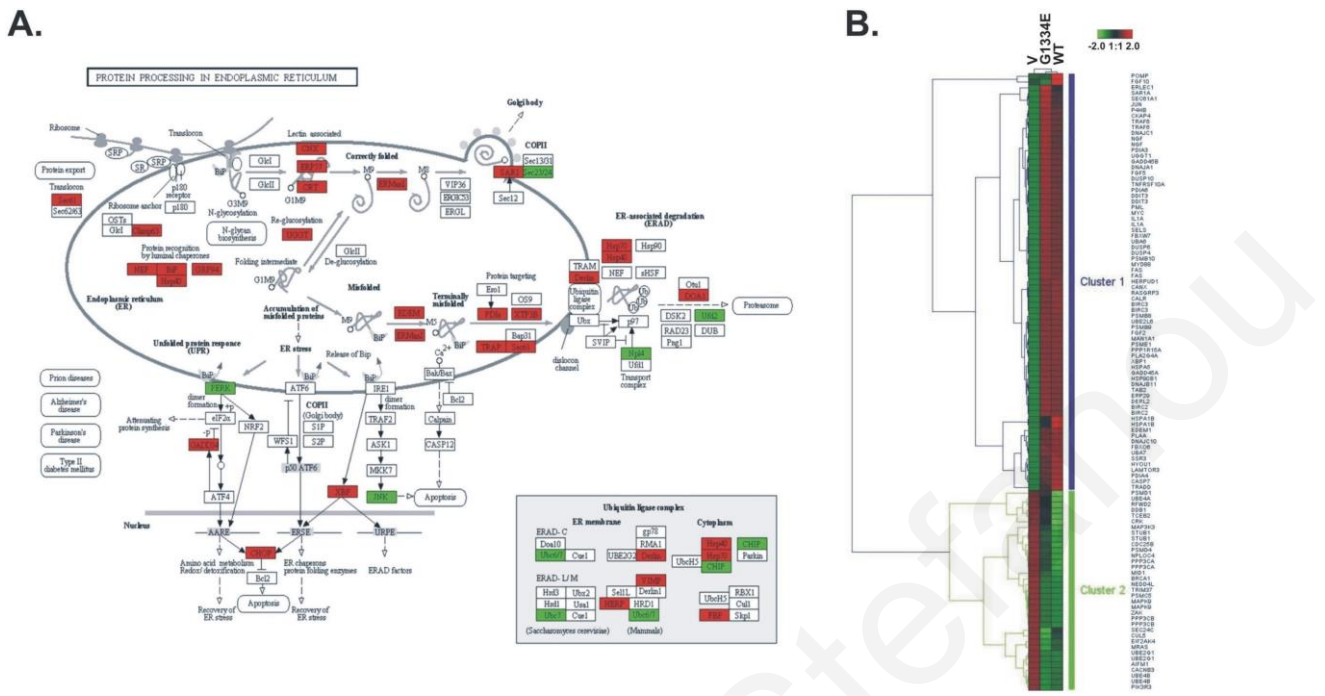

Figure 21: Enrichment analysis on significantly deregulated pathways: Deregulation of the UPR pathway

(A) Enrichment analysis presenting the deregulated pathway of protein processing in the endoplasmic reticulum in transfected cells. The KEGG pathway demonstrates the molecules that participate in the protein processing in the ER. The highlighted molecules were significantly deregulated in the cells transfected with the mutant COL4A3-p.G1334E or the COL4A3-wt chain versus those transfected with an empty vector. Significantly upregulated genes in the pathway are shown in red, whereas significantly downregulated genes in green (see also supplementary table 3). (B) Unsupervised hierarchical cluster based on 118 genes involved directly in the protein processing in the endoplasmic reticulum recognizes two main gene clusters. Color saturation is directly proportional to the measured expression ratio magnitude. Euclidian distance was used as the metric. Rows represent individual probe sets. Columns represent the three experimental conditions: empty vector (V), WT, or G1334E. Red bars indicate high expression, and green bars indicate low expression.

G1334E vector *(Figure 22A, white versus black bars)*. This trend was also evident in the microarray data but did not reach significance. Therefore, it was decided that the mRNA levels of particular UPR markers in human podocytes equally expressing *COL4A3*-wt chain or the *COL4A3*-p.G1334E mutation, should be compared.

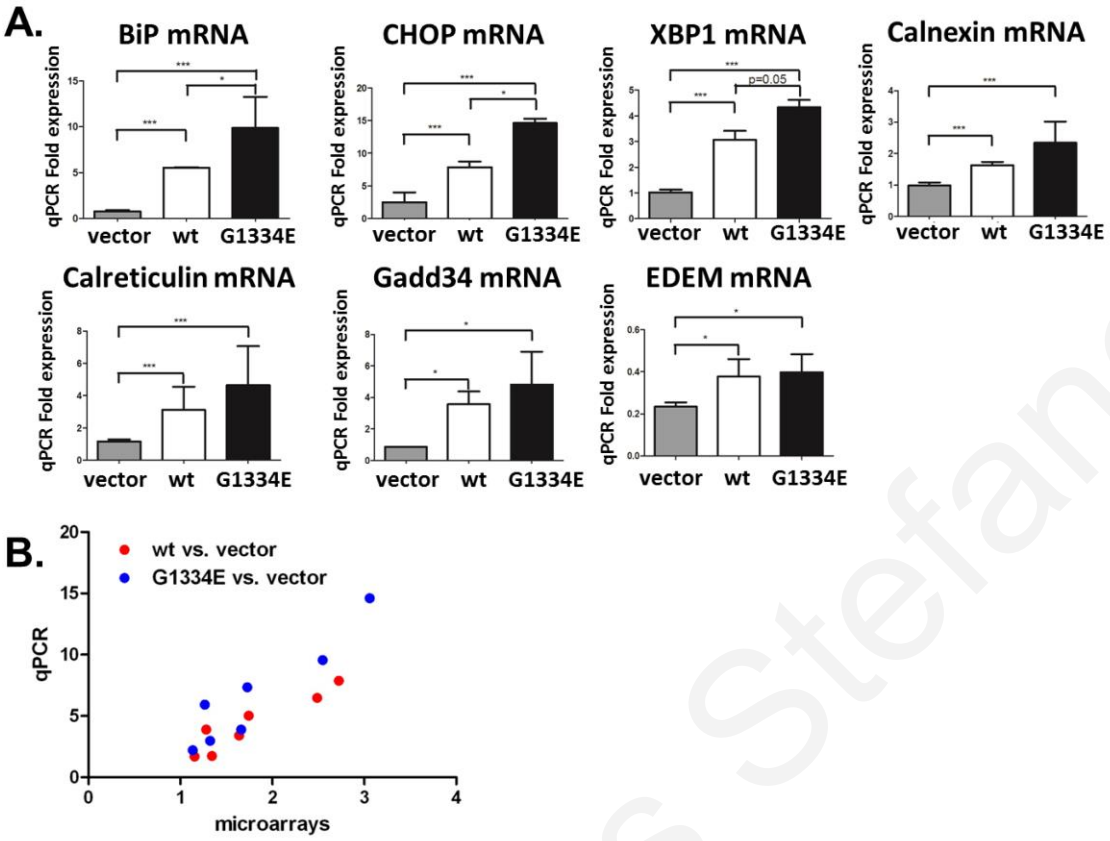

Figure 22: Verification of microarray results by qPCR

*(A) Graph plots of qPCR data showing fold increase in mRNA levels of various UPR genes in cells expressing vector only (gray bars), COL4A3-wt (white bars), or COL4A3-p.G1334E mutant chain (black bars) compared with cells expressing vector only. All mRNAs of UPR genes were significantly upregulated in cells expressing wt or mutant COL4A3 compared with cells expressing vector only, thus verifying the microarray data. BiP, CHOP, and XBP1 mRNAs were significantly increased in mutant expressing cells compared with controls (Data are means ±SEM, n>3 independent experiments; *P<0.05; **P<0.01). (B) Positive correlation between microarrays and qPCR experimentation. qPCR results agree with the microarray data both for the wt versus vector (R^2=0.87; 95% confidence interval [95% CI], 0.62 to 0.99; P=0.0020) and for the G1334E versus vector (R^2=0.88; 95% CI, 0.62 to 0.99; P=0.0019) experiments. Results are presented as scatterplot.*

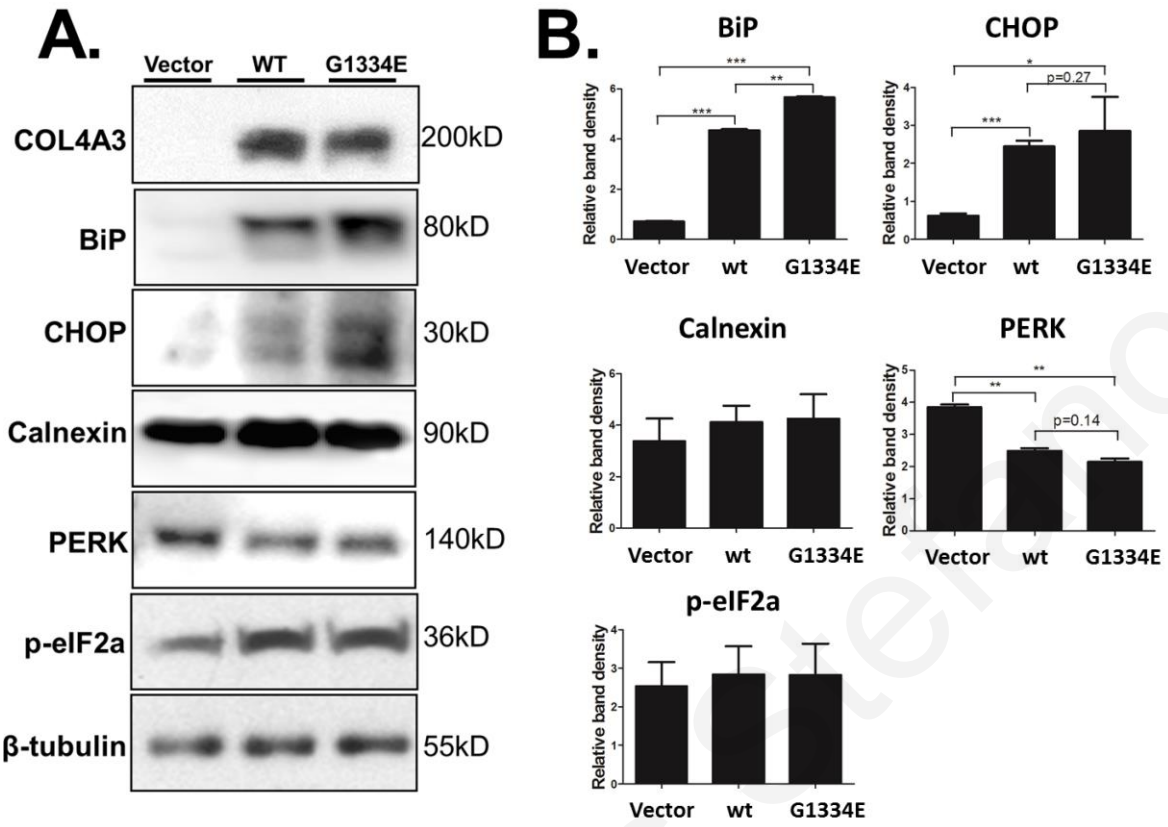

Figure 23: UPR proteins are deregulated in AB8/13 cells transfected with wild type or mutant COL4A3

*(A) Human undifferentiated podocyte cells were transiently transfected with the COL4A3-wt, COL4A3-p.G1334E or the empty pcDNA6/HA vector (vector; used as a negative control). Protein levels of the UPR markers BiP, CHOP, calnexin, PERK and p-eIF2a were measured 48 hours post transfection via Western blotting. β-tubulin expression in the same samples was used as a loading control. Shown is a representative blot with differential levels of the various proteins. (B) Western blotting is quantified via densitometric analysis. Data are means ±SEM of three independent experiments. Calnexin and p-eIF2a remained intact, whereas BiP and CHOP showed upregulation in cells overexpressing the wt or mutant collagen IV chain. Additionally, PERK was also found to be downregulated when comparing lysates originating from cells overexpressing the wt or mutant collagen IV chain. *P<0.05; **P<0.01; ***P<0.001.*

The ratios indicating gene expression changes are presented as fold-change and are compared with the microarray data in *Figure 22B*. These validation experiments showed that the expression patterns of the genes tested were similar to the microarray data. There was very good agreement between the microarrays and the qPCR results both for the *wt* versus vector (R^2=0.87; 95% confidence interval, 0.62 to 0.99; P=0.0020) and for the G1334E versus vector experiments (R^2=0.88; 95% confidence interval, 0.62 to 0.99; P=0.0019) *(Figure 22B)*. This reinforced the reliability of the data acquired from global microarray analysis.

Furthermore, all the above findings were further confirmed by testing protein expression of the UPR markers BiP, CHOP, calnexin, and PERK, as well as phosphorylation of the eIF2a protein, the latter being an important player in protein synthesis shutdown in the UPR cascade. Results demonstrated a significant increase in BiP protein levels, when comparing the vector with the *COL4A3*-wt and the *COL4A3*-p.G1334E expressing cells. Most importantly, BiP protein levels also show a significant increase when comparing the *wt*- with the mutant-expressing cells *(Figure 23)*. Moreover, a significant increase in CHOP protein levels was observed when comparing the vector and the collagen (*wt* or mutant)-expressing cells. A significant decrease was also evident in the total protein levels of the PERK protein in cells expressing the *wt* or the mutant COL4A3 chain compared with vector-only–expressing cells. These results were in agreement with the microarray analysis. No significant change was observed in the calnexin and phosphorylated p-eIF2a levels *(Figure 23)*.

2.3.5 Overexpression of *wt* and mutant COL4A3 chains induce ER stress, as shown by XBP1 splicing

Accumulation of unfolded or misfolded proteins in the endoplasmic reticulum can trigger ER stress, which leads to the activation of the UPR. In addition to the upregulation of protein markers (e.g. BiP, p-eIF2a), UPR signaling involves other the splicing of X-box binding protein-1 (XBP1) mRNA, frequently used as a marker for ER stress. In this set of experiments, an established assay was employed allowing the detection and verification of XBP1 splicing, marking UPR activation.

Obvious splicing of the XBP1 mRNA was observed in podocytes expressing the *COL4A3-wt* chain when compared with cells expressing vector-only cDNA *(Figure 24A)*. In addition, cells overexpressing the GFP protein or the slit diaphragm protein filtrin (NEPH3) cloned in the same vector were used, in order to evaluate whether the splicing effect is specific for the collagen protein or is a general effect. No splicing was observed in GFP or the filtrin expressing cells (results not shown).

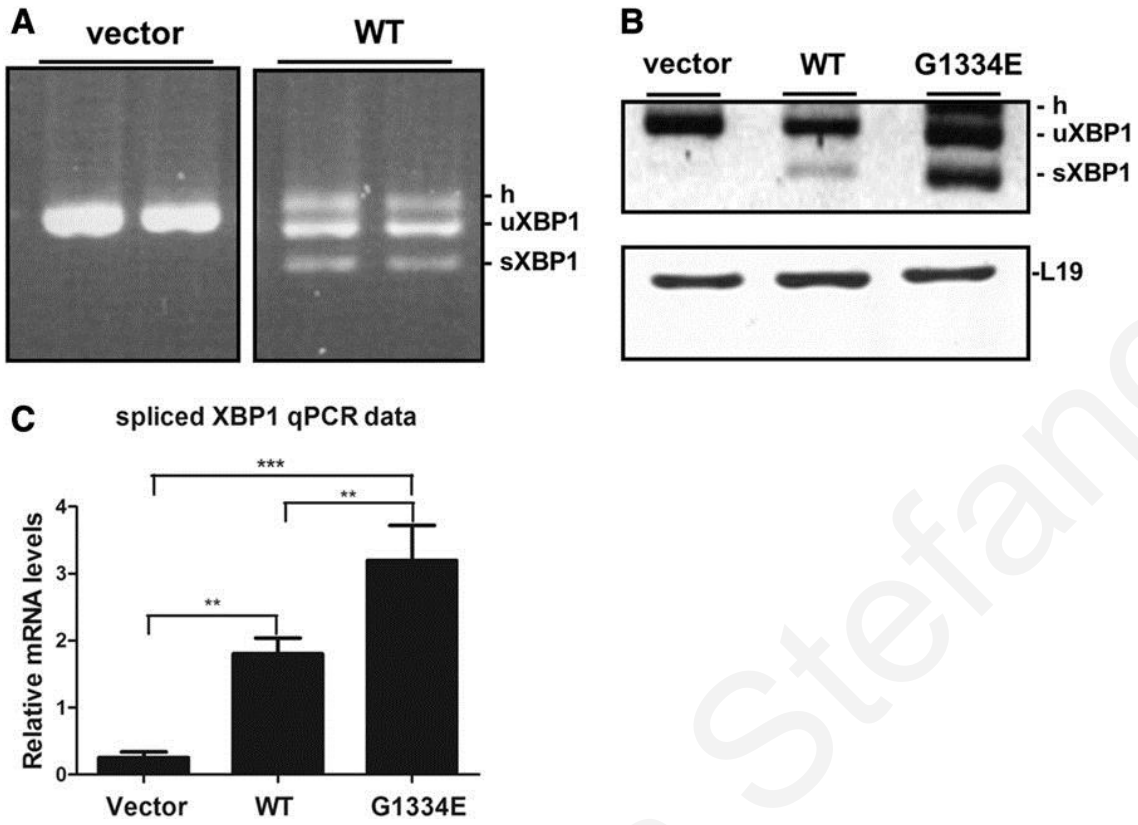

Figure 24: Single-chain expression of wt or COL4A3-p.G1334E induces XBP1 splicing in AB8/13 cells

*(A) Representative experiment of RT-PCR of the XBP1 mRNA in AB8/13 cells transiently expressing COL4A3-wt collagen chain or the empty pcDNA6/HA vector (vector). PCR products were ran on 3% agarose gel. It is apparent that overexpression of the wt chain induces XBP1 splicing, as evidenced by the appearance of the smaller spliced form (sXBP1) and the heteroduplex species formed between unspliced and spliced chains (h). The spliced molecules are smaller by 26 bp. (B) Representative experiment of RT-PCR of the XBP1 mRNA in AB8/13 cells transiently expressing COL4A3-wt, mutant COL4A3-G1334E chain, or the empty pcDNA6/HA vector. PCR products were ran on 3% agarose gel. It is evident that overexpression of both wt and mutant chains results in XBP1 splicing. L19 was used as an internal PCR control. (C) Real-time PCR for direct quantitation of the spliced XBP1 isoform using primers in the spliced-unspliced interface. A highly statistical difference exists in the spliced form between vector-only, wt and mutant expressing cells. Especially important is the differential induction of XBP1 splicing comparing wt with mutant cells. Data are means ± SEM of three independent experiments; **P<0.01; ***P<0.001.*

Surprisingly, expression of the *COL4A3*-p.G1334E mutant into podocytes resulted in significantly more XBP1 splicing when compared with cells expressing the *wt (Figure 24B).* Densitometric analysis of the spliced versus the unspliced product revealed statistical significance in the results obtained from *wt* versus the mutant cells (not shown). The latter was further confirmed by qPCR of the spliced XBP1 isoform using primers in the spliced-unspliced interphase of XBP1's mRNA, as described by (Cawley et al., 2011). Spliced XBP1 was significantly increased in *COL4A3*-p.G1334E versus *COL4A3*-WT–expressing cells *(Figure 24C).*

2.3.6 Knockdown of endogenous COL4A3 chains using small interfering RNA induces ER stress in AB8/13 cells

Both undifferentiated and differentiated AB8/13 cells express the COL4A3, COL4A4, and COL4A5 chains, with differentiated cells demonstrating increased expression (supplementary figure 1).

When the COL4A3 chain was knocked down in differentiated podocytes with the use of small interfering RNA (siRNA), the UPR pathway was activated. This was confirmed by the upregulation of BiP and phosphorylated protein kinase–like endoplasmic reticulum kinase (PERK), and by the trend for an increase in p-eIF2a *(Figure 25).* Interestingly, the proapoptotic marker CHOP remained unaltered.

2.3.7 BiP expression is increased in kidney biopsy specimens from *COL4A3*-p.G1334E mutation carriers

In order to examine whether the UPR pathway is involved in the pathogenic process among patients with TBMN, biopsy samples originating from two patients who were carriers of the *COL4A3*-p.G1334E mutation were evaluated with BiP protein staining. Immunohistochemistry findings in these biopsies, demonstrated increased BiP expression in the glomeruli of these patients *(Figure 26B)* when compared with specimens from obese individuals who were used as negative controls (samples provided by Dr. Demetris Goumenos, University Hospital of Patras) *(Figure 26C).* BiP expression in tubular epithelial cells was similar in both the *COL4A3*-p.G1334E patients and obese individuals. A biopsy sample from a patient with breast carcinoma was stained as a positive control *(Figure 26A).*

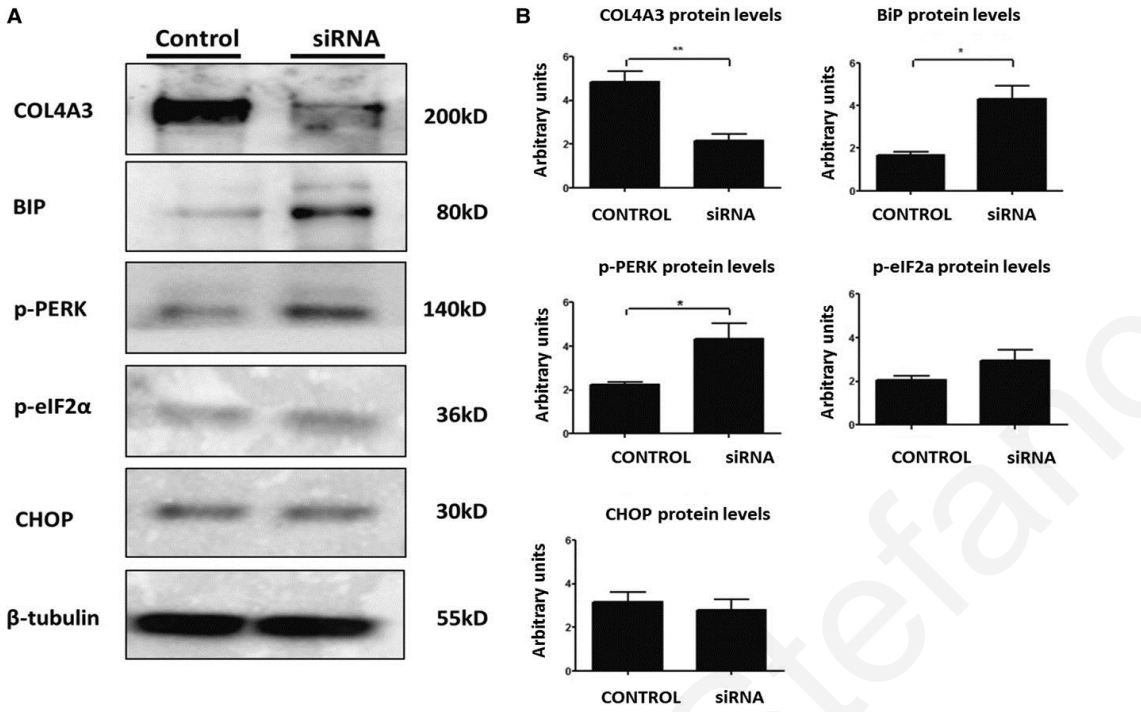

Figure 25: Knockdown of endogenous COL4A3 in differentiated podocytes activates the UPR pathway

*Differentiated cells were transfected with COL4A3 siRNA in order to knock down the endogenous COL4A3 expression. (A) Protein expression of the UPR markers BiP, CHOP, p-PERK, and p-eIF2a was measured 72 hours post transfection via Western blotting. β-tubulin expression in the same samples was used as loading control. Scrambled siRNA was used as a negative control in all experiments. Shown is a representative blot, with differential levels of the various proteins. Note the effective downregulation of the target gene and the upregulation of UPR markers. (B) Western blotting in A was quantified via densitometric analysis. Data are means ±SEM of three independent experiments. While CHOP remained unaltered, BiP and p-PERK were upregulated in cells being treated with COL4A3 siRNA. *P<0.05; **P<0.01.*

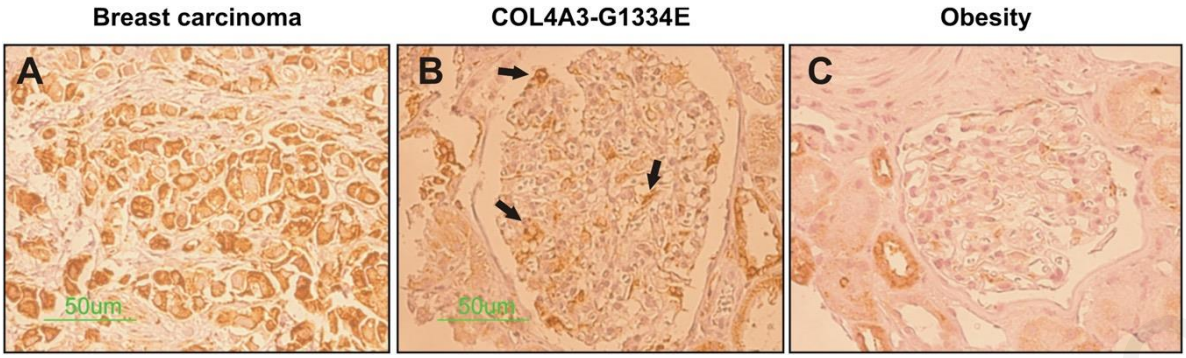

Figure 26: BiP protein expression is increased in renal biopsies of COL4A3-p.G1334E heterozygous carriers

Detection of BiP expression in the glomerulus from renal biopsy specimens of two patients diagnosed with TBMN and confirmed heterozygous carriers of the COL4A3-G1334E mutation, using immunohistochemical staining (B). Kidney biopsy specimens from a patient with breast carcinoma (A) and six obese people (C) were used as positive and negative controls, respectively. In the patients with confirmed COL4A3-G1334E mutation, serial sections show strong perinuclear BiP immunoreactivity in the glomerulus compared with the obese controls. Tubular cells of both the patient with COL4A3-G1334E and the obese individuals are stained positive for BiP. All samples are sex and age matched.

2.3.8 Activation of the UPR pathway in a mouse carrying the *Col4a3*-p.G1332E missense mutation

In order to evaluate the mechanisms by which the *COL4A3*-p.G1334E mutation causes pathology in vivo, a relevant mouse model was created in our facilities. To achieve this, gene-targeting technology was used to successfully generate a knockin mouse for the *Col4a3*-p.G1332E mutation, the corresponding mutation to the *COL4A3*-p.G1334E mutation in patients diagnosed with AS and TBMN. These mice express the COL4A3 chain normally and in equal amounts, as evidenced by both qPCR (results not shown) and Western blot experiments *(Supplemental Figure 2)*. Additionally, EM analysis of homozygous *Col4a3*-p.G1332E mice revealed thin GBM with areas of mild (3-month-old mice) or severe (7-month-old mice) thickening, consistent with AS nephritis *(Figure 27)*.

In these mice the UPR activation was evaluated in the kidney of mutant heterozygous (WT/M) and homozygous (M/M) 3-month-old animals versus their *wt* littermates (WT/WT). Reverse transcription PCR revealed XBP1 splicing in both heterozygous and homozygous mice, in contrast to the *wt (Figure 28A)*. Moreover, quantitative PCR analysis using primers on the spliced-unspliced interphase suggested increased XBP1 splicing in homozygous mice

versus the control *(Figure 28B)*. Additionally, quantification of BiP mRNA demonstrated significantly upregulated levels of this marker in the homozygous mouse compared to the *wt* littermates, while CHOP mRNA levels remained unaltered *(Figure 28C)*. Furthermore, BiP, p-PERK and p-eIF2a protein levels were significantly upregulated in homozygous mice versus their control littermates *(Figure 28, D and E)*. Lastly, using Dynabeads we isolated glomeruli from mutant homozygous mice and their *wt* littermates and studied UPR activation specifically in glomerular cells. The UPR marker BiP was significantly upregulated in mRNA isolated from mutant mice glomeruli (M/M) versus controls (WT/WT) *(Figure 29A)*. An increased trend in spliced XBP1 mRNA was also detected as measured by qPCR, while the XBP1 splicing assay showed the presence of a spliced band in mutant mice *(Figure 29B)*.

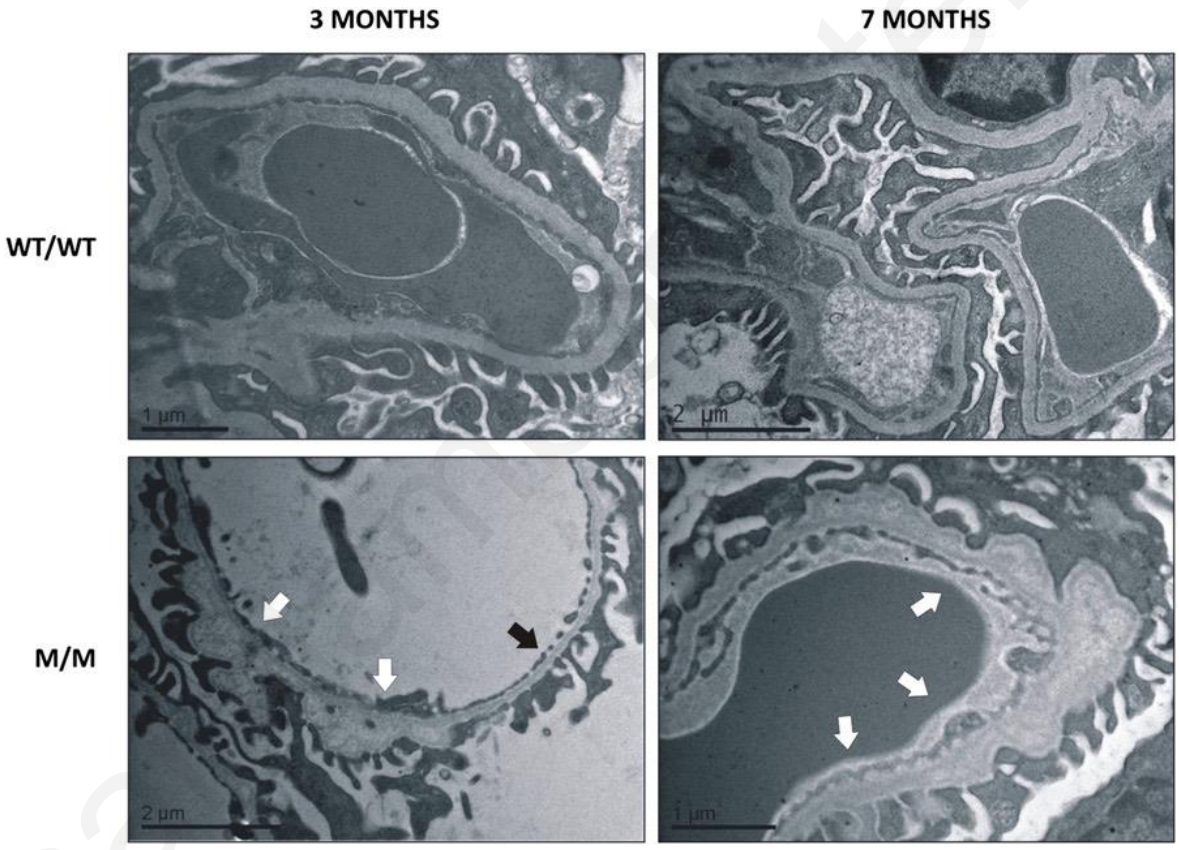

Figure 27: EM analysis of the mutant knockin mice

EM analysis of the mutant knockin mice resulted in the diagnosis of Alport Syndrome nephritis. WT mice (WT/WT) display normal GBM thickness, 280–300 nm range, while G1332E/G1332E (M/M) homozygous mice demonstrate thin GBMs, 140–160 nm range (black arrow), with areas of mild (3-month-old mice) or severe (7- month-old mice) irregular thickening (white arrows), consistent with AS nephritis.

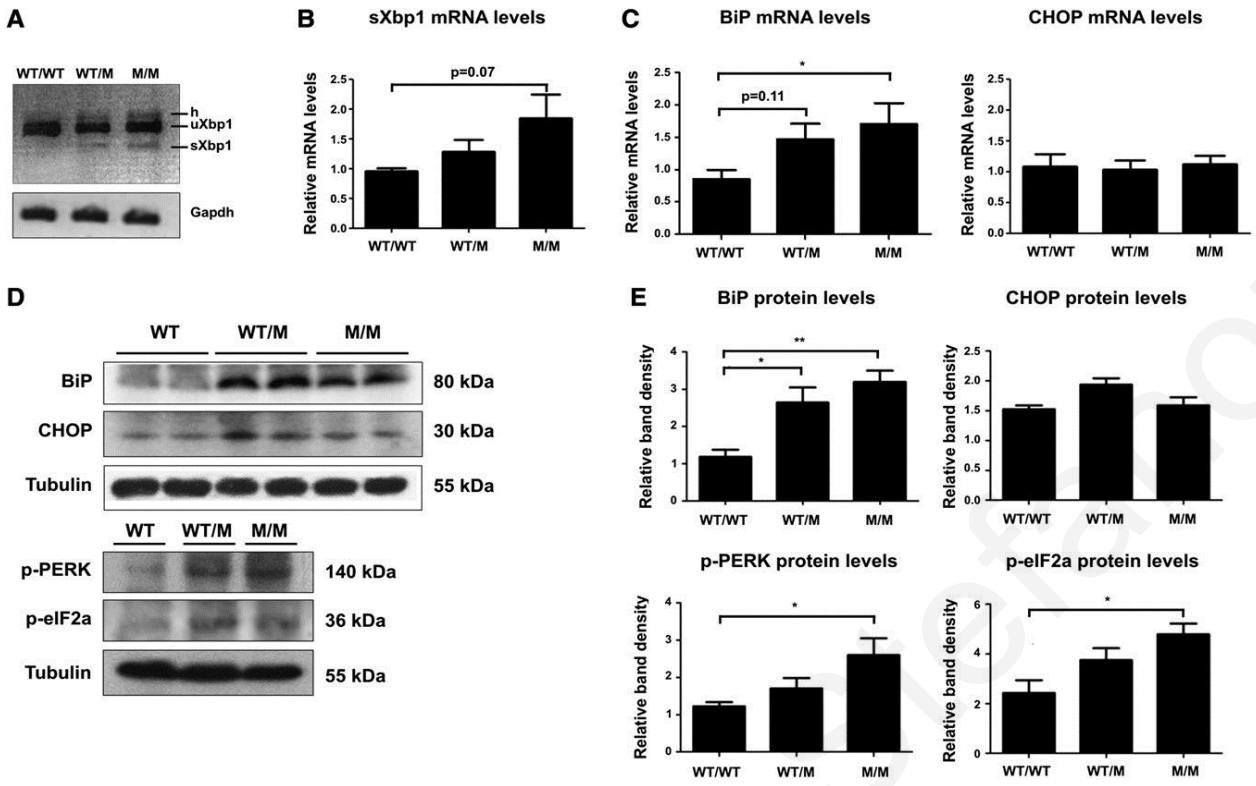

Figure 28: The UPR pathway is activated in whole kidney lysates of Col4a3-p.G1332E mice

*(A) XBP1 splicing assay using RNA extracted from whole kidney lysate of WT, Col4a3-p.G1332E heterozygous (WT/M) and Col4a3-p.G1332E homozygous (M/M) mice. The detection of a smaller size band on a 2% agarose gel, proves the splicing event. Mouse glyceraldehyde 3-phosphate dehydrogenase (GAPDH) was used as an endogenous control. Observe the presence of the spliced band in the heterozygous (WT/M) and homozygous (M/M) mice. (B) Quantification of spliced XBP1 isoform was accomplished using real-time PCR. Replications, did not produce a significant result, nevertheless they presented an obvious trend toward spliced XBP1 increase in homozygous (M/M) mice. Data are means ±SEM of three independent experiments. (C) Quantification of BiP and CHOP mRNA levels through qPCR. RNAs were extracted from whole kidney tissue of WT, Col4a3-p.G1332E heterozygous (WT/M) and Col4a3-p.G1332E homozygous (M/M) mice. Significant upregulation of the BiP is evident but not in the case of CHOP mRNA levels. (D) Representative Western blot demonstrating protein expression level change in the lysates of whole kidney from 3-month-old WT or Col4a3-p.G1332E heterozygous (WT/M) or homozygous (M/M) knock-in mice. Equal amounts of protein lysates were resolved by SDS-PAGE followed by Western blot. Differential expression of proteins between wt and mutant mice were noticed. (E) Quantification of representative blots shown in graphic form. The expression levels of BiP, CHOP, p-PERK, and p-eIF2a were normalized against β-tubulin levels (*P<0.05; **P<0.01, n>3); M/M, homozygous for the Col4a3-p.G1332E mutation; WT/M, heterozygous for the Col4a3-p.G1332E mutation. Three mice were used for each condition. All UPR genes with the exception of CHOP were significantly overexpressed. h, hybrid; sXBP1, spliced XBP1; uXBP1, unspliced XBP1.*

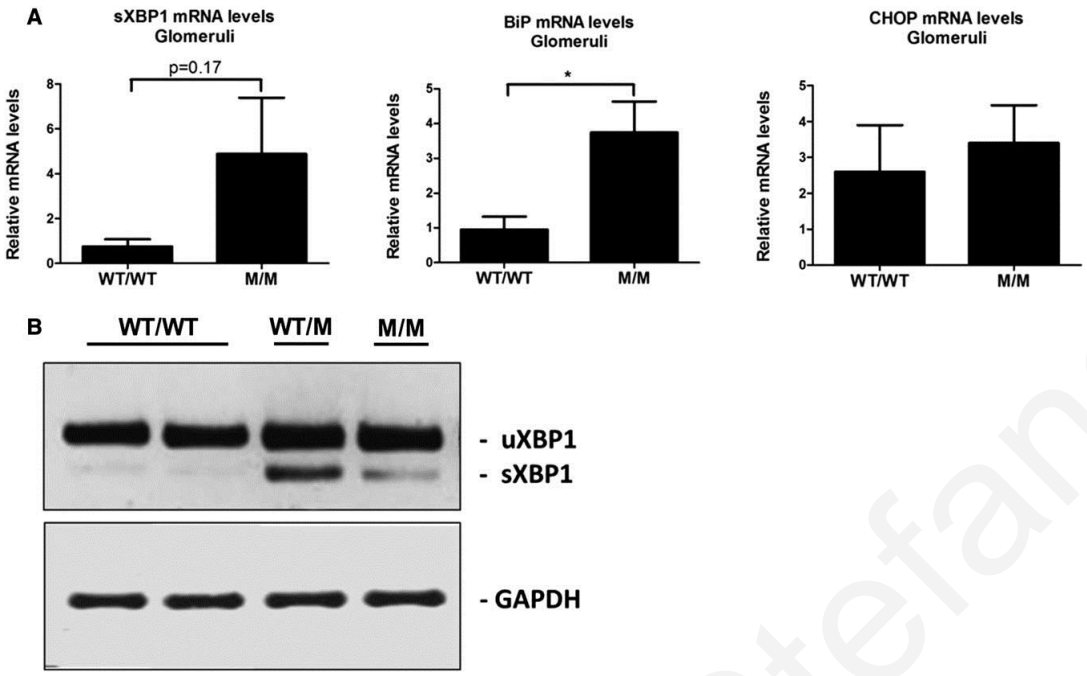

Figure 29: Upregulation of UPR marker mRNA in glomeruli isolated from Col4a3-p.G1332E knock-in mice

*(A) Quantitative evaluation of BiP and CHOP mRNA levels using qPCR. RNAs were extracted from isolated mouse glomeruli of wt and Col4a3-p.G1332E homozygous mutant (M/M) mice. The significant upregulation of BiP is demonstrated but that is not the case for CHOP mRNA levels. Spliced XBP1 mRNA levels show an obvious increase trend. (B) Representative experiment of reverse transcription PCR of the XBP1 mRNA in RNA isolated from wt or mutant mice glomeruli. PCR products were ran on 3% agarose gel. The lower band (smaller spliced form-sXBP1) proves the induction of XBP1 splicing in mutant mice. Mouse glyceraldehyde 3-phosphate dehydrogenase (GAPDH) was used as an endogenous control. M/M, homozygous mouse; WT/M, heterozygous mouse; WT/WT, WT mice. *P<0.05; n=3.*

2.4 Discussion

Alport syndrome and TBMN are heritable kidney diseases mostly caused by mutations in the *COL4A3/A4/A5* genes, triggering complex cellular pathomechanisms. Most of these mechanisms, involve extracellular effects due to reduced or no secretion of collagen IV heterotrimers in the GBM. Nonetheless, no one can exclude effects caused by collagen mutations in intracellular pathways, since collagen IV α3/α4/α5 chains are exclusively produced in podocytes.

This study focused on the putative intracellular effects of the *wt* or mutant (p.G1334E) *COL4A3* chain transiently overexpressed in human podocytes. Undifferentiated cells demonstrated statistically significant reduced secretion of the single p.G1334E mutant chain in the cellular medium in contrast with the *wt* chain. Moreover, immunocytochemistry experiments revealed that overexpression of the wt or mutant *COL4A3* in human podocytes caused ER retention of both proteins with the mutant form demonstrating a more obvious colocalization with an ER marker. This could explain the reduced secretion of the mutant *COL4A3* in the cellular medium. These experiments were performed in an artificial in vitro system, which points out the uncertainty of the single-chain secretion into the cellular medium. However, it is strongly believed that *COL4A3* chain secretion could be an event happening due to the association of the overexpressed chain with the endogenous *COL4A4* and *COL4A5* chains. Additionally, this interaction could also account for the formation of misfolded trimers that trigger the UPR activation. Nevertheless, expression and secretion of single collagen chains is a set of experiments, described previously in studies using both human embryonic kidney 293 and Chinese hamster ovary cells (Kobayashi and Uchiyama, 2003, Leinonen et al., 1999, Fukuda et al., 1997).

Moreover, global mRNA profiling and qPCR assays identified and verified the UPR pathway in human undifferentiated podocytes overexpressing *wt* or mutant COL4A3 chains. A similar differential increased expression was evident in the activated form of XBP1 demonstrated by the splicing assay in cells expressing again the *wt* or mutant collagen chain. It is not surprising that the overexpression of the *wt* or the mutant collagen IV chain activates the UPR signaling cascade on its own. However, the reason behind the increased UPR upregulation when overexpressing the mutant chain is intriguing. Two possible explanations could support these observations. The first one is that the differential UPR upregulation occurs because the cell is capable of applying quality control on the nascent single collagen

chain level. Additionally, since the mutant *COL4A3* chain has a lower affinity to the endogenous *COL4A4* and *COL4A5* chains, this could actually cause accumulation of the misfolded protein, leading to ER retention and subsequently higher activation of particular UPR genes depending on a dose dependent effect. Remarkably, previous studies of cases of hemorrhagic stroke in humans showed intracellular accumulation of mutant *COL4A1* and *COL4A2* chains in the cell's ER activating the UPR pathway (Jeanne et al., 2012). Interestingly mutations in collagen type I gene have been shown to form trimers, which aggregate in the ER. This activates the autophagy-lysosome pathway, in an effort to eliminate the aggregated procollagen trimers, localized in the ER (Ishida et al., 2009).

Importantly, knockdown of endogenous COL4A3 in differentiated human podocytes exhibited activation of the UPR pathway, as shown by upregulation of BiP and increased phosphorylation of PERK.

The current study clearly demonstrated that the UPR pathway can be triggered when podocytes overexpress a collagen chain as well as when the endogenously expressed COL4A3 chain is knocked down through siRNA silencing. In both cases UPR activation was evident by the elevation of BiP, indicating that cells could actually sense the protein chain imbalance exerting its quality control in the ER. Remarkably, the pathway has been shown to be differentially activated under these two conditions resulting in similar outcomes. In greater detail, COL4A3 overexpression resulted in the activation of the proapoptotic branch of the UPR as demonstrated by the upregulation of the proapoptotic marker CHOP. Nevertheless, COL4A3 downregulation activated PERK UPR branch as indicated by the increased levels of p-eIF2a, whereas CHOP levels remained unaltered. These results establish that UPR is a multipronged response that is cytoprotective or proapoptotic, depending on the nature and/or the severity of the stress the cell is facing agreeing with the current literature (Inagi et al., 2008, Tabas and Ron, 2011).

Moreover, considering that the *in vitro* experiments could extrapolate the results obtained, evaluation of the activation of the UPR in human biopsies was followed. This was based on the fact that AS and TBMN are diseases which take many years to become established whereas the cellular work we performed was accomplished in a relative brief experimental time frame in transiently transfected cells. UPR activation was demonstrated by the detection of increased BiP levels in patients carrying the *COL4A3*-p.G1334E mutation as compared to obese individuals. Particularly, BiP staining was more evident in the glomerulus of *COL4A3*-p.G1334E carriers, while BiP expression levels in the tubules remained unaffected when patients were compared with obese individuals. However, further experiments are needed in

order to examine if BiP upregulation in glomeruli of these patients is caused by the collagen accumulation or if it is a result of other downstream effects. Nevertheless, these data are in agreement with the findings of previous studies describing upregulation of ER stress proteins in kidney biopsy specimens obtained from patients diagnosed with other nephropathies, including diabetic nephropathy, FSGS and membranous nephropathy (Lindenmeyer et al., 2008, Bek et al., 2006, Markan et al., 2009).

Regarding the phenotypic analysis in a relevant *in vivo* knockin mouse carrying the *Col4A3*-p.G1332E mutation, activation of the UPR pathway was demonstrated for the first time. Interestingly, electron microscopy studies of kidney biopsies originating from this mouse model, revealed severe AS-like GBM pathology as early as at 3 months of age. At the 7-month time point, the histologic phenotype became more evident, while the mice also presented hematuria and proteinuria (not shown). UPR activation was apparent in the mutant mice by significant upregulation of the UPR markers BiP, p-PERK, and p-eIF2a in mRNA and protein levels, as well as nearly significant increase of XBP1 splicing. Results obtained from this model at the age of 3-months were conflicting with the *in vitro* overexpression findings showing, CHOP upregulation. However, the *in vivo* data were consistent with the COL4A3 knockdown experiments, as both demonstrated significant upregulation of the markers p-PERK and p-eIF2a whereas no change was observed in the proapoptotic marker CHOP. These conflicting results between overexpressing cells and the mouse model could in fact be explained through the assumption that the overexpression of the mutant chains in the cellular system results in severe stress by initiating the proapoptotic branch of the UPR, whereas various homeostatic mechanisms are activated *in vivo* shifting the UPR pathway toward the adaptive cytoprotective direction. However, studies using older mice are currently in progress in an effort to evaluate whether collagen IV mutations induce the proapoptotic branch of the UPR pathway at a later stage. Nevertheless, the significant eIF2a activation observed in these mice could actually demonstrate a translational attenuation event disrupting the highly coordinated podocyte's secretory capacity and thus leading to defective GBMs. Similar results were demonstrated by Tsang et al. who proved UPR activation in a transgenic mouse model expressing mutant collagen X in chondrocytes. Their findings did not show induction of cell death, but an effect on the differentiation and function of chondrocytes leading to chondrodysplasia was revealed (Tsang et al., 2007). Nevertheless, this appears to be the first time that UPR upregulation is evident in a knock-in Col4a3 mouse. Therefore, it would be interesting to test a similar UPR activation in the current established models of AS since it is reasonable to assume that knocking down or entirely knocking out one chain leaves

the other two *wt* chains in excess and susceptible to degradation, perhaps as a result of the quality control applied by the ER machinery and UPR activation. In fact, it would be interesting to look into whether autophagy is also activated in either of the two mice models, the knockout and the knockin.

To the best of our knowledge, this is the first study providing evidence of UPR activation generated through combined results originating from a podocyte culture model, human kidney biopsy specimens and a knockin mouse model carrying the *Col4a3*-p.G1332E mutation. Therefore, on the basis of these data it can be assumed that UPR activation could be an important player in the pathogenesis of AS/TBMN phenotype at the intracellular level. Moreover, it can also be speculated that different amino acid substitutions may activate the UPR pathway differentially and thereby lead to dissimilar phenotypes.

2.5 Conclusions and future perspectives

To conclude, combined experimental data originating from human podocytes cultures, human renal biopsy specimens and a knockin mouse model for a Col4a3 mutation were shown, that mutually associate the UPR pathway with the disease process. To date the exact pathogenic mechanism resulting from COL4 mutations in patients with AS or TBMN is poorly characterized. However, several connective tissue disorders associated with the expression of mutant extracellular matrix proteins have indicated ER stress and UPR activation to be the principal pathogenic mechanism leading to these conditions. ER stress in renal pathophysiology is a relatively new area of research. Therefore, identifying the implication of this mechanism in collagen IV trafficking defects would greatly improve AS/TBMN patient prognosis paving ways for the development of novel therapeutics, including the use of molecular chaperones. Finally, the clinical heterogeneity observed in patients with AS/TBMN could be related to the variation observed in UPR activation. Since UPR activation is directly linked to the extent and severity of the ER stress, this could lead to diverse clinical outcomes. Therefore, UPR related genes could be included in the pursuit for modifier genes.

Chapter 3: A new interacting partner of filtrin and a functional variant in the *NEPH3* gene conferring high risk of renal failure in primary hematuric glomerulopathies and of microalbuminuria in the general population

3.1 Scientific hypothesis and specific aims

As previously reported, microscopic hematuria, sporadic or familial, is a common condition with underestimated risks (Badenas et al., 2002, Buzza et al., 2001, Fogazzi et al., 2008, Hoefele et al., 2010, Kashtan, 2005a, Lemmink et al., 1996, Pierides et al., 2009, Slajpah et al., 2007, Temme et al., 2012, Voskarides et al., 2007). Recent findings from the MMRC and other groups, demonstrated that 50% of patients with *COL4A3/COL4A4* heterozygous mutations, a prevalent cause of familial microscopic hematuria, develop proteinuria with secondary focal segmental glomerulosclerosis (FSGS), after their third decade of life. In a significant percentage of patients, this is followed by chronic or end-stage kidney disease (CKD/ESKD) mostly at ages over 50-years (Voskarides et al., 2007, Voskarides et al., 2008b, Pierides et al., 2009, Deltas et al., 2011, Temme et al., 2012, Deltas et al., 2013a). Other genetic causes of familial hematuria that have been identified include, mutations in the *CFHR5* (Gale et al., 2010, Athanasiou et al., 2011) and *MYH9* (Seri et al., 2000) genes. About half the patients maintain throughout their life a benign microscopic hematuria or microscopic hematuria plus minimal proteinuria and normal kidney function. Conversely, the majority of non-heritable hematuria cases are attributable to IgA nephropathy. IgA nephropathy is considered by many to be a benign condition, despite the fact that longitudinal follow-up studies have revealed that 9-50% of patients progress to ESKD within 20 years of onset (Yoshida et al., 1995, Hsu et al., 2000, Cheng et al., 2011).

In TBMN and Alport syndrome, studies in animal models support the existence of genetic loci that influence disease progression (Andrews et al., 2002, Beirowski et al., 2006). In humans, an association of the *NPHS2*-p.R229Q variant with proteinuria and CRF in patients with TBMN (Tonna et al., 2008a) and familial hematuria has been reported (Voskarides et al., 2012). Modifier genes have been identified in other human inherited renal diseases, such as polycystic kidney disease and renal ciliopathies (Khanna et al., 2009, Liu et al., 2010). In addition, other environmental or co-morbidity factors may contribute to the progression in familial hematuria patients, including nutrition (e.g. high fat diet), hypertension, obesity, diabetes etc. None of these factors have been studied in depth yet.

For this study, it was hypothesized that the phenotypic heterogeneity seen in primary hematurias can be explained by the co-inheritance of modifier genes, associated with the

structure and function of the glomerulus, other than the variant *NPHS2*-p.R229Q (Voskarides et al., 2008b, Deltas et al., 2011, Hoefele et al., 2010). Specific objectives were as follows:

1. *To evaluate if genetic variants identified on important slit-diaphragm genes can actually serve as modifiers of disease severity in a cohort of 103 adult TBMN patients, who are heterozygous for known COL4A3 or COL4A4 mutations, performing a rigorous in silico analysis and genetic testing of several candidate genes.*

2. *To evaluate the role of the statistically significant variants in independent cohorts of primary hematuria and in cohorts of the general population.*

3. *To evaluate the effect of the statistically significant variants in vitro, through functional studies.*

4. *To detect and verify novel interacting partners for filtrin.*

3.2 Materials and methods

3.2.1 Study cohorts

HEMATURIA is a pooled cohort involving four different sub-groups (A, B, C and D) consisting of patients diagnosed with familial TBMN, familial or sporadic microscopic hematuria or IgA nephropathy *(Table 11).*

Sub-cohort A includes 103 patients with TBMN, members of 19 large Cypriot families archived at our Biobank at the MMRC. Seventy-eight patients of sub-cohort A are carriers of the *COL4A3*-p.G1334E mutation, 19 of 103 are heterozygous for the *COL4A3*-p.G871C mutation while six of 103 are heterozygous for the *COL4A4*-c.3854delG mutation. Individuals with "mild disease" (see below) and younger than 50-yo (born after January 1963) were excluded from this group, in an effort to reduce the number of patients with a falsely negative mild phenotype.

For this study, three additional hematuric sub-cohorts were included. Sub-cohort B, consisting of 69 familial microscopic hematuria cases of unknown cause (even though during the attainment of this study some of these patients were found to carry a *COL4A3* or a *COL4A4* mutation), sub-cohort C comprising 34 unrelated familial or sporadic microscopic hematuria cases (with a TBMN biopsy or with genetic studies in which hematuria segregated in their family with the *COL4A3/COL4A4* locus or mutations, or both) kindly provided by Prof. Judy Savige (Australia) and sub-cohort D involving 318 unrelated patients with biopsy-proven IgA nephropathy from Crete-Greece (72 patients) and the UK (246 patients). Likewise, for estimating the frequency of *NEPH3*-p.V353M in the general population, 462 anonymized DNA samples of healthy individuals were used from the MMRCs' Biobank collection.

Finally, for evaluating the association of *NEPH3*-p.V353M with microalbuminuria in the general population, three independent population-based samples were enlisted: 6531 DNA samples from the Framingham Heart Study (FHS), 3037 samples from the German KORAF4 and 1690 samples from Austrian SAPHIR study (Baumeister et al., 2010, Wichmann et al., 2005, Heid et al., 2006).

The study was designed and implemented according to the provisions of the Declaration of Helsinki and was approved by the Cyprus National Bioethics Committee. All participants gave their signed informed consent.

3.2.2 Clinical Assessment and Study Outcomes

Patients of sub-cohorts A, B, and C diagnosed with microscopic or macroscopic hematuria in the absence of chronic renal failure, or with hematuria and a low grade of proteinuria (<300 mg/24 hrs, but no chronic renal failure) were included in the "Mild" category. Individuals with "mild disease" and younger than 50-yo (born after January 1963) were excluded, in order to eliminate any false negative patient with mild phenotype *(Table 11)*.

Moreover, patients of sub-cohorts A, B and C diagnosed with hematuria and proteinuria ≥500 mg/24 hrs or with hematuria, proteinuria and chronic renal failure or ESKD were included in the "Severe" category. Renal failure was defined as the medical condition in which serum creatinine increases over 1.5 mg/dl. Patients diagnosed with any other related renal disease (e.g. over five years of diabetes, vesicoureteral reflux etc.) and described with a borderline proteinuria, or with an extreme body weight (outside ±2 SD of the cohort mean) were excluded from this category. Furthermore, there was no information about the existence or not of proteinuria regarding patients of sub-cohort D (IgAN); therefore they were included in the "Severe" subcategory, in the presence of chronic renal impairment (serum creatinine >1.5 mg/dL) or ESKD. Patients with serum creatinine <1.5mg/dL for at least 5 years following the diagnosis, were considered as "Mild". Patients for which there is inadequate information (i.e. patients with unknown course of renal function years after diagnosis) were excluded from this study. UK patients were enrolled from the MRC/Kidney Research UK National DNA Bank for Glomerulonephritis.

For the FHS sample group (cohort 2), urine albumin concentration was calculated using immuno-turbimetry (Tina-quant Albumin assay; Roche Diagnostics, Indianapolis, IN). Creatinine concentration in urine was quantified with a modified Jaffe method; urinary albumin was indexed to urinary creatinine to account for differences in urine concentrations (UACR; g:mg/g). UACR is a reliable measure of urinary albumin excretion and correlates with albumin excretion rates obtained from 24-hour urine collection (Bakker, 1999, Nathan et al., 1987). Microalbuminuria was defined as a UACR of >25 mg/g for women and UACR of >17 mg/g for men (National Kidney, 2002). The same approach was applied for cohorts KORAF4 and SAPHIR.

3.2.3 Candidate genes and SNPs selection

For this project, all registered non-synonymous SNPs (available in Ensembl database, www.ensembl.org) detected in genes expressing proteins of the SD (*NPHS1*, *NPHS2*,

NEPH1, *NEPH2*, *NEPH3*, *CD2AP*, *TRPC6*, *TJP1 (ZO1)*, *FAT1*, and *FAT2*), were selected in an attempt to assess their effect on hematuric glomerulopathies.

All candidate SNPs were carefully selected based on findings from genetic studies, animal model studies and functional studies, validating their effect on SD's function and integrity. This study mainly focused on nephrin and nephrin-like proteins (*NPHS1, NEPH1, NEPH2, NEPH3)*, since their extra-cellular Ig-like domains have been proven to have a noteworthy role in the formation of the SD (Tryggvason et al., 2006, Patrakka and Tryggvason, 2010). Single Nucleotide Polymorphism (SNP) selection was performed using two different prediction algorithms, SNPs3D (http://www.snps3d.org/) and SIFT (http://sift.jcvi.org/) (Yue et al., 2006, Ng and Henikoff, 2001). SNPs, predicted to be "deleterious" by both algorithms (high score), were further evaluated using any available population genetics data in Ensembl. Moreover, SNPs with a minor allele frequency ≥ 3% in Caucasian populations were selected for genotyping in sub-cohort A. Finally, SNPs being significant in sub-cohort A (*p*-values <0.05), were further evaluated using the pooled *HEMATURIA* cohort.

3.2.4 DNA Genotyping

All variants of interest were genotyped using the PCR-RFLP method (restriction enzymes were purchased from New England Biolabs, USA). Polymorphism *TJP1*-p.I790V was tested, using a modified forward primer, for creating a restriction site for *RsaI* enzyme. All PCR products were digested and electrophoresed on 2-3% (depending on cleavage sizes) agarose gels *(supplementary table 4)*.

Genotyping of UK IgA and FHS DNA samples was performed by the KASPar method (KBioscience-Herts, UK). Moreover, DNA samples of the KORAF4 and SAPHIR were genotyped using a TaqMan assay.

Finally, the flanking regions and the exons of *NEPH3* gene were further evaluated in 12 patients, using Sanger DNA sequencing ABI PRISM™ 3130*xl* (California, USA).

3.2.5 Splicing analysis of the *NEPH3* variant by an ex vivo assay

In order to evaluate the effect of *NEPH3*-p.V353M in splicing due to a change on the first nucleotide of exon 9, the region encompassing part of introns 7 and 10 and all sequences in between, was cloned in a pcDNA3.1 vector (Invitrogen, USA). A PCR product from a *NEPH3*-p.V353M heterozygous individual was subcloned in the *KpnI*/*AgeI* sites of the plasmid. Standard transformation was followed using *E. Coli* cells. Colony PCR-RFLP was performed for detecting the wild type and mutant colonies. Adequate plasmid DNA quantity

was isolated from wild type and mutant plasmids through the Hi-Speed Plasmid Midi Kit (Qiagen, Hilden, Germany). Plasmids were sequenced for sequence verification. Wild type and mutant constructs were transiently transfected into HEK293T cells. Two independent transfection experiments were performed for each construct. Cells were harvested 24 hours after transfection and total RNA was extracted using the RNeasy Mini Kit (Qiagen, Hilden, Germany), followed by reverse transcription (New England Biolabs, USA).

The cDNA amplification reaction was performed through primers complementary to sequences on exons 8 and 10. RT-PCR products (342 bp for normal splicing) were analysed on a 3% 3:1 agarose gel (Eurobio, France) for maximum resolution.

3.2.6 Bioinformatic analysis of *NEPH3* protein and mRNA

In order to predict the 2D structure of the *NEPH3*-wt and *NEPH3*-p.V353M (protein and mRNA), the CLC main workbench V.6.9.1 software was used, employing the Hidden Markov Model algorithm.

Moreover, protein and mRNA sequences were extracted in FASTA format (Ensembl database) and aligned using ClustalW algorithm (CLC main workbench), implementing multiple alignments for *NEPH3* protein orthologs and paralogs.

3.2.7 Site-directed mutagenesis, subcloning and transformation

Variant *NEPH3*-p.V353M was inserted in the pCMV6-*NEPH3*-wt-Myc/DDK (Origene-RC215405) using the QuickChange II XL-site directed mutagenesis kit (Stratagene®).

Following mutagenesis, heat shock competent DH5a competent cells™ (Invitrogen™) were transformed, followed by incubation of the transformed cells on LB agar plates containing kanamycin. Colonies were selected and incubated in LB broth in order to isolate the mutated vector using NucleonSpin® Plasmid (Macherey-Nagel®). Plasmids were sequenced to confirm the insertion of *NEPH3*-p.V353M. Additionally, cDNA of *NEPH3*-wt was subcloned from the pCMV6-*NEPH3*-wt-Myc/DDK to the pCMV6-AC-HA vector. Briefly, both vectors were double digested using BamHI and NotI. Insert and vector were isolated by gel purification and ligated with a sticky end ligase. Ligation products were transformed using DH5a™ (Invitrogen™) cells for isolating the pCMV6-AC-*NEPH3*-wt-HA vector. Subcloning was confirmed via sequencing and restriction digestion.

Moreover, for evaluating the interaction and co-localization of *NEPH3*-wt or *NEPH3*-p.V353M with nephrin-wt (*NPHS1*) and itself (*NEPH3*-wt or *NEPH3*-p.V353M), human *NPHS1* (nephrin) cDNA was cloned into a modified pcDNA6 expression vector coding for

the CD5 signal peptide fused to the V5-tag sequence (sV5-tag) followed by restriction sites to insert the cDNA. Additionally, both *NEPH3* cDNA variants (353V, 353M) were also sub-cloned into the pcDNA6 expression vector coding for the CD5 signal peptide fused to the V5-tag sequence (sV5-tag) (kindly provided by Prof. T. Benzing lab, Cologne, Germany).

3.2.8 Cell culture and transfection

For the *in vitro* experiments, two different cells lines were recruited: human immortalized podocytes (kindly provided by Prof. M. Saleem lab, Bristol, UK) and human embryonic kidney cells HEK293T (ATCC). Both cell lines were used in an effort to identify new interacting partners of Neph3 and to evaluate the effect of *NEPH3*-p.V353M in the interaction and localization of the mutated protein.

Immortalized human podocytes were cultured in RPMI 1640-based medium supplemented with 200 units/ml penicillin and streptomycin (Roche Applied Science), insulin-transferrin-selenium (ITS) (Gibco) and 10% fetal bovine serum (Gibco) as described previously. The podocytes were grown in 75-cm^2 flasks at 33°C and 5% CO_2 and were differentiated by thermo switching at the nonpermissive temperature of 37°C in 5% CO_2 for fourteen days as previously described (Saleem et al., 2002).

Human embryonic kidney cells were cultured in DMEM medium with the addition of 200 units/ml penicillin and streptomycin (Roche Applied Science) and 10% fetal bovine serum (Gibco). HEK293T were grown in 75-cm^2 flasks at 37°C and 5% CO_2.

Cells were transiently transfected at 70% confluency, using Lipofectamine 2000 (Invitrogen) according to the manufacturers' protocol and the requirements of the current experiment. Forty-eight hours post transfection samples were collected for immunoprecipitation, immunoblotting or immunofluorescence experiments. Transfection efficiency was confirmed in all samples through immunofluorescence. When indicated, transfected podocytes were incubated post transfection for 14 h with 10ug/mL with tunicamycin (Sigma) prior to sample collection as previously described (Weichert et al., 2011).

3.2.9 Co-immunoprecipitation

Immunoprecipitation experiments were performed as described previously (Huber et al., 2003a). Briefly, for the detection of new interacting partners or for the evaluation of the effect in the interaction of the *NEPH3*-p.V353M with the new found binding partners, human undifferentiated podocytes were transiently transfected with full-length pCMV6-*NEPH3*-wt-FLAG or pCMV6-*NEPH3*-p.V353M-FLAG using Lipofectamine 2000 (Invitrogen).

Following a 48-hour incubation, a total of 2-5 100-cm^2-culture dishes were washed in PBS and lysed in lysis buffer (50 mM Tris HCl, pH 7.4, with 150 mM NaCl, 1 mM EDTA, and 1% TRITON X-100) containing 2X protease inhibitors (Roche).

Following centrifugation at 12,000 *g* (10 min; 4°C), supernatants containing equal amounts of total protein were incubated overnight at 4°C with 20 ul of anti-FLAG M2 affinity gel (Sigma). Resin was later centrifuged and washed for several times with wash buffer (0.5 M Tris HCl, pH 7.4, with 1.5 M NaCl). Immunoprecipitated FLAG fused *NEPH3* was eluted by heating in 2x sample buffer (125 mM Tris HCl, pH 6.8, with 4% SDS, 20% (v/v) glycerol, and 0.004 % bromphenol blue). In order to minimize the denaturation of the antibody, no reducing agent was added to the sample buffer. Proteins were separated on a 7.5% SDS-PAGE for Brilliant Blue G-Colloidal Concentrate staining (Sigma) or for immunoblotting as described (Lehtonen et al., 2005, Pieri et al., 2014).

For estimating the effect of *NEPH3*-p.V353M on the interaction with *NEPH3*-wt, *NEPH3*-p.V353M or with *NPHS1*-wt, co-immunoprecipitation experiments were performed using the following combinations:

i) Neph3-Nphs1 cross-interaction: Comparison between *NEPH3*-353V-FLAG binding to *NPHS1*-wt-V5 and *NEPH3*-353M-FLAG binding to *NPHS1*-wt-V5

ii) Neph3-Neph3 (testing homodimerization): Comparison between *NEPH3*-wt-HA binding to *NEPH3*-wt-FLAG, *NEPH3*-wt-HA binding to *NEPH3*-353M-FLAG and *NEPH3*-353M-HA binding to *NEPH3*-353M-FLAG.

For this set of experiments, HEK 293T cells were transiently doubly transfected using Lipofectamine 2000 (Invitrogen), and incubated at 37°C for 48 hrs. Cells were washed in PBS and lysed in lysis buffer (50 mM Tris HCl, pH 7.4, with 150 mM NaCl, 1 mM EDTA, and 1% TRITON X-100) containing 2X protease inhibitors (Roche).

Following centrifugation at 12,000 *g* (10 min; 4°C), supernatants containing equal amounts of total protein were incubated overnight at 4°C with 20 ul of anti-FLAG M2 affinity gel (Sigma). Resin was later centrifuged and washed for several times with wash buffer (0.5 M Tris HCl, pH 7.4, with 1.5 M NaCl). Immunoprecipitated FLAG fused *NEPH3* was eluted by heating in 2x sample buffer (125 mM Tris HCl, pH 6.8, with 4% SDS, 20% (v/v) glycerol, and 0.004 % bromphenol blue).

As stated above, in order to minimize the denaturation of the antibody, no reducing agent was added in the sample buffer. Proteins were separated on a 7.5% SDS-PAGE for Brilliant Blue G-Colloidal Concentrate staining (Sigma) or for immunoblotting as described (Lehtonen et al., 2005, Pieri et al., 2014).

3.2.10 Mass spectrometry

As previously described, co-immunoprecipitation was performed in equal amounts of lysates from human undifferentiated podocytes as previously described. Bound proteins were separated by 7.5% SDS-PAGE, fixed and stained with Brilliant Blue G-Colloidal Concentrate (Sigma) according to the manufacturers' protocol.

Bands differing between the control and *NEPH3*-wt-FLAG transfected cells, were excised from the gel and sent for liquid chromatography-mass spectrometry (LC-MSMS) (Orbitrap) analysis at the European Molecular Biology Laboratory (EMBL) Proteomics Core Facility.

Briefly, removed bands were digested with trypsin in-gel and peptides were analysed with LC-MSMS according to EMBLs' protocol. For protein identification, Mascot software (Matrix Science) was employed as the default search engine.

3.2.11 Immunoblotting

Equal volumes of precipitates were separated by 7.5% SDS-PAGE and transferred to polyvinylidene difluoride membranes (Millipore). Transblots were incubated with primary antibodies (anti-FLAG; Santa Cruz Biotechnology, anti-V5; Invitrogen, anti-NEPH3; R&D, anti-MYH9; Abcam) followed by incubation with HRP-goat anti-rabbit and anti-mouse secondary antibodies (Santa Cruz Biotechnology).

In order to evaluate the UPR activation, ER stress antibody sampler kit (Cell Signaling) or anti-BiP, anti-PERK, anti-IRE1a, anti-pPERK, anti-peIF2a and anti-CHOP (Santa Cruz Biotechnology) were used followed by incubation with HRP-goat anti-rabbit secondary antibody (Santa Cruz Biotechnology).

Proteins were detected using the Enhanced ChemiLuminescence (Amersham Biosciences, Buckinhamshire, United Kingdom) and visualized using the ChemiDOC XRS documentation system (Biorad, CA, USA). Densitometry was performed through the publicly available ImageJ Software (NIH, Bethesda, USA).

3.2.12 Double indirect immunocytochemistry

For double indirect immunocytochemistry experiments, human differentiated podocytes were utilized in order to demonstrate the co-localization of the endogenously expressed Neph3 and the newfound interacting partners. Podocytes were cultured on glass coverslips and differentiated by thermo switching to 37°C (incubation at 5% CO_2) for 14 days.

Moreover, in order to test the effect of the *NEPH3*-p.V353M on the localization of itself and of other interacting partners (*NEPH3*-wt, *NPHS1*-wt and *MYH9*) human undifferentiated podocytes were transiently transfected, using the combinations described in *Table 9*.

Table 9: *Combinations employed for evaluating localization effect of NEPH3-p.V353M to itself and other interacting partners*

NEPH3-wt-HA	*NEPH3*-wt-FLAG
NEPH3-wt-HA	*NEPH3*-p.V353M-FLAG
NEPH3-wt-FLAG	*NPHS1*-wt-V5
NEPH3-p.V353M-FLAG	*NPHS1*-wt-V5
NEPH3-wt-FLAG	endo-MYH9
NEPH3-p.V353M-FLAG	endo-MYH9

Following a 48-hour incubation period, coverslips were fixed with 3% paraformaldehyde in PBS for 10 minutes and permeabilized in 0.1% Triton X-100 for one minute. All cells were blocked with 2% BSA in PBST (0.1%) for an hour and incubated as indicated with primary and secondary antibodies in blocking solution overnight at 4^{o}C or for one hour at room temperature respectively. For nucleus staining, cells were incubated with Hoechst solution (Invitrogen) at a dilution of 1:10000 for one minute and mounted in fluorescence mounting medium (DAKO).

3.2.13 Mouse kidney immunohistochemistry

For this set of experiments, we utilized adult mice kidneys in order to evaluate the colocalization of Neph3 with the newfound interacting partners.

Briefly, mice were anesthetized by an intraperitoneal injection of Avertin (2,2,2-tribromoethyl and tertiary amyl alcohol; 0,2mL/10gr mouse body weight) and perfused with MEMFA through the heart. Later, kidneys were removed and placed again in MEMFA solution, at 4^{o}C for 40 minutes with rotation. Tissues were washed in PBS and placed in a 15% sucrose solution overnight and the next day they were further incubate in 30% sucrose, until they settled at the bottom of the tube. Soon afterwards, both kidneys were placed in cryomolds covered with OCT and snap frozen using isopentane.

Using a cryostat, tissues were cut in 7-μm slices and mounted on positively charged slides. For antigen retrieval, kidney sections were incubated with 6M Urea, Glycine-HCl 0,1M pH 3.5 solution at 4^{o}C for 30 minutes. Moreover, these kidney sections were washed with PBS

and incubated with blocking solution for 60 minutes at room temperature. Next, tissues were placed in a humidified immunochamper and incubated simultaneously with primary anti-MYH9; Abcam and anti-NEPH3; R&D overnight at 4^{o}C. The following day, after several washes with PBS kidney sections were incubated with anti-mouse or anti-rabbit fluorescent secondary antibodies respectively for one hour at room temperature. For nucleus staining, cells were incubated with Hoechst solution (Invitrogen) at a dilution of 1:10000 for one min and mounted in fluorescence mounting medium (DAKO).

3.2.14 Fluorescence microscopy

Immunofluorescence preparations (cells and kidney tissues) were examined on a Zeiss Axiovert 200M inverted fluorescence microscope equipped with the Zeiss Axiovision 4.2 software, on a laser scanning confocal microscope Leica TCS SP2 equipped with the Leica LCS software and on a laser scanning confocal microscope Zeiss LSM 710 equipped with the ZEN 2010 software. Digital images were recorded and composed using Adobe Photoshop 5.0.

3.2.15 Statistical analysis

Data analysis, including the genotypic and allelic statistical analysis, the calculations of the odds ratios and the accomplishment of independent t-tests, was performed using the SPSS v.13 or the Graph Prism v.5.01.

Both dominant and recessive models of inheritance were tested when this was possible. Moreover, *p*-values were calculated using the Pearson Chi-square test or the Fischer's exact test (two sided) while logistic regression was applied for adjusting for gender and age. R statistical package v.3.0.1 was used for the calculations regarding the KORAF4 and SAPHIR cohorts and for the meta-analysis.

Allelic association analysis for the *HEMATURIA* cohort was corrected for the presence of related individuals using a quasi-likelihood score function (QLS test) in order to estimate the allele frequencies and their significance in large inbreeding pedigrees, based on kinship coefficients.

A p-value < 0.05 was considered as the cut-off level.

3.3 Results

3.3.1 Identification of Myh9 as a Neph3 interacting protein

Protein extracts from immunoprecipitation experiments of undifferentiated podocytes transiently transfected with *NEPH3*-wt-FLAG and immunoprecipitated with anti-FLAG M2 affinity gel (Sigma), were separated by SDS/PAGE and stained with Brilliant Blue G-Colloidal Concentrate (Sigma). This resulted in the identification of seven different bands interacting specifically to *NEPH3*-wt-FLAG but not the control FLAG *(Figure 30)*. Each band was excised, digested with trypsin and identified with mass spectrometry. The proteins detected through the mass spectrometry analysis are stated below.

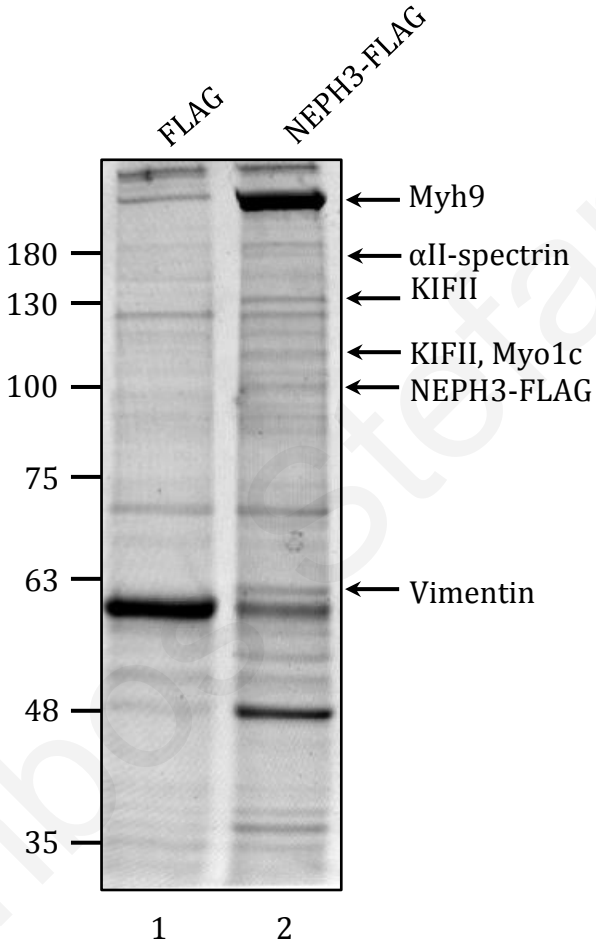

Figure 30: Identification of Neph3 interaction partners

Identification of NEPH3 interaction partners by NEPH3-FLAG immunoprecipitation assays and mass spectrometry. Neph3-FLAG or FLAG were incubated with podocytes lysate, and the bound proteins were separated by 7.5% SDS-PAGE followed by Brilliant Blue G-Colloidal Concentrate staining. The bands observed in Neph3-FLAG precipitates (lane 2) were identified by mass spectrometry as myosin 9, αII-spectrin, KIFII, MyoIc and vimentin.

The band detected at about 200-kDa was identified as myosin 9 (Myh9) while the 180-kDa band contained Myh9 and αII-spectrin. Moreover, the 130-kDa band was shown to be the ATP-dependent RNA helicase A and kinesin-like protein KIFII. Additionally, the 110-kDa band was shown to contain the unconventional myosin Ic, kinesin-like protein KIFII and kinesin I heavy chain.

The 100-kDa and 90-kDa bands were identified as *NEPH3*-FLAG as expected, while the band at 60-kDa contained vimentin.

All the above proteins (Myh9, αII-spectrin, Myo1c and vimentin) are known to be expressed in human podocytes and to interact with proteins of the slit diaphragm. Interestingly, Myh9 has been shown to be expressed in the glomerulus as well as in tubular and endothelial cells (Noris, 2012). Moreover, αII-spectrin has been proven to be part of the nephrin multiprotein complex (Lehtonen et al., 2005). It is important to note that Arif et al. have recently demonstrated the interaction of motor protein Myo1c with Neph1, which enables the transport of Neph1, a homologue of Neph3, to the plasma membrane of the podocyte (Arif et al., 2011).

3.3.2 Neph3 interacts with Myh9 in vitro

In order to confirm the interaction of Neph3 and Myh9, *NEPH3*-wt-FLAG was transiently transfected in human undifferentiated podocytes and precipitated using anti-FLAG M2 affinity gel (Sigma). The immunoprecipitated complex was further analysed using western blot, in order to prove the presence of Myh9 in *NEPH3*-wt-FLAG precipitates *(Figure 31A)*.

Moreover, similar reciprocal experiments were performed, this time precipitating the endogenously expressed Myh9 in human undifferentiated podocytes transiently transfected with *NEPH3*-wt-FLAG. Again, *NEPH3*-wt-FLAG was detected in the precipitates of Myh9 *(Figure 31B)*. Additional data supporting the interaction of the endogenously expressed Neph3 and Myh9 were obtained by precipitating the Myh9 from human undifferentiated podocytes. This time, the endogenously expressed Neph3 was detected with immunoblotting in precipitates of Myh9 *(Figure 31C)*.

3.3.3 Neph3 colocalizes with Myh9, nephrin and actin cytoskeleton in cultured podocytes

Immunofluorescence experiments were performed in order to study the colocalization of Neph3 with Myh9 in human differentiated podocytes. Moreover, dual immunofluorescence experiments were carried out using phalloidin for actin staining or anti-nephrin with anti-Neph3, to validate the co-localization of Neph3 with actin cytoskeleton and nephrin.

Neph3 in differentiated podocytes showed homogenous expression at the cell periphery and not just at the cell-cell junctions. Additionally, Neph3 displayed filamentous cytoplasmic expression and nuclear staining.

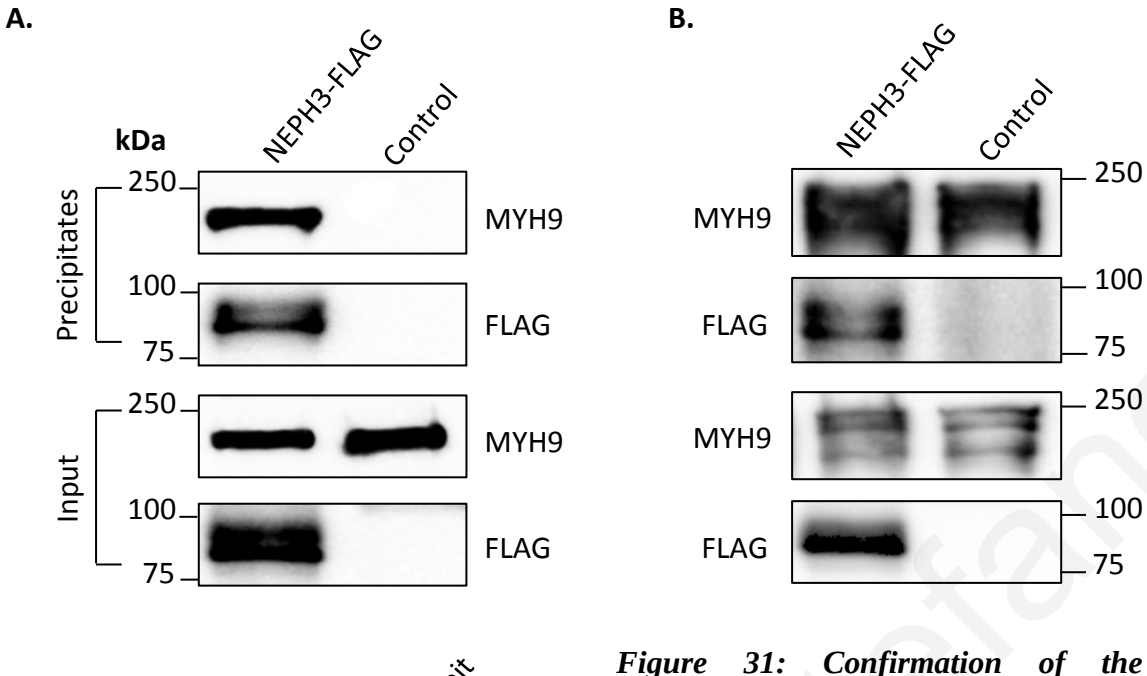

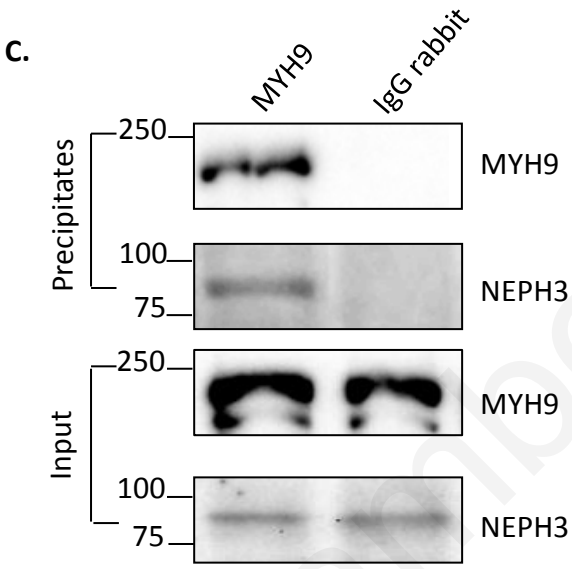

Figure 31: Confirmation of the interaction between Neph3 and Myh9

Eluates from Neph3-FLAG (A) and MYH9 (B, C) affinity columns were separated on SDS-PAGE and subjected to immunoblotting, in order to confirm the results from mass spectrometry analysis.

Immunoprecipitation was performed in human undifferentiated podocytes transiently transfected with NEPH3-FLAG. (A) The MYH9 was present in the precipitates using anti-FLAG affinity gel, while NEPH3-FLAG was found in the precipitates of Myh9 (B).

Immunoprecipitation of the endogenous Myh9 in human undifferentiated podocytes was able to pull down the endogenous Neph3 (C) confirming in that way all the previous results.

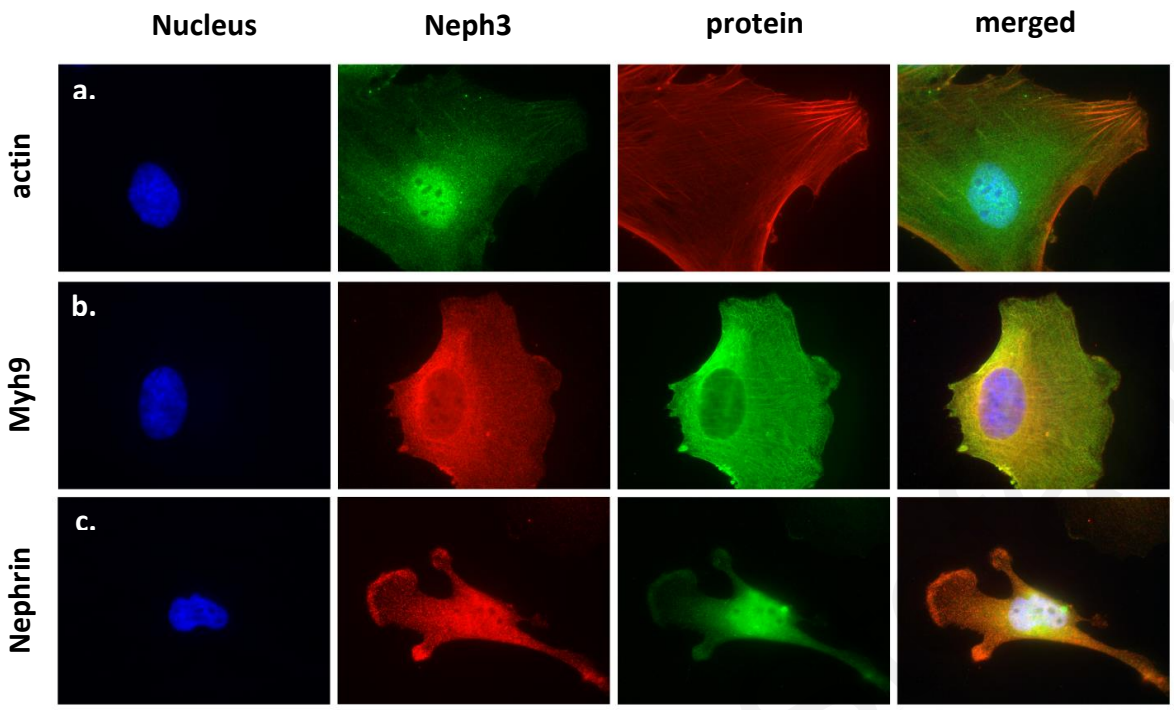

Figure 32: Subcellular localization of Neph3 with Myh9, nephrin and actin

Double immunolabelling experiments were performed on cultured differentiated podocytes and analyzed by confocal microscopy. Column 1: nucleus (blue). Column 2: Neph3. Column 3: (a), actin (b), MYH9 (c), nephrin. Colocalization of Neph3 and studied proteins, observed as a merged signal in yellow staining (Column 4) with the Zeiss Axiovision 4.2 analysis software.

Double labelling of Neph3 and phalloidin revealed co-localization of Neph3 with actin filaments in the cytoplasm, at the tips of cell processes and cell surfaces in forming processes. Myh9 distribution was observed in a filamentous pattern extending to the cell surface, analogous to the pattern of Neph3 expression described above. This was confirmed through the co-localization of the two molecules, with both proteins showing a cytoplasmic linear distribution and an increased expression at the cell surface, in membrane ruffles *(Figure 32)*.

3.3.4 Neph3 and Myh9 are localized in the glomerular epithelium in mouse kidney

Next, immunofluorescence experiments were performed on semithin cryosections from mice kidney to determine the localization of the putative interaction and co-localization of Neph3 with Myh9 demonstrated in cellular lysates and cytoimmunofluorescence experiments. Both proteins are expressed in glomeruli. Staining for Neph3 and Myh9 was confined to the foot process layer that lines the capillary loops of the podocytes. Interestingly Myh9 was detected

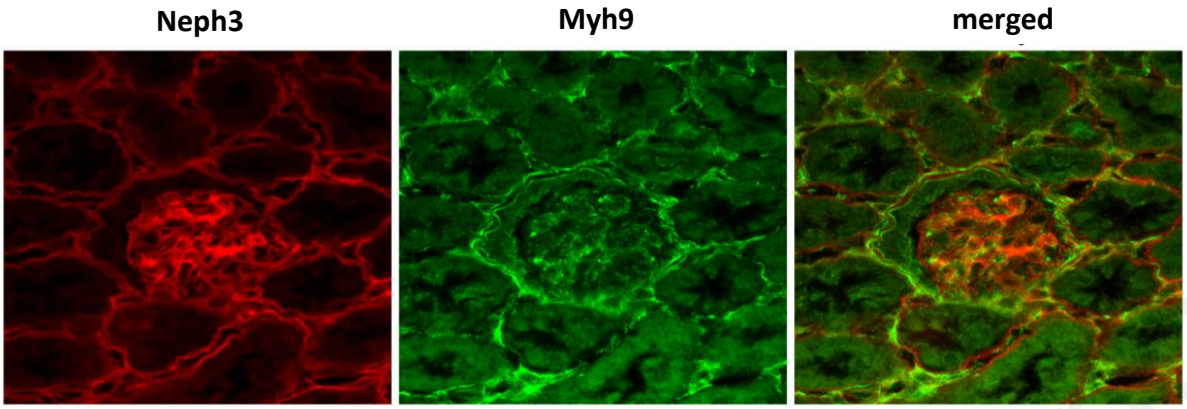

Figure 33: Localization of Neph3 and Myh9 in adult mouse glomeruli

Neph3 and Myh9 are distributed in a pattern along the glomerular capillaries. Double labeling with Neph3 shows that Myh9 and Neph3 colocalize in the foot process layer of podocytes. Mouse kidneys were cryoprotected, infiltrated with glucose, and processed for semithin cryosectioning. Mouse kidneys were perfusion-fixed with MEMFA before processing for semithin cryosectioning. Sections were labeled with anti-Neph3 and anti-Myh9 and examined by immunofluorescence.

in kidney tubules as well as in glomeruli, whereas Neph3 was restricted to podocytes. Thus, the Myh9 identified in the Neph3 complex was found to be expressed in podocytes and to codistribute with Neph3 in the foot processes *(Figure 33)*.

3.3.5 Candidate SNPs genotyping – The emergence of *NEPH3*-p.V353M variant in the *HEMATURIA* cohort

In order to evaluate the severity of all registered non-synonymous single nucleotide polymorphisms (SNPs) found in genes expressing vital proteins of the SD (Nphs1, Nphs2, Neph1, Neph2, Neph3, CD2AP, TRPC6, TJP1 (known as ZO1), FAT1 and FAT2), two different algorithms were employed, the SNPs3D (http://www.snps3d.org/) and the SIFT (http://sift.jcvi.org/).

According to this evaluation, six SNPs located in 4 different genes, *TJP1*-I790V, *TJP1*-N471S, *FAT1*-R1273H, *FAT2*-R574C, *FAT2*-G1515S and *NEPH3*-V353M, were predicted to cause a functionally defective protein.

Table 10: *Genotype associations for four SNPs in sub-cohort A*						
SNP	**Alleles**		**11+12 Vs 22**		**22+12 Vs 11**	
	1	**2**	***p*-value**	**OR (95% CI)**	***p*-value**	**OR (95% CI)**
***NEPH3*-p.V353M (rs 35423326)**	**V**	**M**	-	-	**0.036***	**NA**
***TJP1*-p.I790V (rs 7179270)**	I	V	0.505*	NA	0.195	0.53 (0.20-1.20)
FAT2-p.R574C (rs 1432862)	R	C	0.276	1.66 (0.66-4.17)	0.341*	0.46 (0.11-1.87)
FAT2-p.G1515S (rs 2278370)	G	S	-	-	0.542	1.63 (0.45-5.54)

These non-synonymous SNPs were initially genotyped in sub-cohort A of the *HEMATURIA* cohort, in order to detect SNPs acting as modifiers regarding the severity of the disease. *TJP1*-N471S and *FAT1*-R1273H were non-instructive due to genotypic homogeneity. *TJP1*-I790V, *FAT2*-R574C and *FAT2*-G1515S were not associated with disease severity but *NEPH3*-V353M (rs35423326) was suggestive for association with a severe phenotype in renal disease (p=0.036 for genotypic association) *(Table 10)*.

In order to confirm this finding, *NEPH3*-V353M was further evaluated in three additional hematuric sub-cohorts of the *HEMATURIA* cohort. Among the 301 severely affected patients, 24 were heterozygous, one was homozygous while among the 223 mildly affected patients, three were heterozygous genotypes *(Table 11)*. A genotypic association analysis presented a statistical significance with a *p*-value equal to 3.0×10^{-4} (OR=6.64, CI 1.98-22.29), while following adjustment for gender and age the *p*-value was equal to 3.0×10^{-3}. Moreover, an allelic association analysis indicated a statistical significance with a *p*-value equal to 2.0×10^{-4} and 4.2×10^{-3} after adjusting for patients' kinships *(Table 11)*. Additionally, genotyping of the general population for calculating the allele frequency of the variant 353M resulted in a value equal to 2.7%, which is comparable with other populations (www.ensembl.org). Interestingly, the only homozygous 353M/M patient that was identified belongs to the severely affected category. These results were consistent with Hardy-Weinberg equilibrium.

Table 11: *Frequencies and statistical analysis of variant NEPH3-V353M in the various hematuric sub-cohorts, based on disease severity. The four sub-cohorts presented here comprise the larger HEMATURIA cohort*

		Genotype counts			Genotype frequency			Allele counts		Allele frequency		Statistics		
Cohort	N	VV	VM	MM	VV	VM	MM	V	M	V	M	"Mild" v. "Severe" [a]	"Mild" v. "Severe" [b]	Odds Ratio (Dominant model)
General population	462	437	25	0	0.946	0.054	0	899	25	0.973	0.027			
Mild														
A	44	0	0	0	1.0	0	0	88	0	1.0	0			
B	35	0	0	0	1.0	0	0	70	0	1.0	0			
C	22	0	0	0	1.0	0	0	44	0	1.0	0			
D	122	119	3	0	0.975	0.025	0	241	3	0.988	0.012			
Total	**223**	**220**	**3**	**0**	0.987	0.013	0	**443**	**3**	0.993	0.007			
Severe														
A	59	53	6	0	0.898	0.102	0	112	6	0.949	0.051	**3.6×10^{-2}**		
B	34	32	2	0	0.941	0.059	0	66	2	0.971	0.029			
C	12	10	2	0	0.833	0.167	0	22	2	0.917	0.083			
D	196	181	14	1	0.923	0.071	0.006	376	16	0.959	0.041			
Total	**301**	**276**	**24**	**1**	0.917	0.080	0.003	**576**	**26**	0.957	0.033	**3.0×10^{-4}**	**2.0×10^{-4}**	**6.64 (1.98, 22.29)**
												3.0×10^{-3}	**4.2×10^{-3}**	**6.63 (1.94, 22.68)**

3.3.6 Testing for association of *NEPH3*-p.V353M with microalbuminuria in cohorts of the general population

Genotyping of the *NEPH3*-V353M variant in 6531 DNA samples from participants of the Framingham Heart Study (FHS), revealed an association between the rare homozygous genotype 353M/M and microalbuminuria (p=1.0x10-3 adjusting for gender and age, OR=5.92). Association among serum creatinine or cystatin values with 353M/M was not proven (results not shown).

Moreover, in order to reproduce the result of the association between 353M/M and microalbuminuria, *NEPH3*-V353M was further evaluated in two additional general population cohorts, KORAF4 and SAPHIR. Statistical analysis confirmed the association; however, genotyping results regarding SAPHIR did not reach a statistical significance due to the low number of homozygous genotypes M/M *(Table 12).*

A final meta-analysis, including 11,258 subjects, revealed a *p*-value of p=1.3x10-5 for the recessive model with an OR of 7.46 (95% CI 2.50-22.23) *(Table 13).*

Additionally, no other non-synonymous SNPs on *NEPH3* were found to be in linkage disequilibrium with the 353M allele, after direct re-sequencing of the exons of the *NEPH3* gene in 12 patients from the HEMATURIA cohort. However, two synonymous variants, p.G164G and p.A351A in *NEPH3,* were found in partial linkage disequilibrium with V353M, but without reaching a statistical significance as modifiers (results not shown).

Table 12: *Demographic data of the three general population cohorts genotyped for NEPH3-V353M*

	Microalbuminuria: CASES	No microalbuminuria: CONTROLS	*p*-values
Cohort: FHS	603 (0.090)	5.928 (0.908)	
Age of urine test time	55.9 (±13.3)	46.3 (±12.2)	<0.001
Women	325 out of 603 (0.539)	3.168 out of 5.928 (0.534)	0.831
Cohort: SAPHIR	165 (0.098)	1.525 (0.902)	
Age at urine test time	51.5 (±5.4)	51.4 (±6.0)	0.96
Women	52 out of 165 (0. 315)	578 out of 1.525 (0.379)	0.11
Cohort: KORAF4	397 (0.131)	2.640 (0.869)	
Age at urine test time	63.8 (±13.1)	55.0 (±12.9)	<2.2e-16
Women	160 out of 397 (0.403)	1.410 out of 2.640 (0.534)	1.01e-06

Table 13: *Frequencies and statistics of NEPH3-V353M in the general population cohorts including a meta-analysis*

		Genotype counts			Genotype frequency			Allele counts		Allele frequency		Statistics		
Cohort	N	VV	VM	MM	VV	VM	MM	V	M	V	M	Dominant model	Recessive model	Odds Ratio (Recessive model)
Controls (without MA)														
FHS	5928	5508	415	5	0.929	0.070	0.001	11431	425	0.964	0.036			
KORAF4	2640	2487	152	1	0.942	0.057	0.001	5126	154	0.971	0.029			
SAPHIR	1525	1423	101	1	0.933	0.066	0.001	2947	103	0.966	0.034			
Total (meta-analysis)	**10093**	**9418**	**668**	**7**	0.933	0.066	0.001	**19504**	**682**	0.966	0.034			
Cases (with MA)														
FHS	603	561	39	3	0.930	0.065	0.005	1161	45	0.963	0.037	0.946	**$1.0x10^{-3}$**	**5.92** (1.41-24.85)
KORAF4	397	380	15	2	0.957	0.037	0.006	775	19	0.976	0.024	ND	**$1.8x10^{-3}$**	**13.36** (1.21-147.71)
SAPHIR	165	153	11	1	0.927	0.067	0.006	317	13	0.961	0.039	0.738	0.147	**9.29** (0.58-149.27)
Total (meta-analysis)	**1165**	**1094**	**65**	**6**	0.939	0.056	0.005	**2253**	**77**	0.967	0.033	ND	**$1.3x10^{-5}$**	**7.46** (2.50-22.23)

3.3.7 Splicing analysis of the *NEPH3* variant

Variant 353M results from the substitution of the first nucleotide of exon 9 (GTG>ATG); therefore it was hypothesized that this might affect mRNA splicing. A 342 bp fragment, extending from intron 7 to intron 10, was cloned and transfected in HEK293T cells. Comparison of the RT-PCR products for the normal and mutant allele failed to show a distinct band that could be interpreted as a product of aberrant splicing, implying that 353M does not affect normal splicing of *NEPH3 (Figure 34).*

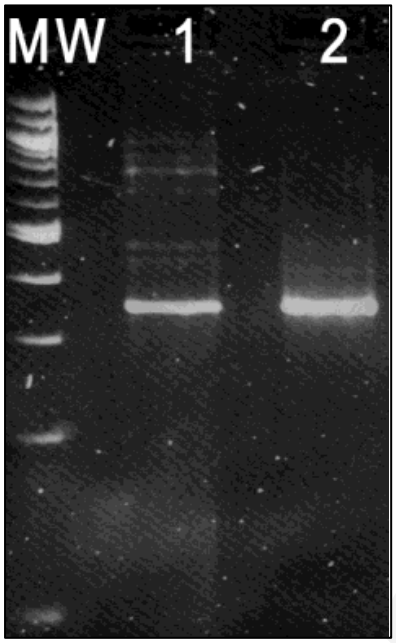

Figure 34: RT-PCR electrophoresis, testing for abnormal splicing

The only RT-PCR band that was strongly visible was common for both alleles, as represented by the 342 bp expected band. No other distinct band exists that could be interpreted as a product of aberrant splicing. This result was also confirmed by fluorescent PCR [capillary electrophoresis in ABI PRISM3130xl genetic analyzer (Applied Biosystems, Foster City, CA)]. MW: Molecular Weight; Lane 1: RT-PCR from cDNA containing the 353-GTG (V) codon; Lane 2: RT-PCR from cDNA containing the 353-ATG (M) codon.

3.3.8 Bioinformatic analysis

At protein level, valine at position 353 of the protein is highly conserved across evolution *(Figure 35)* and is located within the 4th Ig-like domain (Neph3 has five Ig-like domains) of the extra-cellular N-terminal region of the Neph3 protein. Its substitution by a methionine residue is predicted to eliminate a local β-strand domain of the protein *(Figure 36).* At the mRNA level, guanine to adenine substitution does not seem to cause any significant structural change, as tested with the 2D mRNA prediction model using the CLC Main Workbench 6 software package *(Figure 37).*

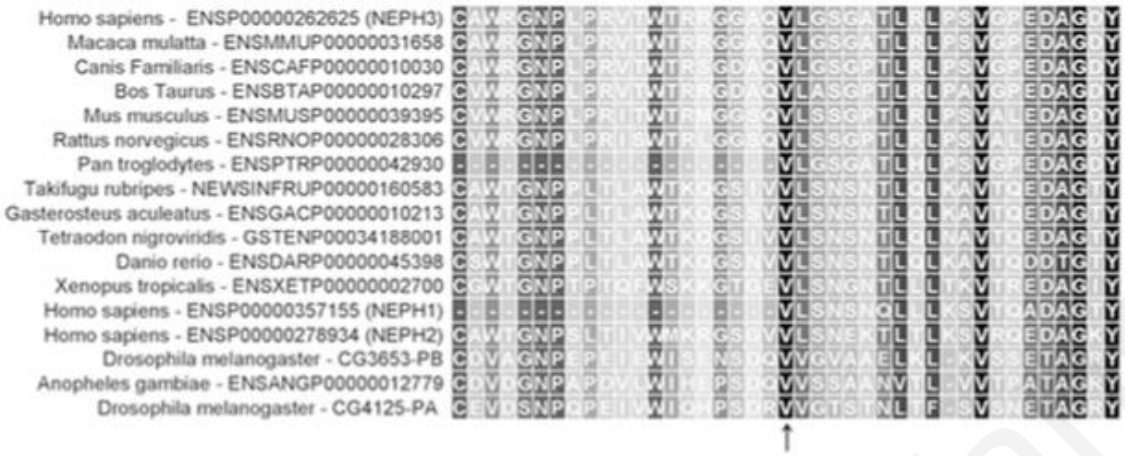

Figure 35: Alignment of orthologs and paralogs sequences of the Neph3 protein around the 353V residue position.

Arrow indicates the conserved valine at position 353 among different species

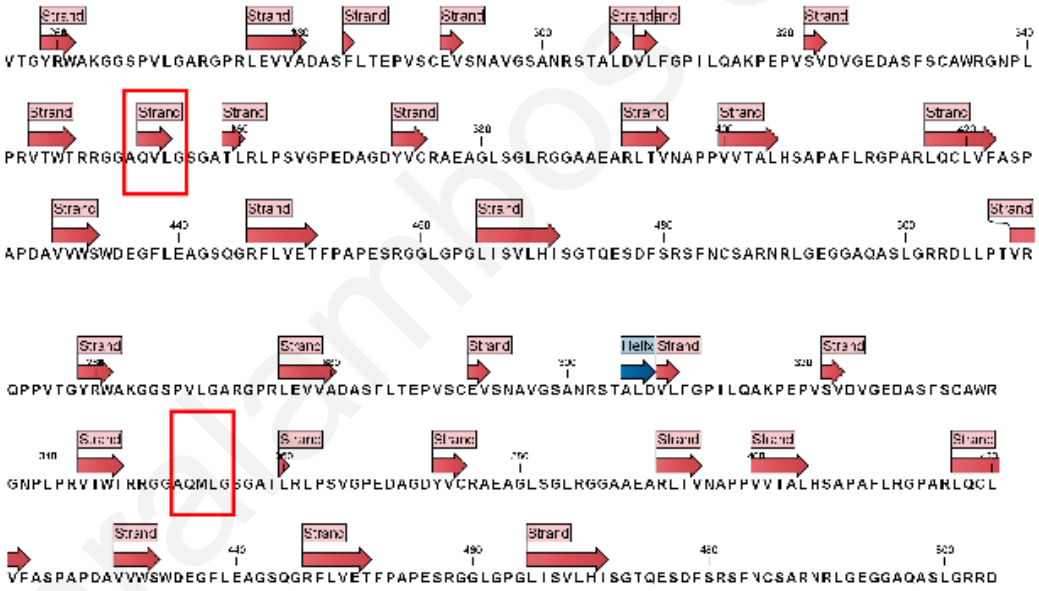

Figure 36: 2D protein structure prediction of the two variants of Neph3 (filtrin) protein (353V, 353M).

The red box indicates the 353 amino-acid residue and neighbouring residues. It is predicted that methionine substitution causes a conformation change due to loss of a β strand (CLC Main Workbench 6 software package).

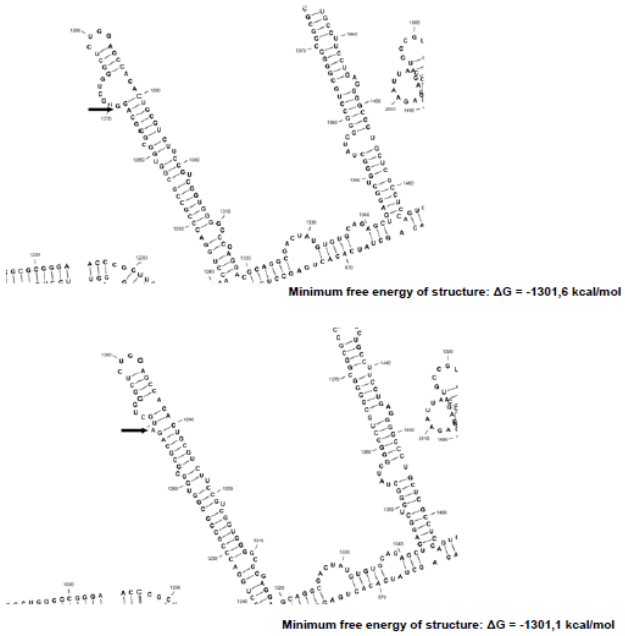

Figure 37: 2D mRNA structure prediction of the two variants of NEPH3 mRNA

Minimum free energy estimation is similar for both variants, indicating that no significant changes occur in the mRNA secondary structure (GTG:Val, ATG:Met; black arrows)

3.3.9 Assays for filtrin homo-dimerization and for hetero-dimerization with nephrin and myosin

Co-immunoprecipitation experiments were performed in order to identify any homo-dimerization and hetero-dimerization alterations of the NEPH3 protein in the presence or not of the *NEPH3*-p.V353M variant. Each co-immunoprecipitation experiment was performed in triplicate.

Western blot analysis from transiently transfected HEK293T cells revealed a slight decrease in the interaction between the *NEPH3*-wt and *NEPH3*-p.V353M variant, when compared to the interaction of *NEPH3*-wt with itself. Unpaired t-test showed statistical significance with p=0.0492. On the contrary, there was a slight increase in the interaction between the *NEPH3*-p.V353M and *NPHS1*-wt, as compared to the interaction of *NEPH3*-wt with *NPHS1*-wt. Unpaired t-test showed statistical significance with p=0.012 *(Figure 38)*.

Moreover in order to evaluate the effect of *NEPH3*-p.V353M in the interaction of Neph3 with Myh9, co-immunoprecipitation experiments (triplicates) were performed using transiently transfected human podocytes either with *NEPH3*-wt or with *NEPH3*-p.V353M.

Immunoblotting results revealed an increased interaction between *NEPH3*-p.V353M and the endogenously expressed Myh9 compared to the interaction of the *NEPH3*-wt. Unpaired t-test showed statistical significance with p=0.001 *(Figure 39)*.

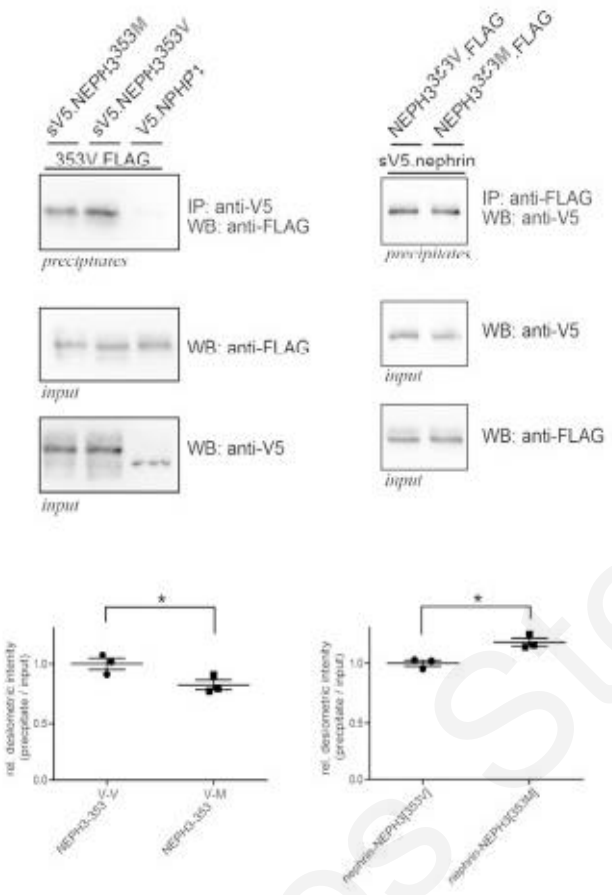

Figure 38: Co-immunoprecipitation experiments, testing for the binding effectiveness of Neph3 protein with methionine (M) at the 353 position

(A) *sV5-Neph3[353**V**] and sV5-Neph3[353**M**] were immuno-precipitated with anti-V5 antibody and analyzed by western blot using an anti-FLAG antibody (for FLAG-Neph3[353**V**]). Neph3 [353**V**]-Neph3[353**M**] homodimers are slightly impaired compared with the Neph3[353**V**]-Neph3[353**V**] ones. FLAG-Neph3[353**V**] and FLAG-Neph3[353**M**] were immuno-precipitated with anti-FLAG antibody and then analyzed by western blot using an anti-V5 antibody (for sV5-Nephrin]. Nephrin-Neph3[353**M**] heterodimers are slightly increased compared with the Nephrin -Neph3[353**V**] ones. Anti-V5 and anti-FLAG western blots from lysates (input) were used for loading normalization. V5-NPHP1 (nephrocystin) served as an experiment control.* ***(B)*** *Statistics of densitometry of the blots. Intensity (±SEM) is given as a percentage of wild-type intensity, which is set by definition at 1.0 (100%). There is statistical significance (unpaired t-test) for the homodimerization and heterodimerization comparisons.*

A.

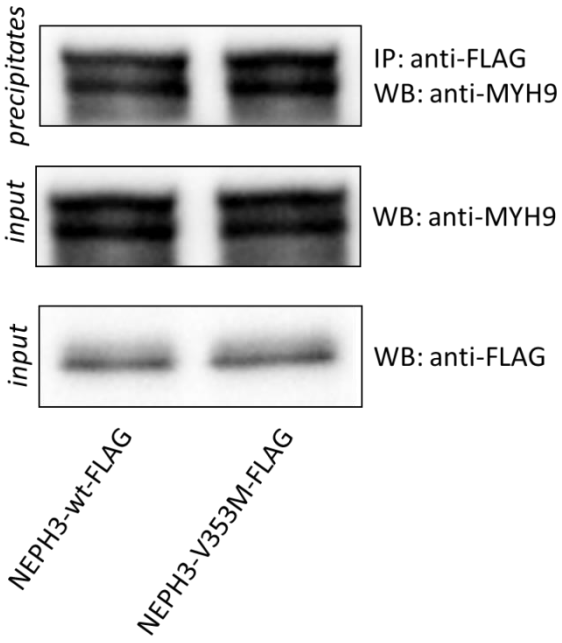

B.

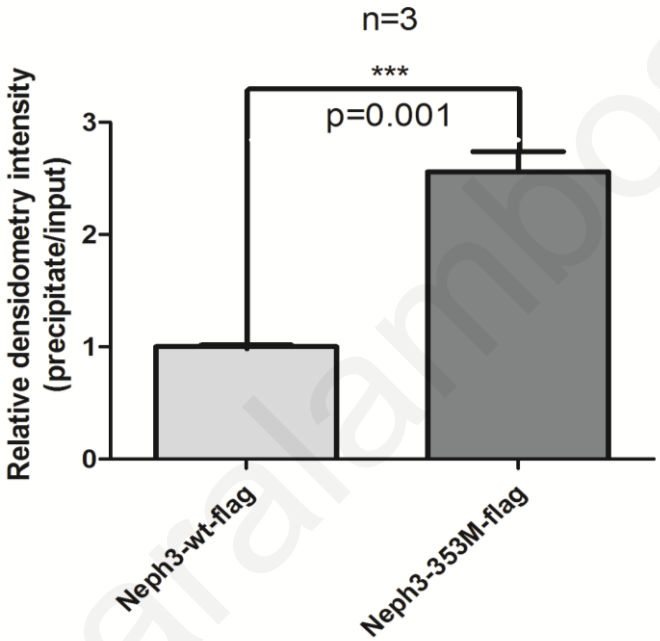

Figure 39: Co-immunoprecipitation of transiently expressed NEPH3-FLAG and Myh9

(A) The panel to the bottom shows expressed wild-type (wt) and mutant (p.V353M) filtrin after transient transfection in human undifferentiated podocytes. Shown above is the result of western analysis of the precipitates using anti-FLAG resin for the immunoprecipitation, and anti-FLAG and anti-MYH9 antibody for immunodetection. (B) Densitometry of the wt and p.V353M bands from repeated paired experiments. Intensity (with error bars indicating SEM) is given as a percentage of wild-type intensity, which is set by definition at 1.00.

3.3.10 Overexpressed *NEPH3*-353M variant results in up-regulation of unfolded protein response markers in the presence of tunicamycin

In an effort to evaluate the activation of the UPR pathway, human podocytes were transiently transfected either with *NEPH3*-wt or *NEPH3*-p.V353M variant were no significant upregulation of any UPR marker was observed.

Bearing in mind that the *NEPH3*-p.V353M variant is hypothesised to act as a modifier gene on the background of another mutation and does not have a pathogenic effect on its own, it was not surprising that no distinguishable differences were observed between the variant and the wild type overexpressing cells. To evaluate the mutant variant in overexpressing cells under external stress factors, transfected podocytes were exposed to tunicamycin, a potent ER-stressor inhibiting the N-linked glycosylation as previously described. Remarkably, after exposure to tunicamycin, the tested UPR markers were considerably more pronounced in the *NEPH3*-p.V353M expressing cells compared to *NEPH3*-wt expressing cells. It is worth noting that pPERK did not reach statistical significance, despite the obvious trend observed in

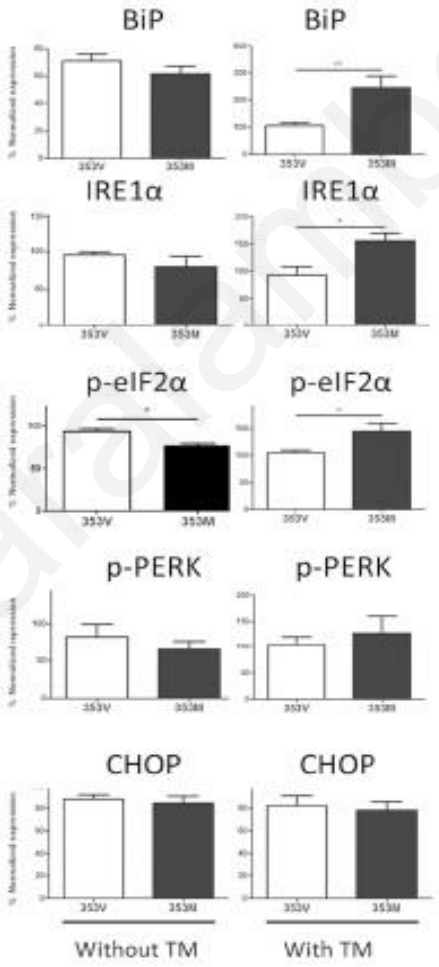

Figure 40: Expression of the NEPH3-p.V353M-FLAG mutant exacerbates ER stress

Results of the densitometry analysis of western blots where the elevation of markers of the unfolded protein response pathway was assayed in the presence of the two NEPH3 alleles (normal "V" vs mutant "M"). Note that in the presence of tunicamycin (TM, a potent factor adding additional cellular stress), three markers are rising significantly (asterisks mark the significance) for the "M" allele.

cells transfected with the mutant NEPH3-p.V353M allele. On the other hand, CHOP marker did not demonstrate any detectable alteration in expression in the presence of tunicamycin. These results indicate that the NEPH3-p.V353M mutant variant is more prone to additional elevation of ER stress, compared to the wild type upon exposure to an external stressor *(Figure 40).*

3.3.11 Effects of wild type and mutant NEPH3 on the distribution of nephrin and Myh9

Since *NEPH3*-p.V353M has been shown to behave as a modifier in the progress of the disease in patients of the *HEMATURIA* cohort, it was hypothesized that *NEPH3*-p.V353M might exert a deleterious effect on the localization of filtrin and its binding partners, nephrin and the new found Myh9. Therefore, membrane targeting of the wild type or *NEPH3*-p.V353M was studied in human podocyte cell lines, transiently co-expressing wild type nephrin construct or stable expressing the Myh9 protein.

In perfect accordance with the clinical data, nephrin-wt was localized properly to the plasma membrane when co-expressed with wild-type NEPH3, but was retained in the cytoplasm showing perinuclear localization, when coexpressed with *NEPH3*-p.V353M *(Figure 41)*.

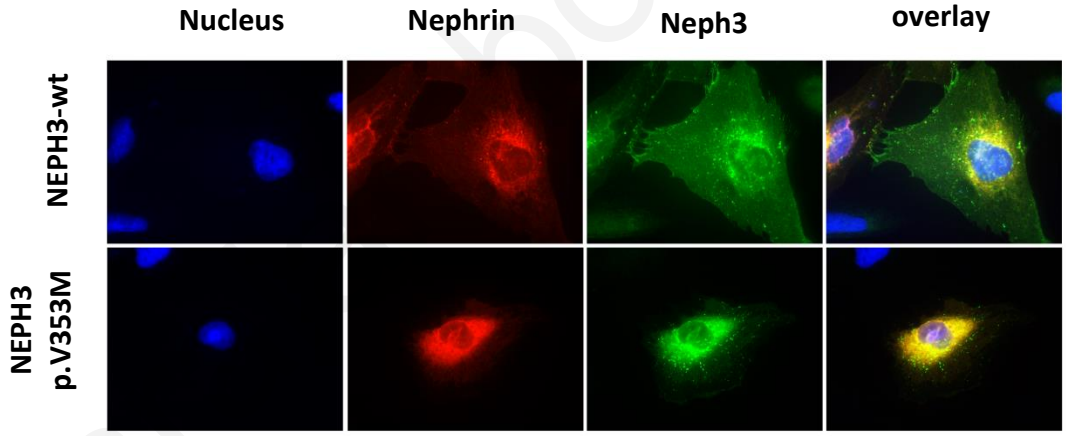

Figure 41: Double-labelling immunofluorescence of wild-type nephrin and wild-type or missense mutated Neph3

Human podocyte cell line was transiently doubly transfected with the wild-type nephrin, and the with wild-type or each missense mutated NEPH3 cDNAs, followed by immunostaining with V5 antibody and FLAG antibody. Wild-type nephrin colocalizes with wild-type NEPH3, both properly localizing to the plasma membrane. On the contrary, the p.V353M variant was shown to interfere with the normal trafficking of both proteins, demonstrating a perinuclear staining.

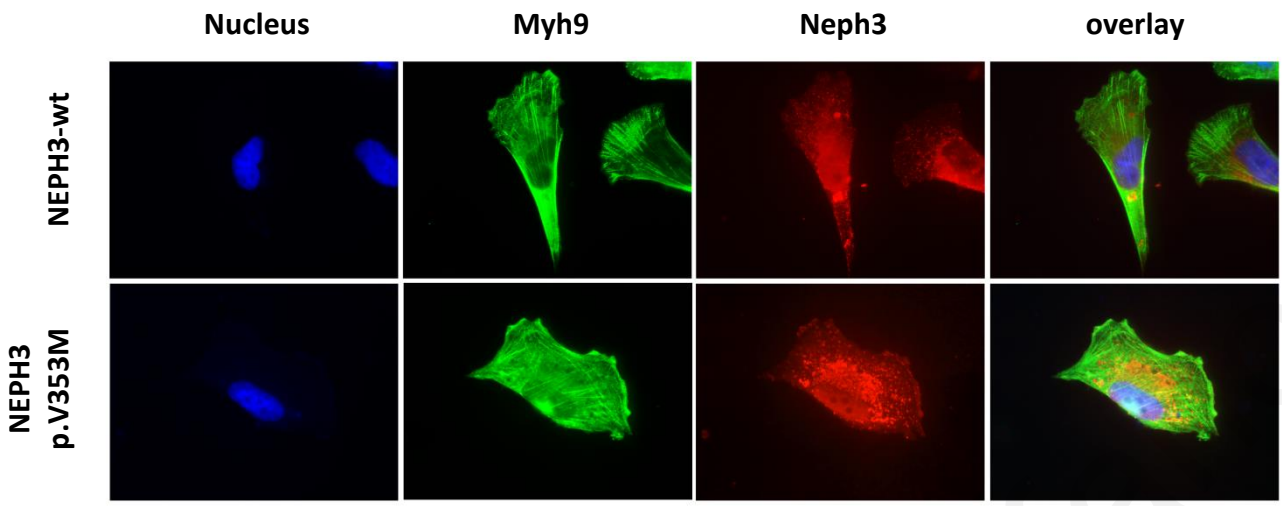

Figure 42: Double-labelling immunofluorescence of endogenously expressed wild-type Myh9 and wild-type or mutated Neph3

Human podocyte cell line was transiently transfected with the wild-type or missense mutated NEPH3 cDNAs, followed by immunostaining with Myh9 and FLAG antibody. Wild-type NEPH3 colocalizes with MYH9, both properly localizing to the plasma membrane. On the contrary p.V353M NEPH3 demonstrated a perinuclear staining with no effect on the localization of the endogenously expressed Myh9.

Moreover, NEPH3-p.V353M had no effect on the localization of the endogenously expressed MYH9, even though NEPH3-p.V353M demonstrated a perinuclear staining *(Figure 42)*.

3.4 Discussion

As previously mentioned, progression in primary hematuric glomerulopathies is still a debate in nephrology. In this project, we have focused on known non-synonymous SNPs found in specific genes expressing proteins of the multiprotein complex of the SD. Many of these genes have been associated with a number of inherited glomerulopathies. Therefore, we hypothesized that missense variants found on these genes could act as hypomorphic mutations, contributing to the progression of a subset of hematuric patients. Application of an *in silico* analysis strategy led us to focus on filtrin (Neph3), a protein of unknown function, which has been presented to interact with several slit diaphragm proteins. After suggestive significance in a previously well-studied TBMN sub-cohort, we extended the evaluation of the *NEPH3*-p.V353M in the pooled hematuric cohort *HEMATURIA*, consisting mainly by an important number of patients diagnosed with TBMN or IgA nephropathy. Statistical analysis revealed a high risk for the carriers of this variant (genotypic association: $p=3.0x10^{-3}$, OR=6.64 adjusting for gender/age; allelic association: $p=2.0x10^{-4}$). Even though this data should be replicated by additional research groups, we suggest that variant *NEPH3*-p.V353M may have a significant predictive value for an adverse outcome, when co-inherited in patients with a background of another primary hematuric glomerulopathy, such as TBMN and IgA nephropathy. This qualifies the *NEPH3*-p.V353M variant as a hypomorphic allele, as on its own is not adequate to cause any perceptible symptom; but instead, aggravates the situation when co-inherited with another causative mutation. An analogous inheritance pattern has been described in some rare severe and early onset cases of autosomal dominant polycystic kidney disease, when hypomorphic *PKD1* mutations were co-inherited with variants in the *PKHD1* or the *HNF-1β* gene (Vujic et al., 2010, Bergmann et al., 2011).

Moreover, it was examined whether this variant could be associated with the development of microalbuminuria in the general population. Genotyping and analyzing 6,531 subjects of the FHS revealed association of the homozygous genotype 353M/M with microalbuminuria in this population ($p=1.0x10^{-3}$ adjusting for gender and age, OR=5.92). In the process of verifying this result, this variant was genotyped in two different general population-based samples, SAPHIR and KORAF4. A meta-analysis for all three cohorts, confirmed that 353M/M homozygotes are in higher risk for developing microalbuminuria (adjusted $p=1.3x10^{-5}$, OR=7.46). Based on these findings, it is suggested that one dose of this hypomorphic mutation on the background of a primary hematuric glomerulopathy is sufficient enough to predispose to kidney impairment while two doses are required to predispose a healthy individual to manifest microalbuminuria. Remarkably, recent findings

reinforced the importance of Neph3 in the prevention of the glomerular protein leakage, since it was demonstrated that non-synonymous variants in *NEPH3* gene can cause nephrotic syndrome in dogs (Littman et al., 2013)**.**

Furthermore, in an effort to detect new interacting partners of Neph3 other than Nphs1, Neph1 and Nphs2, an experimental approach implicating IP, mass spectrometry and immune-staining experiments was employed. This process provided for the first time convincing evidence of direct or indirect interaction of Neph3 with Myh9; an important cytoskeletal protein primarily expressed in glomerular podocytes, implicated in the development of FSGS and other rare diseases known as MYH9 related diseases (Sekine et al., 2010, Alhindawi and Al-Jbour, 2009, Epstein et al., 1972, Ghiggeri et al., 2003, Moxey-Mims et al., 1999, Naito et al., 1997, Peterson et al., 1985, Turi et al., 1992, Yap et al., 2009, Clare et al., 1979). Fluorescent microscopy demonstrated co-localization of Neph3 with Myh9 in cultured podocytes and mouse kidney biopsies thereby increasing the significance of the previous findings. Immunoprecipitation experiments also showed that 353M variant of filtrin interacts more strongly with Myh9. Further co-immunoprecipitation experiments displayed an effect on the interaction of Neph3 with nephrin and itself, demonstrating the significance of the substitution of valine to methionine at position 353. This could be attributed to the fact that V353M is located in the 4th Ig-like domain of filtrin, which is important for the interaction between members of the Ig- superfamily proteins. Interestingly, 2D structure prediction showed a possible alteration caused by the methionine substitution in Neph3 structure. According to these findings, it is suggested that a functionally deleterious variant like 353M, can accelerate the collapse of the SD integrity or even assist the degeneration of the interactions between adjacent podocytes during the aging process in a healthy individual, or most importantly on the background of another primary glomerular disease. In spite of the fact that these results were obtained from triplicate experiments, we suggest further investigation should occur confirming these slight but perceptible quantitative protein changes. Moreover, it is important to note that if this variant had a more dramatic effect on protein-protein interactions, it might have been a serious primary mutation and not a hypomorphic variant predisposing to proteinuria over a period of many decades.

Additionally, in the present work potential activation of the UPR pathway was evaluated, employing semi-quantification of the protein levels of the UPR markers, including BiP, IRE1a, p-eIF2α, p-PERK, and CHOP. This was performed in cells overexpressing the 353V or the 353M variant of filtrin. Interestingly UPR marker activation was shown to be similar for both 353V and 353M overexpressing cells. However, in order to create a more realistic

representation of the podocyte environment in the glomerulus, transfected cells were exposed to tunicamycin, a pharmacological ER stress activator. In this setup, cells were imposed in stress pressure caused by the genetic background of the filtrin and by the exposure to the stress-causing agent. Remarkably, the cells expressing the 353M variant were prone to further elevating UPR markers than the *wt* expressing cells. This is interesting since one might hypothesise that the 353M variant could potentially raise susceptibility of the cell in the presence of other predisposing factors, genetic or environmental, such as an inherited pathogenic mutation (like in TBMN patients), a locally increased osmotic or mechanical pressure, toxic chemicals etc. Taking everything into account, it is suggested that *NEPH3*-p.V353M imposes a slowly degenerating process on podocytes that needs several decades to manifest.

3.5 Conclusions and future perspectives

To conclude, it has been shown that the candidate gene approach followed in this study in searching for non-synonymous variants in ten SD genes using a bioinformatics approach could be valuable for diseases such as glomerulopathies, particularly when dealing with rare variants. In the cohorts investigated, consisting of patients diagnosed with microscopic hematuria, the obtained results imply that testing for the presence of the rare *NEPH3-p.*V353M could have a highly positive predictive value for renal impairment. This, however, needs to be confirmed in appropriate prospective cohort studies. Moreover, it is important to note that the new findings regarding the interaction of Neph3 with Myh9, possibly point to new directions for research in podocytes and SD. Interestingly, these data could be beneficial for understanding the unresolved issue of how slit diaphragm proteins are trafficked to the filtration slit, since the only existing evidence for this question is the direct interaction of Myo1c with Neph1(Arif et al., 2011).

Chapter 4: Co-inheritance of functional podocin variants with heterozygous collagen IV mutations is a potential cause of renal failure

4.1 Scientific hypothesis and specific aims

As previously reported, TBMN was long considered as a benign renal condition reserved for individuals having persistent isolated microscopic hematuria and a uniformly thinned GBM due to heterozygous mutations in the *COL4A3 or COL4A4* genes (Kashtan, 2005a, Savige et al., 2013). However, several reports suggest that occasionally, TBMN can progress to chronic renal failure of variable degree (Voskarides et al., 2007, Pierides et al., 2009, Lin et al., 2014a). In more recent publications, a significant number of *COL4A3/COL4A4* heterozygous mutation carriers has been demonstrated to develop FSGS (Voskarides et al., 2007, Pierides et al., 2009) or even ultrastructural GBM histology of alternate thinning/thickening and splitting, which is pathognomonic of AS (Marcocci et al., 2009). In more detail, this study proves that in a large Greek-Cypriot cohort, more than 50% of TBMN patients with known *COL4A3/COL4A4* heterozygous mutations progress to clinically significant proteinuria and CRF, due to late-onset FSGS manifesting after the age of 30 years. Equally importantly in a Greek-Cypriot cohort of 230 patients about 30% of the patients reached ESKD by the age of 70 years (Deltas et al., 2013b). Multiple factors were shown to cause an effect on the spectrum of symptoms in TBMN, including the mutated gene, the position and type of mutation, environmental factors and genetic modifiers that, on their own, cannot result in a Mendelian condition but have been invoked in explaining the progressive nature of TBMN in a subset of patients. Recently, two different studies provided evidence that variant p.R229Q detected in the *NPHS2* gene, represents a genetic risk factor, predisposing TBMN patients to proteinuria and renal failure (Tonna et al., 2008a, Voskarides et al., 2012)**.**

In the current study, it was hypothesized that additional putative variants in the *NPHS2* gene, besides *NPHS2*-p.R229Q, could also act as modifiers predisposing to an adverse disease outcome in TBMN during aging. Specific objectives were as follows:

1. *To re-sequence the coding region of the NPHS2 gene in a previously described TBMN cohort, focusing on families that segregated TBMN due to a primary founder mutation COL4A3-p.G1334E.*
2. *To evaluate the effect of the found variants on podocin and nephrin localization in vitro.*
3. *To evaluate the effect of the found variants on podocin cross-interaction with nephrin and itself in vitro.*

4.2 Materials and methods

4.2.1 Patients - Clinical Assessment and Study Outcomes

For the current study 122 patients with TBMN, carriers of a heterozygous *COL4A3* or *COL4A4* mutation, all of Greek-Cypriot origin, were classified as "Mild" or "Severe" *(supplementary table 5)*. This cohort was employed due to the fact that it includes an important number of patients with common mutations as a result of two major founder effects. Specifically, among the 122 TBMN patients, 87 carry the *COL4A3*-p.G1334E mutation, 18 carry the *COL4A3*-p.G871C mutation, seven carry the *COL4A4*-c.3854delG mutation, four carry the *COL4A3*-p.G1077D, three the *COL4A4*-p.G143V mutation, two the *COL4A4*-p.G208D mutation and lastly one carries the *COL4A3*-p.G484R mutation. Patients younger than 50-yo without evidence of severe disease were excluded since young individuals with apparently mild disease could develop a severe phenotype at later ages. Regarding TBMN patients, disease was considered mild by the presence of MH only or MH and clinically not significant proteinuria, with no CRF. "Severe" disease was distinguished by hematuria along with proteinuria ≥300 mg/24h, with or without CRF/ESKD. CRF was defined as serum creatinine, elevated over 1.5 mg/dL. Severely affected patients were excluded if another renal disease was described or with a clinical history of diabetes mellitus for at least five years, or at the extreme of body weight (outside ±2 SD of the cohort mean).

For calculating the allele frequency of *NPHS2*-p.E237Q in the general population, 96 DNA samples obtained from healthy individuals were used. The *NPHS2*-p.R229Q allele frequency in the general population was assessed as part of a previous work of our team (Voskarides et al., 2012).

The study was approved by the Cyprus National Bioethics Committee and participants gave their signed informed consent, unless they were included anonymously after testing for purely diagnostic purposes.

4.2.2 *NPHS2* re-sequencing and analysis of the found variants

All eight exons of the *NPHS2* gene of 35 TBMN severe patients were amplified by PCR using flanking intronic primers and subsequently re-sequenced employing Sanger method. Direct re-sequencing was performed using the Big Dye terminator technology and the ABI-3130*xl* Genetic Analyzer (Applied Biosystems).

Any identified non-synonymous variant was genotyped in the remaining 87 TBMN patients again by DNA re-sequencing. Genotypic statistical analysis was accomplished by SPSS v.13

(IBM, USA). The significance level alpha was set to 0.05. Segregation analysis was performed for the two variants we identified in two families, by calculating the Mendelian probabilities.

4.2.3 Plasmid Vectors

For the cellular studies, a pCMV6-entry vector containing the full-length human podocin (*NPHS2*) cDNA was acquired from Origene (Rockville, MD, USA). Moreover, the cDNA of *NPHS2*-wt was subcloned from pCMV6-*NPHS2*-wt-Myc/DDK to pCMV6-AC-HA vector. The pcDNA6/HIS containing the full-length human nephrin (*NPHS1*) cDNA was kindly provided by Prof. T. Benzing lab, Cologne, Germany. The vectors were confirmed for expression of C-terminal fusion of the podocin with the FLAG or HA tag and of N-terminal fusion of the nephrin with the V5 tag via western blotting.

Podocin missense mutations were introduced in the human podocin full-length cDNA using the QuikChange Site-Directed Mutagenesis Kit and according to the manufacturer's protocol (Stratagene, La Jolla, CA, USA). Mutagenic primers were as follows:

NPHS2-p.R229Q-For:
CCACTATGAAGCGTCTCCTAGCACATCAATCCCTCACTGAAATTCTTCTAGAGAG;
NPHS2-p.R229Q-Rev:
CTCTCTAGAAGAATTTCAGTGAGGGATTGATGTGCTAGGAGACGCTTCATAGTG;
NPHS2-p.E237Q-For:
CTCACTGAAATTCTTCTACAGAGGAAGAGCATCGCCCAAGATG;
NPHS2-p.E237Q-Rev:
CATCTTGGGCGATGCTCTTCCTCTGTAGAAGAATTTCAGTGAG.

For ensuring that no undesired mutations had occurred during the mutagenesis procedure, all constructs were resequenced.

4.2.4 Cell lines and transfections

The human embryonic kidney cell line HEK293T was grown in Dulbecco's modified Eagle's medium (D-MEM) (Life Technologies, Gaithersburg, MD, USA) supplemented with 10% FBS (Invitrogen, Carlsbad, CA) and 100 U/mL penicillin/streptomycin, in 37^{o}C incubator with 5% CO_2. The AB8/13 undifferentiated human podocyte cells (kindly provided by Dr. M. Saleem, Bristol, UK) were incubated at 33°C at 5% CO_2 and cultured in RPMI medium,

supplemented with 10% FBS, 1% of 100 U/ml penicillin/streptomycin (Invitrogen), and 1% insulin-transferrin-selenium (Invitrogen, Carlsbad, CA).

At 70% confluence, cells were transiently transfected with the vectors containing the nephrin and podocin cDNAs, *wt* or mutants, using Lipofectamine 2000 (Invitrogen, USA) and according to the manufacturer's instructions. Following a 48hr incubation period, cells were washed and subsequently lysed in Laemmli Sample Buffer. Transfection efficiency was assessed by immunofluorescence using an anti-FLAG, anti-HA (Santa Cruz Biotechnology) or an anti-V5 antibody (Invitrogen, Carlsbad, CA) in a transfection control sample; transfection efficiency was typically approximately 60%. Podocin and nephrin expression was similar in all transfected cells as assessed by western blot at each single experiment, using an anti-FLAG, anti-HA or anti-V5 antibody respectively against the engineered terminal tags. Expression levels of both proteins after transfection strongly increased compared with non-transfected cells.

4.2.5 Immunofluorescence

In order to determine the intracellular localization of the proteins of interest, AB8/13 undifferentiated human podocyte cells were cultured on glass coverslips and transiently co-transfected with nephrin or podocin cDNAs (wild type or mutant) for further incubation period, reaching 48 hours. Cells were washed and fixed in 3% paraformaldehyde in PBS for 10 minutes. After three washes in PBS, cells were permeabilized for 30 seconds in 0.1% Triton X100, washed in PBS and blocked with PBS containing 1% Bovine Serum Albumin (BSA) for an hour at room temperature. Cells were incubated with the appropriate primary antibody, in blocking buffer, overnight at 4^{o}C. After three washes, cells were incubated with the appropriate secondary antibody for an hour at room temperature. Then, after three additional washes, coverslips were mounted on slides using Fluorescence Mounting Medium (DAKO, Denmark). Immunofluorescence preparations were analysed on a Zeiss Axiovert200M inverted fluorescence microscope equipped with Zeiss Axiovision 4.2 software and on a laser scanning confocal microscope Zeiss LSM 710 equipped with the ZEN 2010 software. Digital images were recorded and composed using Adobe Photoshop 5.0.

4.2.6 Co-immunoprecipitation

To determine the protein binding of the missense podocin mutants to the wild-type podocin or nephrin, HEK293T cells were transiently co-transfected with the cDNAs expressing the wild-type podocin or nephrin carrying the HA or V5 tag respectively and the wild-type or

mutant podocin carrying the FLAG tag. Following a 48hr incubation at 37^{o}C, cells were washed in PBS and lysed in lysis buffer (50 mM Tris-HCl, pH 7.4, with 150 mM NaCl, 1 mM EDTA, and 1% TRITON X-100) containing protease inhibitors (Roche).

Lysates were centrifuged for 10 minutes at 12.000 rpm and the supernatants were transferred in a new tube and incubated with anti-FLAG M2 affinity gel for 3 hours at 4°C.

Resin was then centrifuged and washed for three times with wash buffer (0.5 M Tris-HCl, pH 7.4, with 1.5 M NaCl). Immunoprecipitated FLAG fused podocin was eluted with 2x sample buffer (125 mM Tris-HCl, pH 6.8, with 4% SDS, 20% (v/v) glycerol, and 0.004% bromphenol blue). In order to minimize the denaturation of the antibody, no reducing agent was included in the sample buffer. The eluates were then applied for immunoblotting of nephrin and podocin.

4.2.7 Immunoblotting and densitometry

Samples of HEK293T cells transiently transfected with wild type or missense mutated podocin constructs, and the immunoprecipitated samples mentioned above were separated on 7.5% SDS-PAGE under reducing conditions. Then they were transferred overnight at 4°C to polyvinylidene difluoride membranes (Millipore, Massachusetts, USA) and incubated for one hour at room temperature with anti-FLAG (1:6000), anti-HA (1:10000) or anti-V5 (1:6000) antibody. The membranes were incubated for 60 minutes at room temperature with a 1:6000 diluted HRP-labeled goat anti-rabbit or goat anti-mouse antibody. Proteins were detected using the Enhanced ChemiLuminescencePlus Blotting Detection system (GE Healthcare, Little Chalfont, United Kingdom) and visualized using the ChemiDocXRS+ system (Biorad, California, USA). Band density was defined by the ImageJ Software (NIH, Maryland, USA).

4.3 Results

4.3.1 Genetics studies

In our searching for putative functional variants in the *NPHS2* gene that could putatively act as adverse genetic modifiers in the presence of TBMN, we were led to the re-sequencing of the coding region of the *NPHS2* gene, in severely affected TBMN patients. This hypothesis was entirely based on previous results according to which a known variant, *NPHS2*-p.R229Q was shown to predispose such patients to proteinuria and severe CRF. Re-sequencing of the *NPHS2* gene in 35 severely affected TBMN patients detected a previously described rare non-synonymous variant, *NPHS2*-p.E237Q in exon 5 in three patients. Due to this finding, exon 5 of *NPHS2* was also genotyped in the remaining patients of the MMRC TBMN cohort. Three p.E237Q and four p.R229Q heterozygous patients were found among the 82 "severe" patients and none among the 40 "mild" patients. Genotypic association analysis by Pearson Chi-square resulted in a *p*-value of 0.05 *(Table 14).*

Table 14: *Combined frequencies and statistics of NPHS2-R229Q and NPHS2-E237Q variants, among patients with thin basement membrane nephropathy and according to disease severity*

		Genotype counts			**Genotype frequency %**			***p*-values**
Cohort	n	RR/ EE	RQ or EQ	QQ/ QQ	RR/ EE	RQ/ EQ	QQ/ QQ	
TBMN-Mild	40	40	0	0	100.0	0	0	
TBMN-Severe	82	75	7	0	91.5	8.5	0	0.09 (2-sited Fisher's Exact test) 0.08 (Bernard Test) 0.05 (Pearson Chi Square)

These data supported further evaluation of two clinically described families, which interestingly co-segregated the *COL4A3*-p.G1334E as the primary TBMN mutation with one of the two *NPHS2* variants. For these two families, CY5304 and CY5376, DNA samples were available for seven and eleven TBMN patients respectively. Remarkably, in the family

CY5304 an *NPHS2*-p.E237Q homozygous individual (III-4) was detected, negative for the *COL4A3*-p.G1334E mutation, aged 81-yo, with no known renal phenotype *(Figure 43)*. The three "severe" patients of this family were heterozygous carriers of *NPHS2*-p.E237Q whereas the four "mild" ones were negative for *NPHS2*-p.E237Q variant. This indicated a positive correlation of the p.E237Q with a severe phenotype, when is found on the background of *COL4A3*-p.G1334E. The probability for this to happen is low. According to the genotyping of subjects in generation III (no DNA samples are available from generation II), both parents II-1 and II-2 were obligate heterozygous for the *NPHS2*-p.E237Q, whereas in the case of spouses/parents II-3 and II-4 most probably only one was positive (heterozygous) for this variant *(Figure 43).*

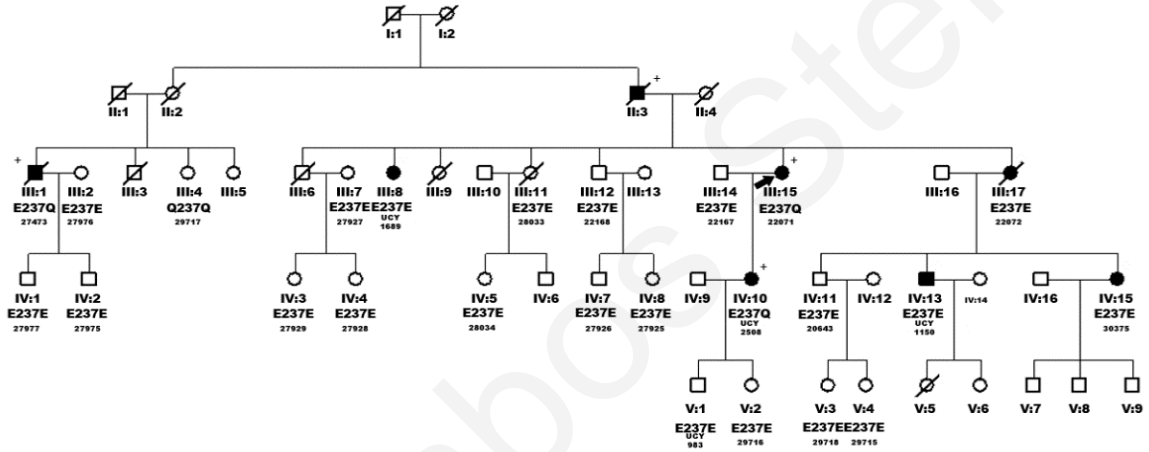

Figure 43: Family CY5304 where NPHS2-p.E237Q was found to segregate with the severe phenotypes.

Black symbols show the TBMN patients, heterozygous for the founder mutation COL4A3-p. G1334E. Patients with a cross symbol have a severe phenotype.

Thus, the probability for the *NPHS2*-p.E237Q to segregate by chance in the seven individuals with TBMN, is (0,75) x $(0,5)^4$ = 0,05. The probability of 0,75 is attributed to patient III-1 who has a healthy homozygous sibling, III-4; therefore both parents are obligate carriers. Moreover, in family CY5376 *(Figure 44)* segregation of *NPHS2*-p.R229Q was observed in patients who fulfilled the criteria for a severe phenotype (II-2, II-4, II-9, III-13). Mildly affected subjects were not considered because of their young age, thereby not satisfying the set criteria. According to the genotyping data in generation II *(Figure 44)* it is assumed that only one of the two parents I-1 and I-2 is heterozygous for this variant. Hence, the probability of *NPHS2*-p.R229Q to segregate by chance in the four patients is $(0,5)^4$=0,06 (nearly significant). Studying the clinical record of individual II7, it was found that he also suffers

from vesicoureteral reflux (VUR), a second renal phenotype. This might explain his progression to ESKD at age 55-years, without having inherited *NPHS2*-p.R229Q. Additional evidence was found, demonstrating that VUR can contribute to TBMN severity when it was realized that his nephew, individual III-13, also has VUR and he reached ESKD at the fairly young age of 37 years. This patient has reached ESKD at the youngest age among all our Greek-Cypriot patients with TBMN. This was attributed to both *NPHS2*-p.R229Q variant inheritance and VUR on the background of TBMN.

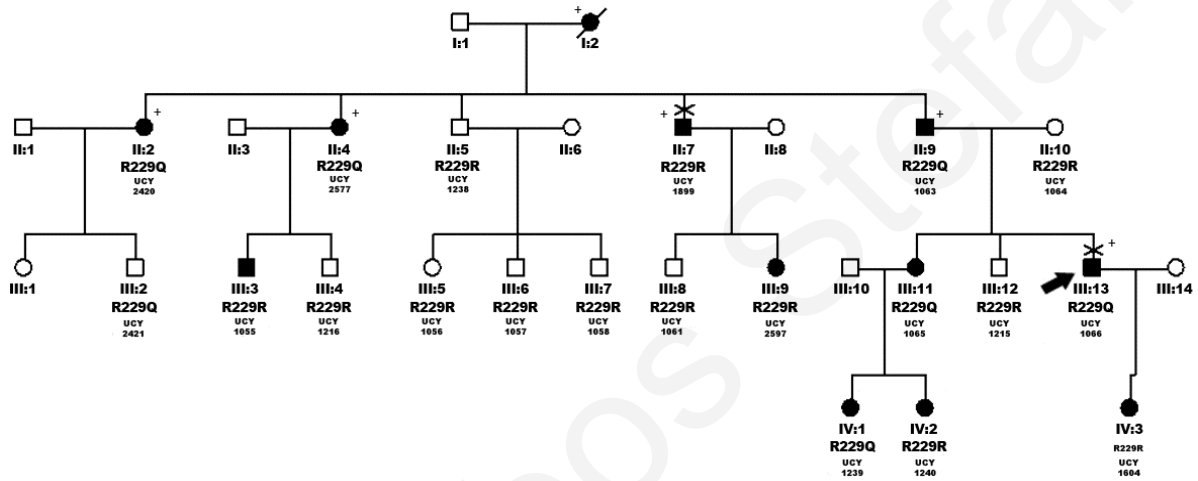

Figure 44: Family CY5376 where NPHS2-p.R229Q was found to segregate with the severe phenotypes.

Black symbols show the TBMN patients, heterozygous for the founder mutation COL4A3-p.G1334E. Patients with a cross symbol have a mild phenotype, probably due to the young of their age (this is why they are not included among the 123 TBMN patients of this cohort). The two patients marked with an X symbol are the ones that co-inherit the VUR phenotype.

4.3.2 Immunofluorescence findings

Since both *NPHS2* variants have been shown to behave as modifiers in the progress of TBMN in patients co-inheriting a *COL4A3* mutation, both podocin variants were further evaluated under the assumption of causing altered localization to the wild-type protein. Both mutants were co-expressed with the wild type protein in human undifferentiated podocytes and studied in dually expressing cells. Confocal microscopy analysis revealed altered localization of both variants as compared to the wild type protein *(Figure 45).*

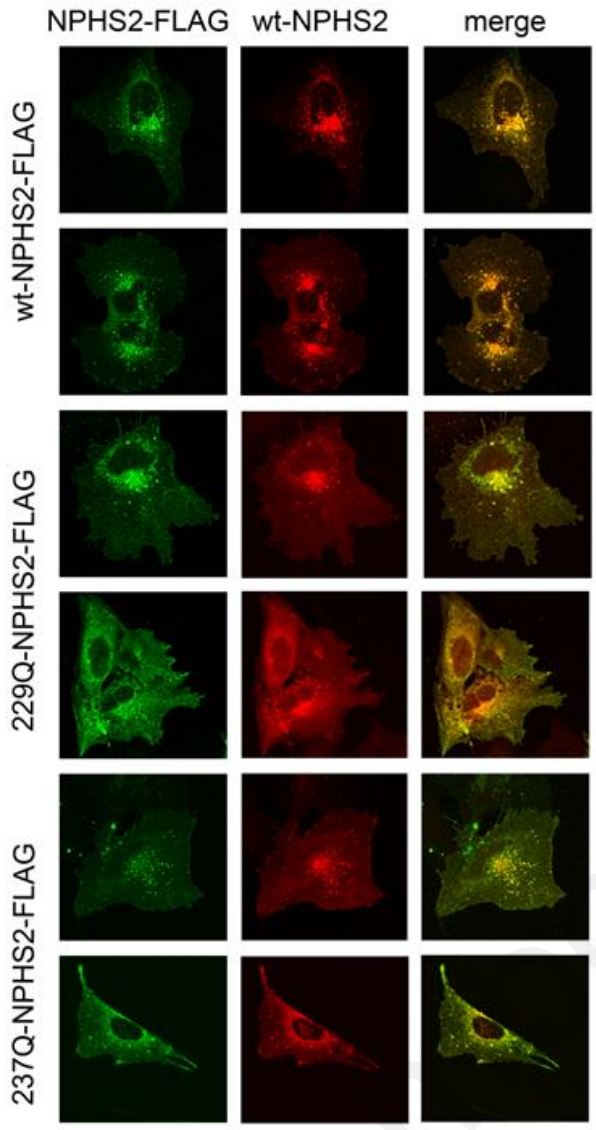

Figure 45: Double-labelling immunofluorescence of wild-type HA tagged and either wild-type or mutant FLAG tagged podocin constructs

Human podocyte cell line was transiently double transfected with the wild-type and wild-type or mutant podocin cDNAs carrying different epitope tags, followed by immunostaining with FLAG antibody and HA antibody. Wild-type FLAG and HA proteins co-localise fully (upper two panels), contrary to p.R229Q (middle two panels) or p.E237Q (lower two panels), where both variants showed reduced colocalization with the wild type proteins.

Moreover, both podocin variants were further evaluated in causing an effect on nephrin localization. Nephrin is a vital component of the slit diaphragm and a known partner of podocin. For this set of experiments, undifferentiated human podocytes were transiently co-transfected with podocin constructs expressing the wild type or mutant forms of podocin and with a construct expressing nephrin. Confocal microscopy observation revealed that when wild-type podocin was expressed with wild-type nephrin, both proteins were properly localized to the plasma membrane, contrary to p.R229Q or p.E237Q, where both variants showed to interfere with the normal trafficking of nephrin, exhibiting a dominant negative effect in altering its localization in a perinuclear fashion *(Figure 46)*.

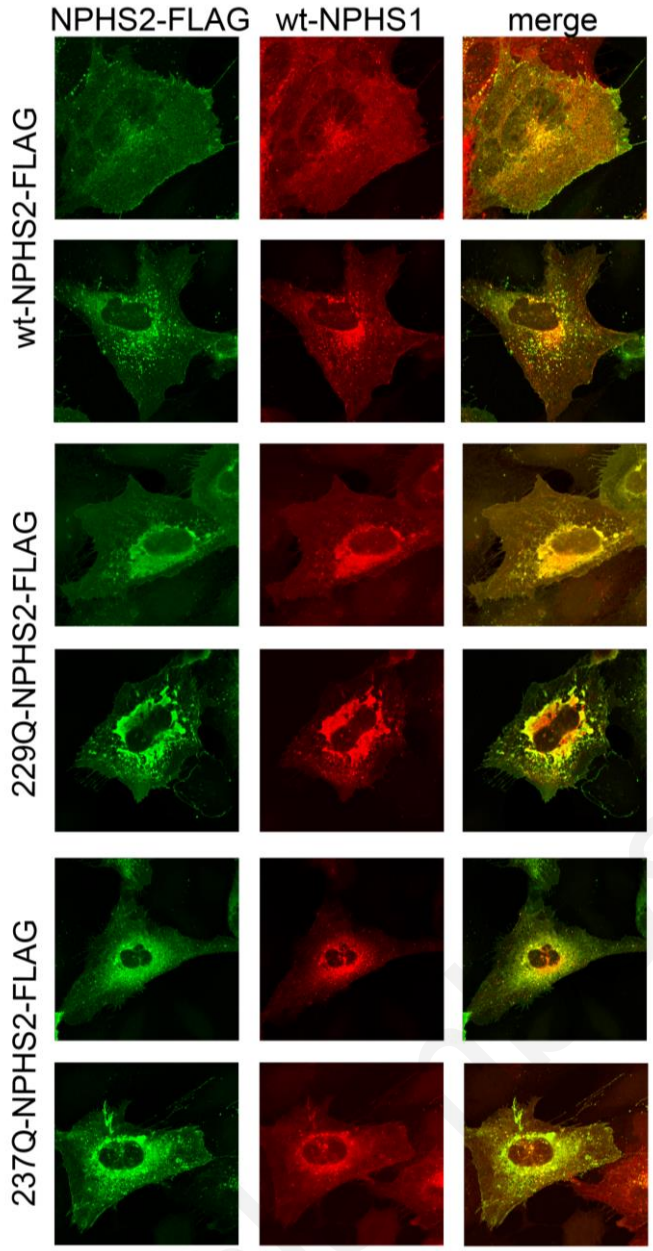

Figure 46: Double labelling immunofluorescence of wild-type nephrin and wild-type or missense mutated podocin

Human podocyte cell line was transiently double transfected with the wild type nephrin and with either wild-type or each missense mutated podocin cDNAs, followed by immunostaining with V5 antibody and FLAG antibody. Wild-type nephrin colocalizes with wild-type podocin, both properly localizing to the plasmas membrane, contrary to p.R229Q or p.E237Q, where both variants showed to interfere to the normal trafficking of both proteins, demonstrating a more prominent perinuclear staining.

4.3.3 Co-Immunoprecipitation

Based on the fact that podocin variants demonstrated altered cellular localization, podocin homodimerization was further tested, in order to evaluate if both variants exert an effect on the interaction of podocin with itself. Co-immunoprecipitation experiments were carried out, using HEK293T cells transiently co-transfected with either the *wt* podocin and/or the mutant podocin constructs tagged with a different epitope. Importantly, the results showed that the *wt* podocin interacts significantly stronger with the variants as compared to the *wt* protein *(Figure 47)*. Specifically, *wt* podocin had 209% stronger binding to p.R229Q (n=5, p=0.048) podocin and 244% to p.E237Q (n=5, p=0.035) (unpaired two-tailed *t* tests).

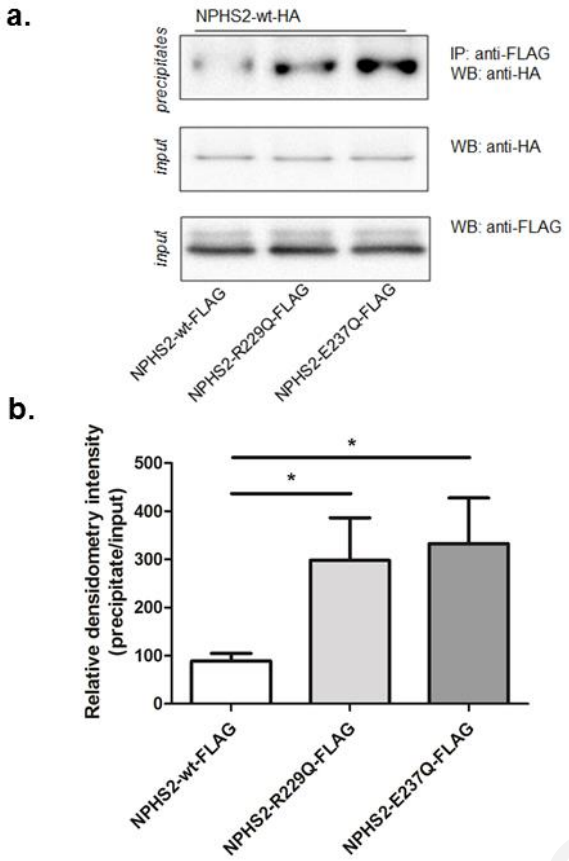

Figure 47: Podocin homodimerization experiments

(a) Podocin homodimerization experiments: Podocin co-precipitates with both variants (R229Q and E237Q). FLAG- and HA-tagged proteins were expressed in HEK293T cells and precipitated with anti-FLAG antibody as indicated. Western blot analysis was performed with HA and FLAG specific antibodies. Expression levels of HA-tagged wild type podocin and FLAG-tagged variant constructs in the lysates are shown below. (b) Densitometry of the p.R229Q and p.E237Q bands from repeated experiments (n=5). Intensity (with error bars indicating SEM) is given as percentage of wild-type intensity, which is set by definition at 100%. As shown, both podocin variants demonstrate significantly increased homodimerization with the wild type protein. With R229Q there is 209% increase (p=0.048) and with E237Q there is 244% increase (p=0.035).

Since co-expression of mutant podocin also alters nephrin localization, the interaction properties of the two proteins were next examined in the presence of the two variants. HEK293T cells were transiently co-transfected with the cDNAs of the *wt* nephrin and the *wt* or mutant podocin. In these immunoprecipitation assays, nephrin was observed to interact with lower affinity to *wt* podocin than with either of the two mutants *(Figure 48)*. The normalized intensity of nephrin immunoprecipitated by p.R229Q podocin demonstrated a 149% increase, compared to *wt* podocin (*n*=4 unpaired comparisons, p= 0.049 in an unpaired

two-tailed *t* test), while the normalized intensity of nephrin immunoprecipitated by p. E237Q podocin showed a 297% increase compared to *wt* podocin (*n*=4 unpaired comparisons, p= 0.0074 in an unpaired two-tailed *t* test). In the absence of podocin, nephrin did not immunoprecipitate while the western blot analysis indicated equivalent amounts of podocin were immunoprecipitated in each reaction.

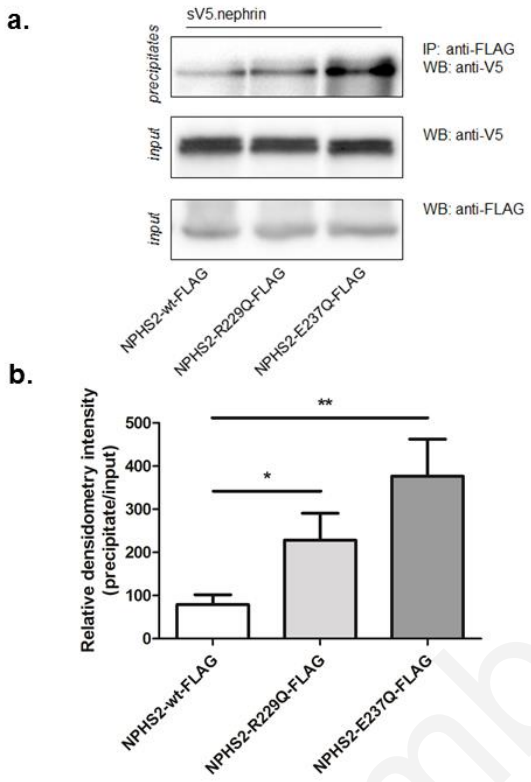

Figure 48: Podocin and nephrin interaction experiments

(a) Podocin and nephrin interaction experiments. Nephrin co-precipitates with both podocin variants p.R229Q and p.E237Q. FLAG- and V5-tagged proteins were expressed in HEK293T cells and precipitated with anti-FLAG antibody as indicated. Western blot analysis was performed with a V5 and FLAG specific antibodies. Expression levels of FLAG podocin and V5 nephrin constructs in the lysates are shown below. (b) Densitometry of the p.R229Q and p.E237Q bands from repeated experiments (n=4). Intensity (with error bars indicating SEM) is given as percentage of wild-type intensity, which is set by definition at 100%. As shown, both podocin variants demonstrate significantly increased interaction with wild type nephrin. With p.R229Q there is 149% increase (p=0.049) and with p.E237Q there is 297% increase (p=0.0074).

4.4 Discussion

Keeping in mind the great phenotypic heterogeneity observed among our TBMN patients, it was hypothesized that modifier genes could play an important role in the prognosis of this disease. Founder effects for two mutations in the *COL4A3* gene found in Cyprus, allowed for the identification of modifier variants due to less prominent genetic background "noise". Findings from previously published data (Tonna et al., 2008a, Voskarides et al., 2012) led to direct re-sequencing of the entire coding region of the *NPHS2* gene in "severe" patients, in an effort to detect more candidate modifier variants. Seven of the severely affected TBMN patients, were found to carry variants p.E237Q or p.R229Q, whereas none of the mildly affected patients had inherited any non-synonymous variant of obvious significance (p=0.05). Variant p.R229Q in heterozygosity is continuously reported in bibliography, with uncertain findings. However, it is well recognized that p.R229Q is a frequent cause of nephrotic syndrome when is inherited in compound heterozygosity with other *NPHS2* mutations (Voskarides et al., 2008a, Machuca et al., 2009, Caridi et al., 2009, Santin et al., 2011, Tory et al., 2014). Nevertheless, the actual effect of this variant when is found in heterozygosity is still under investigation. For example, Pereira et al (Pereira et al., 2004) in a general population study described p.R229Q as a putative cause of micro-albuminuria whereas Tonna et al (Tonna et al., 2008b) contradicted these findings, reporting that p.R229Q could not be considered as a risk factor for proteinuria in the general population. Moreover, Kottgen et al (Kottgen et al., 2008) did not corroborate any significant association between p.R229Q and GFR in either white or black individuals. Jungraithmayr et al (Jungraithmayr et al., 2011) suggested a possible association of p.R229Q with kidney transplant rejection. Based on a very detailed review and meta-analysis article by Franceschini et al (Franceschini et al., 2006), the p.R229Q variant gives a non-significant increased risk for FSGS by 20 to 70% in populations of European descent.

Data from Cyprus, report a frequency of 2% for the p.R229Q allele (Voskarides et al., 2012) and a frequency of 2,1% for the p.E237Q allele (4 heterozygous in 96 DNA samples of the general population studied here). Opposing to what is available for variant p.R229Q information about p.E237Q is still scanty. A number of investigators described this variant in heterozygosity in a few sporadic cases of nephrotic syndrome and FSGS, reporting that its significance is unknown (Weber et al., 2004, Ruf et al., 2004, Tonna et al., 2008b). Moreover, the frequency of p.E237Q in the general population is a debatable issue since two different studies report-contradicting results. In the first study, Ruf et al (Ruf et al., 2004)

were unable to find this variant in controls, while Weber et al (Weber et al., 2004) detected the p.E237Q in a frequency equal to the 0,3% in the general population.

Segregation studies in the families presented in this study provide evidence that p.R229Q and p.E237Q variants can act as modifiers for TBMN, probably through the development and the progression of histological FSGS, this being the case for individual IV:10 in family CY5304. The combined probability for these observations to have occurred by chance is very small, 0,003. Furthermore, this is the first report of a homozygous individual for the p.E237Q variant. Remarkably, homozygosity for this variant alone does not seem to cause a conspicuous phenotype.

Functional studies performed by Tsukaguchi et al (Tsukaguchi et al., 2002) demonstrated that p.R229Q could cause a reduction in the binding capacity of podocin to nephrin. More recently Tory et al (Tory et al., 2014) found that disease-associated 3′ mutations of podocin exert a dominant-negative effect on p.R229Q podocin but behave as recessive alleles when associated with *wt* podocin. Equivalent functional studies for variant p.E237Q do not exist. Both variants concern evolutionarily conserved aminoacid residues. In this study, it was hypothesized that both variants may adversely affect the interactions of slit diaphragm proteins, thereby predisposing to mechanical instability and deterioration of the filtration barrier as a long-term effect. It was shown that in the current experimental setting both variants appear to increase both podocin homodimerization as well as binding of podocin with nephrin. Moreover, immunofluorescence microscopy observations demonstrated that both p.E237Q and p.R229Q cause a peri-nuclear trapping of podocin. Binding assay shows that p.R229Q podocin binds more strongly on *wt* nephrin, in contrast to previous results (Tsukaguchi et al., 2002). The fact that these results were repeated for variant p.E237Q, in contrast to the *wt* podocin, is an indication for trusting these results, in this series of experiments. Even though these may be subtle effects, one should consider that these variants in heterozygosity on their own are recessive and have not been associated with a Mendelian disorder. We hypothesize that they only exert an effect, which becomes evident when co-inherited on the background of another glomerulopathy and only after many years during aging. Interestingly, Tory et al (Tory et al., 2014) found evidence that 237E and 229R are two residues that are structurally connected. In the authors' words: "Arg229 is stabilized in the core of the globular head domain by at least two hydrogen bonds involving Glu233, Glu237 or Asp244". This reinforces the genetic and functional findings for the two SNPs studied here, since they concern the same two residues.

4.5 Conclusions and future perspectives

In conclusion, these findings reinforce earlier published results, providing more evidence that certain non-synonymous variants in podocin are risk factors for proteinuria and renal impairment when found on the background of TBMN. These results conform to the rare variant-strong effect scenario for both p.R229Q and p.E237Q variants. These modifiers may be viewed as hypomorphic mutations, similar to what it was demonstrated for hypomorphic mutations in the *PKD* genes that were found to be responsible for severe and very early onset of autosomal dominant polycystic kidney disease (Bergmann et al., 2011). In that paper, Bergmann et al showed that some variants, which on their own are either recessive or neutral resulting in no perceptible phenotype, can lead to severe phenotype in childhood when co-inherited with mutations in the *PKD1/PKD2* genes, which normally are accompanied by late onset disease. Environmental factors such as smoking, high protein and sodium intake, in combination with genetic background, may increase even more the risk for these patients. Gender difference also appeared as a significant contributing factor for disease progression between "Severe" and "Mild" patients in our cohort. This shows that men risk behaviour hormones etc. can be an encumbering factor. Other existing kidney anomalies such as VUR may accelerate the progression, behaving in an additive manner together with genetic and environmental factors. This study confirmed this in one of the families studied at the present work. Results obtained from this set of experiments, showed that close clinical guidance and re-sequencing of the entire coding region of *NPHS2* gene in young TBMN patients, may warn for more careful long term follow-up, for a closer genetic counselling and advice regarding life style and for more timely therapeutic interventions, all aiming to delay or prevent progression to ESKD. This work, also suggests the probable existence of other rare podocin variants while it indicates that additional genetic factors definitely play a negative role of unknown degree in predisposing TBMN patients to an adverse disease outcome. This is simply based on the fact that many "severe" patients did not carry either of the two variants.

General Conclusion

TBMN and AS are hereditary collagen IV glomerulopathies primarily caused by mutations in the COL4A3/A4/A5 genes, with AS presenting hematuria, progressive nephritis with proteinuria and declining renal function, leading to end-stage renal disease, while TBMN is typically characterized by persistent microscopic hematuria of glomerular origin, minimal proteinuria, normal arterial blood pressure and normal renal function. Nonetheless, a number of limited reports suggest that, occasionally, TBMN can be progressive, leading to impairment of renal function of variable degree causing even focal segmental glomerulosclerosis (FSGS). The cause of this phenotypic variability observed in TBMN patients and the molecular mechanisms by which these mutations exert their deleterious effects on the glomerulus remain elusive.

This dissertation was focused in highlighting the molecular mechanism behind collagen IV mutations found in patients with TBMN and in identifying modifier genes resulting in the observed TBMN variability.

On the collagen mechanism, we found that defective trafficking of the COL4A3 chain causes a strong intracellular effect on the cell responsible for COL4A3 expression, the podocyte. To this end, normal and mutant COL4A3 chains (*COL4A3*-p.G1334E mutation) were overexpressed in human undifferentiated podocytes in order to verify their effects in various intracellular pathways employing a microarray approach. COL4A3 overexpression caused chain retention in the endoplasmic reticulum (ER) leading to the activation of unfolded protein response (UPR)–related markers of ER stress. Notably, the overexpression of normal or mutant COL4A3 chains differentially activated the UPR pathway. Similar results were observed in a novel knockin mouse carrying the *Col4a3*-p.G1332E mutation, which produced a phenotype consistent with AS and in biopsy specimens from patients with TBMN carrying a heterozygous *COL4A3*-p.G1334E mutation.

On the modifier gene part, we found that genetic modifiers could explain the observed variability of symptoms in TBMN patients. To this end, *in silico* analysis and re-sequencing in genes expressed in the slit diaphragm was performed, in an effort to detect potentially deleterious non-synonymous SNPs. Genotyping for six high-scored variants in 103 TBMN adult patients with founder mutations, who were classified as mildly or severely affected, pointed to an association with variant *NEPH3*-p.V353M (filtrin) (p=0.036). This result prompted testing in a larger pooled cohort (HEMATURIA) of 524 patients, which also included IgA nephropathy patients, categorized as “Severe” or “Mild”. This indicated an

association of the *NEPH3*-p.V353M variant with disease severity under the dominant model ($p=5.0x10^{-3}$). Subsequently, genotyping 6,531 subjects of the Framingham Heart Study (FHS) revealed an association of the homozygous 353M/M genotype with microalbuminuria ($p=1.0x10^{-3}$). Two further general population cohorts, KORAF4 and SAPHIR confirmed the association, and a meta-analysis of all three cohorts (11,258 individuals) was highly significant ($p=1.3x10^{-5}$). Moreover, functional studies exhibited a slight distortion in homodimerization or heterodimerization of Neph3 with nephrin caused by the *NEPH3*-p.V353M. Interestingly, a combination of a proteomics approach followed by immunoprecipitation and immunofluorescence experiments, identified Myh9 as a new interacting partner of filtrin. The filtrin *NEPH3*-p.V353M substitution resulted in a significantly stronger interaction with Myh9 protein. Additionally, overexpression of *NEPH3*-p.V353M in the presence of tunicamycin, exhibited a differential activation of the UPR pathway.

Furthermore, resequencing of *NPHS2* led to the detection of *NPHS2*-p.(E237Q) and *NPHS2*-p.(R229Q) in seven severely affected TBMN patients, belonging in two families which segregated mutation *COL4A3*-p.(G1334E) (combined concordance probability 0,003). Immunofluorescence experiments suggested altered localization of *wt* podocin or nephrin when co-expressed with each of the two these variants, demonstrating perinuclear staining. Additionally, immunoprecipitation experiments showed stronger binding of mutant podocin to *wt* podocin or nephrin.

These results suggest that ER stress arising from defective localization of collagen IV chains in human podocytes contributes to the pathogenesis of TBMN and AS through activation of the UPR, a finding that may pave the way for novel therapeutic interventions for a variety of collagenopathies. Moreover, genetics and functional studies support a "rare variant-strong effect" role for *NEPH3*-V353M, by exerting a negative modifier effect on primary hematuria. Additionally, genetic studies support a role in predisposing homozygous subjects of the general population to micro-albuminuria. Finally, genetics and functional studies support the hypothesis that certain hypomorphic podocin variants may act as adverse modifiers when co-inherited with *COL4A3/A4* mutations, thus predisposing to FSGS and severe kidney function decline. Overall the current study, using an interdisciplinary approach, shed light to the pathophysiology of TBMN, a serious health issue in Cyprus and around the world.

References

AALTONEN, P. & HOLTHOFER, H. 2007. The nephrin-based slit diaphragm: new insight into the signalling platform identifies targets for therapy. *Nephrol Dial Transplant,* 22**,** 3408-10.

ABRAHAMSON, D. R. 2012. Role of the podocyte (and glomerular endothelium) in building the GBM. *Semin Nephrol,* 32**,** 342-9.

ABRAHAMSON, D. R., HUDSON, B. G., STROGANOVA, L., BORZA, D. B. & ST JOHN, P. L. 2009. Cellular origins of type IV collagen networks in developing glomeruli. *J Am Soc Nephrol,* 20**,** 1471-9.

ALBERTS B, J. A., LEWIS J 2002. *Molecular Biology of the Cell,* New York, Garland Science.

ALHINDAWI, E. & AL-JBOUR, S. 2009. Epstein syndrome with rapid progression to end stage renal disease. *Saudi J Kidney Dis Transpl,* 20**,** 1076-8.

ALPORT, A. C. 1927. Hereditary Familial Congenital Haemorrhagic Nephritis. *Br Med J,* 1**,** 504-6.

ANDREWS, K. L., MUDD, J. L., LI, C. & MINER, J. H. 2002. Quantitative trait loci influence renal disease progression in a mouse model of Alport syndrome. *Am J Pathol,* 160**,** 721-30.

ANTIGNAC, C., ZHOU, J., SANAK, M., COCHAT, P., ROUSSEL, B., DESCHENES, G., GROS, F., KNEBELMANN, B., HORS-CAYLA, M. C., TRYGGVASON, K. & ET AL. 1992. Alport syndrome and diffuse leiomyomatosis: deletions in the 5' end of the COL4A5 collagen gene. *Kidney Int,* 42**,** 1178-83.

ARIF, E., WAGNER, M. C., JOHNSTONE, D. B., WONG, H. N., GEORGE, B., PRUTHI, P. A., LAZZARA, M. J. & NIHALANI, D. 2011. Motor protein Myo1c is a podocyte protein that facilitates the transport of slit diaphragm protein Neph1 to the podocyte membrane. *Mol Cell Biol,* 31**,** 2134-50.

ATHANASIOU, Y., VOSKARIDES, K., GALE, D. P., DAMIANOU, L., PATSIAS, C., ZAVROS, M., MAXWELL, P. H., COOK, H. T., DEMOSTHENOUS, P., HADJISAVVAS, A., KYRIACOU, K., ZOUVANI, I., PIERIDES, A. & DELTAS, C. 2011. Familial C3 glomerulopathy associated with CFHR5 mutations: clinical characteristics of 91 patients in 16 pedigrees. *Clin J Am Soc Nephrol,* 6**,** 1436-46.

BADENAS, C., PRAGA, M., TAZON, B., HEIDET, L., ARRONDEL, C., ARMENGOL, A., ANDRES, A., MORALES, E., CAMACHO, J. A., LENS, X., DAVILA, S., MILA, M., ANTIGNAC, C., DARNELL, A. & TORRA, R. 2002. Mutations in

theCOL4A4 and COL4A3 genes cause familial benign hematuria. *J Am Soc Nephrol,* 13**,** 1248-54.

BAKKER, A. J. 1999. Detection of microalbuminuria. Receiver operating characteristic curve analysis favors albumin-to-creatinine ratio over albumin concentration. *Diabetes Care,* 22**,** 307-13.

BAUMEISTER, S. E., BOGER, C. A., KRAMER, B. K., DORING, A., EHEBERG, D., FISCHER, B., JOHN, J., KOENIG, W. & MEISINGER, C. 2010. Effect of chronic kidney disease and comorbid conditions on health care costs: A 10-year observational study in a general population. *Am J Nephrol,* 31**,** 222-9.

BEIROWSKI, B., WEBER, M. & GROSS, O. 2006. Chronic renal failure and shortened lifespan in COL4A3+/- mice: an animal model for thin basement membrane nephropathy. *J Am Soc Nephrol,* 17**,** 1986-94.

BEK, M. F., BAYER, M., MULLER, B., GREIBER, S., LANG, D., SCHWAB, A., AUGUST, C., SPRINGER, E., ROHRBACH, R., HUBER, T. B., BENZING, T. & PAVENSTADT, H. 2006. Expression and function of C/EBP homology protein (GADD153) in podocytes. *Am J Pathol,* 168**,** 20-32.

BEKHEIRNIA, M. R., REED, B., GREGORY, M. C., MCFANN, K., SHAMSHIRSAZ, A. A., MASOUMI, A. & SCHRIER, R. W. 2010. Genotype-phenotype correlation in X-linked Alport syndrome. *J Am Soc Nephrol,* 21**,** 876-83.

BENZING, T. 2004. Signaling at the slit diaphragm. *J Am Soc Nephrol,* 15**,** 1382-91.

BERGMANN, C., VON BOTHMER, J., ORTIZ BRUCHLE, N., VENGHAUS, A., FRANK, V., FEHRENBACH, H., HAMPEL, T., PAPE, L., BUSKE, A., JONSSON, J., SARIOGLU, N., SANTOS, A., FERREIRA, J. C., BECKER, J. U., CREMER, R., HOEFELE, J., BENZ, M. R., WEBER, L. T., BUETTNER, R. & ZERRES, K. 2011. Mutations in multiple PKD genes may explain early and severe polycystic kidney disease. *J Am Soc Nephrol,* 22**,** 2047-56.

BORZA, D. B., BONDAR, O., NINOMIYA, Y., SADO, Y., NAITO, I., TODD, P. & HUDSON, B. G. 2001. The NC1 domain of collagen IV encodes a novel network composed of the alpha 1, alpha 2, alpha 5, and alpha 6 chains in smooth muscle basement membranes. *J Biol Chem,* 276**,** 28532-40.

BOUCHIREB, K., BOYER, O., GRIBOUVAL, O., NEVO, F., HUYNH-CONG, E., MORINIERE, V., CAMPAIT, R., ARS, E., BRACKMAN, D., DANTAL, J., ECKART, P., GIGANTE, M., LIPSKA, B. S., LIUTKUS, A., MEGARBANE, A., MOHSIN, N., OZALTIN, F., SALEEM, M. A., SCHAEFER, F., SOULAMI, K.,

TORRA, R., GARCELON, N., MOLLET, G., DAHAN, K. & ANTIGNAC, C. 2014. NPHS2 mutations in steroid-resistant nephrotic syndrome: a mutation update and the associated phenotypic spectrum. *Hum Mutat,* 35**,** 178-86.

BOUTE, N., GRIBOUVAL, O., ROSELLI, S., BENESSY, F., LEE, H., FUCHSHUBER, A., DAHAN, K., GUBLER, M. C., NIAUDET, P. & ANTIGNAC, C. 2000. NPHS2, encoding the glomerular protein podocin, is mutated in autosomal recessive steroid-resistant nephrotic syndrome. *Nat Genet,* 24**,** 349-54.

BRINKKOETTER, P. T., ISING, C. & BENZING, T. 2013. The role of the podocyte in albumin filtration. *Nat Rev Nephrol,* 9**,** 328-36.

BUZZA, M., DAGHER, H., WANG, Y. Y., WILSON, D., BABON, J. J., COTTON, R. G. & SAVIGE, J. 2003. Mutations in the COL4A4 gene in thin basement membrane disease. *Kidney Int,* 63**,** 447-53.

BUZZA, M., WANG, Y. Y., DAGHER, H., BABON, J. J., COTTON, R. G., POWELL, H., DOWLING, J. & SAVIGE, J. 2001. COL4A4 mutation in thin basement membrane disease previously described in Alport syndrome. *Kidney Int,* 60**,** 480-3.

CARIDI, G., GIGANTE, M., RAVANI, P., TRIVELLI, A., BARBANO, G., SCOLARI, F., DAGNINO, M., MURER, L., MURTAS, C., EDEFONTI, A., ALLEGRI, L., AMORE, A., COPPO, R., EMMA, F., DE PALO, T., PENZA, R., GESUALDO, L. & GHIGGERI, G. M. 2009. Clinical features and long-term outcome of nephrotic syndrome associated with heterozygous NPHS1 and NPHS2 mutations. *Clin J Am Soc Nephrol,* 4**,** 1065-72.

CAWLEY, K., DEEGAN, S., SAMALI, A. & GUPTA, S. 2011. Assays for detecting the unfolded protein response. *Methods Enzymol,* 490**,** 31-51.

CHENG, H. & HARRIS, R. C. 2010. The glomerulus--a view from the outside--the podocyte. *Int J Biochem Cell Biol,* 42**,** 1380-7.

CHENG, W., ZHOU, X., ZHU, L., SHI, S., LV, J., LIU, L. & ZHANG, H. 2011. Polymorphisms in the nonmuscle myosin heavy chain 9 gene (MYH9) are associated with the progression of IgA nephropathy in Chinese. *Nephrol Dial Transplant,* 26**,** 2544-9.

CHEONG, H. I., KASHTAN, C. E., KIM, Y., KLEPPEL, M. M. & MICHAEL, A. F. 1994. Immunohistologic studies of type IV collagen in anterior lens capsules of patients with Alport syndrome. *Lab Invest,* 70**,** 553-7.

CICCARESE, M., CASU, D., KI WONG, F., FAEDDA, R., ARVIDSSON, S., TONOLO, G., LUTHMAN, H. & SATTA, A. 2001. Identification of a new mutation in the

alpha4(IV) collagen gene in a family with autosomal dominant Alport syndrome and hypercholesterolaemia. *Nephrol Dial Transplant,* 16**,** 2008-12.

CLARE, N. M., MONTIEL, M. M., LIFSCHITZ, M. D. & BANNAYAN, G. A. 1979. Alport's syndrome associated with macrothrombopathic thrombocytopenia. *Am J Clin Pathol,* 72**,** 111-7.

CONTI, M. A., EVEN-RAM, S., LIU, C., YAMADA, K. M. & ADELSTEIN, R. S. 2004. Defects in cell adhesion and the visceral endoderm following ablation of nonmuscle myosin heavy chain II-A in mice. *J Biol Chem,* 279**,** 41263-6.

COSGROVE, D., MEEHAN, D. T., GRUNKEMEYER, J. A., KORNAK, J. M., SAYERS, R., HUNTER, W. J. & SAMUELSON, G. C. 1996a. Collagen COL4A3 knockout: a mouse model for autosomal Alport syndrome. *Genes Dev,* 10**,** 2981-92.

COSGROVE, D., SAMUELSON, G. & PINNT, J. 1996b. Immunohistochemical localization of basement membrane collagens and associated proteins in the murine cochlea. *Hear Res,* 97**,** 54-65.

CROCKETT, D. K., PONT-KINGDON, G., GEDGE, F., SUMNER, K., SEAMONS, R. & LYON, E. 2010. The Alport syndrome COL4A5 variant database. *Hum Mutat,* 31**,** E1652-7.

CYBULSKY, A. V. 2010. Endoplasmic reticulum stress in proteinuric kidney disease. *Kidney Int,* 77**,** 187-93.

CYBULSKY, A. V., TAKANO, T., PAPILLON, J. & BIJIAN, K. 2005. Role of the endoplasmic reticulum unfolded protein response in glomerular epithelial cell injury. *J Biol Chem,* 280**,** 24396-403.

CYBULSKY, A. V., TAKANO, T., PAPILLON, J., BIJIAN, K., GUILLEMETTE, J. & KENNEDY, C. R. 2009. Glomerular epithelial cell injury associated with mutant alpha-actinin-4. *Am J Physiol Renal Physiol,* 297**,** F987-95.

CYBULSKY, A. V., TAKANO, T., PAPILLON, J., KHADIR, A., LIU, J. & PENG, H. 2002. Complement C5b-9 membrane attack complex increases expression of endoplasmic reticulum stress proteins in glomerular epithelial cells. *J Biol Chem,* 277**,** 41342-51.

DEEN, W. M. 2004. What determines glomerular capillary permeability? *J Clin Invest,* 114**,** 1412-4.

DELTAS, C., PIERIDES, A. & VOSKARIDES, K. 2011. The role of molecular genetics in diagnosing familial hematuria(s). *Pediatr Nephrol*.

DELTAS, C., PIERIDES, A. & VOSKARIDES, K. 2012. The role of molecular genetics in diagnosing familial hematuria(s). *Pediatr Nephrol,* 27**,** 1221-31.

DELTAS, C., PIERIDES, A. & VOSKARIDES, K. 2013a. Molecular genetics of familial hematuric diseases. *Nephrol Dial Transplant*.

DELTAS, C., PIERIDES, A. & VOSKARIDES, K. 2013b. Molecular genetics of familial hematuric diseases. *Nephrol Dial Transplant,* 28**,** 2946-60.

DEMOSTHENOUS, P., VOSKARIDES, K., STYLIANOU, K., HADJIGAVRIEL, M., ARSALI, M., PATSIAS, C., GEORGAKI, E., ZIROGIANNIS, P., STAVROU, C., DAPHNIS, E., PIERIDES, A., DELTAS, C. & HELLENIC NEPHROGENETICS RESEARCH, C. 2012. X-linked Alport syndrome in Hellenic families: phenotypic heterogeneity and mutations near interruptions of the collagen domain in COL4A5. *Clin Genet,* 81**,** 240-8.

DROZDOVA, T., PAPILLON, J. & CYBULSKY, A. V. 2013. Nephrin missense mutations: induction of endoplasmic reticulum stress and cell surface rescue by reduction in chaperone interactions. *Physiol Rep,* 1**,** e00086.

EPSTEIN, C. J., SAHUD, M. A., PIEL, C. F., GOODMAN, J. R., BERNFIELD, M. R., KUSHNER, J. H. & ABLIN, A. R. 1972. Hereditary macrothrombocytopathia, nephritis and deafness. *Am J Med,* 52**,** 299-310.

EREMINA, V., JEFFERSON, J. A., KOWALEWSKA, J., HOCHSTER, H., HAAS, M., WEISSTUCH, J., RICHARDSON, C., KOPP, J. B., KABIR, M. G., BACKX, P. H., GERBER, H. P., FERRARA, N., BARISONI, L., ALPERS, C. E. & QUAGGIN, S. E. 2008. VEGF inhibition and renal thrombotic microangiopathy. *N Engl J Med,* 358**,** 1129-36.

FALLERINI, C., DOSA, L., TITA, R., DEL PRETE, D., FERIOZZI, S., GAI, G., CLEMENTI, M., LA MANNA, A., MIGLIETTI, N., MANCINI, R., MANDRILE, G., GHIGGERI, G. M., PIAGGIO, G., BRANCATI, F., DIANO, L., FRATE, E., PINCIAROLI, A. R., GIANI, M., CASTORINA, P., BRESIN, E., GIACHINO, D., DE MARCHI, M., MARI, F., BRUTTINI, M., RENIERI, A. & ARIANI, F. 2014. Unbiased next generation sequencing analysis confirms the existence of autosomal dominant Alport syndrome in a relevant fraction of cases. *Clin Genet,* 86**,** 252-7.

FAN, Q., ZHANG, H., DING, J., LIU, S., MIAO, J., XING, Y., YU, Z. & GUAN, N. 2009. R168H and V165X mutant podocin might induce different degrees of podocyte injury via different molecular mechanisms. *Genes Cells,* 14**,** 1079-90.

FEEHALLY, J., FLOEGE, J. & JOHNSON, R. C. 2007. *Comprehensive Clinical Nephrology,* Philadelphia, Mosby Elsevier.

FOGAZZI, G. B., EDEFONTI, A., GARIGALI, G., GIANI, M., ZOLIN, A., RAIMONDI, S., MIHATSCH, M. J. & MESSA, P. 2008. Urine erythrocyte morphology in patients with microscopic haematuria caused by a glomerulopathy. *Pediatr Nephrol,* 23**,** 1093-100.

FRANCESCHINI, N., NORTH, K. E., KOPP, J. B., MCKENZIE, L. & WINKLER, C. 2006. NPHS2 gene, nephrotic syndrome and focal segmental glomerulosclerosis: a HuGE review. *Genet Med,* 8**,** 63-75.

FUKASAWA, H., BORNHEIMER, S., KUDLICKA, K. & FARQUHAR, M. G. 2009. Slit diaphragms contain tight junction proteins. *J Am Soc Nephrol,* 20**,** 1491-503.

FUKUDA, K., HORI, H., UTANI, A., BURBELO, P. D. & YAMADA, Y. 1997. Formation of recombinant triple-helical [alpha 1(IV)]2 alpha 2(IV) collagen molecules in CHO cells. *Biochem Biophys Res Commun,* 231**,** 178-82.

GALE, D. P., DE JORGE, E. G., COOK, H. T., MARTINEZ-BARRICARTE, R., HADJISAVVAS, A., ADAM, G., MCLEAN, A. G., PUSEY, C. D., PIERIDES, A., KYRIACOU, K., ATHANASIOU, Y., VOSKARIDES, K., DELTAS, C., PALMER, A., FREMEAUX-BACCHI, V., CORDOBA, S., MAXWELL, P. H. & PICKERING, M. C. 2010. Complement Factor H-Related protein 5 (CFHR5) Nephropathy: an edemic cause of renal disease in Cyprus. *Lancet,* 376**,** 794-801.

GENOVESE, G., FRIEDMAN, D. J., ROSS, M. D., LECORDIER, L., UZUREAU, P., FREEDMAN, B. I., BOWDEN, D. W., LANGEFELD, C. D., OLEKSYK, T. K., USCINSKI KNOB, A. L., BERNHARDY, A. J., HICKS, P. J., NELSON, G. W., VANHOLLEBEKE, B., WINKLER, C. A., KOPP, J. B., PAYS, E. & POLLAK, M. R. 2010. Association of trypanolytic ApoL1 variants with kidney disease in African Americans. *Science,* 329**,** 841-5.

GHIGGERI, G. M., CARIDI, G., MAGRINI, U., SESSA, A., SAVOIA, A., SERI, M., PECCI, A., ROMAGNOLI, R., GANGAROSSA, S., NORIS, P., SARTORE, S., NECCHI, V., RAVAZZOLO, R. & BALDUINI, C. L. 2003. Genetics, clinical and pathological features of glomerulonephritis associated with mutations of nonmuscle myosin IIA (Fechtner syndrome). *Am J Kidney Dis,* 41**,** 95-104.

GODEL, M., OSTENDORF, B. N., BAUMER, J., WEBER, K. & HUBER, T. B. 2013. A novel domain regulating degradation of the glomerular slit diaphragm protein podocin in cell culture systems. *PLoS One,* 8**,** e57078.

GRAHAMMER, F., SCHELL, C. & HUBER, T. B. 2013. The podocyte slit diaphragm--from a thin grey line to a complex signalling hub. *Nat Rev Nephrol,* 9**,** 587-98.

GROSS, O., FRIEDE, T., HILGERS, R., GORLITZ, A., GAVENIS, K., AHMED, R. & DURR, U. 2012. Safety and Efficacy of the ACE-Inhibitor Ramipril in Alport Syndrome: The Double-Blind, Randomized, Placebo-Controlled, Multicenter Phase III EARLY PRO-TECT Alport Trial in Pediatric Patients. *ISRN Pediatr,* 2012**,** 436046.

GROSS, O., NETZER, K. O., LAMBRECHT, R., SEIBOLD, S. & WEBER, M. 2002. Meta-analysis of genotype-phenotype correlation in X-linked Alport syndrome: impact on clinical counselling. *Nephrol Dial Transplant,* 17**,** 1218-27.

GROSS, O., PERIN, L. & DELTAS, C. 2014. Alport syndrome from bench to bedside: the potential of current treatment beyond RAAS blockade and the horizon of future therapies. *Nephrol Dial Transplant,* 29 Suppl 4**,** iv124-30.

HALLMAN, N., NORIO, R. & KOUVALAINEN, K. 1967. Main features of the congenital nephrotic syndrome. *Acta Paediatr Scand***,** Suppl 172:75-8.

HARALDSSON, B. & JEANSSON, M. 2009. Glomerular filtration barrier. *Curr Opin Nephrol Hypertens,* 18**,** 331-5.

HARALDSSON, B., NYSTROM, J. & DEEN, W. M. 2008. Properties of the glomerular barrier and mechanisms of proteinuria. *Physiol Rev,* 88**,** 451-87.

HARTLEBEN, B., SCHWEIZER, H., LUBBEN, P., BARTRAM, M. P., MOLLER, C. C., HERR, R., WEI, C., NEUMANN-HAEFELIN, E., SCHERMER, B., ZENTGRAF, H., KERJASCHKI, D., REISER, J., WALZ, G., BENZING, T. & HUBER, T. B. 2008. Neph-Nephrin proteins bind the Par3-Par6-atypical protein kinase C (aPKC) complex to regulate podocyte cell polarity. *J Biol Chem,* 283**,** 23033-8.

HAYS, T., MA'AYAN, A., CLARK, N. R., TAN, C. M., TEIXEIRA, A., TEIXEIRA, A., CHOI, J. W., BURDIS, N., JUNG, S. Y., BAJAJ, A. O., O'MALLEY, B. W., HE, J. C., HYINK, D. P. & KLOTMAN, P. E. 2014. Proteomics analysis of the non-muscle myosin heavy chain IIa-enriched actin-myosin complex reveals multiple functions within the podocyte. *PLoS One,* 9**,** e100660.

HEID, I. M., WAGNER, S. A., GOHLKE, H., IGLSEDER, B., MUELLER, J. C., CIP, P., LADURNER, G., REITER, R., STADLMAYR, A., MACKEVICS, V., ILLIG, T., KRONENBERG, F. & PAULWEBER, B. 2006. Genetic architecture of the APM1 gene and its influence on adiponectin plasma levels and parameters of the metabolic syndrome in 1,727 healthy Caucasians. *Diabetes,* 55**,** 375-84.

HEIDET, L., ARRONDEL, C., FORESTIER, L., COHEN-SOLAL, L., MOLLET, G., GUTIERREZ, B., STAVROU, C., GUBLER, M. C. & ANTIGNAC, C. 2001. Structure of the human type IV collagen gene COL4A3 and mutations in autosomal Alport syndrome. *J Am Soc Nephrol,* 12**,** 97-106.

HEIDET, L., CAI, Y., GUICHARNAUD, L., ANTIGNAC, C. & GUBLER, M. C. 2000. Glomerular expression of type IV collagen chains in normal and X-linked Alport syndrome kidneys. *Am J Pathol,* 156**,** 1901-10.

HEIKKILA, E., RISTOLA, M., HAVANA, M., JONES, N., HOLTHOFER, H. & LEHTONEN, S. Trans-interaction of nephrin and Neph1/Neph3 induces cell adhesion that associates with decreased tyrosine phosphorylation of nephrin. *Biochem J,* 435**,** 619-28.

HEIKKILA, E., RISTOLA, M., HAVANA, M., JONES, N., HOLTHOFER, H. & LEHTONEN, S. 2011. Trans-interaction of nephrin and Neph1/Neph3 induces cell adhesion that associates with decreased tyrosine phosphorylation of nephrin. *Biochem J,* 435**,** 619-28.

HERTZ, J. M., THOMASSEN, M., STOREY, H. & FLINTER, F. 2012. Clinical utility gene card for: Alport syndrome. *Eur J Hum Genet,* 20.

HOEFELE, J., LANGE-SPERANDIO, B., RUESSMANN, D., GLOCKNER-PAGEL, J., ALBERER, M., BENZ, M. R., NAGEL, M. & WEBER, L. T. 2010. Novel heterozygous COL4A3 mutation in a family with late-onset ESRD. *Pediatr Nephrol,* 25**,** 1539-42.

HOLLIEN, J. & WEISSMAN, J. S. 2006. Decay of endoplasmic reticulum-localized mRNAs during the unfolded protein response. *Science,* 313**,** 104-7.

HOLTHOFER, H. 2007. Molecular architecture of the glomerular slit diaphragm: lessons learnt for a better understanding of disease pathogenesis. *Nephrol Dial Transplant,* 22**,** 2124-8.

HSU, S. I., RAMIREZ, S. B., WINN, M. P., BONVENTRE, J. V. & OWEN, W. F. 2000. Evidence for genetic factors in the development and progression of IgA nephropathy. *Kidney Int,* 57**,** 1818-35.

HUANG, Y., SHI, H., ZHOU, H., SONG, X., YUAN, S. & LUO, Y. 2006. The angiogenic function of nucleolin is mediated by vascular endothelial growth factor and nonmuscle myosin. *Blood,* 107**,** 3564-71.

HUBER, T. B., HARTLEBEN, B., KIM, J., SCHMIDTS, M., SCHERMER, B., KEIL, A., EGGER, L., LECHA, R. L., BORNER, C., PAVENSTADT, H., SHAW, A. S.,

WALZ, G. & BENZING, T. 2003a. Nephrin and CD2AP associate with phosphoinositide 3-OH kinase and stimulate AKT-dependent signaling. *Mol Cell Biol,* 23**,** 4917-28.

HUBER, T. B., SCHERMER, B., MULLER, R. U., HOHNE, M., BARTRAM, M., CALIXTO, A., HAGMANN, H., REINHARDT, C., KOOS, F., KUNZELMANN, K., SHIROKOVA, E., KRAUTWURST, D., HARTENECK, C., SIMONS, M., PAVENSTADT, H., KERJASCHKI, D., THIELE, C., WALZ, G., CHALFIE, M. & BENZING, T. 2006. Podocin and MEC-2 bind cholesterol to regulate the activity of associated ion channels. *Proc Natl Acad Sci U S A,* 103**,** 17079-86.

HUBER, T. B., SIMONS, M., HARTLEBEN, B., SERNETZ, L., SCHMIDTS, M., GUNDLACH, E., SALEEM, M. A., WALZ, G. & BENZING, T. 2003b. Molecular basis of the functional podocin-nephrin complex: mutations in the NPHS2 gene disrupt nephrin targeting to lipid raft microdomains. *Hum Mol Genet,* 12**,** 3397-405.

HUDSON, B. G., REEDERS, S. T. & TRYGGVASON, K. 1993. Type IV collagen: structure, gene organization, and role in human diseases. Molecular basis of Goodpasture and Alport syndromes and diffuse leiomyomatosis. *J Biol Chem,* 268**,** 26033-6.

HUTCHINGS, N. J., CLARKSON, N., CHALKLEY, R., BARCLAY, A. N. & BROWN, M. H. 2003. Linking the T cell surface protein CD2 to the actin-capping protein CAPZ via CMS and CIN85. *J Biol Chem,* 278**,** 22396-403.

IHALMO, P., PALMEN, T., AHOLA, H., VALTONEN, E. & HOLTHOFER, H. 2003. Filtrin is a novel member of nephrin-like proteins. *Biochem Biophys Res Commun,* 300**,** 364-70.

IHALMO, P., SCHMID, H., RASTALDI, M. P., MATTINZOLI, D., LANGHAM, R. G., LUIMULA, P., KILPIKARI, R., LASSILA, M., GILBERT, R. E., KERJASCHKI, D., KRETZLER, M. & HOLTHOFER, H. 2007. Expression of filtrin in human glomerular diseases. *Nephrol Dial Transplant,* 22**,** 1903-9.

INAGI, R., KUMAGAI, T., NISHI, H., KAWAKAMI, T., MIYATA, T., FUJITA, T. & NANGAKU, M. 2008. Preconditioning with endoplasmic reticulum stress ameliorates mesangioproliferative glomerulonephritis. *J Am Soc Nephrol,* 19**,** 915-22.

INAGI, R., NANGAKU, M., ONOGI, H., UEYAMA, H., KITAO, Y., NAKAZATO, K., OGAWA, S., KUROKAWA, K., COUSER, W. G. & MIYATA, T. 2005a. Involvement of endoplasmic reticulum (ER) stress in podocyte injury induced by excessive protein accumulation. *Kidney Int,* 68**,** 2639-50.

INAGI, R., NANGAKU, M., USUDA, N., SHIMIZU, A., ONOGI, H., IZUHARA, Y., NAKAZATO, K., UEDA, Y., OISHI, H., TAKAHASHI, S., YAMAMOTO, M., SUZUKI, D., KUROKAWA, K., VAN YPERSELE DE STRIHOU, C. & MIYATA, T. 2005b. Novel serpinopathy in rat kidney and pancreas induced by overexpression of megsin. *J Am Soc Nephrol,* 16**,** 1339-49.

ISHIDA, Y., YAMAMOTO, A., KITAMURA, A., LAMANDE, S. R., YOSHIMORI, T., BATEMAN, J. F., KUBOTA, H. & NAGATA, K. 2009. Autophagic elimination of misfolded procollagen aggregates in the endoplasmic reticulum as a means of cell protection. *Mol Biol Cell,* 20**,** 2744-54.

JAIS, J. P., KNEBELMANN, B., GIATRAS, I., DE MARCHI, M., RIZZONI, G., RENIERI, A., WEBER, M., GROSS, O., NETZER, K. O., FLINTER, F., PIRSON, Y., DAHAN, K., WIESLANDER, J., PERSSON, U., TRYGGVASON, K., MARTIN, P., HERTZ, J. M., SCHRODER, C., SANAK, M., CARVALHO, M. F., SAUS, J., ANTIGNAC, C., SMEETS, H. & GUBLER, M. C. 2003. X-linked Alport syndrome: natural history and genotype-phenotype correlations in girls and women belonging to 195 families: a "European Community Alport Syndrome Concerted Action" study. *J Am Soc Nephrol,* 14**,** 2603-10.

JAIS, J. P., KNEBELMANN, B., GIATRAS, I., DE MARCHI, M., RIZZONI, G., RENIERI, A., WEBER, M., GROSS, O., NETZER, K. O., FLINTER, F., PIRSON, Y., VERELLEN, C., WIESLANDER, J., PERSSON, U., TRYGGVASON, K., MARTIN, P., HERTZ, J. M., SCHRODER, C., SANAK, M., KREJCOVA, S., CARVALHO, M. F., SAUS, J., ANTIGNAC, C., SMEETS, H. & GUBLER, M. C. 2000. X-linked Alport syndrome: natural history in 195 families and genotype-phenotype correlations in males. *J Am Soc Nephrol,* 11**,** 649-57.

JEANNE, M., LABELLE-DUMAIS, C., JORGENSEN, J., KAUFFMAN, W. B., MANCINI, G. M., FAVOR, J., VALANT, V., GREENBERG, S. M., ROSAND, J. & GOULD, D. B. 2012. COL4A2 mutations impair COL4A1 and COL4A2 secretion and cause hemorrhagic stroke. *Am J Hum Genet,* 90**,** 91-101.

JOHNSTONE, D. B. & HOLZMAN, L. B. 2006. Clinical impact of research on the podocyte slit diaphragm. *Nat Clin Pract Nephrol,* 2**,** 271-82.

JONES, N., BLASUTIG, I. M., EREMINA, V., RUSTON, J. M., BLADT, F., LI, H., HUANG, H., LAROSE, L., LI, S. S., TAKANO, T., QUAGGIN, S. E. & PAWSON, T. 2006. Nck adaptor proteins link nephrin to the actin cytoskeleton of kidney podocytes. *Nature,* 440**,** 818-23.

JUNGRAITHMAYR, T. C., HOFER, K., COCHAT, P., CHERNIN, G., CORTINA, G., FARGUE, S., GRIMM, P., KNUEPPEL, T., KOWARSCH, A., NEUHAUS, T., PAGEL, P., PFEIFFER, K. P., SCHAFER, F., SCHONERMARCK, U., SEEMAN, T., TOENSHOFF, B., WEBER, S., WINN, M. P., ZSCHOCKE, J. & ZIMMERHACKL, L. B. 2011. Screening for NPHS2 mutations may help predict FSGS recurrence after transplantation. *J Am Soc Nephrol,* 22**,** 579-85.

JURKIN, J., HENKEL, T., NIELSEN, A. F., MINNICH, M., POPOW, J., KAUFMANN, T., HEINDL, K., HOFFMANN, T., BUSSLINGER, M. & MARTINEZ, J. 2014. The mammalian tRNA ligase complex mediates splicing of XBP1 mRNA and controls antibody secretion in plasma cells. *EMBO J,* 33**,** 2922-36.

KALLURI, R. 2003. Basement membranes: structure, assembly and role in tumour angiogenesis. *Nat Rev Cancer,* 3**,** 422-33.

KALLURI, R., SHIELD, C. F., TODD, P., HUDSON, B. G. & NEILSON, E. G. 1997. Isoform switching of type IV collagen is developmentally arrested in X-linked Alport syndrome leading to increased susceptibility of renal basement membranes to endoproteolysis. *J Clin Invest,* 99**,** 2470-8.

KANEKO, K., TANAKA, S., HASUI, M., NOZU, K., KROL, R. P., IIJIMA, K., SUGIMOTO, K. & TAKEMURA, T. 2010. A family with X-linked benign familial hematuria. *Pediatr Nephrol,* 25**,** 545-8.

KAO, W. H., KLAG, M. J., MEONI, L. A., REICH, D., BERTHIER-SCHAAD, Y., LI, M., CORESH, J., PATTERSON, N., TANDON, A., POWE, N. R., FINK, N. E., SADLER, J. H., WEIR, M. R., ABBOUD, H. E., ADLER, S. G., DIVERS, J., IYENGAR, S. K., FREEDMAN, B. I., KIMMEL, P. L., KNOWLER, W. C., KOHN, O. F., KRAMP, K., LEEHEY, D. J., NICHOLAS, S. B., PAHL, M. V., SCHELLING, J. R., SEDOR, J. R., THORNLEY-BROWN, D., WINKLER, C. A., SMITH, M. W., PAREKH, R. S., FAMILY INVESTIGATION OF, N. & DIABETES RESEARCH, G. 2008. MYH9 is associated with nondiabetic end-stage renal disease in African Americans. *Nat Genet,* 40**,** 1185-92.

KASHTAN, C. E. 2005a. Familial hematurias: what we know and what we don't. *Pediatr Nephrol,* 20**,** 1027-35.

KASHTAN, C. E. 2005b. The nongenetic diagnosis of thin basement membrane nephropathy. *Semin Nephrol,* 25**,** 159-62.

KATAYAMA, K., NOMURA, S., TRYGGVASON, K. & ITO, M. 2014. Searching for a treatment for Alport syndrome using mouse models. *World J Nephrol,* 3**,** 230-6.

KEFALIDES, N. A. 1966. A collagen of unusual composition and a glycoprotein isolated from canine glomerular basement membrane. *Biochem Biophys Res Commun,* 22**,** 26-32.

KEFALIDES, N. A. & WINZLER, R. J. 1966. The chemistry of glomerular basement membrane and its relation to collagen. *Biochemistry,* 5**,** 702-13.

KESTILA, M., LENKKERI, U., MANNIKKO, M., LAMERDIN, J., MCCREADY, P., PUTAALA, H., RUOTSALAINEN, V., MORITA, T., NISSINEN, M., HERVA, R., KASHTAN, C. E., PELTONEN, L., HOLMBERG, C., OLSEN, A. & TRYGGVASON, K. 1998. Positionally cloned gene for a novel glomerular protein--nephrin--is mutated in congenital nephrotic syndrome. *Mol Cell,* 1**,** 575-82.

KHANNA, H., DAVIS, E. E., MURGA-ZAMALLOA, C. A., ESTRADA-CUZCANO, A., LOPEZ, I., DEN HOLLANDER, A. I., ZONNEVELD, M. N., OTHMAN, M. I., WASEEM, N., CHAKAROVA, C. F., MAUBARET, C., DIAZ-FONT, A., MACDONALD, I., MUZNY, D. M., WHEELER, D. A., MORGAN, M., LEWIS, L. R., LOGAN, C. V., TAN, P. L., BEER, M. A., INGLEHEARN, C. F., LEWIS, R. A., JACOBSON, S. G., BERGMANN, C., BEALES, P. L., ATTIE-BITACH, T., JOHNSON, C. A., OTTO, E. A., BHATTACHARYA, S. S., HILDEBRANDT, F., GIBBS, R. A., KOENEKOOP, R. K., SWAROOP, A. & KATSANIS, N. 2009. A common allele in RPGRIP1L is a modifier of retinal degeneration in ciliopathies. *Nat Genet,* 41**,** 739-45.

KHOSHNOODI, J., HILL, S., TRYGGVASON, K., HUDSON, B. & FRIEDMAN, D. B. 2007. Identification of N-linked glycosylation sites in human nephrin using mass spectrometry. *J Mass Spectrom,* 42**,** 370-9.

KHOSHNOODI, J., PEDCHENKO, V. & HUDSON, B. G. 2008. Mammalian collagen IV. *Microsc Res Tech,* 71**,** 357-70.

KOBAYASHI, T. & UCHIYAMA, M. 2003. Characterization of assembly of recombinant type IV collagen alpha3, alpha4, and alpha5 chains in transfected cell strains. *Kidney Int,* 64**,** 1986-96.

KOPP, J. B. 2010. Glomerular pathology in autosomal dominant MYH9 spectrum disorders: what are the clues telling us about disease mechanism? *Kidney Int,* 78**,** 130-3.

KOPP, J. B., SMITH, M. W., NELSON, G. W., JOHNSON, R. C., FREEDMAN, B. I., BOWDEN, D. W., OLEKSYK, T., MCKENZIE, L. M., KAJIYAMA, H., AHUJA, T. S., BERNS, J. S., BRIGGS, W., CHO, M. E., DART, R. A., KIMMEL, P. L., KORBET, S. M., MICHEL, D. M., MOKRZYCKI, M. H., SCHELLING, J. R.,

SIMON, E., TRACHTMAN, H., VLAHOV, D. & WINKLER, C. A. 2008. MYH9 is a major-effect risk gene for focal segmental glomerulosclerosis. *Nat Genet,* 40**,** 1175-84.

KOTTGEN, A., HSU, C. C., CORESH, J., SHULDINER, A. R., BERTHIER-SCHAAD, Y., GAMBHIR, T. R., SMITH, M. W., BOERWINKLE, E. & KAO, W. H. 2008. The association of podocin R229Q polymorphism with increased albuminuria or reduced estimated GFR in a large population-based sample of US adults. *Am J Kidney Dis,* 52**,** 868-75.

KOZUTSUMI, Y., SEGAL, M., NORMINGTON, K., GETHING, M. J. & SAMBROOK, J. 1988. The presence of malfolded proteins in the endoplasmic reticulum signals the induction of glucose-regulated proteins. *Nature,* 332**,** 462-4.

KRAMER-ZUCKER, A. G., WIESSNER, S., JENSEN, A. M. & DRUMMOND, I. A. 2005. Organization of the pronephric filtration apparatus in zebrafish requires Nephrin, Podocin and the FERM domain protein Mosaic eyes. *Dev Biol,* 285**,** 316-29.

KRUEGEL, J., RUBEL, D. & GROSS, O. 2013. Alport syndrome--insights from basic and clinical research. *Nat Rev Nephrol,* 9**,** 170-8.

LEHTONEN, S., RYAN, J. J., KUDLICKA, K., IINO, N., ZHOU, H. & FARQUHAR, M. G. 2005. Cell junction-associated proteins IQGAP1, MAGI-2, CASK, spectrins, and alpha-actinin are components of the nephrin multiprotein complex. *Proc Natl Acad Sci U S A,* 102**,** 9814-9.

LEINONEN, A., NETZER, K. O., BOUTAUD, A., GUNWAR, S. & HUDSON, B. G. 1999. Goodpasture antigen: expression of the full-length alpha3(IV) chain of collagen IV and localization of epitopes exclusively to the noncollagenous domain. *Kidney Int,* 55**,** 926-35.

LEMMINK, H. H., NILLESEN, W. N., MOCHIZUKI, T., SCHRODER, C. H., BRUNNER, H. G., VAN OOST, B. A., MONNENS, L. A. & SMEETS, H. J. 1996. Benign familial hematuria due to mutation of the type IV collagen alpha4 gene. *J Clin Invest,* 98**,** 1114-8.

LENNON, R., BYRON, A., HUMPHRIES, J. D., RANDLES, M. J., CARISEY, A., MURPHY, S., KNIGHT, D., BRENCHLEY, P. E., ZENT, R. & HUMPHRIES, M. J. 2014. Global analysis reveals the complexity of the human glomerular extracellular matrix. *J Am Soc Nephrol,* 25**,** 939-51.

LI, M., ARMELLONI, S., EDEFONTI, A., MESSA, P. & RASTALDI, M. P. 2013. Fifteen years of research on nephrin: what we still need to know. *Nephrol Dial Transplant,* 28**,** 767-70.

LIN, F., BIAN, F., ZOU, J., WU, X., SHAN, J., LU, W., YAO, Y., JIANG, G. & GALE, D. P. 2014a. Whole exome sequencing reveals novel COL4A3 and COL4A4 mutations and resolves diagnosis in Chinese families with kidney disease. *BMC Nephrol,* 15**,** 175.

LIN, X., SUH, J. H., GO, G. & MINER, J. H. 2014b. Feasibility of repairing glomerular basement membrane defects in Alport syndrome. *J Am Soc Nephrol,* 25**,** 687-92.

LINDENMEYER, M. T., RASTALDI, M. P., IKEHATA, M., NEUSSER, M. A., KRETZLER, M., COHEN, C. D. & SCHLONDORFF, D. 2008. Proteinuria and hyperglycemia induce endoplasmic reticulum stress. *J Am Soc Nephrol,* 19**,** 2225-36.

LITTMAN, M. P., WILEY, C. A., RADUCHA, M. G. & HENTHORN, P. S. 2013. Glomerulopathy and mutations in NPHS1 and KIRREL2 in soft-coated Wheaten Terrier dogs. *Mamm Genome,* 24**,** 119-26.

LIU, L., DONE, S. C., KHOSHNOODI, J., BERTORELLO, A., WARTIOVAARA, J., BERGGREN, P. O. & TRYGGVASON, K. 2001. Defective nephrin trafficking caused by missense mutations in the NPHS1 gene: insight into the mechanisms of congenital nephrotic syndrome. *Hum Mol Genet,* 10**,** 2637-44.

LIU, M., SHI, S., SENTHILNATHAN, S., YU, J., WU, E., BERGMANN, C., ZERRES, K., BOGDANOVA, N., COTO, E., DELTAS, C., PIERIDES, A., DEMETRIOU, K., DEVUYST, O., GITOMER, B., LAAKSO, M., LUMIAHO, A., LAMNISSOU, K., MAGISTRONI, R., PARFREY, P., BREUNING, M., PETERS, D. J., TORRA, R., WINEARLS, C. G., TORRES, V. E., HARRIS, P. C., PATERSON, A. D. & PEI, Y. 2010. Genetic variation of DKK3 may modify renal disease severity in ADPKD. *J Am Soc Nephrol,* 21**,** 1510-20.

LIU, X. L., DONE, S. C., YAN, K., KILPELAINEN, P., PIKKARAINEN, T. & TRYGGVASON, K. 2004. Defective trafficking of nephrin missense mutants rescued by a chemical chaperone. *J Am Soc Nephrol,* 15**,** 1731-8.

LU, W., PHILLIPS, C. L., KILLEN, P. D., HLAING, T., HARRISON, W. R., ELDER, F. F., MINER, J. H., OVERBEEK, P. A. & MEISLER, M. H. 1999. Insertional mutation of the collagen genes Col4a3 and Col4a4 in a mouse model of Alport syndrome. *Genomics,* 61**,** 113-24.

MACHUCA, E., HUMMEL, A., NEVO, F., DANTAL, J., MARTINEZ, F., AL-SABBAN, E., BAUDOUIN, V., ABEL, L., GRUNFELD, J. P. & ANTIGNAC, C. 2009. Clinical and epidemiological assessment of steroid-resistant nephrotic syndrome associated with the NPHS2 R229Q variant. *Kidney Int,* 75**,** 727-35.

MALONE, A. F., PHELAN, P. J., HALL, G., CETINCELIK, U., HOMSTAD, A., ALONSO, A. S., JIANG, R., LINDSEY, T. B., WU, G., SPARKS, M. A., SMITH, S. R., WEBB, N. J., KALRA, P. A., ADEYEMO, A. A., SHAW, A. S., CONLON, P. J., JENNETTE, J. C., HOWELL, D. N., WINN, M. P. & GBADEGESIN, R. A. 2014. Rare hereditary COL4A3/COL4A4 variants may be mistaken for familial focal segmental glomerulosclerosis. *Kidney Int,* 86**,** 1253-9.

MARCOCCI, E., ULIANA, V., BRUTTINI, M., ARTUSO, R., SILENGO, M. C., ZERIAL, M., BERGESIO, F., AMOROSO, A., SAVOLDI, S., PENNESI, M., GIACHINO, D., ROMBOLA, G., FOGAZZI, G. B., ROSATELLI, C., MARTINHAGO, C. D., CARMELLINI, M., MANCINI, R., DI COSTANZO, G., LONGO, I., RENIERI, A. & MARI, F. 2009. Autosomal dominant Alport syndrome: molecular analysis of the COL4A4 gene and clinical outcome. *Nephrol Dial Transplant,* 24**,** 1464-71.

MARKAN, S., KOHLI, H. S., JOSHI, K., MINZ, R. W., SUD, K., AHUJA, M., ANAND, S. & KHULLAR, M. 2009. Up regulation of the GRP-78 and GADD-153 and down regulation of Bcl-2 proteins in primary glomerular diseases: a possible involvement of the ER stress pathway in glomerulonephritis. *Mol Cell Biochem,* 324**,** 131-8.

MENCARELLI, M. A., HEIDET, L., STOREY, H., VAN GEEL, M., KNEBELMANN, B., FALLERINI, C., MIGLIETTI, N., ANTONUCCI, M. F., CETTA, F., SAYER, J. A., VAN DEN WIJNGAARD, A., YAU, S., MARI, F., BRUTTINI, M., ARIANI, F., DAHAN, K., SMEETS, B., ANTIGNAC, C., FLINTER, F. & RENIERI, A. 2015. Evidence of digenic inheritance in Alport syndrome. *J Med Genet*.

MEUSSER, B., HIRSCH, C., JAROSCH, E. & SOMMER, T. 2005. ERAD: the long road to destruction. *Nat Cell Biol,* 7**,** 766-72.

MINER, J. H. 2012a. The glomerular basement membrane. *Exp Cell Res,* 318**,** 973-8.

MINER, J. H. 2012b. Life without nephrin: it's for the birds. *J Am Soc Nephrol,* 23**,** 369-71.

MINER, J. H. & SANES, J. R. 1996. Molecular and functional defects in kidneys of mice lacking collagen alpha 3(IV): implications for Alport syndrome. *J Cell Biol,* 135**,** 1403-13.

MORSE, E., SCHROTH, J., YOU, Y. H., PIZZO, D. P., OKADA, S., RAMACHANDRARAO, S., VALLON, V., SHARMA, K. & CUNARD, R. 2010.

TRB3 is stimulated in diabetic kidneys, regulated by the ER stress marker CHOP, and is a suppressor of podocyte MCP-1. *Am J Physiol Renal Physiol,* 299**,** F965-72.

MOXEY-MIMS, M. M., YOUNG, G., SILVERMAN, A., SELBY, D. M., WHITE, J. G. & KHER, K. K. 1999. End-stage renal disease in two pediatric patients with Fechtner syndrome. *Pediatr Nephrol,* 13**,** 782-6.

MULLER, T., RUMPEL, E., HRADETZKY, S., BOLLIG, F., WEGNER, H., BLUMENTHAL, A., GREINACHER, A., ENDLICH, K. & ENDLICH, N. 2011. Non-muscle myosin IIA is required for the development of the zebrafish glomerulus. *Kidney Int,* 80**,** 1055-63.

NAITO, I., NOMURA, S., INOUE, S., KAGAWA, M., KAWAI, S., GUNSHIN, Y., JOH, K., TSUKIDATE, C., SADO, Y. & OSAWA, G. 1997. Normal distribution of collagen IV in renal basement membranes in Epstein's syndrome. *J Clin Pathol,* 50**,** 919-22.

NAKANISHI, K., YOSHIKAWA, N., IIJIMA, K., KITAGAWA, K., NAKAMURA, H., ITO, H., YOSHIOKA, K., KAGAWA, M. & SADO, Y. 1994. Immunohistochemical study of alpha 1-5 chains of type IV collagen in hereditary nephritis. *Kidney Int,* 46**,** 1413-21.

NATHAN, D. M., ROSENBAUM, C. & PROTASOWICKI, V. D. 1987. Single-void urine samples can be used to estimate quantitative microalbuminuria. *Diabetes Care,* 10**,** 414-8.

NATIONAL KIDNEY, F. 2002. K/DOQI clinical practice guidelines for chronic kidney disease: evaluation, classification, and stratification. *Am J Kidney Dis,* 39**,** S1-266.

NELSON, R. K. W. E. 2011. Nelson textbook of pediatrics. 19th ed. Philadelphia, PA: Elsevier/Saunders.

NG, P. C. & HENIKOFF, S. 2001. Predicting deleterious amino acid substitutions. *Genome Res,* 11**,** 863-74.

NISHIBORI, Y., LIU, L., HOSOYAMADA, M., ENDOU, H., KUDO, A., TAKENAKA, H., HIGASHIHARA, E., BESSHO, F., TAKAHASHI, S., KERSHAW, D., RUOTSALAINEN, V., TRYGGVASON, K., KHOSHNOODI, J. & YAN, K. 2004. Disease-causing missense mutations in NPHS2 gene alter normal nephrin trafficking to the plasma membrane. *Kidney Int,* 66**,** 1755-65.

NORIS, M., REMUZZI, G 2012. Non-muscle myosins and the podocyte. *Clinical Kidney Journal,* 5**,** 94-101.

OHASHI, T., UCHIDA, K., UCHIDA, S., SASAKI, S. & NIHEI, H. 2003. Intracellular mislocalization of mutant podocin and correction by chemical chaperones. *Histochem Cell Biol,* 119**,** 257-64.

OHSE, T., INAGI, R., TANAKA, T., OTA, T., MIYATA, T., KOJIMA, I., INGELFINGER, J. R., OGAWA, S., FUJITA, T. & NANGAKU, M. 2006. Albumin induces endoplasmic reticulum stress and apoptosis in renal proximal tubular cells. *Kidney Int,* 70**,** 1447-55.

PAPAZACHARIOU, L., DEMOSTHENOUS, P., PIERI, M., PAPAGREGORIOU, G., SAVVA, I., STAVROU, C., ZAVROS, M., ATHANASIOU, Y., IOANNOU, K., PATSIAS, C., PANAGIDES, A., POTAMITIS, C., DEMETRIOU, K., PRIKIS, M., HADJIGAVRIEL, M., KKOLOU, M., LOUKAIDOU, P., PASTELLI, A., MICHAEL, A., LAZAROU, A., ARSALI, M., DAMIANOU, L., GOUTZIAMANI, I., SOLOUKIDES, A., YIOUKAS, L., ELIA, A., ZOUVANI, I., POLYCARPOU, P., PIERIDES, A., VOSKARIDES, K. & DELTAS, C. 2014. Frequency of COL4A3/COL4A4 Mutations amongst Families Segregating Glomerular Microscopic Hematuria and Evidence for Activation of the Unfolded Protein Response. Focal and Segmental Glomerulosclerosis Is a Frequent Development during Ageing. *PLoS One,* 9**,** e115015.

PATRAKKA, J. & TRYGGVASON, K. 2007. Nephrin--a unique structural and signaling protein of the kidney filter. *Trends Mol Med,* 13**,** 396-403.

PATRAKKA, J. & TRYGGVASON, K. 2009. New insights into the role of podocytes in proteinuria. *Nat Rev Nephrol,* 5**,** 463-8.

PATRAKKA, J. & TRYGGVASON, K. 2010. Molecular make-up of the glomerular filtration barrier. *Biochem Biophys Res Commun,* 396**,** 164-9.

PAVENSTADT, H., KRIZ, W. & KRETZLER, M. 2003. Cell biology of the glomerular podocyte. *Physiol Rev,* 83**,** 253-307.

PEISSEL, B., GENG, L., KALLURI, R., KASHTAN, C., RENNKE, H. G., GALLO, G. R., YOSHIOKA, K., SUN, M. J., HUDSON, B. G., NEILSON, E. G. & ET AL. 1995. Comparative distribution of the alpha 1(IV), alpha 5(IV), and alpha 6(IV) collagen chains in normal human adult and fetal tissues and in kidneys from X-linked Alport syndrome patients. *J Clin Invest,* 96**,** 1948-57.

PEREIRA, A. C., PEREIRA, A. B., MOTA, G. F., CUNHA, R. S., HERKENHOFF, F. L., POLLAK, M. R., MILL, J. G. & KRIEGER, J. E. 2004. NPHS2 R229Q functional

variant is associated with microalbuminuria in the general population. *Kidney Int,* 65**,** 1026-30.

PETERSON, L. C., RAO, K. V., CROSSON, J. T. & WHITE, J. G. 1985. Fechtner syndrome--a variant of Alport's syndrome with leukocyte inclusions and macrothrombocytopenia. *Blood,* 65**,** 397-406.

PIERI, M., STEFANOU, C., ZARAVINOS, A., ERGULER, K., STYLIANOU, K., LAPATHITIS, G., KARAISKOS, C., SAVVA, I., PARASKEVA, R., DWEEP, H., STICHT, C., ANASTASIADOU, N., ZOUVANI, I., GOUMENOS, D., FELEKKIS, K., SALEEM, M., VOSKARIDES, K., GRETZ, N. & DELTAS, C. 2014. Evidence for activation of the unfolded protein response in collagen IV nephropathies. *J Am Soc Nephrol,* 25**,** 260-75.

PIERIDES, A., VOSKARIDES, K., ATHANASIOU, Y., IOANNOU, K., DAMIANOU, L., ARSALI, M., ZAVROS, M., PIERIDES, M., VARGEMEZIS, V., PATSIAS, C., ZOUVANI, I., ELIA, A., KYRIACOU, K. & DELTAS, C. 2009. Clinico-pathological correlations in 127 patients in 11 large pedigrees, segregating one of three heterozygous mutations in the COL4A3/ COL4A4 genes associated with familial haematuria and significant late progression to proteinuria and chronic kidney disease from focal segmental glomerulosclerosis. *Nephrol Dial Transplant,* 24**,** 2721-9.

PIERIDES, A., VOSKARIDES, K., KKOLOU, M., HADJIGAVRIEL, M. & DELTAS, C. 2013. X-linked, COL4A5 hypomorphic Alport mutations such as G624D and P628L may only exhibit thin basement membrane nephropathy with microhematuria and late onset kidney failure. *Hippokratia,* 17**,** 207-13.

POLLAK, M. R. 2009. Expanding the spectrum of NPHS1-associated disease. *Kidney Int,* 76**,** 1221-3.

REEVES, W., CAULFIELD, J. P. & FARQUHAR, M. G. 1978. Differentiation of epithelial foot processes and filtration slits: sequential appearance of occluding junctions, epithelial polyanion, and slit membranes in developing glomeruli. *Lab Invest,* 39**,** 90-100.

REIMOLD, A. M., IWAKOSHI, N. N., MANIS, J., VALLABHAJOSYULA, P., SZOMOLANYI-TSUDA, E., GRAVALLESE, E. M., FRIEND, D., GRUSBY, M. J., ALT, F. & GLIMCHER, L. H. 2001. Plasma cell differentiation requires the transcription factor XBP-1. *Nature,* 412**,** 300-7.

REISER, J., SEVER, S. & FAUL, C. 2014. Signal transduction in podocytes--spotlight on receptor tyrosine kinases. *Nat Rev Nephrol,* 10**,** 104-15.

REY, M., VICENTE-MANZANARES, M., VIEDMA, F., YANEZ-MO, M., URZAINQUI, A., BARREIRO, O., VAZQUEZ, J. & SANCHEZ-MADRID, F. 2002. Cutting edge: association of the motor protein nonmuscle myosin heavy chain-IIA with the C terminus of the chemokine receptor CXCR4 in T lymphocytes. *J Immunol,* 169**,** 5410-4.

REYNAUD, E. 2010. *Protein Misfolding and Degenerative Diseases* [Online]. Nature Education. Available: http://www.nature.com/scitable/topicpage/protein-misfolding-and-degenerative-diseases-14434929.

RHEAULT, M. N., KREN, S. M., THIELEN, B. K., MESA, H. A., CROSSON, J. T., THOMAS, W., SADO, Y., KASHTAN, C. E. & SEGAL, Y. 2004. Mouse model of X-linked Alport syndrome. *J Am Soc Nephrol,* 15**,** 1466-74.

RINTA-VALKAMA, J., PALMEN, T., LASSILA, M. & HOLTHOFER, H. 2007. Podocyte-associated proteins FAT, alpha-actinin-4 and filtrin are expressed in Langerhans islets of the pancreas. *Mol Cell Biochem,* 294**,** 117-25.

RISTOLA, M., ARPIAINEN, S., SALEEM, M. A., MATHIESON, P. W., WELSH, G. I., LEHTONEN, S. & HOLTHOFER, H. 2009. Regulation of Neph3 gene in podocytes--key roles of transcription factors NF-kappaB and Sp1. *BMC Mol Biol,* 10**,** 83.

RISTOLA, M. & LEHTONEN, S. 2014. Functions of the podocyte proteins nephrin and Neph3 and the transcriptional regulation of their genes. *Clin Sci (Lond),* 126**,** 315-28.

RODEWALD, R. & KARNOVSKY, M. J. 1974. Porous substructure of the glomerular slit diaphragm in the rat and mouse. *J Cell Biol,* 60**,** 423-33.

RON, D. & WALTER, P. 2007. Signal integration in the endoplasmic reticulum unfolded protein response. *Nat Rev Mol Cell Biol,* 8**,** 519-29.

ROSDAHL, C. B. & KOWALSKI, M. T. 2008. *Textbook of Basic Nursing,* Lippincott Williams & Wilkins.

ROSELLI, S., HEIDET, L., SICH, M., HENGER, A., KRETZLER, M., GUBLER, M. C. & ANTIGNAC, C. 2004a. Early glomerular filtration defect and severe renal disease in podocin-deficient mice. *Mol Cell Biol,* 24**,** 550-60.

ROSELLI, S., MOUTKINE, I., GRIBOUVAL, O., BENMERAH, A. & ANTIGNAC, C. 2004b. Plasma membrane targeting of podocin through the classical exocytic pathway: effect of NPHS2 mutations. *Traffic,* 5**,** 37-44.

ROSTGAARD, J. & QVORTRUP, K. 1997. Electron microscopic demonstrations of filamentous molecular sieve plugs in capillary fenestrae. *Microvasc Res,* 53**,** 1-13.

RUF, R. G., LICHTENBERGER, A., KARLE, S. M., HAAS, J. P., ANACLETO, F. E., SCHULTHEISS, M., ZALEWSKI, I., IMM, A., RUF, E. M., MUCHA, B., BAGGA, A., NEUHAUS, T., FUCHSHUBER, A., BAKKALOGLU, A., HILDEBRANDT, F. & ARBEITSGEMEINSCHAFT FUR PADIATRISCHE NEPHROLOGIE STUDY, G. 2004. Patients with mutations in NPHS2 (podocin) do not respond to standard steroid treatment of nephrotic syndrome. *J Am Soc Nephrol,* 15**,** 722-32.

RUOTSALAINEN, V., LJUNGBERG, P., WARTIOVAARA, J., LENKKERI, U., KESTILA, M., JALANKO, H., HOLMBERG, C. & TRYGGVASON, K. 1999. Nephrin is specifically located at the slit diaphragm of glomerular podocytes. *Proc Natl Acad Sci U S A,* 96**,** 7962-7.

SALEEM, M. A., O'HARE, M. J., REISER, J., COWARD, R. J., INWARD, C. D., FARREN, T., XING, C. Y., NI, L., MATHIESON, P. W. & MUNDEL, P. 2002. A conditionally immortalized human podocyte cell line demonstrating nephrin and podocin expression. *J Am Soc Nephrol,* 13**,** 630-8.

SALMON, A. H., NEAL, C. R. & HARPER, S. J. 2009. New aspects of glomerular filtration barrier structure and function: five layers (at least) not three. *Curr Opin Nephrol Hypertens,* 18**,** 197-205.

SANTIN, S., TAZON-VEGA, B., SILVA, I., COBO, M. A., GIMENEZ, I., RUIZ, P., GARCIA-MASET, R., BALLARIN, J., TORRA, R., ARS, E. & GROUP, F. S. S. 2011. Clinical value of NPHS2 analysis in early- and adult-onset steroid-resistant nephrotic syndrome. *Clin J Am Soc Nephrol,* 6**,** 344-54.

SAVIGE, J., GREGORY, M., GROSS, O., KASHTAN, C., DING, J. & FLINTER, F. 2013. Expert guidelines for the management of Alport syndrome and thin basement membrane nephropathy. *J Am Soc Nephrol,* 24**,** 364-75.

SAVIGE, J., RANA, K., TONNA, S., BUZZA, M., DAGHER, H. & WANG, Y. Y. 2003. Thin basement membrane nephropathy. *Kidney Int,* 64**,** 1169-78.

SCHINDLER, A. J. & SCHEKMAN, R. 2009. In vitro reconstitution of ER-stress induced ATF6 transport in COPII vesicles. *Proc Natl Acad Sci U S A,* 106**,** 17775-80.

SCHUCK, S., PRINZ, W. A., THORN, K. S., VOSS, C. & WALTER, P. 2009. Membrane expansion alleviates endoplasmic reticulum stress independently of the unfolded protein response. *J Cell Biol,* 187**,** 525-36.

SCHWARZ, K., SIMONS, M., REISER, J., SALEEM, M. A., FAUL, C., KRIZ, W., SHAW, A. S., HOLZMAN, L. B. & MUNDEL, P. 2001. Podocin, a raft-associated component of the glomerular slit diaphragm, interacts with CD2AP and nephrin. *J Clin Invest,* 108**,** 1621-9.

SEKINE, T., KONNO, M., SASAKI, S., MORITANI, S., MIURA, T., WONG, W. S., NISHIO, H., NISHIGUCHI, T., OHUCHI, M. Y., TSUCHIYA, S., MATSUYAMA, T., KANEGANE, H., IDA, K., MIURA, K., HARITA, Y., HATTORI, M., HORITA, S., IGARASHI, T., SAITO, H. & KUNISHIMA, S. 2010. Patients with Epstein-Fechtner syndromes owing to MYH9 R702 mutations develop progressive proteinuric renal disease. *Kidney Int,* 78**,** 207-14.

SELLIN, L., HUBER, T. B., GERKE, P., QUACK, I., PAVENSTADT, H. & WALZ, G. 2003. NEPH1 defines a novel family of podocin interacting proteins. *FASEB J,* 17**,** 115-7.

SERI, M., CUSANO, R., GANGAROSSA, S., CARIDI, G., BORDO, D., LO NIGRO, C., GHIGGERI, G. M., RAVAZZOLO, R., SAVINO, M., DEL VECCHIO, M., D'APOLITO, M., IOLASCON, A., ZELANTE, L. L., SAVOIA, A., BALDUINI, C. L., NORIS, P., MAGRINI, U., BELLETTI, S., HEATH, K. E., BABCOCK, M., GLUCKSMAN, M. J., ALIPRANDIS, E., BIZZARO, N., DESNICK, R. J. & MARTIGNETTI, J. A. 2000. Mutations in MYH9 result in the May-Hegglin anomaly, and Fechtner and Sebastian syndromes. The May-Heggllin/Fechtner Syndrome Consortium. *Nat Genet,* 26**,** 103-5.

SIEBER, J., LINDENMEYER, M. T., KAMPE, K., CAMPBELL, K. N., COHEN, C. D., HOPFER, H., MUNDEL, P. & JEHLE, A. W. 2010. Regulation of podocyte survival and endoplasmic reticulum stress by fatty acids. *Am J Physiol Renal Physiol,* 299**,** F821-9.

SLAJPAH, M., GORINSEK, B., BERGINC, G., VIZJAK, A., FERLUGA, D., HVALA, A., MEGLIC, A., JAKSA, I., FURLAN, P., GREGORIC, A., KAPLAN-PAVLOVCIC, S., RAVNIK-GLAVAC, M. & GLAVAC, D. 2007. Sixteen novel mutations identified in COL4A3, COL4A4, and COL4A5 genes in Slovenian families with Alport syndrome and benign familial hematuria. *Kidney Int,* 71**,** 1287-95.

ST JOHN, P. L. & ABRAHAMSON, D. R. 2001. Glomerular endothelial cells and podocytes jointly synthesize laminin-1 and -11 chains. *Kidney Int,* 60**,** 1037-46.

STEFFES, M. W., BARBOSA, J., BASGEN, J. M., SUTHERLAND, D. E., NAJARIAN, J. S. & MAUER, S. M. 1983. Quantitative glomerular morphology of the normal human kidney. *Lab Invest,* 49**,** 82-6.

SUH, J. H. & MINER, J. H. 2013. The glomerular basement membrane as a barrier to albumin. *Nat Rev Nephrol,* 9**,** 470-7.

SUN, C., KILBURN, D., LUKASHIN, A., CROWELL, T., GARDNER, H., BRUNDIERS, R., DIEFENBACH, B. & CARULLI, J. P. 2003. Kirrel2, a novel immunoglobulin superfamily gene expressed primarily in beta cells of the pancreatic islets. *Genomics,* 82**,** 130-42.

TABAS, I. & RON, D. 2011. Integrating the mechanisms of apoptosis induced by endoplasmic reticulum stress. *Nat Cell Biol,* 13**,** 184-90.

TAKAHASHI, K. 2012. WAVE2 Protein Complex Coupled to Membrane and Microtubules. *J Oncol,* 2012**,** 590531.

TAKEMOTO, M., ASKER, N., GERHARDT, H., LUNDKVIST, A., JOHANSSON, B. R., SAITO, Y. & BETSHOLTZ, C. 2002. A new method for large scale isolation of kidney glomeruli from mice. *Am J Pathol,* 161**,** 799-805.

TEMME, J., PETERS, F., LANGE, K., PIRSON, Y., HEIDET, L., TORRA, R., GRUNFELD, J. P., WEBER, M., LICHT, C., MULLER, G. A. & GROSS, O. 2012. Incidence of renal failure and nephroprotection by RAAS inhibition in heterozygous carriers of X-chromosomal and autosomal recessive Alport mutations. *Kidney Int,* 81**,** 779-83.

TONNA, S., WANG, Y. Y., WILSON, D., RIGBY, L., TABONE, T., COTTON, R. & SAVIGE, J. 2008a. The R229Q mutation in NPHS2 may predispose to proteinuria in thin-basement-membrane nephropathy. *Pediatr Nephrol,* 23**,** 2201-7.

TONNA, S. J., NEEDHAM, A., POLU, K., USCINSKI, A., APPEL, G. B., FALK, R. J., KATZ, A., AL-WAHEEB, S., KAPLAN, B. S., JERUMS, G., SAVIGE, J., HARMON, J., ZHANG, K., CURHAN, G. C. & POLLAK, M. R. 2008b. NPHS2 variation in focal and segmental glomerulosclerosis. *BMC Nephrol,* 9**,** 13.

TORY, K., MENYHARD, D. K., WOERNER, S., NEVO, F., GRIBOUVAL, O., KERTI, A., STRANER, P., ARRONDEL, C., CONG, E. H., TULASSAY, T., MOLLET, G., PERCZEL, A. & ANTIGNAC, C. 2014. Mutation-dependent recessive inheritance of NPHS2-associated steroid-resistant nephrotic syndrome. *Nat Genet,* 46**,** 299-304.

TRYGGVASON, K. & PATRAKKA, J. 2006. Thin basement membrane nephropathy. *J Am Soc Nephrol,* 17**,** 813-22.

TRYGGVASON, K., PATRAKKA, J. & WARTIOVAARA, J. 2006. Hereditary proteinuria syndromes and mechanisms of proteinuria. *N Engl J Med,* 354**,** 1387-401.

TSANG, K. Y., CHAN, D., CHESLETT, D., CHAN, W. C., SO, C. L., MELHADO, I. G., CHAN, T. W., KWAN, K. M., HUNZIKER, E. B., YAMADA, Y., BATEMAN, J. F., CHEUNG, K. M. & CHEAH, K. S. 2007. Surviving endoplasmic reticulum stress is coupled to altered chondrocyte differentiation and function. *PLoS Biol,* 5**,** e44.

TSIAKKIS, D., PIERI, M., KOUPEPIDOU, P., DEMOSTHENOUS, P., PANAYIDOU, K. & DELTAS, C. 2012. Genotype-phenotype correlation in X-linked Alport syndrome patients carrying missense mutations in the collagenous domain of COL4A5. *Clin Genet,* 82**,** 297-9.

TSUKAGUCHI, H., SUDHAKAR, A., LE, T. C., NGUYEN, T., YAO, J., SCHWIMMER, J. A., SCHACHTER, A. D., POCH, E., ABREU, P. F., APPEL, G. B., PEREIRA, A. B., KALLURI, R. & POLLAK, M. R. 2002. NPHS2 mutations in late-onset focal segmental glomerulosclerosis: R229Q is a common disease-associated allele. *J Clin Invest,* 110**,** 1659-66.

TURI, S., KOBOR, J., ERDOS, A., BODROGI, T., VIRAG, I. & ORMOS, J. 1992. Hereditary nephritis, platelet disorders and deafness-Epstein's syndrome. *Pediatr Nephrol,* 6**,** 38-43.

VAN DER LOOP, F. T., HEIDET, L., TIMMER, E. D., VAN DEN BOSCH, B. J., LEINONEN, A., ANTIGNAC, C., JEFFERSON, J. A., MAXWELL, A. P., MONNENS, L. A., SCHRODER, C. H. & SMEETS, H. J. 2000. Autosomal dominant Alport syndrome caused by a COL4A3 splice site mutation. *Kidney Int,* 58**,** 1870-5.

VERMA, R., KOVARI, I., SOOFI, A., NIHALANI, D., PATRIE, K. & HOLZMAN, L. B. 2006. Nephrin ectodomain engagement results in Src kinase activation, nephrin phosphorylation, Nck recruitment, and actin polymerization. *J Clin Invest,* 116**,** 1346-59.

VERMA, R., WHARRAM, B., KOVARI, I., KUNKEL, R., NIHALANI, D., WARY, K. K., WIGGINS, R. C., KILLEN, P. & HOLZMAN, L. B. 2003. Fyn binds to and phosphorylates the kidney slit diaphragm component Nephrin. *J Biol Chem,* 278**,** 20716-23.

VICENTE-MANZANARES, M., MA, X., ADELSTEIN, R. S. & HORWITZ, A. R. 2009. Non-muscle myosin II takes centre stage in cell adhesion and migration. *Nat Rev Mol Cell Biol,* 10**,** 778-90.

VOGLER, C., MCADAMS, A. J. & HOMAN, S. M. 1987. Glomerular basement membrane and lamina densa in infants and children: an ultrastructural evaluation. *Pediatr Pathol,* 7**,** 527-34.

VOLKER, L. A., PETRY, M., ABDELSABOUR-KHALAF, M., SCHWEIZER, H., YUSUF, F., BUSCH, T., SCHERMER, B., BENZING, T., BRAND-SABERI, B., KRETZ, O., HOHNE, M. & KISPERT, A. Comparative analysis of Neph gene expression in mouse and chicken development. *Histochem Cell Biol,* 137**,** 355-66.

VOLKER, L. A., PETRY, M., ABDELSABOUR-KHALAF, M., SCHWEIZER, H., YUSUF, F., BUSCH, T., SCHERMER, B., BENZING, T., BRAND-SABERI, B., KRETZ, O., HOHNE, M. & KISPERT, A. 2012. Comparative analysis of Neph gene expression in mouse and chicken development. *Histochem Cell Biol,* 137**,** 355-66.

VOLKER, L. A., SCHUREK, E. M., RINSCHEN, M. M., TAX, J., SCHUTTE, B. A., LAMKEMEYER, T., UNGRUE, D., SCHERMER, B., BENZING, T. & HOHNE, M. 2013. Characterization of a short isoform of the kidney protein podocin in human kidney. *BMC Nephrol,* 14**,** 102.

VOSKARIDES, K., ARSALI, M., ATHANASIOU, Y., ELIA, A., PIERIDES, A. & DELTAS, C. 2012. Evidence that NPHS2-R229Q predisposes to proteinuria and renal failure in familial hematuria. *Pediatr Nephrol,* 27**,** 675-9.

VOSKARIDES, K., DAMIANOU, L., NEOCLEOUS, V., ZOUVANI, I., CHRISTODOULIDOU, S., HADJICONSTANTINOU, V., IOANNOU, K., ATHANASIOU, Y., PATSIAS, C., ALEXOPOULOS, E., PIERIDES, A., KYRIACOU, K. & DELTAS, C. 2007. COL4A3/COL4A4 mutations producing focal segmental glomerulosclerosis and renal failure in thin basement membrane nephropathy. *J Am Soc Nephrol,* 18**,** 3004-16.

VOSKARIDES, K., DEMOSTHENOUS, P., PAPAZACHARIOU, L., ARSALI, M., ATHANASIOU, Y., ZAVROS, M., STYLIANOU, K., XYDAKIS, D., DAPHNIS, E., GALE, D. P., MAXWELL, P. H., ELIA, A., PATTARO, C., PIERIDES, A. & DELTAS, C. 2013. Epistatic role of the MYH9/APOL1 region on familial hematuria genes. *PLoS One,* 8**,** e57925.

VOSKARIDES, K., MAKARIOU, C., PAPAGREGORIOU, G., STERGIOU, N., PRINTZA, N., ALEXOPOULOS, E., ELIA, A., PAPACHRISTOU, F., PIERIDES, A., GEORGAKI, E. & DELTAS, C. 2008a. NPHS2 screening with SURVEYOR in Hellenic children with steroid-resistant nephrotic syndrome. *Pediatr Nephrol,* 23**,** 1373-5.

VOSKARIDES, K., PIERIDES, A. & DELTAS, C. 2008b. COL4A3/COL4A4 mutations link familial hematuria and focal segmental glomerulosclerosis. glomerular epithelium destruction via basement membrane thinning? *Connect Tissue Res,* 49**,** 283-8.

VUJIC, M., HEYER, C. M., ARS, E., HOPP, K., MARKOFF, A., ORNDAL, C., RUDENHED, B., NASR, S. H., TORRES, V. E., TORRA, R., BOGDANOVA, N. & HARRIS, P. C. 2010. Incompletely penetrant PKD1 alleles mimic the renal manifestations of ARPKD. *J Am Soc Nephrol,* 21**,** 1097-102.

WALSER, M. & THROPE, B. 2004. *Coping with Kidney Disease: A 12-Step Treatment Program to Help You Avoid Dialysis,* Wiley.

WALTER, P. & RON, D. 2011. The unfolded protein response: from stress pathway to homeostatic regulation. *Science,* 334**,** 1081-6.

WANG, Y. Y. & SAVIGE, J. 2005. The epidemiology of thin basement membrane nephropathy. *Semin Nephrol,* 25**,** 136-9.

WEBER, S., GRIBOUVAL, O., ESQUIVEL, E. L., MORINIERE, V., TETE, M. J., LEGENDRE, C., NIAUDET, P. & ANTIGNAC, C. 2004. NPHS2 mutation analysis shows genetic heterogeneity of steroid-resistant nephrotic syndrome and low post-transplant recurrence. *Kidney Int,* 66**,** 571-9.

WEICHERT, N., KALTENBORN, E., HECTOR, A., WOISCHNIK, M., SCHAMS, A., HOLZINGER, A., KERN, S. & GRIESE, M. 2011. Some ABCA3 mutations elevate ER stress and initiate apoptosis of lung epithelial cells. *Respir Res,* 12**,** 4.

WELSH, G. I. & SALEEM, M. A. 2010. Nephrin-signature molecule of the glomerular podocyte? *J Pathol,* 220**,** 328-37.

WELSH, G. I. & SALEEM, M. A. 2012. The podocyte cytoskeleton--key to a functioning glomerulus in health and disease. *Nat Rev Nephrol,* 8**,** 14-21.

WICHMANN, H. E., GIEGER, C., ILLIG, T. & GROUP, M. K. S. 2005. KORA-gen--resource for population genetics, controls and a broad spectrum of disease phenotypes. *Gesundheitswesen,* 67 Suppl 1**,** S26-30.

XIE, J., WU, X., REN, H., WANG, W., WANG, Z., PAN, X., HAO, X., TONG, J., MA, J., YE, Z., MENG, G., ZHU, Y., KIRYLUK, K., KONG, X., HU, L. & CHEN, N. 2014. COL4A3 mutations cause focal segmental glomerulosclerosis. *J Mol Cell Biol,* 6**,** 498-505.

YAMADA, E. 1955. The fine structure of the renal glomerulus of the mouse. *J Biophys Biochem Cytol,* 1**,** 551-66.

YAP, D. Y., TSE, K. C., CHAN, T. M. & LIE, A. K. 2009. Epstein syndrome presenting as renal failure in young patients. *Ren Fail,* 31**,** 582-5.

YOSHIDA, H., MITARAI, T., KAWAMURA, T., KITAJIMA, T., MIYAZAKI, Y., NAGASAWA, R., KAWAGUCHI, Y., KUBO, H., ICHIKAWA, I. & SAKAI, O. 1995. Role of the deletion of polymorphism of the angiotensin converting enzyme gene in the progression and therapeutic responsiveness of IgA nephropathy. *J Clin Invest,* 96**,** 2162-9.

YUE, P., MELAMUD, E. & MOULT, J. 2006. SNPs3D: candidate gene and SNP selection for association studies. *BMC Bioinformatics,* 7**,** 166.

ZHANG, K. W., TONNA, S., WANG, Y. Y., RANA, K., PADAVARAT, S. & SAVIGE, J. 2007. Do mutations in COL4A1 or COL4A2 cause thin basement membrane nephropathy (TBMN)? *Pediatr Nephrol,* 22**,** 645-51.

ZHANG, S. Y., MARLIER, A., GRIBOUVAL, O., GILBERT, T., HEIDET, L., ANTIGNAC, C. & GUBLER, M. C. 2004. In vivo expression of podocyte slit diaphragm-associated proteins in nephrotic patients with NPHS2 mutation. *Kidney Int,* 66**,** 945-54.

ZHOU, J., MOCHIZUKI, T., SMEETS, H., ANTIGNAC, C., LAURILA, P., DE PAEPE, A., TRYGGVASON, K. & REEDERS, S. T. 1993. Deletion of the paired alpha 5(IV) and alpha 6(IV) collagen genes in inherited smooth muscle tumors. *Science,* 261**,** 1167-9.

ZHOU, J. & REEDERS, S. T. 1996. The alpha chains of type IV collagen. *Contrib Nephrol,* 117**,** 80-104.

Appendix I

Supplementary table 1

A) Differentially expressed genes between wild type (*wt*) and Vector (V). Top 20 up-regulated genes in *wt* vs V.

Gene ID	Gene name	*p*-value (*wt* vs V)	Log2 fold change (*wt* vs V)
IFI44L	Interferon-induced protein 44-like	4.40E-08	6.128073
MX1	Mixovirus (influenza virus) resistance 1, interferon-inducible protein p78 (mouse)	5.73E-08	6.030455
IFITM1	Interferon induced transmembrane protein 1 (9-27)	8.22E-07	5.393325
IFI27	Interferon, alpha-inducible protein 27	2.25E-06	5.249378
IFI6	Interferon, alpha-inducible protein 6	9.24E-07	5.043366
IFI44	Interferon, alpha-inducible protein 44	8.34E-07	5.139564
EPSTI1	Epithelial stromal interaction 1 (breast)	2.13E-06	4.924327
HERC6	Hect domain and RLD 6	8.58E-08	4.748837
ISG20	Interferon stimulated exonuclease gene 20kDa	4.43E-06	4.272059
XAF1	XIAP associated factor 1	4.38E-06	4.314879
BST2	Bone marrow stromal cell antigen 2	3.37E-07	4.282297
DDX58	DEAD (Asp-Glu-Ala-Asp) box polypeptide 58	1.78E-06	4.202594
IFIH1	Interferon induced with helicase C domain 1	2.21E-06	4.244243
COL4A3	Collagen, type IV, alpha 3 (Goodpasture antigen)	0.00075	4.096923
TRIM22	Tripartite motif containing 22	0.000002	4.12346
ISG15	ISG15 ubiquitin-like modifier	3.66E-08	3.984095
OAS3	2'-5'-olgiadenylate synthetase 3, 100kDa	1.89E-07	3.847259
CMPK2	Cytidine monophosphate (UMP-CMP) kinase 2, mitochondrial	0.000021	3.935589
IFIT1	Interferon-induced protein with	6.51E-07	3.934508

	tetratricopeptide repeats 1		
OAS1	2', 5'-oligoadenylate synthetase 1, 40/46 kDa		

B) Differentially expressed genes between wild type (*wt*) and Vector (V). Top 20 down-regulated genes in *wt* vs V.

Gene ID	Gene name	*p*-value (*wt* vs V)	Log2 fold change (*wt* vs V)
MCTP1	Multiple C2 domains, transmembrane 1	0.0009	-0.910214
GUCY1B3	Guanylate cyclase 1, soluble, beta 3	0.0002	-1.004274
GPR125	G protein-coupled receptor 125	0.0002	-0.945474
FAM173B	Family with sequence similarity 173, member B	0.0082	-1.000825
SUMF1	Sulfatase modifying factor 1	0.0000	-0.993077
FAM171A1	Family with sequence similarity 171, member A1	0.0001	-1.083245
CERK	Ceramide kinase	0.0018	-1.211266
CGNL1	Cingulin-like 1	0.0015	-1.155014
WRB	Tryptophan rich basic protein	0.0000	-1.222404
TMEM168	Transmembrane protein 168	0.0009	-1.129653
KIAA0114	KIAA0114	0.0000	-1.226387
SLN	Sarcolipin	0.0097	-1.433262
FAM172A	Family qith sequence similarity 172, member A	0.0020	-1.22797
RAB4A	RAB4A, member RAS oncogene family	0.0000	-1.224384
SPHAR	S-phase response (cyclin related)	0.0023	-1.272674
NT5DC2	5'-nucleotidase domain containing 2	0.0012	-1.543241
DCDC2	Doublecortin domain containing 2	0.0031	-1.615536
RPL27A	Ribosomal protein L27a	0.0002	-1.539911
ACO1	Acotinase 1, soluble	0.0001	-1.628394
CDKN1C	Cyclin-dependent kinase inhibitor 1C (p57, Kip2)	0.0000	-1.732839

C) Differentially expressed genes between G1334E and Vector (V). Top 20 up-regulated genes in G1334E vs V.

Gene ID	Gene name	*p*-value (*wt* vs V)	Log2 fold change (*wt* vs V)
IFI44L	Interferon-induced protein 44-like	4.30E-08	6.16
MX1	Myxovirus (influenza virus) resistance 1, interferon-inducible protein	5.84E-08	6.00
IFITM1	Interferon induced transmembrane protein 1 (9-27)	8.18E-07	5.40
IFI27	Interferon, alpha-inducible protein 27	2.12E-06	5.33
IFI6	Interferon, alpha-inducible protein 6	8.93E-07	5.09
IFI44	Interferon induced protein 44	8.79E-07	5.07
EPSTI1	Epithelial stromal interaction 1 (breast)	2.08E-06	4.95
HERC6	Hect domain and RLD6	8.30E-08	4.79
ISG20	Interferon stimulated exonuclease gene 20kDa	4.72E-06	4.31
XAF1	XIAP associated factor 1	4.46E-06	4.30
BST2	Bone marrow stromal cell antigen 2	3.37E-07	4.28
DDX58	DEAD (Aps-Glu-Ala-Asp) box polypeptide 58	1.69E-06	4.26
IFIH1	Interferon induced with helicase C domain 1	2.27E-06	4.22
COL4A3	Collagen, type IV, alpha 3 (Goodpasture antigen)	0.0007	4.15
TRIM22	Tripartite motif containing 22	2.37E-06	4.04
ISG15	ISG15 ubiquitin-like modifier	3.61E-08	4.00
OAS3	2'-5'-oligoadenylate synthetase 3, 100kDa	1.65E-07	3.98
CMPK2	Cytidine monophosphate (UMP-CMP) kinase 2, mitochondrial	0.00002	3.95
IFIT1	Interferon-induced protein with tetratricopeptide repeats 1	6.70E-07	3.91
OAS1	2', 5'-oligoadenylate synthetase 1, 40/46	1.84E-06	3.86

	kDa

D) Differentially expressed genes between G1334E and Vector (V). Top 20 down-regulated genes in G1334E vs V.			
Gene ID	**Gene name**	***p*-value (*wt* vs V)**	**Log2 fold change (*wt* vs V)**
MCTP1	Multiple C2 domains, transmembrane 1	0.0009	-0.93
GUCY1B3	Guanylate cyclase 1, soluble, beta 3	0.0002	-0.95
GPR125	G protein-coupled receptor 125	0.0002	-0.95
FAM173B	Family with sequence similarity 173 member B	0.0083	-1.00
SUMF1	Sulfatase modifying factor 1	0.0000	-1.10
FAM171A1	Family with sequence similarity 171, member A1	0.0001	-1.11
CERK	Ceramide kinase	0.0018	-1.11
CGNL1	Cingulin-like 1	0.0015	-1.11
WRB	Tryptophan rich basic protein	0.0000	-1.21
TMEM168	Transmembrane protein 168	0.0007	-1.22
KIAA0114	KIAA0114	0.0000	-1.25
SLN	Sarcolipin	0.0134	-1.30
FAM172A	Family with sequence similarity 172, member A	0.0015	-1.32
RAB4A	RAB4A, member RAS oncogene family	0.0000	-1.35
SPHAR	S-phase response (cyclin related)	0.0018	-1.37
NT5DC2	5'-nucleotidase domain containing 2	0.0015	-1.44
DCDC2	Doublecortin domain containing 2	0.0039	-1.51
RPL27A	Ribosomal protein L27a	0.0002	-1.56
ACO1	Acotinase 1, soluble	0.0001	-1.58
CDKN1C	Cyclin-dependent kinase inhibitor 1C (p57, Kip2)	0.0000	-1.77

E) Differentially expressed genes between G1334E and wild type (*wt*). Top 5 up-regulated genes in G1334E vs *wt*.

Gene ID	Gene name	Log2 fold change (*wt* vs V)
EGR1	Early growth response 1	0.341932
DYRK3	Dual-specificity tyrosine-(Y)-phosphorylation regulated kinase 3	0.310839
PFDN6	Prefoldin subunit 6	0.308013
DUSP5	Dual specificity phosphatase 5	0.295127
MORN1	MORN repeat containing 1	0.249616

F) Differentially expressed genes between G1334E and wild type (*wt*). Top 5 down-regulated genes in G1334E vs *wt*.

Gene ID	Gene name	Log2 fold change (*wt* vs V)
SNHG9	Small nucleolar RNA host gene (non-protein coding)	-0.352206
PTPN2	Protein tyrosine phosphatase, non-receptor 2	-0.310232
ZDBF2	Zinc finger, DBF-type containing 2	-0.305589
HAUS6	HAUS augmin-like complex, subunit 6	-0.294768
ZNF468	Zinc finger protein 468	-0.248545

Supplementary table 2

Showing 10 pathways linked with up-regulated genes with p<0.05 after Benjamini correction

	Pathway	***p*-value**
1	Unfolded protein response	<0.00001
2	p53 signalling pathway	0.0023
3	Glyoxylate and dicarboxylate metabolism	0.0048
4	Antigen processing and presentation	0.0053
5	NOD-like receptor signalling pathway	0.0088
6	Ubiquitin mediated proteolysis	0.0116
7	RIG-1-like receptor signalling pathway	0.0235
8	Toll-like receptor signalling pathway	0.0281
9	Pyrimidine metabolism	0.0368
10	Apoptosis	0.0416

Supplementary table 3

Showing the thirty-one and seven genes that were either upregulated (red colour) or downregulated (green colour) respectively in the "Protein processing in endoplasmic reticulum pathway"

Gene symbol	Fold change (G1334E vs V)	Fold change (*wt* vs V)	*p*-value (G1334E vs V)	*p*-value (*wt* vs V)
DDIT3	3.060	2.724	0.0001	0.0001
HSPA5	2.547	2.489	0.0004	0.0004
HERPUD1	2.359	2.439	0.0005	0.0004
FBXO6	1.733	1.813	0.0019	0.0014
PPP1R15A	1.728	1.743	0.0052	0.0049
XBP1	1.662	1.640	0.0021	0.0023
P4HB	1.494	1.402	0.0001	0.0002
HSP90B1	1.454	1.432	0.0014	0.0016
HYOU1	1.454	1.565	0.0005	0.0002
DNAJB11	1.441	1.424	0.0004	0.0005
PDIA3	1.402	1.336	0.0018	0.0032
SAR1A	1.368	1.265	0.0019	0.0053
SELS	1.367	1.332	0.0001	0.0001
CANX	1.325	1.343	0.0020	0.0017
PDIA4	1.324	1.410	0.0001	0.0000
CKAP4	1.314	1.260	0.0095	0.0167

DNAJA1	1.267	1.231	0.0014	0.0022
DNAJC10	1.266	1.294	0.0026	0.0019
CALR	1.266	1.282	0.0075	0.0062
MAN1A1	1.262	1.265	0.0070	0.0067
DNAJC1	1.219	1.177	0.0038	0.0076
PDIA6	1.201	1.179	0.0005	0.0007
ERLEC1	1.195	1.118	0.0004	0.0021
SSR3	1.187	1.229	0.0035	0.0018
SEC61A1	1.184	1.136	0.0010	0.0027
HSPA1B	1.157	1.281	0.0180	0.0029
ERP29	1.155	1.147	0.0046	0.0055
PLAA	1.147	1.164	0.0138	0.0098
DERL2	1.138	1.131	0.0012	0.0015
EDEM1	1.135	1.155	0.0045	0.0028
UGGT1	1.131	1.113	0.0018	0.0030
STUB1	0.883	0.855	0.0069	0.0030
MAPK9	0.873	0.868	0.0056	0.0048
NPLOC4	0.849	0.804	0.0103	0.0038
UBE2G1	0.841	0.844	0.0079	0.0084
SEC24C	0.802	0.871	0.0032	0.0162
EIF2AK4	0.796	0.830	0.0008	0.0018

UBE4B	0.667	0.692	0.0002	0.0002

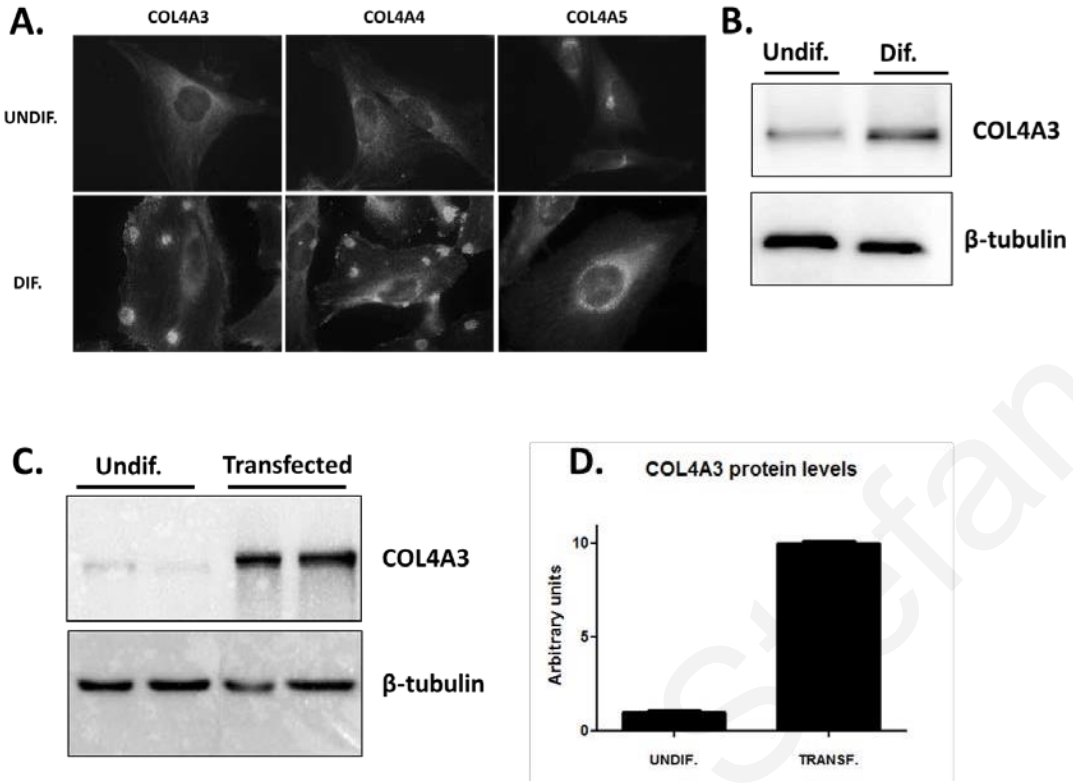

Supplementary figure 1: Relative expression of the Collagen IV chains in undifferentiated, differentiated and transfected AB8/13 cells

Immunofluorescence showing the expression of COL4A3, COL4A4 and COL4A5 chains in undifferentiated and differentiated AB8/13 cells (A). Notice that all chains are expressed in AB8/13 cells, even in the undifferentiated state. Western blotting showing the increased expression of the COL4A3 chain in cells after differentiation (B). Western blotting showing the increase in COL4A3 expression in undifferentiated podocytes when cells are transfected with the pCMV6-AC-HA vector expressing the COL4A3 chain. A 10-fold increase in COL4A3 expression was observed after transfection (D). Primary antibodies used against the human COL-IV chains were as follows: anti-COL4A3 (Novus Biologicals, UK), anti-COL4A4 and anti-COL4A5 (Santa Cruz Biotechnology, CA).

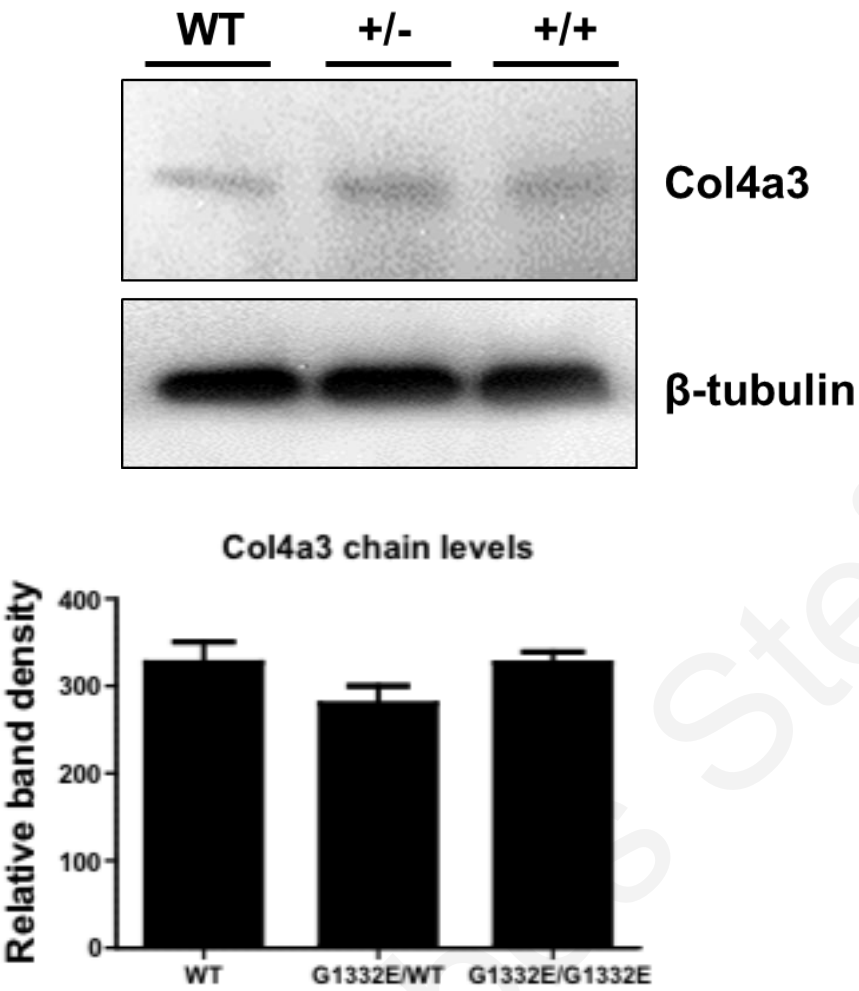

Supplementary figure 2: Showing expression of the Col4a3 protein chain in G1332E knockin mice

The Col4a3 chain is normally expressed in the knockin mouse model as shown by Western blotting and quantified by densitometry.

Appendix II

Supplementary table 4
PCR primers and restriction enzymes used for SNPs genotyping

SNP	Forward primer	Reverse primer	PCR size (bp)	Tm (^{0}C)	Restriction enzyme	Cleavage products (bp)
***NEPH3*–V353M**	CTAGAGGGTGTGGTGTTTCTGTG	CTAAAAGCCTCGCCTTCAATAG	590	60.5	*EcoNI*	300 + 180 + 82 + 28 (V allele)
***TJP1*–I790V**	CCCTCGGAAACCCATACCAGCT GGTTTTGCTGTTGTTGTA	TACTTTCTTGGAAAGCTTCCTG TTGTGTTAACACCTGCTG	300	64	*RsaI*	261 + 39 (V allele)
***FAT2*–R574C**	AGTTGTGGGTGAGGCATAGTTT	GTCACCTATTCCATTGCTGGAC	483	64	*AciI*	244 + 239 (R allele)
***FAT2*–G1515S**	CAACTCTGTCTCGTGCATGG	CAGCTGGACCCAAGCAGT	209	58	*AluI*	156 + 53 (S allele)

Supplementary table 5
Description of TBMN patients ("Mild" patients born before 01/1963) under study

Patients	Origin	N	Mild				Severe			
			N (%)	Age: mean (SD)	Females: N (%)	With ESKD: N (%)	N (%)	Age: mean (SD)	Females: N (%)	With ESKD: N (%)
Heterozygous *COL4A3/COL4A4* mutation carriers	Cyprus	122	40 (33%)	60.9 (±11.1)	28 (%70)	0	82 (67%)	59.6 (±13.1)	34 (41%)	25 (30%)

Appendix III

Evidence for Activation of the Unfolded Protein Response in Collagen IV Nephropathies

Myrtani Pieri,* Charalambos Stefanou,* Apostolos Zaravinos,* Kamil Erguler,* Kostas Stylianou,† George Lapathitis,‡ Christos Karaiskos,‡ Isavella Savva,* Revekka Paraskeva,* Harsh Dweep,§ Carsten Sticht,§ Natassa Anastasiadou,| Ioanna Zouvani,| Demetris Goumenos,¶ Kyriakos Felekkis,** Moin Saleem,†† Konstantinos Voskarides,* Norbert Gretz,§ and Constantinos Deltas*

*Molecular Medicine Research Center, Department of Biological Sciences, University of Cyprus, Nicosia, Cyprus; †Department of Nephrology, Heraklion University Hospital, Crete, Greece; ‡The Cyprus Institute of Neurology and Genetics, Nicosia, Cyprus; §Medical Research Center, University of Heidelberg, Mannheim, Germany; |Department of Histopathology, Nicosia General Hospital, Nicosia, Cyprus; ¶Departments of Internal Medicine-Nephrology, University Hospital of Patras, Patras, Greece; **Department of Life and Health Sciences, University of Nicosia, Nicosia, Cyprus; and ††Children's and Academic Renal Unit, Southmead Hospital-University of Bristol, Bristol, United Kingdom

ABSTRACT

Thin-basement-membrane nephropathy (TBMN) and Alport syndrome (AS) are progressive collagen IV nephropathies caused by mutations in COL4A3/A4/A5 genes. These nephropathies invariably present with microscopic hematuria and frequently progress to proteinuria and CKD or ESRD during long-term follow-up. Nonetheless, the exact molecular mechanisms by which these mutations exert their deleterious effects on the glomerulus remain elusive. We hypothesized that defective trafficking of the COL4A3 chain causes a strong intracellular effect on the cell responsible for COL4A3 expression, the podocyte. To this end, we overexpressed normal and mutant COL4A3 chains (G1334E mutation) in human undifferentiated podocytes and tested their effects in various intracellular pathways using a microarray approach. COL4A3 overexpression in the podocyte caused chain retention in the endoplasmic reticulum (ER) that was associated with activation of unfolded protein response (UPR)–related markers of ER stress. Notably, the overexpression of normal or mutant COL4A3 chains differentially activated the UPR pathway. Similar results were observed in a novel knockin mouse carrying the Col4a3-G1332E mutation, which produced a phenotype consistent with AS, and in biopsy specimens from patients with TBMN carrying a heterozygous COL4A3-G1334E mutation. These results suggest that ER stress arising from defective localization of collagen IV chains in human podocytes contributes to the pathogenesis of TBMN and AS through activation of the UPR, a finding that may pave the way for novel therapeutic interventions for a variety of collagenopathies.

J Am Soc Nephrol 25: 260–275, 2014. doi: 10.1681/ASN.2012121217

Alport syndrome (AS) and thin-basement-membrane nephropathy (TBMN) are genetic diseases of the glomerular basement membrane (GBM), an important key component of the glomerular filtration barrier. They are caused by pathogenic changes in the genes encoding the a3/a4/a5 chains of type IV collagen, an abundant constituent of the GBM, and can lead to total or partial loss of its network.[1,2] Mutations have been identified in all three genes that encode the collagen IV chains in patients with AS and TBMN, while the number of these

Received December 21, 2012. Accepted August 8, 2013.

M.P. and C.S. contributed equally to this work.

Published online ahead of print. Publication date available at www.jasn.org.

Correspondence: Prof. Constantinos Deltas, Molecular Medicine Research Center and Laboratory of Molecular and Medical Genetics, Department of Biological Sciences, University of Cyprus, Kallipoleos 75, 1678 Nicosia, Cyprus. Email: Deltas@ucy.ac.cy

mutations exceeds 500 to date (Human Gene Mutation Database). AS is invariably associated with CKD and ESRD usually before 30 years of age, often accompanied by sensorineural deafness and/or ocular abnormalities. TBMN is characterized primarily by microscopic hematuria and was classically thought to be a benign disease with excellent prognosis. Still, our group and others have described particular COL4A3/COL4A4 mutations in patients with the dual diagnosis of TBMN and FSGS who developed CKD/ESRD, thus establishing TBMN as a far-from-benign condition, at least in a subset of patients.[3,4] Nonetheless, the exact molecular mechanisms by which these mutations exert their pathogenic effect remain unclear.

Physiologically, the collagen IV α3, α4, and α5 chains assemble through recognition of their carboxy-terminal NC1 domains and form helical heterotrimers that undergo several enzymatic post-translational modifications in the cell's endoplasmic reticulum (ER) before being secreted into the GBM. Once in the extracellular space, they form a multistructural network that has a dual role in providing strength to the membrane and participating in dynamic biological processes by interacting with many other proteins.[5,6] Previous studies showed that numerous COL4A3/A4/A5 mutations in the NC1 domains share destructive effects on heterotrimer formation and/or secretion of the heterotrimer from cells.[7–9] Therefore, mutant collagen IV heterotrimers could potentially cause deleterious extracellular effects due to their absence from the GBM, as well as putative intracellular effects due to accumulation of misfolded protein inside the producing cells. Importantly, it has been shown that the adult GBM collagen IV chains are solely produced by the podocyte and not by the endothelial or adjacent cells.[10] This fact confers the podocyte a central role as the collagen IV producing and secreting cell. Of note, Heidet et al. demonstrated that in the AS podocyte, the COL4A3 protein, even when absent from the GBM, is detected within the cell, a finding that is distinct among patients with AS.[11]

Herein, we addressed the putative effect of overexpression of both normal and mutant COL4A3 chains on various intracellular pathways of the human podocyte. To target this, we profiled mRNA on human cultured podocytes that overexpressed the wild-type (WT) or mutant COL4A3-G1334E chain for panoramic assessment of gene expression. One of the pathways that emerged as highly deregulated in our analysis is the unfolded protein response pathway (UPR). Inside the cell, an imbalance between protein load and proper protein folding is called ER stress. As a defense mechanism against this imbalance, the cells have at hand a robust mechanism termed the UPR and activated by intracellular retention of unfolded protein.[12] UPR allows cells to recover from stress by temporarily halting protein translation and activating signaling pathways that lead to the production of molecular chaperones involved in protein folding. Once activated, this adaptive pathway may protect the cell from future insults.[13] However, in cases of prolonged or deregulated ER stress owing to genetic or other factors, this pathway could become maladaptive and cytotoxic and lead to apoptosis.[14]

We further examined this pathway by testing whether chaperone binding immunoglobulin protein (BiP), a central marker of UPR activation, is upregulated in renal biopsy specimens from patients with a confirmed COL4A3-G1334E mutation. Finally, we examined UPR activation using a relevant knockin mouse model we recently generated in our laboratory carrying the Col4a3-G1332E mutation (the equivalent of the COL4A3-G1334E mutation in patients with AS and TBMN). To our knowledge, this is the first mouse model carrying a missense glycine COL4A3 mutation, which causes AS and TBMN in humans.[4,15,16]

RESULTS

Overexpression of COL4A3-WT and COL4A3-G1334E Chains in AB8/13 Podocyte Cells

Transient transfection of podocytes with equal amounts of normal COL4A3-WT and mutant COL4A3-G1334E constructs resulted in equal expression of genes as tested in each transfection experiment by quantitative real-time PCR (qPCR) analysis (not shown). Cells expressing the mutant chain showed significantly reduced secretion of the mutant protein, as revealed by Western blotting of the cellular medium 48 hours after transfection ($P > 0.01$) (Figure 1, A and B). The mutant COL4A3-G1334E demonstrated more accumulation into the cellular lysate compared with the WT chain, but this finding did not reach significance at the 48-hour time point (Figure 1B). To determine the cellular location of the expressed chains, we performed immunocytochemistry experiments on the same cells grown on coverslips. Results strongly suggest that overexpressed collagen chains were mainly retained into the cell's ER and were colocalized with the well-established ER marker, calnexin (Figure 2, A and B). This colocalization was more evident for the mutant COL4A3-G1334E chain. Intensity correlation analysis plots indicated that the colocalization of collagen and calnexin in the WT is more random, as opposed to the improved association seen in the mutant (Figure 2, C–H).

Identification of Significantly Deregulated Genes Using Microarrays

To study in a high-throughput manner which cellular pathways are affected by collagen overexpression in the podocyte, we performed microarray profiling and identified 1835 differentially expressed genes among the empty vector, the COL4A3-WT– and the COL4A3-G1334E–expressing cells. Of these, 1512 genes were significantly deregulated between the WT and vector and 1553 between the G1334E and vector, respectively. The top 40 (20 top upregulated and 20 top downregulated) significantly deregulated genes in the vector versus the COL4A3-WT are depicted in Supplemental Table 1, A and B. A similar pattern was observed for the vector versus the

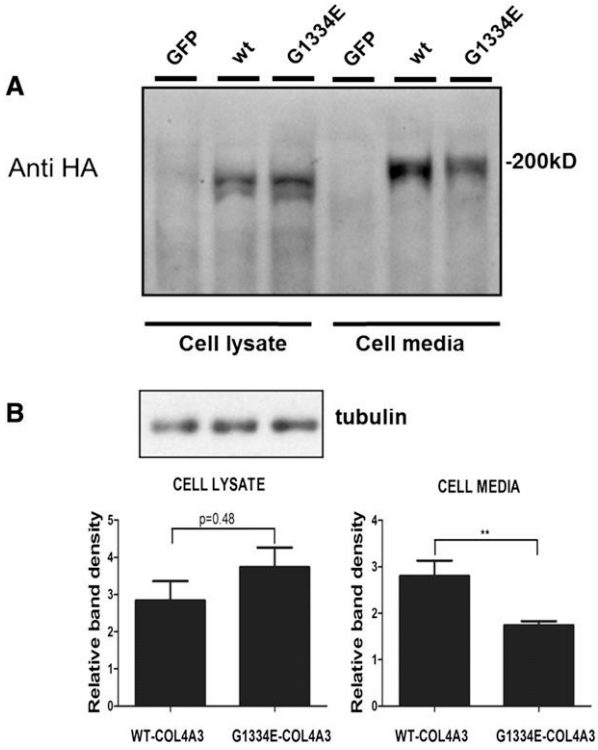

Figure 1. Mutant COL4A3 chain is secreted less efficiently when expressed in AB8/1 cells. (A) AB8/13 cells were transiently transfected with expression vectors containing WT (COL4A3-WT) collagen chain or mutated COL4A3 (COL4A3-G1334E) cDNAs, which included an HA epitope at C-terminus of the protein. Single chain expression and secretion were measured via Western blot analysis of the cell lysate and the cell medium, respectively, 48 hours after transfection. No HA antigen was detected in AB8/13 cells transfected with a vector expressing the green fluorescent protein (GFP). (B) The extracellular levels of the COL4A3-G1334E chain were significantly lower, reaching 70% of WT COL4A3 levels. A shows a representative Western blot and B shows relative band density that corresponds to HA tag immunoreactivity (i.e., COL4A3) that was normalized to tubulin expression for the cell lysate. Data are represented as means±SEM of n≥3 independent experiments; **P<0.01.

COL4A3-G1334E–expressing cells (Supplemental Table 1, C and D). No genes were significantly deregulated, under the strict criteria we applied, between the cells that overexpressed the WT or the mutant chains. The deregulated genes were further clustered using unsupervised two-way hierarchical clustering with Euclidian distance and were separated into three main groups (Figure 3A). Gene clustering with the K-means algorithm verified the existence of three main gene clusters (Figure 3B).

Enrichment Analysis on Significantly Deregulated Pathways: Deregulation of the UPR Pathway

The significantly deregulated genes identified above were separated into two groups: upregulated and downregulated in the vector versus the COL4A3-WT. The pattern was the same for the vector versus COL4A3-G1334E. We found 10 pathways linked with deregulated genes, with $P<0.05$ after Benjamini correction (Supplemental Table 2). Among them, the top three pathways were the UPR ($P<0.001$), the p53 (P=0.0023), and the glyoxylate and dicarboxylate metabolism pathway (P=0.0048). Because the UPR pathway was the top linked pathway with the deregulated genes, we used the "protein processing in the endoplasmic reticulum" pathway from the Kyoto Encyclopedia of Genes and Genomes (KEGG) database to depict the most deregulated genes that play a significant role in it (P=1.7E-9; Fisher exact test) (Figure 4A). Furthermore, we focused on 118 genes involved directly in the protein processing in the ER and we clustered them, as described above (Figure 4B). Thirty-one and seven genes were upregulated or downregulated, respectively, in the "protein processing in endoplasmic reticulum" pathway (Supplemental Table 3). Among them, the genes selected for further validation were the ones encoding the protein chaperones BiP, calnexin, and calreticulin; the downstream transcription factor X-box binding protein 1 (XBP1); the UPR target genes Gadd34 and EDEM; and the proapoptotic marker C/EBP homologous protein (CHOP).

Verification of UPR Activation Using qPCR and Western Blotting

Use of qPCR confirmed the results obtained by the microarray experiments showing significantly increased expression of all UPR markers identified by the arrays in cells expressing WT or the COL4A3-G1334E mutant versus the empty vector (Figure 5A, gray versus white and gray versus black bars). Remarkably, the qPCR method revealed statistically significant differences in comparing the variable expression of the BiP, CHOP, and XBP1 genes between the WT versus vector on one hand and between the G1334E versus vector-expressing cells on the other (Figure 5A, white versus black bars). This trend was also evident in the microarray data but did not reach significance. Therefore, it was interesting to observe that expression of the G1334E mutation into human podocytes results in significantly increased expression of the mRNA levels of particular UPR markers compared with equal expression of the WT chain.

The ratios representing gene expression changes are shown as fold-change and are correlated with the microarray data in Figure 5B. The validation experiments showed that the expression patterns of the genes tested were similar to the microarray data. There was very good agreement between the microarrays and the qPCR results both for the WT versus vector (R^2=0.87; 95% confidence interval, 0.62 to 0.99; P=0.0020) and for the G1334E versus vector experiments (R^2=0.88; 95% confidence interval, 0.62 to 0.99; P=0.0019) (Figure 5B). This supported the reliability of the data obtained from global microarray analysis.

Additionally, we tested protein expression of the UPR markers BiP, CHOP, calnexin, and PERK, as well as phosphorylation of

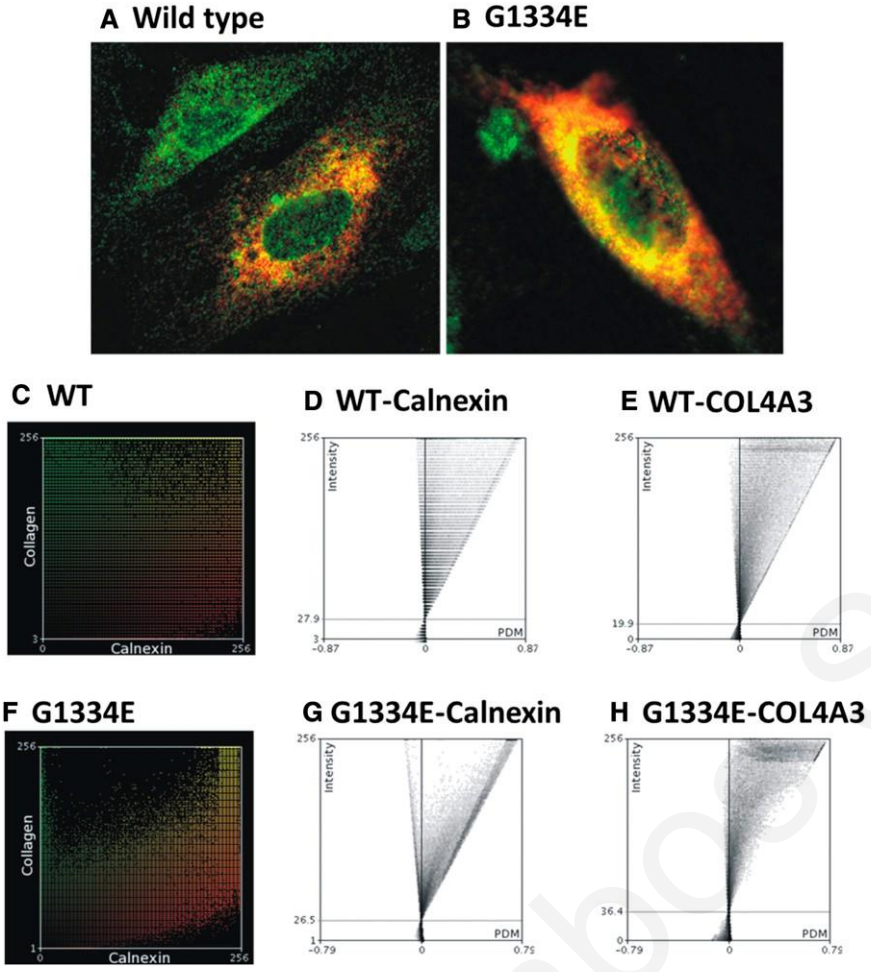

Figure 2. Mutant collagen IV chain is more prominently localized in the ER when expressed in AB8/13 cells. Equal expression of the WT (A) or the G1334E mutant protein (B) is retained in the cells' ER, as shown by colocalization (yellow) of the ER marker calnexin (green) with COL4A3 chain (red). Intensity correlation analysis of the immunocytochemistry images C and F show the color scatter plots of the red (collagen) and green (calnexin) channels. (D, E, G, and H) Intensity correlation analysis plots where for each pixel the product of differences from the mean value is plotted with respect to its intensity. As indicated, the co-localization of collagen and calnexin in the WT is more random as opposed to the improved association seen in the mutant. The intensity correlation analysis was performed using the ImageJ software.

the eIF2a protein, the latter being an important player in protein synthesis shutdown in the UPR cascade.[17] Results show a significant increase in BiP protein levels between the vector and the COL4A3-WT as well as between the vector and the G1334E-COL4A3–expressing cells. Interestingly, results show a significant increase in BiP protein levels between the WT- and the mutant-expressing cells as well (Figure 6). Furthermore, a significant increase is evident in CHOP protein levels between the vector and the collagen (WT or mutant)-expressing cells. A significant decrease is observed in the total protein levels of the PERK protein in cells expressing the WT or the mutant COL4A3 chain compared with vector-only–expressing cells, in agreement with the microarray analysis. No significant change was observed in the calnexin and phosphorylated p-eIF2a levels (Figure 6).

Overexpression of WT and Mutant COL4A3 Chains Induce ER Stress, as Shown by XBP1 Splicing

An established assay to examine UPR activation is the widely used XBP1 splicing assay.[18] Accumulation of misfolded protein within the cell's ER causes the dissociation of BiP from IRE1, resulting in its dimerization and subsequent activation. Full-length XBP1 requires the endoribonuclease domain of active IRE1 for processing into active sXBP1; thus, the splicing of XBP1 is a key marker for UPR activation. When podocytes expressed the COL4A3-WT chain, there was obvious splicing of the XBP1 mRNA compared with cells expressing vector-only cDNA (Figure 7A). Additionally, cells overexpressing the GFP protein or the slit diaphragm protein filtrin (NEPH3), cloned in the same vector, were examined in parallel experiments to assess whether the splicing effect is specific for the collagen protein or a general effect. No splicing was observed in GFP or the filtrin-expressing cells (results not shown). Surprisingly, expression of the COL4A3-G1334E mutant into podocytes resulted in significantly more XBP1 splicing compared with cells expressing the WT and under identical experimental conditions (Figure 7B). Densitometric analysis of the spliced versus the unspliced product in gels like the one in Figure 7B revealed statistical significance in the results obtained from WT versus the mutant cells (not shown). The latter was more directly confirmed by qPCR of the spliced XBP1 isoform using primers in the spliced-unspliced interphase of XBP1's mRNA, as described by Cawley et al.[19] Spliced XBP1 was significantly increased in COL4A3-G1334E– versus COL4A3-WT–expressing cells (Figure 7C).

Knockdown of Endogenous COL4A3 Chains Using Small Interfering RNA Induces ER Stress in AB8/13 Cells

Both undifferentiated and differentiated AB8/13 cells express the COL4A3, COL4A4, and COL4A5 chains, with expression increasing upon differentiation (Supplemental Figure 1). In differentiated podocytes, when the COL4A3 chain is knocked down using small interfering RNA (siRNA), there is activation of the UPR pathway, as shown by upregulation of BiP and increased phosphorylation of protein kinase–like endoplasmic

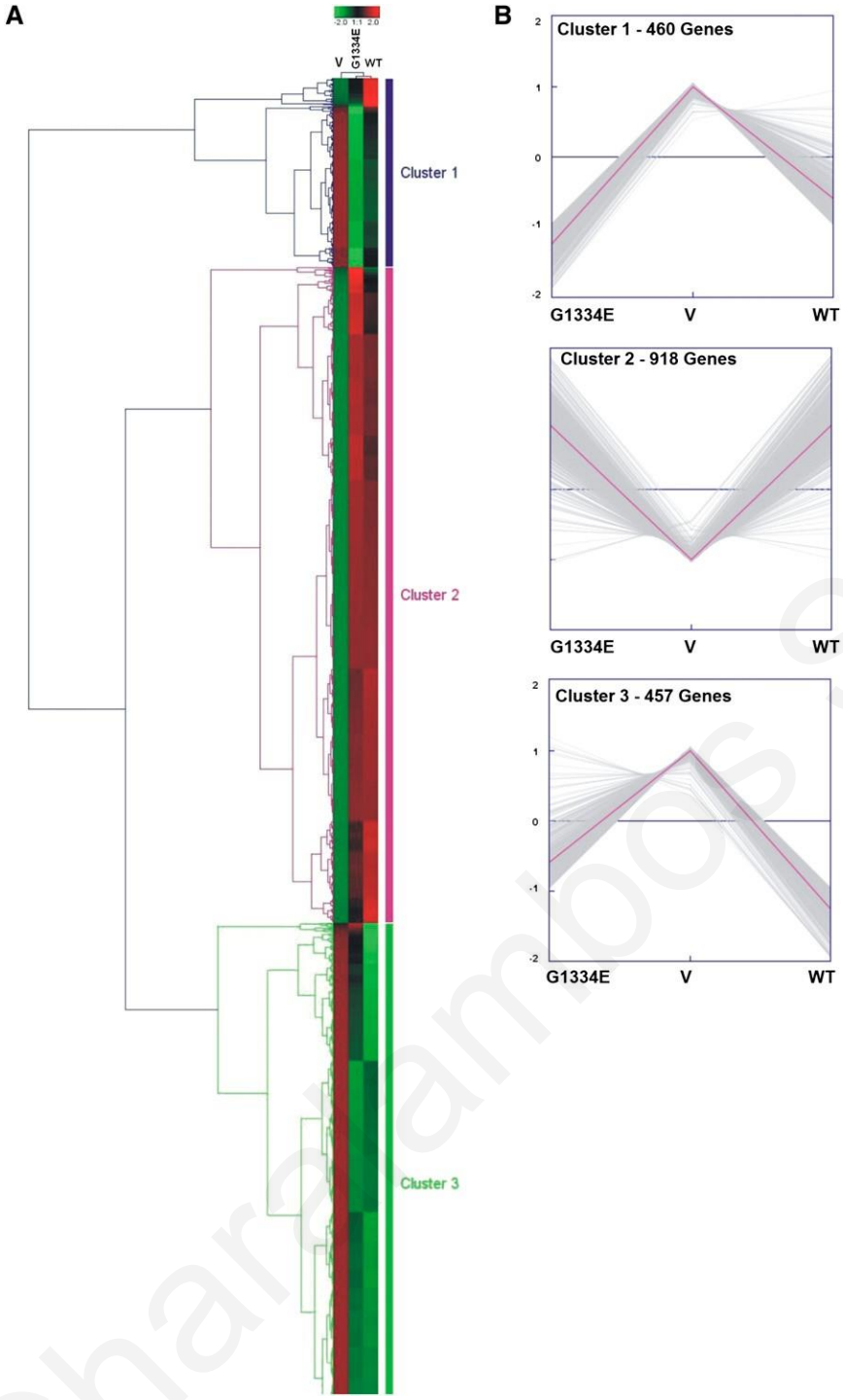

Figure 3. Unsupervised hierarchical cluster illustrating differentially expressed genes between vector only (V), WT, and COL4A3-G1334E (G1334E)–expressing cells. (A) Unsupervised hierarchical cluster based on 1835 probe sets with highest variation in three different transfections in podocytes: with empty pcDNA6-HA vector (V) and vectors expressing the WT COL4A3 chain or the mutant COL4A3-G1334E chain (G1334E). Three main gene clusters were noticed. Color saturation is directly proportional to the measured expression ratio magnitude. Euclidian distance was used as the metric. Rows represent individual probe sets. Columns represent the three experimental conditions. Red bars indicate high expression, and green bars indicate low expression. (B) K-means clustering verified the existence of three main gene clusters: cluster 1 (460 genes), cluster 2 (918 genes), and cluster 3 (457 genes).

reticulum kinase (PERK), as well as a trend for an increase in p-eIF2a (Figure 8). Interestingly, the proapoptotic marker CHOP remains unaltered.

BiP Expression Is Increased in Kidney Biopsy Specimens from COL4A3-G1334E Mutation Carriers

To examine whether the UPR pathway is involved in the pathogenic process among patients with TBMN, we examined BiP protein staining in biopsy samples from two patients who were confirmed heterozygous carriers of the COL4A3-G1334E mutation. BiP expression was increased in the glomeruli of these patients (Figure 9B) compared with expression in biopsy specimens from obese individuals who were used as controls (Figure 9C). BiP expression in tubular epithelial cells was similar in both the COL4A3-G1334E patients and obese individuals. A biopsy sample from a patient with breast carcinoma was stained as a positive control (Figure 9A).

Activation of the UPR Pathway in a Mouse Carrying the Col4a3-G1332E Missense Mutation

To investigate the mechanisms whereby the COL4A3-G1334E mutation causes pathology in vivo, we generated a relevant mouse model. To achieve this, we used gene-targeting technology to successfully generate a knockin mouse for the Col4a3-G1332E mutation, the equivalent of the COL4A3-G1334E mutation in patients with AS and TBMN (Supplemental Figure 2). These mice express the COL4A3 chain normally and in equal amounts, as evidenced by both qPCR (results not shown) and Western blot experiments (Supplemental Figure 3). Additionally, the ultrastructural analysis of homozygous Col4a3-G1332E mice demonstrated thin GBM with areas of mild (3-month-old mice) or severe (7-month-old mice) thickening, consistent with AS nephritis (Figure 10). In these mice we assessed for evidence of UPR activation in the kidney of mutant heterozygous (WT/M) and homozygous (M/M) 3-month-old animals versus their WT littermates (WT/WT). In contrast to the WT, reverse transcription PCR revealed XBP1 splicing in both heterozygous and homozygous mice (Figure 11A). qPCR analysis using primers

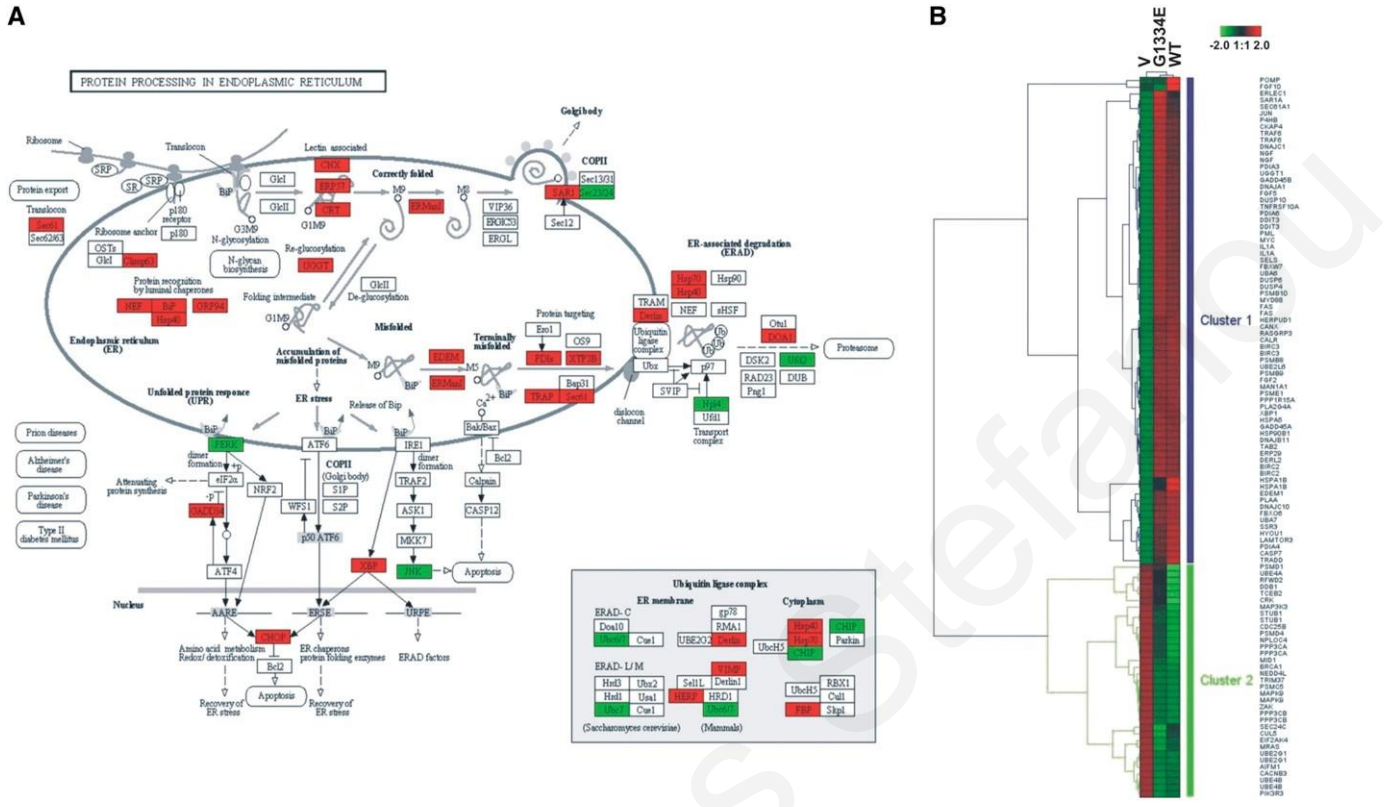

Figure 4. (A) Enrichment analysis showing that the protein processing in the endoplasmic reticulum pathway is greatly deregulated in transfected cells. The KEGG pathway depicts the molecules that take part in the protein processing in the ER. The highlighted molecules were significantly deregulated in the cells transfected with the mutant COL4A3-G1334E or the COL4A3-WT chain versus those transfected with an empty vector. Significantly upregulated genes in the pathway are shown in red, whereas significantly downregulated genes are green (see also Supplemental Table 3). (B) Unsupervised hierarchical cluster based on 118 genes involved directly in the protein processing in the endoplasmic reticulum recognizes two main gene clusters. Color saturation is directly proportional to the measured expression ratio magnitude. Euclidian distance was used as the metric. Rows represent individual probe sets. Columns represent the three experimental conditions: empty vector (V), WT, or G1334E. Red bars indicate high expression, and green bars indicate low expression.

on the spliced-unspliced interphase suggested increased XBP1 splicing in homozygous mice versus control (Figure 11B). Also, BiP mRNA was significantly upregulated in the homozygous mouse versus the WT littermates, whereas CHOP mRNA levels remained unaltered (Figure 11C). Additionally, BiP, p-PERK, and p-eIF2a protein levels were significantly upregulated in homozygous mice versus their control littermates (Figure 11, D and E). Finally, we isolated glomeruli from mutant homozygous mice and their WT littermates and examined UPR activation specifically in glomerular cells. The UPR marker BiP was significantly upregulated in mRNA isolated from mutant mice glomeruli (M/M) versus controls (WT/WT) (Figure 12A). We also observed an increased trend in spliced XBP1 mRNA as measured by qPCR, while the XBP1 splicing assay showed the presence of a spliced band in mutant mice (Figure 12B).

DISCUSSION

Mutations in the COL4A3/A4/A5 genes result in heritable kidney diseases, such as AS and TBMN, collectively referred to as collagen IV nephropathies.[20] The cellular pathomechanisms of these diseases are complex and clearly include extracellular effects due to reduced or no secretion of collagen IV heterotrimers in the GBM. Additionally, one cannot rule out effects caused by collagen mutations on intracellular pathways, something that to our knowledge has not been previously tested in human podocytes. Because collagen IV a3/a4/a5 chains originate solely from podocytes,[10] one can anticipate that the glomerular phenotypes of AS/TBMN are caused by defects that concern specifically or mainly the podocyte. Interestingly, it has been shown via biopsy immunofluorescence that in the patients with X-linked AS, the COL4A3 chain is still expressed and appears to accumulate within the podocyte.[11]

Collagen IV Secretion and UPR Phenotype in a Podocyte Cellular Model

We first focused on the putative intracellular effects of WT or mutant (G1334E) COL4A3 chain overexpression on podocyte function. In experiments using transiently transfected undifferentiated podocytes, we showed reduced secretion of the single G1334E mutant chain in the cellular medium compared with the WT chain (Figure 1). Immunocytochemistry

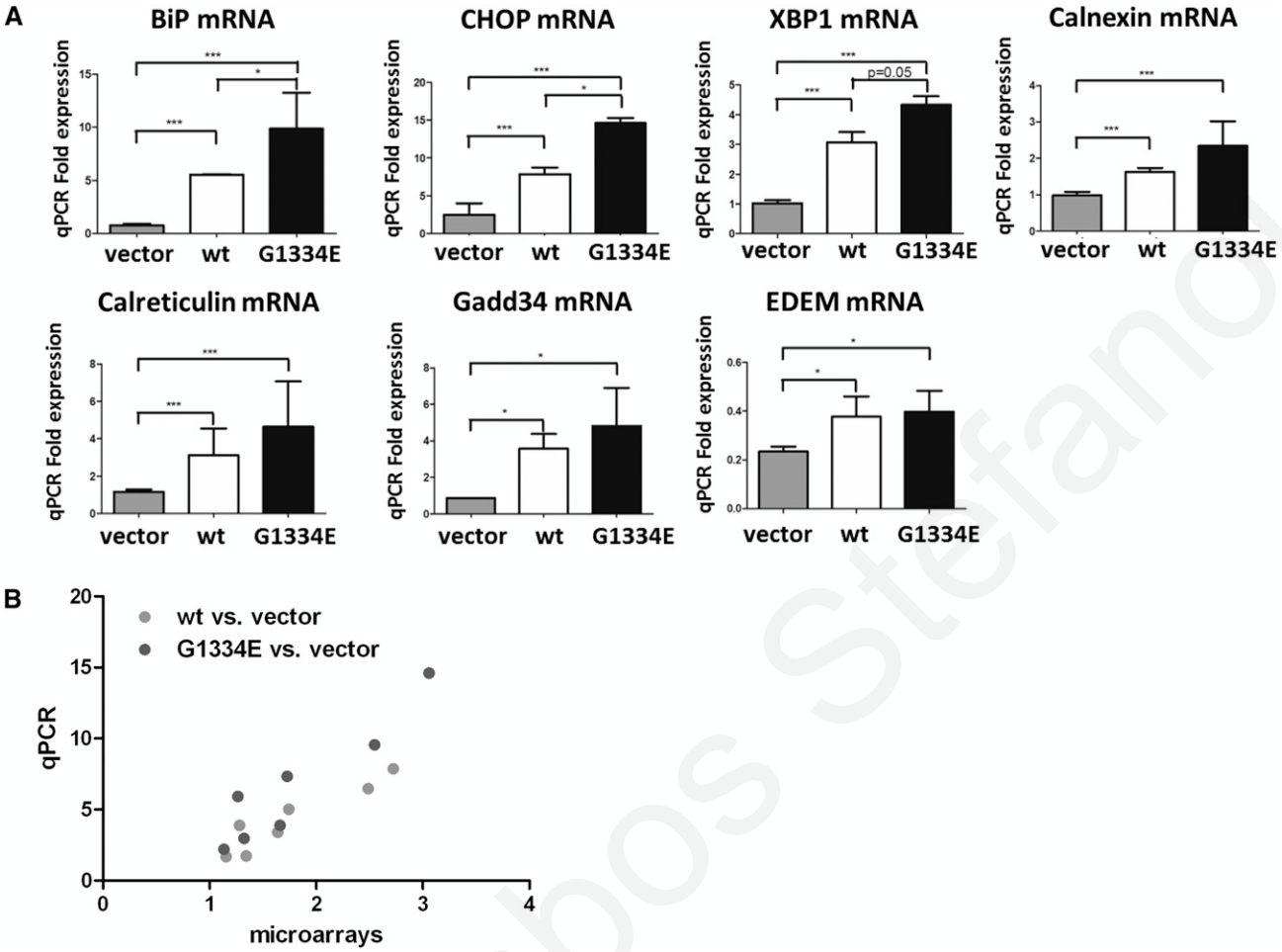

Figure 5. The deregulation of selected genes based on microarray data is verified by qPCR. (A) Graph plots of qPCR data in showing fold increase in mRNAs of various UPR genes in cells expressing vector only (gray bars), WT COL4A3 (white bars), or COL4A3-G1334E mutant chain (black bars) compared with cells expressing vector only. All mRNAs of UPR genes were significantly upregulated in cells expressing WT or mutant COL4A3 compared with cells expressing vector only, thus verifying the microarray data. BiP, CHOP, and XBP1 mRNAs are significantly increased in mutant expressing cells compared with controls (Data are means±SEM, n≥3 independent experiments; *P < 0.05; **P < 0.01. (B) Positive correlation between microarrays and qPCR experimentation. Good agreement is identified between the microarrays and the qPCR results both for the WT versus vector (R^2=0.87; 95% confidence interval [95% CI], 0.62 to 0.99; P=0.0020) and for the G1334E versus vector (R^2=0.88; 95% CI, 0.62 to 0.99; P=0.0019) experiments. Results are presented as scatterplot. EDEM, ER degradation enhancer, mannosidase α-like.

experiments revealed that the COL4A3 single chains are retained in the cell's ER, both in the WT- and mutant-overexpressing cells, but this fact is more evident in the latter (Figure 2). This differential behavior of the cells could explain the reduced secretion of the mutant in the cellular medium. Collagen IV is known to be secreted as a trimer;[21–23] therefore, we should point out that it is questionable whether the single-chain secretion actually takes place in vivo or is a phenomenon observed only in an artificial in vitro system after overexpression of the single chains. Here, secretion of the COL4A3 chain could be due to association of the overexpressed chain with the endogenous COL4A4 and COL4A5 chains that have been shown to be expressed, even at lower levels, in the undifferentiated podocytes (Supplemental Figure 1). The association of the transfected COL4A3 mutant chains with normal endogenous chains could also account for and explain the formation of misfolded trimers that triggered the UPR activation upon quality control in the ER. Nonetheless, secretion of single collagen chains was previously reported in both human embryonic kidney 293 and Chinese hamster ovary cells overexpressing single collagen IV chains.[8,24,25]

Furthermore, global mRNA profiling identified and verified the UPR pathway, among others, as a downstream prime aftermath of overexpression of WT or mutant COL4A3 chains in human undifferentiated podocytes. The UPR pathway arose as the most highly deregulated pathway associated with COL4A3-WT or COL4A3-G1334E overexpression (Supplemental Table 2). Importantly, we validated the microarray data for several UPR genes using qPCR (Figure 5). During

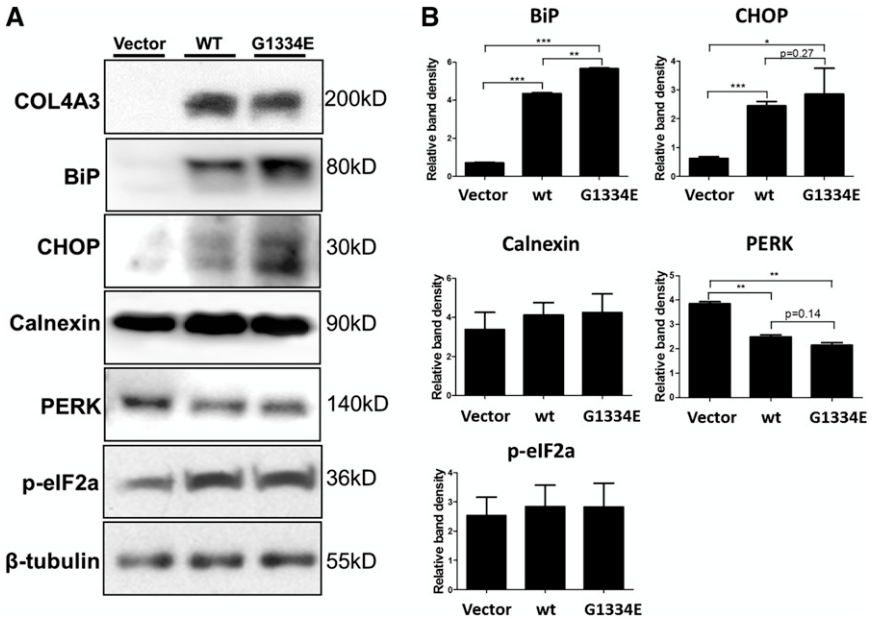

Figure 6. UPR proteins are deregulated in AB8/13 cells transfected with wild type or mutant COL4A3. (A) Undifferentiated cells are transfected with equal amounts of COL4A3-WT (WT), COL4A3-G1334E (G1334E), or the empty pcDNA6/HA vector (Vector; used as a negative control). Protein expression of the UPR markers BiP, CHOP, calnexin, PERK, and p-eIF2a was measured 48 hours after transfection via Western blotting. b-Tubulin expression in the same samples was used as an equal loading control. Shown is a representative blot, with differential levels of the various proteins. (B) Western blotting is quantified via densitometric analysis. Data are means6SEM of three independent experiments. While calnexin and p-eIF2a remain unaltered, BiP and CHOP are upregulated in cells overexpressing the WT or mutant collagen IV chain, and PERK is downregulated. *P , 0.05; **P , 0.01; ***P , 0.001.

the qPCR verification we demonstrated significant upregulation of the genes BiP and CHOP between cells expressing the WT or the COL4A3-G1334E single chains in equal amounts (Figure 5A). A similar differential increased expression was evident in the activated form of XBP1, as tested by the splicing assay in cells expressing the WT or mutant collagen chain (Figure 7). These results were also supported by over-representation of the respective proteins, although not always reaching statistical significance (Figure 6). It is not clear from these experiments why the PERK gene appears downregulated in the cells and upregulated in the mice (see below).

We recognize that in our experimental set-up we used singly transfected cells, which expressed either a WT or a mutant collagen IV chain. This resulted in intracellular overexpression (nearly 30-fold compared with the endogenous at the mRNA level and 10-fold at the protein level), which was adequate on its own to activate the UPR signaling cascade. An explanation as to why overexpression of the mutant chain results in higher UPR upregulation compared with the WT is not obvious at first sight. There could be two complementary explanations: One is that this differential UPR upregulation occurs because the cell can apply quality control on the nascent single collagen chain level. Another is that the mutant COL4A3 chain associates poorly with the endogenous COL4A4 and COL4A5 chains, resulting in more misfolded protein being retained in the ER and subsequent higher activation of particular UPR genes due to a dose effect.

Notably, previous studies showed that intracellular accumulation of mutant COL4A1 and COL4A2 chains, causative for hemorrhagic stroke in humans, are retained in the cell's ER and activate the UPR pathway.[26]

Importantly, the UPR pathway is triggered both when podocytes overexpress a collagen chain and when the endogenous COL4A3 chain is knocked down by siRNA. Activation is evident in both cases by the increase of the key UPR marker BiP, demonstrating that the cell senses this protein chain imbalance and exerts its quality control in the ER. Of note, the pathway is differentially activated in these two contrasting conditions that result in similar outcomes. COL4A3 overexpression results in activation of the proapoptotic branch of the UPR with upregulation of the proapoptotic marker CHOP. However, in COL4A3 downregulation, CHOP remains unaltered and the PERK UPR branch is activated with increase of eIF2a phosphorylation. These results could reflect the variable activation of the pathway shifting toward the cytoprotective or proapoptotic direction, depending on the nature and/or severity of the stress the cell is facing.

UPR Phenotype on Human Renal Biopsy Specimens

We next tested the activation of the UPR pathway in human biopsy material because we are mindful that extrapolation of the cell culture data obtained herein should be done with caution. This is because in vitro experiments are based on overexpression or downregulation and a relative brief experimental time frame, whereas AS and TBMN are disease processes that take many years to become established. We demonstrated UPR activation, as shown by increased expression of BiP, a sensitive indicator of UPR activation[27,28] in patients carrying the COL4A3-G1334E mutation as compared with obese persons (Figure 8). Notably, BiP staining in the glomerulus of these patients is more evident, whereas tubular BiP expression is similar between patients and obese persons. Further experiments should be carried out in order to examine whether it is collagen accumulation per se that causes BiP upregulation in glomeruli of these patients or it is a result of other downstream mutational effects. Still, our data agree with previous studies depicting an increase in ER stress proteins in kidney biopsy specimens from patients with other

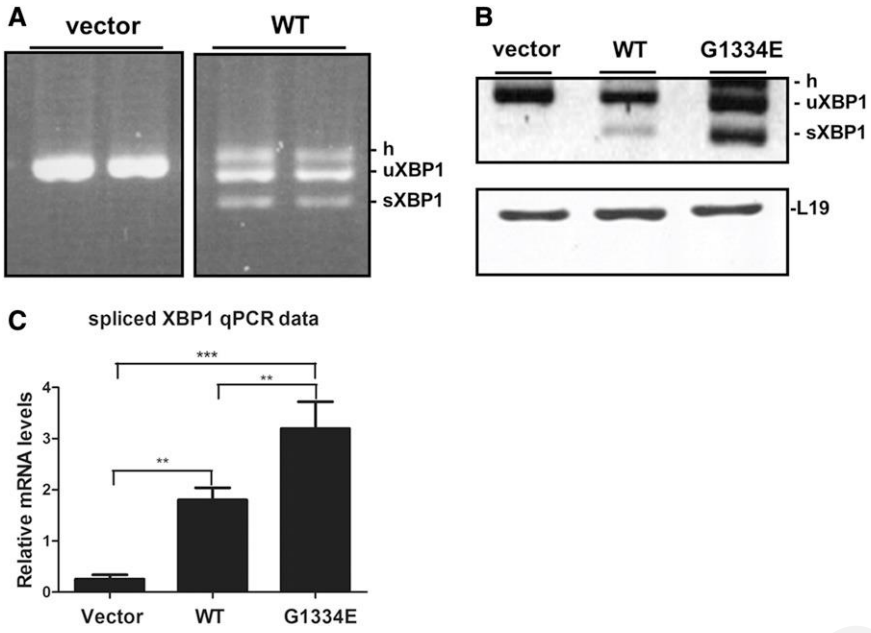

Figure 7. Single-chain expression of WT or COL4A3-G1334E induces XBP1 splicing in AB8/13 cells. (A) Representative experiment of RT-PCR of the XBP1 mRNA in AB8/13 cells transiently expressing COL4A3-WT collagen chain or the empty pcDNA6/HA vector (vector). PCR products were run on 3% agarose gel. It is apparent that overexpression of WT chain induces XBP1 splicing, as evidenced by the appearance of the smaller spliced form (sXBP1) and the heteroduplex species formed between unspliced and spliced chains (h). The spliced molecules are smaller by 26 bp. (B) Representative experiment of RT-PCR of the XBP1 mRNA in AB8/13 cells transiently expressing COL4A3-WT, mutant COL4A3-G1334E chain, or the empty pcDNA6/HA vector. PCR products were run on 3% agarose gel. It is evident that overexpression of both WT and mutant chains results in XBP1 splicing. L19 was used as an internal PCR control. (C) Real-time PCR for direct quantitation of the spliced XBP1 isoform using primers in the spliced-unspliced interface. Notice the highly statistical difference in the spliced form between vector-only–, WT-, and mutant-expressing cells. Especially important is the differential induction of XBP1 splicing comparing WT with mutant cells. Data are means±SEM of three independent experiments; **$P < 0.01$; ***$P < 0.001$. uXBP1, unspliced XBP1.

nephropathies, such as diabetic nephropathy,[29] FSGS, and membranous nephropathy.[30,31]

UPR Phenotype in a Mouse Carrying the Col4A3-G1332E Mutation

Our data demonstrated (for the first time, to our knowledge), UPR activation in a relevant in vivo mouse model, the knockin Col4a3-G1332E mouse. These mice developed severe AS-like GBM pathology as early as at 3 months of age, based on electron microscopy of renal biopsy specimens. The histologic phenotype became more evident at the 7-month time point, while the mice also exhibited hematuria and proteinuria (not shown). UPR activation was evident by significant upregulation of the UPR markers BiP, p-PERK, and p-eIF2a in the mutant mice both at the mRNA and the protein level, as well as nearly significant increase of XBP1 splicing in mutant mice (Figure 11). Contrary to the in vitro overexpression results, in these mice we did not observe CHOP upregulation at the 3-month time point. However, the in vivo data best resembled the COL4A3 knockdown experiments with upregulation of the markers p-PERK and p-eIF2a and no change in the proapoptotic marker CHOP. This finding is interesting because it seems that the stress exerted by the partial knockdown of one chain seems to resemble best the in vivo situation.

Follow-up studies using more and older mice could determine whether collagen IV mutations could evoke the proapoptotic branch of the UPR pathway at a later time point. Still, the significant eIF2a activation observed in these mice could mean translational attenuation, which could still be detrimental in disrupting the highly coordinated events in the podocyte's specialized secretory capacity, leading to defective GBMs. Tsang et al. showed similar results in which transgenic mice expressing mutant collagen X in chondrocytes activated the UPR pathway without inducing cell death but caused altered chondrocyte differentiation and function causing chondrodysplasia.[32] It is interesting that in the in vitro system, overexpression of collagen chains results in significant CHOP upregulation and unaltered p-eIF2a, whereas in the Col4a3-G1332E–carrying mice the opposite is observed and is more similar to the knockdown system. This discrepancy could be due to overexpression of the mutant chains in the cellular system, resulting in severe stress and initiating the proapoptotic branch of the UPR, or it might reflect the various homeostatic mechanisms present in the in vivo situation that shifts the UPR pathway toward the adaptive cytoprotective site. Nonetheless, this appears to be the first time that UPR upregulation is evident in a knock-in Col4a3 mouse. Thus, it would be interesting to examine the current established models of AS[33–36] for a similar UPR activation effect. The existing knockout models are null for the Col4a3 or the Col4a5 chain, meaning that the a3a4a5 collagen protomer is compromised. On the basis of the existing knowledge of collagen biochemistry and protomer formation, it is reasonable to assume that knocking down or entirely knocking out one a chain leaves the other two WT chains in excess and vulnerable to degradation, perhaps as a result of the quality control applied by the ER machinery and UPR activation.

Interestingly, it was previously shown that ectopic expression of COL4A3 and COL4A4 in the lens of transgenic mice

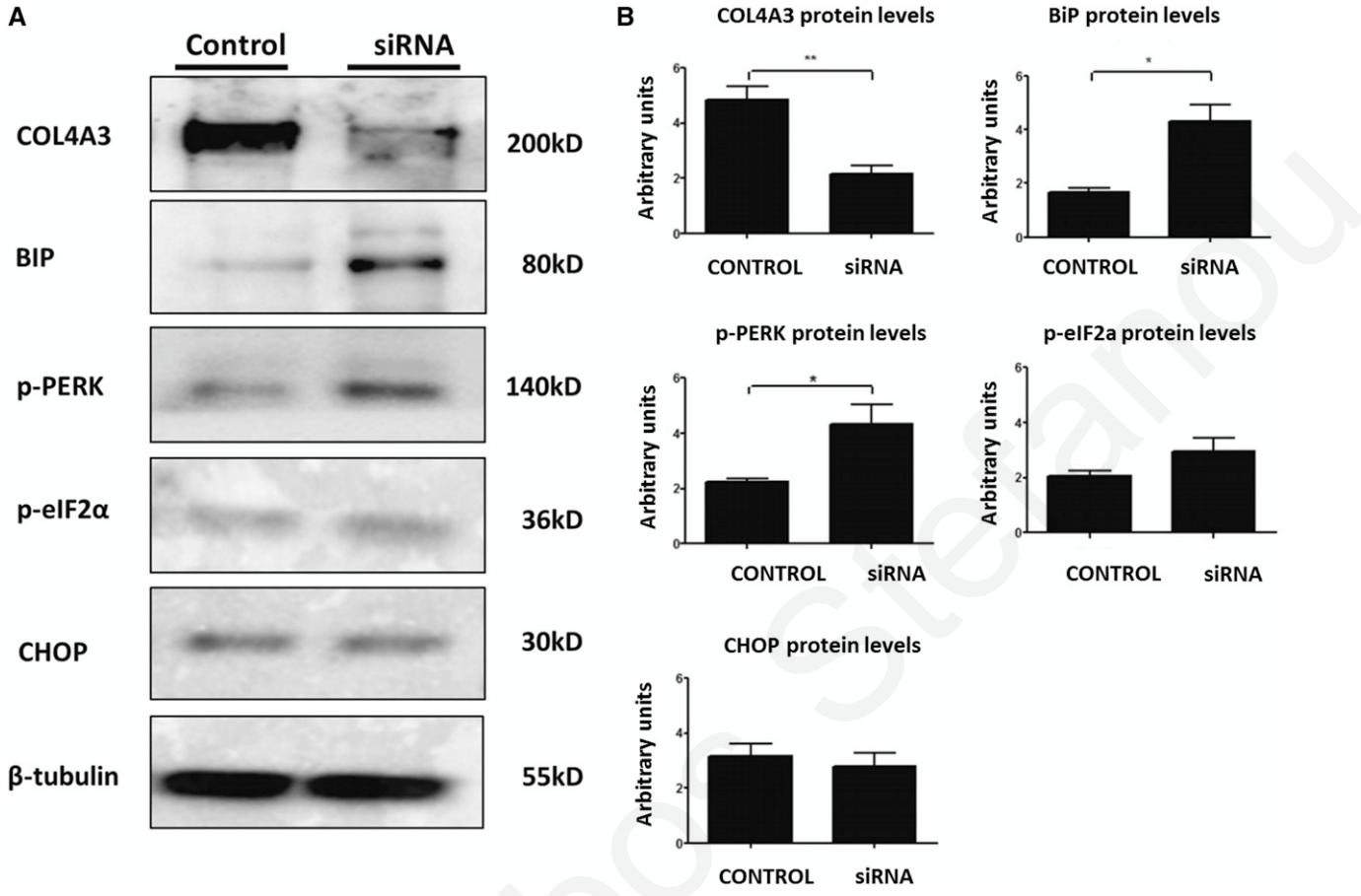

Figure 8. Knockdown of endogenous COL4A3 in differentiated podocytes activates the UPR pathway. Differentiated cells are treated with COL4A3 siRNA to knock down endogenous COL4A3 expression. (A) Protein expression of the UPR markers BiP, CHOP, p-PERK, and p-eIF2a was measured 72 hours after transfection via Western blotting. b-Tubulin expression in the same samples was used as equal loading control. Scrambled siRNA was used as a negative control in all experiments. Shown is a representative blot, with differential levels of the various proteins. Note the effective downregulation of the target gene and the upregulation of UPR markers. (B) Western blotting in A was quantified via densitometric analysis. Data are means6SEM of three independent experiments. While CHOP remained unaltered, BiP and p-PERK were upregulated in cells being treated with COL4A3 siRNA. *P , 0.05; **P , 0.01.

results in cataract,[37] while it is accompanied by UPR activation and ER expansion. This transgene expression had adverse effects on lens fiber cell differentiation and eventually induced cell death in a group of transgenic fiber cells.[37]

To our knowledge, this study is the first to generate results in a podocyte culture model and in human kidney biopsy specimens, as well as results in knockin mice carrying the Col4a3-G1332E mutation that provide evidence of UPR activation. Consequently, on the basis of these data we can hypothesize that UPR activation might be part of the overall AS/TBMN phenotype at the intracellular level. We are also justified in hypothesizing that different amino acid substitutions may activate the UPR pathway differentially and thereby lead to disparate phenotypes.

In conclusion, we herewith showed experimental data based on cultured human podocytes and human renal biopsy specimens as well as preliminary data from a knockin mouse model for a Col4a3 mutation that collectively implicate the UPR pathway in the disease process. To date the exact pathogenic mechanism resulting from COL4 mutations in patients with AS or TBMN is poorly characterized. ER stress and UPR activation make up a central pathogenic mechanism in various conditions, including several connective tissue disorders associated with the expression of mutant extracellular matrix proteins.[14] ER stress in renal pathophysiology is a relatively new area of research.[38–40] Therefore, recognizing its contributory role to the deleterious consequences of collagen IV trafficking defects would greatly improve AS/TBMN patient prognosis and would pave ways for development of novel therapeutics, such as the use of molecular chaperones to improve or ameliorate disease symptoms. Finally, the clinical heterogeneity observed in patients with AS/TBMN could be

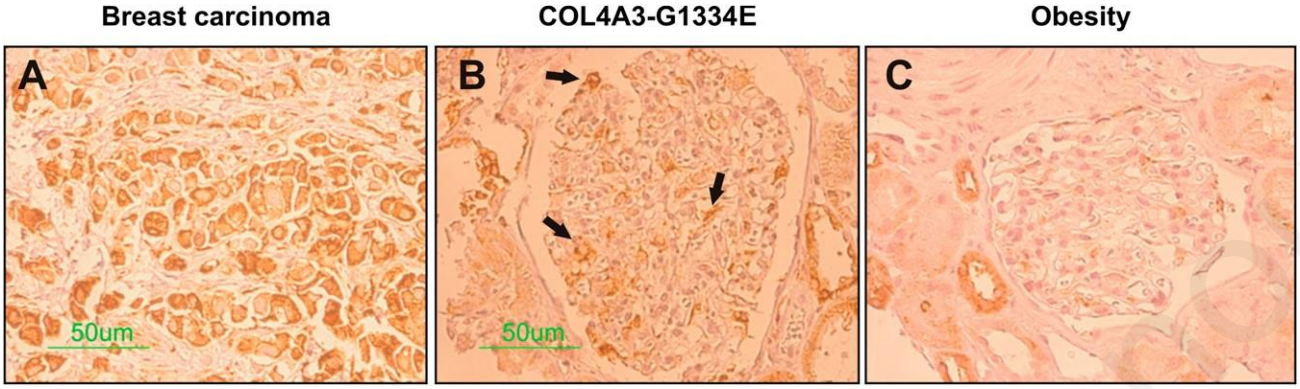

Figure 9. BiP protein expression is increased in renal biopsies of COL4A3-G1334E heterozygous carriers. Detection of BiP expression in the glomerulus from renal biopsy specimens of two patients diagnosed with TBMN and confirmed heterozygous carriers of the COL4A3-G1334E mutation, using immunohistochemical staining (B). Kidney biopsy specimens from a patient with breast carcinoma (A) and six obese persons (C) were used as positive and negative controls, respectively. In the patients with confirmed COL4A3-G1334E mutation, serial sections show strong perinuclear BiP immunoreactivity in the glomerulus compared with the obese controls. Tubular cells of both the patient with COL4A3-G1334E and the obese persons are stained positive for BiP. All samples are sex and age matched.

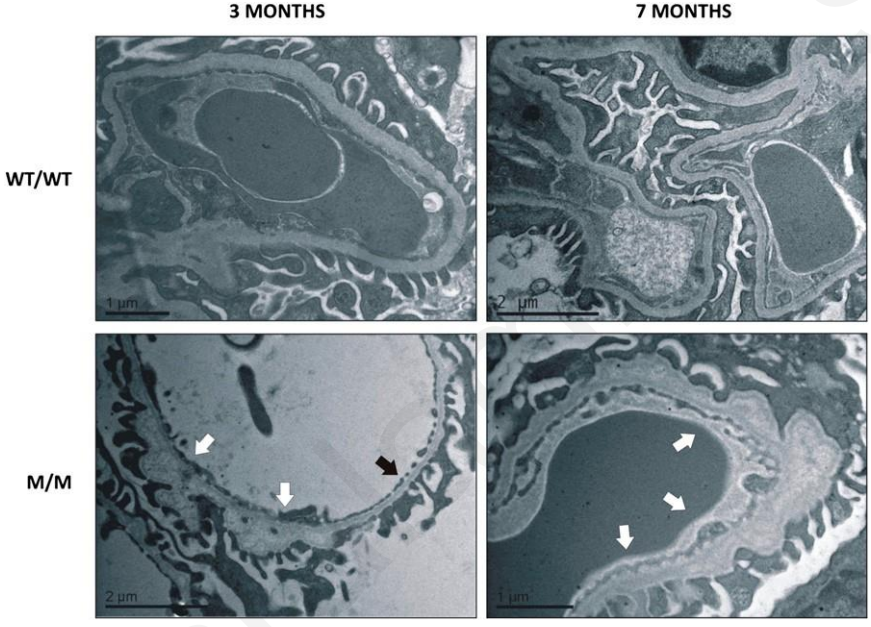

Figure 10. Ultrastractural pathology of the mutant knockin mice is consistent with Alport Syndrome nephritis. WT mice (WT/WT) display normal GBM thickness, 280–300 nm range, while G1332E/G1332E (M/M) homozygous mice demonstrate thin GBMs, 140–160 nm range (black arrow), with areas of mild (3-month-old mice) or severe (7-month-old mice) irregular thickening (white arrows), consistent with AS nephritis.

associated with a varying pattern in UPR activation. Because the level of UPR activation is linked directly to the duration and severity of the ER experienced by the cell, this is something that could vary between individuals carrying different mutations, leading to diverse clinical outcomes. Therefore, the pursuit for modifier genes could include the search for UPR related genes.

CONCISE METHODS

Plasmid Vectors

A plasmid vector containing the full-length human COL4A3 cDNA subcloned into the pCMV6-AC-HA was purchased from Origene. The vector was confirmed for expression of C-terminal fusion of the Collagen a3 with the hemagglutinin (HA) tag. The COL4A3-G1334E point mutation was introduced in the WT COL4A3 by PCR-based site-directed mutagenesis (QuikChange Site-Directed Mutagenesis, Stratagene, La Jolla, CA). Mutagenic primers were as follows: G1334E-A3-For: 59-CCATTGGACCTCCAGAACCAATTGGGCCAAAAGG-39; G1334E-A3-Rev: 59-CCTTTTGGCCCAATTGGTTCTGGAGGTCCAATGG-39. Correct incorporation of the mutation as well as elimination of any nonspecific changes was confirmed by both restriction digest and DNA sequencing. Mutation G1334E was chosen because of its known pathogenic effect; it is endemic in Cyprus and has been found in a cohort of 169 TBMN patients as a strong founder effect.[19]

Cell Culture and Transfections

The AB8/13 undifferentiated podocyte cells[41] were incubated at 33°C at 5% CO_2 and cultured in RPMI medium, supplemented with 10% FBS (Invitrogen, Carlsbad, CA), 1% of 100 U/ml penicillin/streptomycin (Invitrogen), and 1% insulin-transferrin-selenium (Invitrogen). When needed, differentiated podocytes were obtained by culturing the cells at 37°C for 14 days. At 70% confluence, cells were transiently transfected with the vectors containing the collagen cDNAs, WT or mutant, using lipofectamine 2000 according to the manufacturer's instructions.

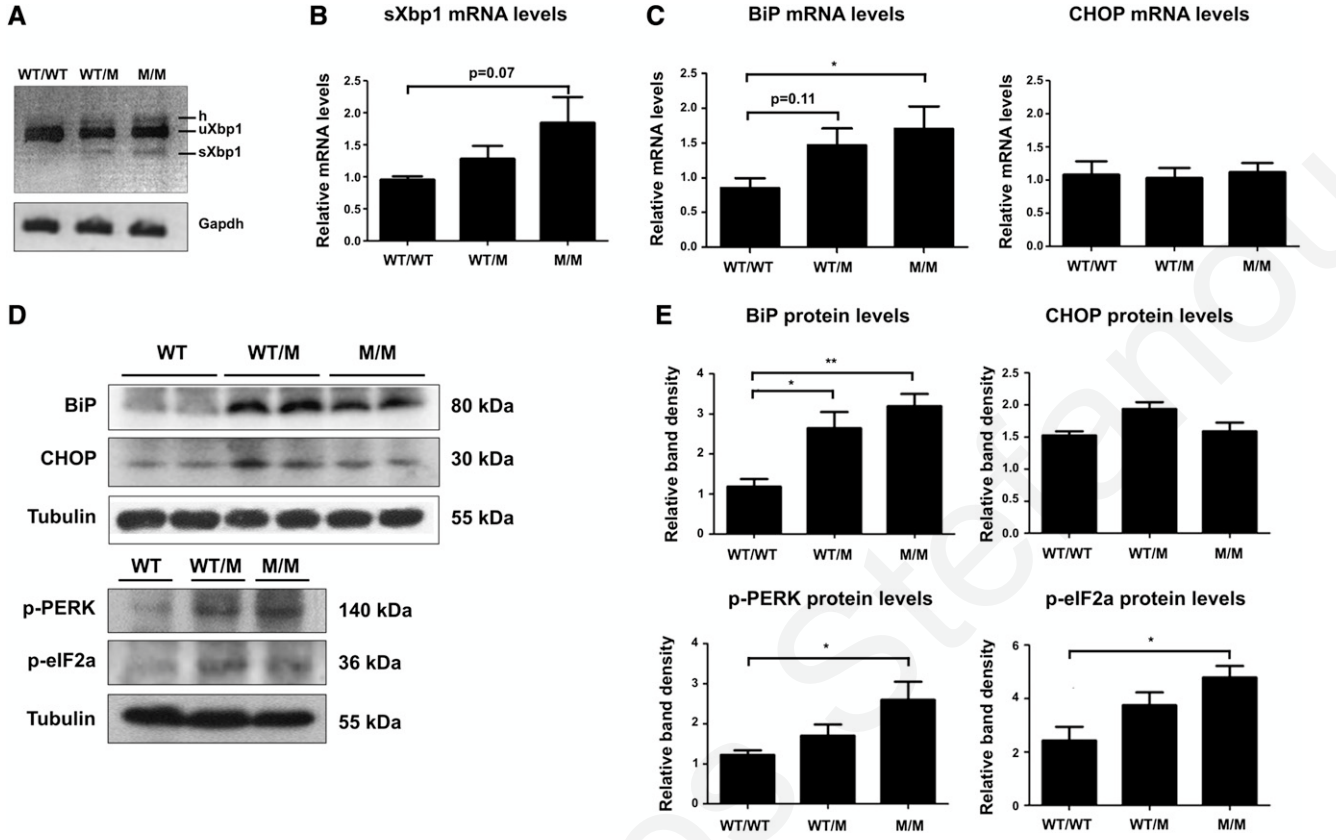

Figure 11. The UPR pathway is activated in whole kidney lysates of Col4a3-G1332E mice. (A) XBP1 splicing assay using RNA from whole kidney lysate from WT, Col4a3-G1332E heterozygous (WT/M), and Col4a3-G1332E homozygous (M/M) mice. Splicing is evident by the presence of the lower-molecular-weight band on 2% agarose gel. Mouse glyceraldehyde 3-phosphate dehydrogenase is used as control. Notice the presence of the spliced band in the heterozygous (WT/M) and homozygous (M/M) mice. (B) Real-time PCR for direct quantitation of the spliced XBP1 isoform using primers in the spliced–unspliced interface. Significance is not reached, but there is an obvious trend toward spliced XBP1 increase in homozygous (M/M) mice. Data are means6SEM of three independent experiments. (C) Examination of BiP and CHOP mRNA levels by qPCR. RNAs were extracted from whole kidney tissue of WT, Col4a3-G1332E heterozygous (WT/M), and Col4a3-G1332E homozygous (M/M) mice. Shown is significant upregulation of the BiP but not CHOP mRNA levels. (D) Representative Western blot to demonstrate protein expression level change in the homogenates of whole kidney lysate from 3-month-old WT or Col4a3-G1332E heterozygous (WT/M) or homozygous (M/M) knock-in mice. Equal amounts of protein homogenates were resolved by SDS-PAGE followed by Western blot. The blots in each panel came from the same gel. Notice differential expression of proteins between WT and mutant mice. (E) Quantification of representative blots as in D is shown in graphic form. The expression levels of BiP, CHOP, p-PERK, and p-eIF2a were normalized to b-tubulin levels (*P , 0.05; **P , 0.01, n$3); M/M, homozygous for the Col4a3-G1332E mutation; WT/M, heterozygous for the Col4a3-G1332E mutation. Three mice were used for each condition. All UPR genes except CHOP were significantly overexpressed. h, hybrid; sXBP1, spliced XBP1; uXBP1, unspliced XBP1.

Forty-eight hours after transfection, cellular lysates and cellular medium were collected for experiments. Importantly, 12 hours before extraction, cells were treated with 50 mg/ml ascorbic acid (Sigma-Aldrich, St. Louis, MO) in serum-free medium. Transfection efficiency was assessed by immunofluorescence using an anti-HA antibody in a transfection control sample; transfection efficiency was typically about 60%. In all experiments, the empty pCMV6-AC-HA plasmid was used as a control to determine transfection toxicity. Collagen construct expression was similar in all transfected cells as assessed by qPCR on the collagen mRNA levels, at each single experiment, using a reverse primer on the engineered C-terminal tag. Primers were as follows: COL4A3-For: CCAGCTGGATCAGATGGAT; HA-FLAG-Rev: AGCGTAATCTGGAACATCGTATGGGTA. COL4A3 mRNA expression after transfection strongly increased (30-fold) compared with nontransfected AB8/13 cells as determined by qPCR (data not shown).

RNA Preparation and Microarray Experimental Design

To study the genetic regulation of COL4A3 overexpression in the podocyte, 24 hours after transfection, total RNA was extracted from podocytes transfected only with the pcDNA6-HA vector or vectors expressing WT COL4A3 or the mutant COL4A3-G1334E chain. Before cDNA synthesis, the quality of total RNA was checked by a 2100 Bioanalyzer (Agilent Technologies, Santa Clara, CA) using an RNA 6000 LabChip kit (Agilent Technologies). All samples were of good quality, and 100 ng RNA was used to synthesize biotin-labeled

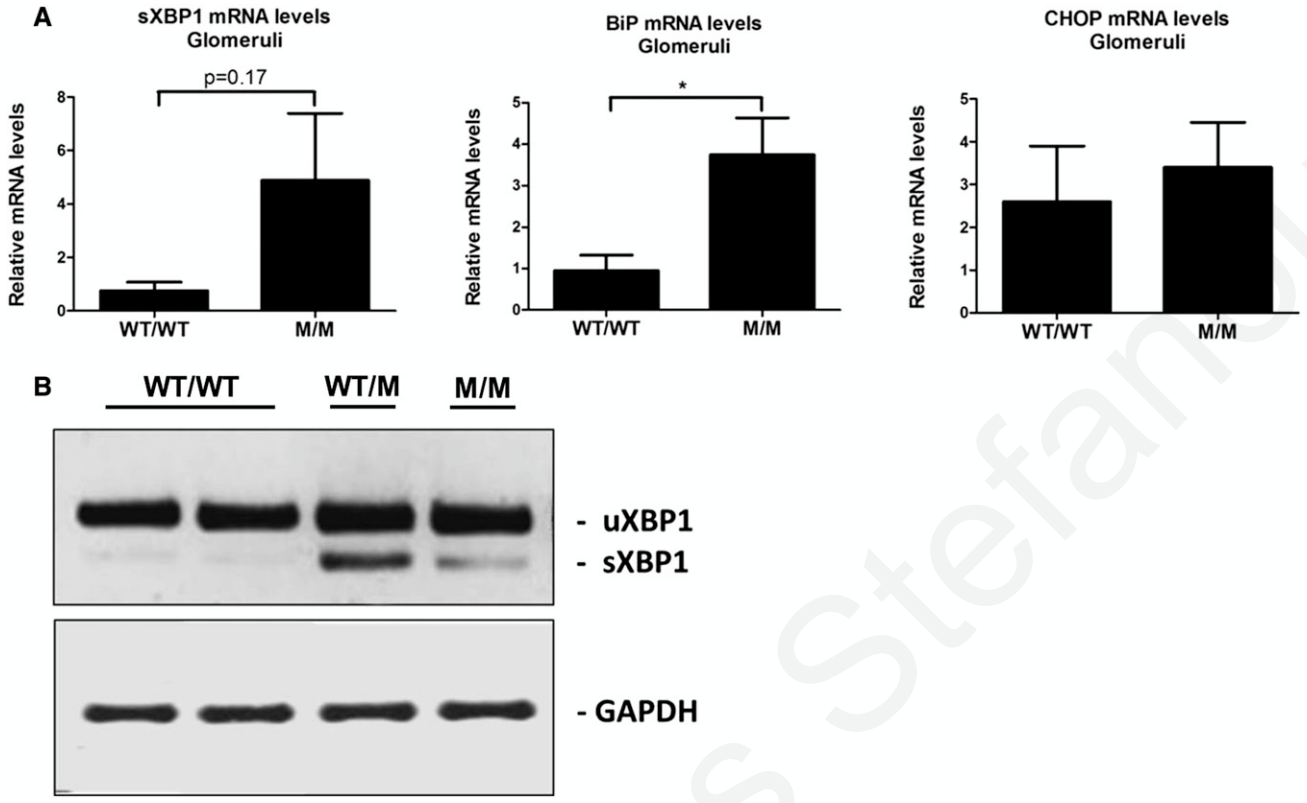

Figure 12. Upregulation of UPR marker mRNA in glomeruli isolated from Col4a3-G1332E knock-in mice. (A) Examination of BiP and CHOP mRNA levels by qPCR. RNAs were extracted from isolated mouse glomeruli of WT and Col4a3-G1332E homozygous mutant (M/M) mice. Shown is significant upregulation of the BiP but not CHOP mRNA levels. Spliced XBP1 mRNA levels show an obvious increase trend. (B) Representative experiment of reverse transcription PCR of the XBP1 mRNA in RNA isolated from WT or mutant mice glomeruli. PCR products were run on 3% agarose gel. It is apparent that there is induction of XBP1 splicing in mutant mice, as evidenced by the appearance of the smaller spliced form (sXBP1). The spliced molecules are smaller by 26 bp. Mouse glyceraldehyde 3-phosphate dehydrogenase is used as control. M/M, homozygous mouse; WT/M, heterozygous mouse; WT/WT, WT mice. *P , 0.05; n53.

target cRNA using the GeneChip 39 IVT Express Kit (Affymetrix, Santa Clara, CA). Two hundred micrograms of the labeled and fragmented RNA from V1 (vector only), WT (WT COL4A3), and G (COL4A3-G1334E) were hybridized for 16 hours to the Affymetrix GeneChip Human Genome U133 Plus 2.0 Array, which represents approximately 39,000 of the best-characterized human genes. The hybridization step was followed by staining and washes using the GeneChip Hybridization, Wash and Stain Kit from Affymetrix as well as the GeneChip Fluicids Station 450 robot (Affymetrix). The arrays were scanned at 5-mm resolution using the Affymetrix GeneChip Scanner 3000 7G. Quality control was performed using the Affymetrix expression Console. The raw microarray data were background corrected, quantile normalized, and $\log_2$ transformed using the SAS JMP7 Genomics, version 4, package (SAS Institute, Cary, NC). Differential mRNA expression was analyzed by one-way ANOVA. A P value of 0.05 with false discovery rate , 10% was considered as the cutoff level of significance.

Pathway Analysis, Gene Ontology, and Clustering

Pathway analysis and gene ontology for the significantly deregulated genes was performed using the KEGG (http://www.genome.jp/kegg/pathway.html) and The Database for Annotation, Visualization and Integrated Discovery (http://david.abcc.ncifcrf.gov/) databases. A P value of 0.05 using the Fisher exact test with Bonferroni correction was set as a cutoff. We used two-way hierarchical clustering and K-means clustering with Euclidean distance as a metric to cluster the most deregulated genes. Clustering was performed using Genesis software, version 1.7.6 (Graz University of Technology).

qPCR

Twenty-four hours after transfection, total RNA was extracted from cells using an RNA extraction kit (Macherey-Nagel, Düren, Germany). The integrity of the RNA was assessed via gel electrophoresis, and the concentration was measured spectrophotometrically (Nanodrop Technologies, Montchanin, DE). One microgram of total RNA from all samples was reverse transcribed simultaneously using an oligo-dT (dT23VN) primer and the ProtoScript First Strand cDNA Synthesis Kit (New England Biolabs, United Kingdom). The qPCR amplifications were performed on a LightCycler system (Roche Applied Science) using the LightCycler FastStart DNA Master SYBR Green I kit (Roche, Germany) in a reaction volume of 20 ml. Relative

quantification analysis was carried out on LightCycler software, version 4.1. The primer sets for the genes whose differential expression was analyzed by qPCR are shown in Table 1. Differences in starting material were compensated by normalization to the endogenous reference genes GAPDH and L19.

Immunoblotting

Forty-eight hours after transfection, cellular lysates or cellular medium were collected for experiments. Cells were lysed in equal volumes of preheated 2× SDS loading buffer (SDS 25 mM, Tris-HCl with pH of 6.8, 20% glycerol, 2% SDS, 2% b-mercaptoethanol, and bromophenol blue) and homogenized via sonication. The transblots were probed with a primary antibody (anti-HA; Santa Cruz Biotechnology), targeted to the fused HA-tag epitope engineered in the carboxyl terminus of the collagen chain. The collagen chains were seen at around 200 kDa. Antibodies used against the ER-stress proteins were anti-BiP, anti-PERK, anticalnexin (Cell Signaling Technology, Danvers, MA) and anti-CHOP, and anti–p-eIF2a (Santa Cruz Biotechnology), followed by peroxidase-labeled secondary antibodies—either goat antimouse or donkey anti-rabbit (Santa Cruz Biotechnology). Proteins were detected using the Enhanced ChemiLuminescence Plus Blotting Detection system (Amersham Biosciences, Buckinghamshire, United Kingdom) and were visualized by autoradiography on photographic film (Kodak X-OMAT; Eastman Kodak, Rochester, NY).

All transblots were reprobed with anti–b-tubulin antibody (Santa Cruz Biotechnology) to prove equal amounts of protein were loaded on the membrane. Band density was defined the ImageJ Software (http://imagej.nih.gov/ij).

Table 1. Sets of qPCR oligonucleotides synthesized to measure expression of the mRNA levels of these genes.

Genes	Primer Sequence (5′ to 3′)
Human genes	
BiP_F	TGTTCAACCAATTATCAGCAAACTC
BiP_R	TTCTGCTGTATCCTCTTCACCAGT
CHOP_F	AGAACCAGGAAACGGAAACAGA
CHOP_R	TCTCCTTCATGCGCTGCTTT
Calnexin_F	TCCGCCTCTCTCTTTACTGC
Calnexin_R	GCAACCACTTCCCTTCCAT
Calreticulin_F	GCAAATTCGTCCTCAGTTCTGG
Calreticulin_R	CCATGCATGTCCTTCTGGTC
Gadd34_F	ATGTATGGTGAGCGAGAGGC
Gadd34_R	GCAGTGTCCTTATCAGAAGGC
EDEM_F	CAAGTGTGGGTACGCCACG
EDEM_R	AAAGAAGCTCTCCATCCGGTC
sXBP-1_F	CTGAGTCCGCAGCAGGTGCAG
sXBP-1_R	CCAGAACATCTCCCCATGGAT
GAPDH_F	TTGGTATCGTGGAAGGACTCA
GAPDH_R	TGTCATCATATTTGGCAGGTTT
L19_F	GCGGAAGGGTACAGCCAAT
L19_R	GCAGCCGGCGCAAA
Mouse genes	
COL4A3_F	CCGAGCCAGTCCATTTATAGAAT
COL4A3_R	CAGCGAAGCCAGCCAGAA
BiP_F	TCATCGGACGCACTTGGAA
BiP_R	CAACCACCTTGAATGGCAAGA
CHOP_F	GTCCCTAGCTTGGCTGACAGA
CHOP_R	TGGAGAGCGAGGGCTTTG
sXbp1_F	CTGAGTCCGCAGCAGGTGCAG
sXbp1_R	CCAGAACATCTCCCCATGGAT
GAPDH_F	GCATGGCCTTCCGTGTTCCTA
GAPDH_R	CCTGCTTCACCACCTTCT
Oligos for Xbp1 splicing assay	
hXbp1_F	GGAGTTAAGACAGCGCTTGG
hXbp1_R	ACTGGGTCCAAGTTGTCCAG
mXbp1_F	GAACCAGGAGTTAAGAACACG
mXbp1_R	AGGCAACAGTGTCAGAGTCC

All supplied by M.W.G., Ebersberg, Germany.

Semiquantitative Analysis and XBP1 Splicing

AB8/13 cells were transfected with COL4A3-WT or COL4A3-G1334E constructs in equal amounts as confirmed by qPCR and Western blots (not shown). Twenty-four hours post-transfection total RNA was isolated and cDNA was synthesized as described above. For every RNA sample, a control reaction without reverse transcription was performed to exclude genomic DNA contamination. cDNA was further used as a template for PCR with XBP or L19 RNA primers (primers shown in Table 1). PCR products were then analyzed on a 3% agarose gel.

Experiments with siRNA

A total of 400,000 podocytes were seeded on a 6-cm culture dish. Differentiated podocytes were transfected with siRNA COL4A3 (Santa Cruz Biotechnology) using the lipofectant RNAiMax (Invitrogen) Briefly, 7.5 ml of the lipofectant was mixed with 80 pmol of siRNA in 1 ml of Opti MEM. The mix was added to 4 ml of complete media without antibiotics to the dishes. Cells were incubated overnight at 37°C and 5% CO_2. The following day, the same concentrations of lipofectant and siRNA in 1 ml of Opti-MEM Were again added to the dishes. Cells were harvested 72 hours after the second transfection.

Immunocytochemistry

Forty-eight hours after transfection, cells on coverslips were fixed with 4% paraformaldehyde in PBS for 10 minutes and permeabilized for an additional 10 minutes with 0.5% Triton X-100 in PBS. All cells were quenched with 50 mM ammonium chloride in PBS for 10 minutes, blocked with 2% BSA, 2% FCS, 0.2% fish skin gelatin in PBS (blocking mix) for 30 minutes, and incubated with primary and then secondary antibodies in PBS, containing 5% blocking mix, either overnight at 4°C or for 1 hour at room temperature. Cells were incubated with Hoechst solution (DAKO, Denmark) at a 1:1000 dilution for 1 minute for nucleus staining and were subsequently mounted with fluorescence mounting medium (DAKO).

Fluorescence Microscopy

Immunofluorescent preparations were analyzed on a Zeiss Axiovert 200M inverted fluorescence microscope equipped with Zeiss Axiovision 4.2 software. Digital images were recorded and composed using Adobe Photoshop 5.0 and Illustrator 10 for Macintosh. Quantification and co-localization were determined using ImageJ software.

Immunohistochemistry

For human kidney staining experiments, kidney sections were cut and mounted on slides coated with suitable tissue adhesive. Then

sections were deparaffinized using xylene and rehydrated through washes in graded alcohols. Endogenous peroxidase was neutralized using 0.5% vol/vol hydrogen peroxide/methanol for 10 minutes. Slides were washed with water. Retrieval was carried out using 0.01 M citrate retrieval solution (pH, 6.0). Sections were subsequently washed with TBS and blocked for 10 minutes using diluted normal serum (Novocastra Protein Block; Leica Microsystems). Sections were incubated with primary antibody anti-BiP (Cell Signaling Technology) diluted 1:200 in antibody diluent solution (DAKO) overnight at 4°C. Slides were then washed and incubated with DAKO REAL EnVision, HRP Rabbit/Mouse (ENV). Subsequently, slides were incubated with a suitable peroxidase substrate, washed thoroughly in running tap water, and counterstained with hematoxylin, before being dehydrated and mounted. Patient tissue was used after bioethics approval and informed consent. The patients who carry mutation G1334E belong to families that have been described before.[4]

Generation of Col4a3-G1332E Knock-In Mice

All animal experiments were carried out in compliance with Cyprus law for protection of animals and were approved by the local authorities. Details on targeting construct generation, production, and genotyping of mice are described in the supplemental materials (Supplemental Figure 2). Comprehensive phenotypic details of this line will be documented elsewhere (M.P. and C.D., unpublished data). Animals were hosted in the Cyprus Institute of Neurology and Genetics animal house under specific pathogen-free conditions.

Electron Microscopy of Mouse Kidney Sections

For electron microscopy studies, left kidney sections were processed as usual and examined under a transmission electron microscope (JEM2100HR; JEOL, Inc., Tokyo, Japan) equipped with an ES500W Erlangshen CCD camera (Gatan GmbH, Munchen, Germany). GBM thickness was measured in open capillary loops using Digital-Micrograph software (Gatan).

Glomeruli Isolation

Glomeruli were isolated following the protocol by Takemoto et al.[42] Briefly, mice were anesthetized by an intraperitoneal injection of Avertin (2,2,2-tribromoethyl and tertiary amyl alcohol; 17 ml/g mouse) and perfused with 8×10^7 Dynabeads through the heart. The kidneys were removed, minced, and digested in collagenase. The digested tissue was gently pressed through a 100-mm cell strainer and the cell suspension was then centrifuged at 200×g for 5 minutes. The supernatant was discarded and the cell pellet was resuspended in HBSS. Glomeruli containing Dynabeads were gathered by a magnetic particle concentrator. Glomeruli total RNA was isolated using a commercially available kit (Macherey-Nagel), according to the manufacturer's instructions.

Statistical Analyses

All statistical analyses with the exception of the microarrays were performed using GraphPad Prism, version 5, statistical software. Data are expressed as mean±SEM; the Mann-Whitney U test was performed for pairwise comparisons. For comparisons involving more than two groups, nonparametric analysis of relative contrasts was performed with Tukey post hoc analysis. No prior transformation of the data was performed. For microarray analysis we used the SAS JMP7 Genomics, version 4, package (SAS Institute). Differential mRNA expression was analyzed by ANOVA. A P value $\leq$ 0.05 with a false discovery rate $\leq$ 10% was considered as the cutoff level of significance. For pathway analysis and gene ontology enrichment, a P value of 0.05 using the Fisher exact test with Bonferonni correction was set as a cutoff.

ACKNOWLEDGMENTS

The authors thank Dr. S. Malas and his student, E. Panayiotou, for assistance with the animal procedures. Part of this work was presented orally during the 8th Meeting of the COST Action BM0702, Kidney and Urine Proteomics, March 29–April 1, 2012, Sounion, Athens, Greece, during the 25th European Renal Cell Study Group meeting in Oxford, United Kingdom, March 21–24, 2013, and as a poster during the 50th Congress of the European Renal Association-European Dialysis and Transplant Association, May 18–21, 2013.

The work was supported mainly by a grant from the Cyprus Research Promotion Foundation, HEALTH/BIOS/0308(BE)/17 and NEW INFRASTRUCTURE/STRATEGIC/0308/24 (cofunding by the EU Structural Funds) to C.D.

DISCLOSURES

None.

REFERENCES

1. Haas M: Alport syndrome and thin glomerular basement membrane nephropathy: a practical approach to diagnosis. Arch Pathol Lab Med 133: 224232, 2009
2. Thorner PS: Alport syndrome and thin basement membrane nephropathy. Nephron Clin Pract 106: c82–c88, 2007
3. Temme J, Peters F, Lange K, Pirson Y, Heidet L, Torra R, Grunfeld JP, Weber M, Licht C, Müller GA, Gross O: Incidence of renal failure and nephroprotection by RAAS inhibition in heterozygous carriers of X-chromosomal and autosomal recessive Alport mutations. Kidney Int 81: 779–783, 2012
4. Voskarides K, Damianou L, Neocleous V, Zouvani I, Christodoulidou S, Hadjiconstantinou V, Ioannou K, Athanasiou Y, Patsias C, Alexopoulos E, Pierides A, Kyriacou K, Deltas C: COL4A3/COL4A4 mutations producing focal segmental glomerulosclerosis and renal failure in thin basement membrane nephropathy. J Am Soc Nephrol 18: 3004–3016, 2007
5. Parkin JD, San Antonio JD, Pedchenko V, Hudson B, Jensen ST, Savige J: Mapping structural landmarks, ligand binding sites, and missense mutations to the collagen IV heterotrimers predicts major functional domains, novel interactions, and variation in phenotypes in inherited diseases affecting basement membranes. Hum Mutat 32: 127–143, 2011
6. Miner JH: The glomerular basement membrane. Exp Cell Res 318: 973–978, 2012
7. Kobayashi T, Kakihara T, Uchiyama M: Mutational analysis of type IV collagen alpha5 chain, with respect to heterotrimer formation. Biochem Biophys Res Commun 366: 60–65, 2008

8. Kobayashi T, Uchiyama M: Characterization of assembly of recombi- nant type IV collagen alpha3, alpha4, and alpha5 chains in transfected cell strains. Kidney Int 64: 1986–1996, 2003
9. Kobayashi T, Uchiyama M: Mutant-type alpha5(IV) collagen in a mild form of Alport syndrome has residual ability to form a heterotrimer. Pediatr Nephrol 25: 1169–1172, 2010
10. Abrahamson DR, Hudson BG, Stroganova L, Borza DB, St John PL: Cellular origins of type IV collagen networks in developing glomeruli. J Am Soc Nephrol 20: 1471–1479, 2009
11. Heidet L, Cai Y, Guicharnaud L, Antignac C, Gubler MC: Glomerular expression of type IV collagen chains in normal and X-linked Alport syndrome kidneys. Am J Pathol 156: 1901–1910, 2000
12. Boot-Handford RP, Briggs MD: The unfolded protein response and its rel- evance to connective tissue diseases. Cell Tissue Res 339: 197–211, 2010
13. Yoshida H: ER stress and diseases. FEBS J 274: 630–658, 2007
14. Rajpar MH, McDermott B, Kung L, Eardley R, Knowles L, Heeran M, Thornton DJ, Wilson R, Bateman JF, Poulsom R, Arvan P, Kadler KE, Briggs MD, Boot-Handford RP: Targeted induction of endoplasmic reticulum stress induces cartilage pathology. PLoS Genet 5: e1000691, 2009
15. Pierides A, Voskarides K, Athanasiou Y, Ioannou K, Damianou L, Arsali M, Zavros M, Pierides M, Vargemezis V, Patsias C, Zouvani I, Elia A, Kyriacou K, Deltas C: Clinico-pathological correlations in 127 patients in 11 large pedigrees, segregating one of three heterozygous muta- tions in the COL4A3/ COL4A4 genes associated with familial haema- turia and significant late progression to proteinuria and chronic kidney disease from focal segmental glomerulosclerosis. Nephrol Dial Trans- plant 24: 2721–2729, 2009
16. Voskarides K, Pierides A, Deltas C: COL4A3/COL4A4 mutations link familial hematuria and focal segmental glomerulosclerosis. Glomerular epithelium destruction via basement membrane thinning? Connect Tissue Res 49: 283–288, 2008
17. Zoll WL, Horton LE, Komar AA, Hensold JO, Merrick WC: Character- ization of mammalian eIF2A and identification of the yeast homolog. J Biol Chem 277: 37079–37087, 2002
18. Oslowski CM, Urano F: Measuring ER stress and the unfolded protein response using mammalian tissue culture system. Methods Enzymol 490: 71–92, 2011
19. Cawley K, Deegan S, Samali A, Gupta S: Assays for detecting the un- folded protein response. Methods Enzymol 490: 31–51, 2011
20. Deltas C, Pierides A, Voskarides K: The role of molecular genetics in diagnosing familial hematuria(s). Pediatr Nephrol 27: 1221–1231, 2012
21. Mayne R, Wiedemann H, Irwin MH, Sanderson RD, Fitch JM, Linsenmayer TF, Kühn K: Monoclonal antibodies against chicken type IV and V collagens: Electron microscopic mapping of the epitopes after rotary shadowing. J Cell Biol 98: 1637–1644, 1984
22. Trüeb B, Gröbli B, Spiess M, Odermatt BF, Winterhalter KH: Basement membrane (type IV) collagen is a heteropolymer. J Biol Chem 257: 5239–5245, 1982
23. Fatemi SH: The role of secretory granules in the transport of basement membrane components: Radioautographic studies of rat parietal yolk sac employing ^{3}H-proline as a precursor of type IV collagen. Connect Tissue Res 16: 1–14, 1987
24. Leinonen A, Netzer KO, Boutaud A, Gunwar S, Hudson BG: Good- pasture antigen: Expression of the full-length alpha3(IV) chain of col- lagen IV and localization of epitopes exclusively to the noncollagenous domain. Kidney Int 55: 926–935, 1999
25. Fukuda K, Hori H, Utani A, Burbelo PD, Yamada Y: Formation of re- combinant triple-helical [alpha 1(IV)]2 alpha 2(IV) collagen molecules in CHO cells. Biochem Biophys Res Commun 231: 178–182, 1997
26. Jeanne M, Labelle-Dumais C, Jorgensen J, Kauffman WB, Mancini GM, Favor J, Valant V, Greenberg SM, Rosand J, Gould DB: COL4A2 mu- tations impair COL4A1 and COL4A2 secretion and cause hemorrhagic stroke. Am J Hum Genet 90: 91–101, 2012
27. Lee AS: The ER chaperone and signaling regulator GRP78/BiP as a monitor of endoplasmic reticulum stress. Methods 35: 373–381, 2005
28. Bertolotti A, Zhang Y, Hendershot LM, Harding HP, Ron D: Dynamic interaction of BiP and ER stress transducers in the unfolded-protein response. Nat Cell Biol 2: 326–332, 2000
29. Lindenmeyer MT, Rastaldi MP, Ikehata M, Neusser MA, Kretzler M, Cohen CD, Schlöndorff D: Proteinuria and hyperglycemia induce en- doplasmic reticulum stress. J Am Soc Nephrol 19: 2225–2236, 2008
30. Bek MF, Bayer M, Müller B, Greiber S, Lang D, Schwab A, August C, Springer E, Rohrbach R, Huber TB, Benzing T, Pavenstädt H: Expression and function of C/EBP homology protein (GADD153) in podocytes. Am J Pathol 168: 20–32, 2006
31. Markan S, Kohli HS, Joshi K, Minz RW, Sud K, Ahuja M, Anand S, Khullar M: Up regulation of the GRP-78 and GADD-153 and down regulation of Bcl-2 proteins in primary glomerular diseases: A possible involvement of the ER stress pathway in glomerulonephritis. Mol Cell Biochem 324: 131–138, 2009
32. Tsang KY, Chan D, Cheslett D, Chan WC, So CL, Melhado IG, Chan TW, Kwan KM, Hunziker EB, Yamada Y, Bateman JF, Cheung KM, Cheah KS: Surviving endoplasmic reticulum stress is coupled to altered chon- drocyte differentiation and function. PLoS Biol 5: e44, 2007
33. Rheault MN, Kren SM, Thielen BK, Mesa HA, Crosson JT, Thomas W, Sado Y, Kashtan CE, Segal Y: Mouse model of X-linked Alport syn- drome. J Am Soc Nephrol 15: 1466–1474, 2004
34. Lu W, Phillips CL, Killen PD, Hlaing T, Harrison WR, Elder FF, Miner JH, Overbeek PA, Meisler MH: Insertional mutation of the collagen genes Col4a3 and Col4a4 in a mouse model of Alport syndrome. Genomics 61: 113–124, 1999
35. Cosgrove D, Meehan DT, Grunkemeyer JA, Kornak JM, Sayers R, Hunter WJ, Samuelson GC: Collagen COL4A3 knockout: A mouse model for autosomal Alport syndrome. Genes Dev 10: 2981–2992, 1996
36. Beirowski B, Weber M, Gross O: Chronic renal failure and shortened lifespan in COL4A3+/- mice: An animal model for thin basement membrane nephropathy. J Am Soc Nephrol 17: 1986–1994, 2006
37. Firtina Z, Danysh BP, Bai X, Gould DB, Kobayashi T, Duncan MK: Ab- normal expression of collagen IV in lens activates unfolded protein response resulting in cataract. J Biol Chem 284: 35872–35884, 2009
38. Kitamura M: Endoplasmic reticulum stress in the kidney. Clin Exp Nephrol 12: 317–325, 2008
39. Inagi R: Endoplasmic reticulum stress in the kidney as a novel mediator of kidney injury. Nephron, Exp Nephrol 112: e1–e9, 2009
40. Dickhout JG, Krepinsky JC: Endoplasmic reticulum stress and renal disease. Antioxid Redox Signal 11: 2341–2352, 2009
41. Saleem MA, O'Hare MJ, Reiser J, Coward RJ, Inward CD, Farren T, Xing CY, Ni L, Mathieson PW, Mundel P: A conditionally immortalized hu- man podocyte cell line demonstrating nephrin and podocin expression. J Am Soc Nephrol 13: 630–638, 2002
42. Takemoto M, Asker N, Gerhardt H, Lundkvist A, Johansson BR, Saito Y, Betsholtz C: A new method for large scale isolation of kidney glomeruli from mice. Am J Pathol 161: 799–805, 2002